TECHNOLOGY DEPT.

JOURNAL OF APPLIED PHYSICS

Vol. 23, No. 11 November, 1952

PUBLIC LIBRARY
DEC 4 1952
DETROIT

New Permanent Magnets from Powdered Manganese Bismuthide. See page 1207.

JOURNAL OF APPLIED PHYSICS

Vol. 23, No. 11 NOVEMBER, 1952

In This Issue

		Page
Temperature Rise in a Heat-Producing Solid behind a Surface Defect	William Karush and Gale Young	1191
Mechanism for Self-Diffusion in Graphite	G. J. Dienes	1194
Studies of Self-Diffusion in Graphite Using C-14 Tracer	M. H. Feldman, W. V. Goeddel, G. J. Dienes, and W. Gossen	1200
New Permanent Magnet from Powdered Manganese Bismuthide	Edmond Adams, William M. Hubbard, and Albert M. Syeles	1207
Polarization of Acoustic Waves in Cubic Crystals	A. E. Fein and Charles S. Smith	1212
Use of Radioactive Material for the Generation of High Voltage	E. G. Linder and S. M. Christian	1213
Application of Fluorescence X-Rays to Metallurgical Microradiography	H. R. Splettstosser and H. E. Seemann	1217
On the Relation between the Conductance and the Noise Power Spectrum of Certain Electronic Streams	J. J. Freeman	1223
Electric Potential Produced by Two Point Current Sources in a Homogeneous Conducting Sphere	Ernest Frank	1225
Scabbing of Metals under Explosive Attack: Multiple Scabbing	John S. Rinehart	1229
Thermal Stresses in a Partially Clamped Elastic Half-Plane	J. H. Huth	1234
Development of Porosity during Diffusion in Substitutional Solid Solutions	R. W. Balluffi and B. H. Alexander	1237
Effect of Cyclotron Bombardment on Self-Diffusion in Silver	R. D. Johnson and A. B. Martin	1245
Effect of Filament Voltage on the Plate Current of a Diode	Henry F. Ivey	1254
X-Ray Diffraction Study of the Hafnium-Hydrogen System	S. S. Sidhu and J. C. McGuire	1257
Barlated Tungsten Emitters	Ray C. Hughes and Patrick P. Coppola	1261
Creep of Copper under Deuteron Bombardment	Warren F. Witzig	1263
Diffraction of a Shock or an Electromagnetic Pulse by a Right-Angled Wedge	Joseph B. Keller	1267
Initial Behavior of a Spherical Blast	J. A. McFadden	1269
Letters to the Editor:		
Note on Love Waves in a Homogeneous Crust Laid upon Heterogeneous Medium	Sushil Chandra Das Gupta	1276
Creep of Zinc Single Crystals under Direct Shear	Elliot H. Weinberg	1277
Creep of Zinc Single Crystals	Donald O. Thompson	1277
Comments on "A Mathematical Analysis of Parallel Connected Magnetic Amplifiers with Resistive Loads"	H. S. Kirschbaum	1278
Comments on H. S. Kirschbaum's Letter	Louis A. Pipes	1279
Remarque on Critical Reflections of Elastic Wages at Free Surfaces	W. S. Jardetzky	1279
Comments on "Remarque on Critical Reflections of Elastic Waves at Free Surfaces"	J. N. Goodier	1280
Resistance of a Truncated Hemisphere	W. R. Smythe	1280
Light Scattering by Pure Polystyrene	F. Bueche	1280
Organization and Entropy	Jerome Rothstein	1281
Preferred Crystal Orientation in Ferromagnetic Ceramics	A. L. Stuyts, G. W. Rathenau, and E. W. Gorter	1282
Electrical Resistivity of Artificial Graphite	Jun Okada and Tatsuo Ikegawa	1282
Emissivity for CO_2 at Elevated Pressures	R. J. Holm, D. Weber, and S. S. Penner	1283
Books Reviewed		1284
Other Books Received		1288
Announcements		1288
Index to Advertisers		xxx

BOARD OF EDITORS

Elmer Hutchisson, *Editor*

Earle C. Gregg, *Assistant Editor*

Associate Editors

Howard H. Aiken
Ray E. Bolz
Lyle D. Borst
Robert D. Heidenreich
James Hillier
Leonard B. Loeb
W. James Lyons
Eric Reissner
Roman Smoluchowski

Publication of the

American Institute of Physics

OFFICERS

George R. Harrison, *Chairman*
George B. Pegram, *Treasurer*

GOVERNING BOARD

Karl K. Darrow
G. J. Dienes
S. A. Goudsmit
G. P. Harnwell
George R. Harrison
F. V. Hunt
Rudolph Kingslake
Hugh S. Knowles
C. C. Lauritsen
F. W. Loomis
William F. Meggers
George B. Pegram
I. I. Rabi
Duane Roller
Frederick Seitz
Francis G. Slack
John C. Steinberg
Richard M. Sutton
Mark W. Zemansky

Consultant on Printing

Melvin Loos

ADMINISTRATIVE STAFF

Henry A. Barton, *Director*
Wallace Waterfall, *Executive Secretary*
Theodore Vorburger, *Advertising Manager*
Ruth F. Bryans, *Publication Manager*
Betty H. Goodfriend, *Assistant Secretary*
Eileen B. Neuberger, *Circulation Manager*
Kathryn Setze *Assistant Treasurer*

The Journal of Applied Physics, published monthly at Prince and Lemon Sts., Lancaster, Pa., is devoted to physics in its role as the science basic to other natural sciences and to the arts and industries. Previous to 1937 this publication was known as Physics. The Journal of Applied Physics publishes editorials and reviews, as well as technical papers of applied physics. Articles appearing in it are indexed regularly, according to their field, by Physics Abstracts, Chemical Abstracts, Engineering Index, Inc., Industrial Arts Index, etc.

Manuscripts should be submitted to Elmer Hutchisson, Editor, Case Institute of Technology, Cleveland 6, Ohio. Unless otherwise stated, submission of a manuscript is a representation that it has been neither copyrighted, published, nor submitted for publication elsewhere. The authors' institutions are requested to pay a **publication charge** of $8 per page which, if honored, entitles them to 100 reprints without further charge. Instructions will be sent with galley proofs.

Subscriptions, renewals, and orders for back numbers should be addressed to the American Institute of Physics, 57 East 55 Street, New York 22, New York.

Subscription Price	U.S. and Canada	Elsewhere
To members of the American Institute of Physics and Affiliated Societies	$10.00	$11.00
To all others	12.00	13.00

Back Number Prices

Yearly back number rate when complete year is available: $14.00. Single copies: $1.25 each.

Changes of address should be sent to the American Institute of Physics; **corrected proofs** should be sent to the Publication Manager, American Institute of Physics. **Advertising rates** supplied on request. Orders, advertising copy, and cuts should be sent to the American Institute of Physics.

Entered as second class matter January 22, 1937, at the Post Office at Lancaster, Pennsylvania, under the Act of March 3, 1879. Accepted for mailing at the special rate of postage provided for in paragraph (d-2), section 34.40, P. L. & R. of 1948, authorized May 2, 1932.

1. Center line of slidewire and shaft
2. Control cams
3. Balancing motor
4. Spring-loaded no-backlash drive
5. Control slidewires
6. Measuring slidewire

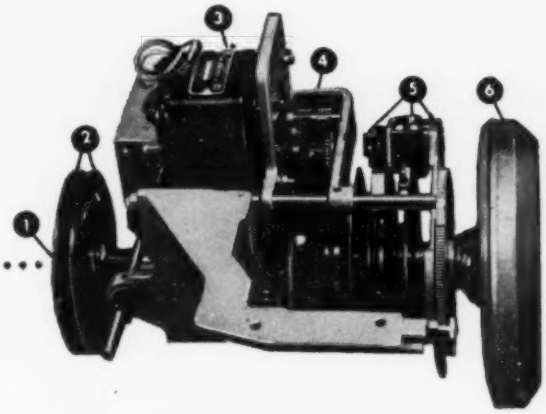

This partially dis-assembled view of Speedomax shows its two-phase Balancing Motor and gears, with a typically "heavy" load of slidewires and contacting cams for signal and control devices. Several more cams, etc., can be added if necessary; only practical limit is physical space on shaft. Smoothness in operating many contacts is an outstanding Speedomax ability.

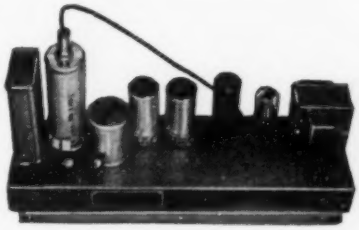

Amplifier which feeds the Speedomax balancing motor the controlling half of its power. Torque gradient is especially high where needed most—around balance point—for prompt, positive balancing. This Amplifier leads its field by large margins in sensitivity and in power output.

Good circuit engineering shows in this Slidewire's non-inductive wiring and in the absence of any flexible leads which might form inductive loops.

POWER IS PERFORMANCE

... and Speedomax Instruments lead with "huge" 12-watt balancing motors!

• Power underlies good performance, in instruments as in automobiles, machine tools or rolling mills. That's why L&N engineers insist that an automatic instrument should operate as positively and promptly as any other high-grade machine.

Even the first null balance potentiometer Recorder we built, back in 1911, which went to a steel mill, had a 110-volt motor instead of a spring drive to run its balancing mechanism, chart and signalling contacts. And, while its pioneering of balance-method measurement attracted the most attention, its ample power certainly helped establish L&N Recorders as the coming idea in process Instrumentation.

Power has done the same for Speedomax instruments. Twenty years ago, Speedomax pioneered the electronic idea of measurement—in a husky, powerful piece of equipment. Today's models have from 2 to 4 times more power in their balancing motors than any other current models of electronic controllers, recorders or indicators.

This power means superior performance in both load-carrying and speed. Load-carrying ability applies especially when the motor operates, in addition, an unusual number of contact devices. But even the most usual Speedomax jobs—automatic control, for instance—can call on the instrument's power for high operating speed in handling the normal number of control devices. The strong, wide-faced, rigidly-mounted cams and gears so typical of Speedomax instruments start moving instantly, move rapidly and stop dead still without coast. Signalling and control action is correspondingly crisp and precise.

Speedomax for industrial use is described in Catalog ND46 (1); additional information for unusual applications is given in Technical Publication ND46(1). Either will be sent on request by our nearest office or from 4978 Stenton Ave., Philadelphia 44, Pa.

LEEDS NORTHRUP

instruments automatic controls • furnaces

CAREER OPPORTUNITIES AT L&N

Expansion program of this long-established firm has many features to attract outstanding recent graduates in engineering and science. Opportunities are in sales field engineering, product and application engineering, research, advertising, market development. Widely-respected policies assure recognition of progress and achievement. Address Personnel Manager for preliminary interview at nearest of 17 L&N offices.

Jrl. Ad. ND46(8)

3 UNIVERTERS

...for extending the coverage of B.R.C. Signal Generators

UNIVERTER—Type 207-A

A frequency converter for use with FM-AM Signal Generators 202-B and 202-C. Output frequency range of Signal Generators is 54 to 216 mc. Additional output when using 207-A:

Frequency Range: 0.1 to 55 mc.

Output: 0.1 to 100,000 microvolts at X1 jack, approximately 7.5 times these values at high output jack.

Frequency Increment Dial: ±300 kc in 5 kc increments.

Modulation: FM and AM controlled by Signal Generator.

Price: $345.00 fob Factory.

UNIVERTER—Type 207-B

A frequency converter for use with FM-AM Signal Generator 202-D. The 202-D is applicable to telemetering problems over frequency range of 175-250 mc. Additional output when using 207-B:

Frequency Range: 0.1 to 55 mc.

Output: 0.1 to 100,000 microvolts at X1 jack and approximately 7.5 times these values at high output jack.

Frequency Increment Dial: ±300 kc in 5 kc increments.

Modulation: FM and AM controlled by Signal Generator.

Price: $345.00 fob Factory.

UNIVERTER—Type 207-C

A frequency converter for use with FM Signal Generator 206-A. The 206-A is applicable to mobile communications problems over a frequency range of 146 to 176 mc. Additional output when using 207-C:

Frequency Range: 0.1 to 50 mc.

Output: 0.1 to 100,000 microvolts at X1 jack and approximately 7.5 times these values at high output jack.

Modulation: FM controlled by Signal Generator.

Price: $345.00 fob Factory.

Write for complete information

BOONTON RADIO Corporation

BOONTON, N. J.

There's a DPi high vacuum measuring instrument for every laboratory and industrial requirement

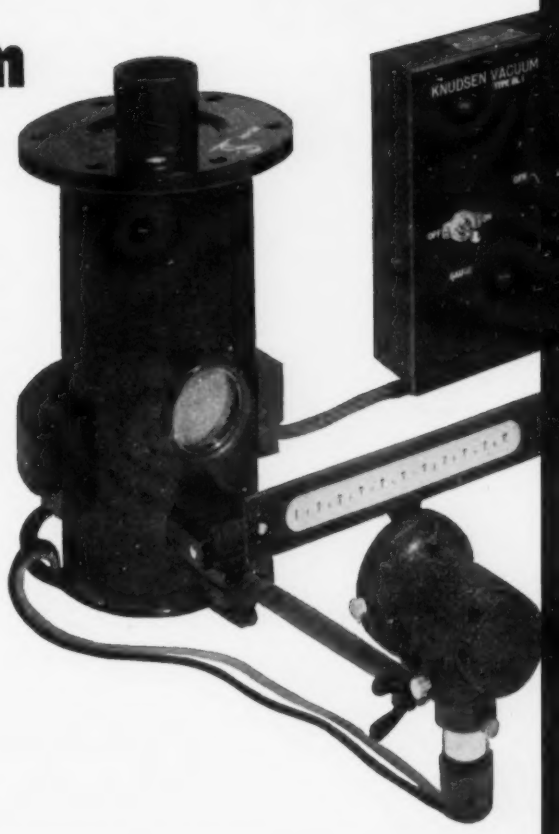

HERE ARE EXAMPLES . . .

For the range from 10^{-3} to 10^{-5} mm Hg, DPi's Knudsen Gauge, Type BL-1, is a radiometer gauge with a constant response that is essentially independent of the nature of most gases. Readings are absolute, giving total gas and vapor pressure. With no incandescent filament, better accuracy is assured in measuring vacuums in systems where gases are subject to decomposition. A magnetic damper provides stable readings without loss of sensitivity. And it can be attached to any system by standard glass or metal joints.

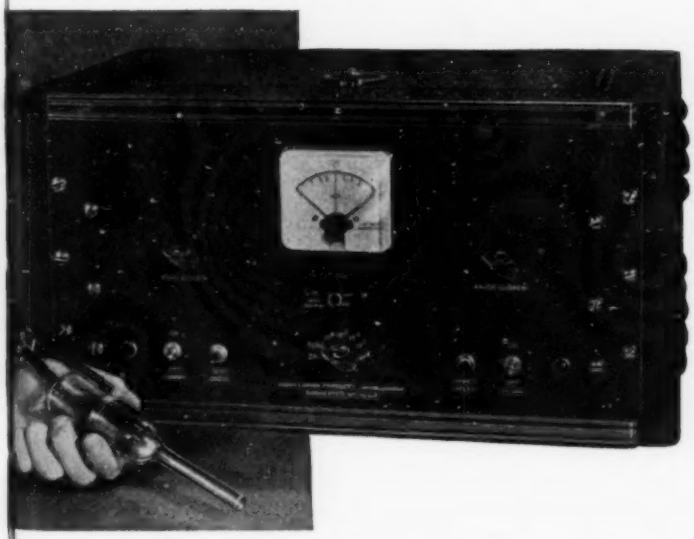

For the range from 1 micron to 1 x 10^{-8} mm Hg, DPi's Type VG-1A Ionization Gauge Tube, sealed in your vacuum system, provides the sensitivity required for measuring pressures as low as 10^{-8} mm Hg, yet is reliable at pressures of 1 micron. Its design reduces electrical leakage and outgassing to a minimum.

The DPi DPA-38 Ionization Gauge Control Circuit affords a completely self-contained power and amplifying unit for an ionization gauge tube—saves you the time and trouble of building your own. Designed for use with the VG-1A tube, but adaptable to others, it provides a tube degassing circuit. An automatic relay turns off gauge tube and turns on power for an alarm system when pressures exceed safe limits. Its very large range and continuous direct readings widen the DPA-38's application and make your work easier.

Both the Knudsen Gauge and the DPA-38 will hold calibration indefinitely and operate from any 115-v a-c outlet. And both are the result of nearly 20 years of experience in making high vacuum easy and economical to produce, measure and use. For more detailed information and prices, or engineering help on any problem involving high vacuum, write to ***Distillation Products Industries,*** Vacuum Equipment Department, 769 Ridge Road West, Rochester 3, N. Y. (Division of Eastman Kodak Company).

DPi

high vacuum research and engineering

Also . . . vitamins A and E . . . distilled monoglycerides . . . more than 3500 Eastman Organic Chemicals for science and industry

Vacuum Fusion Gas Analyzer

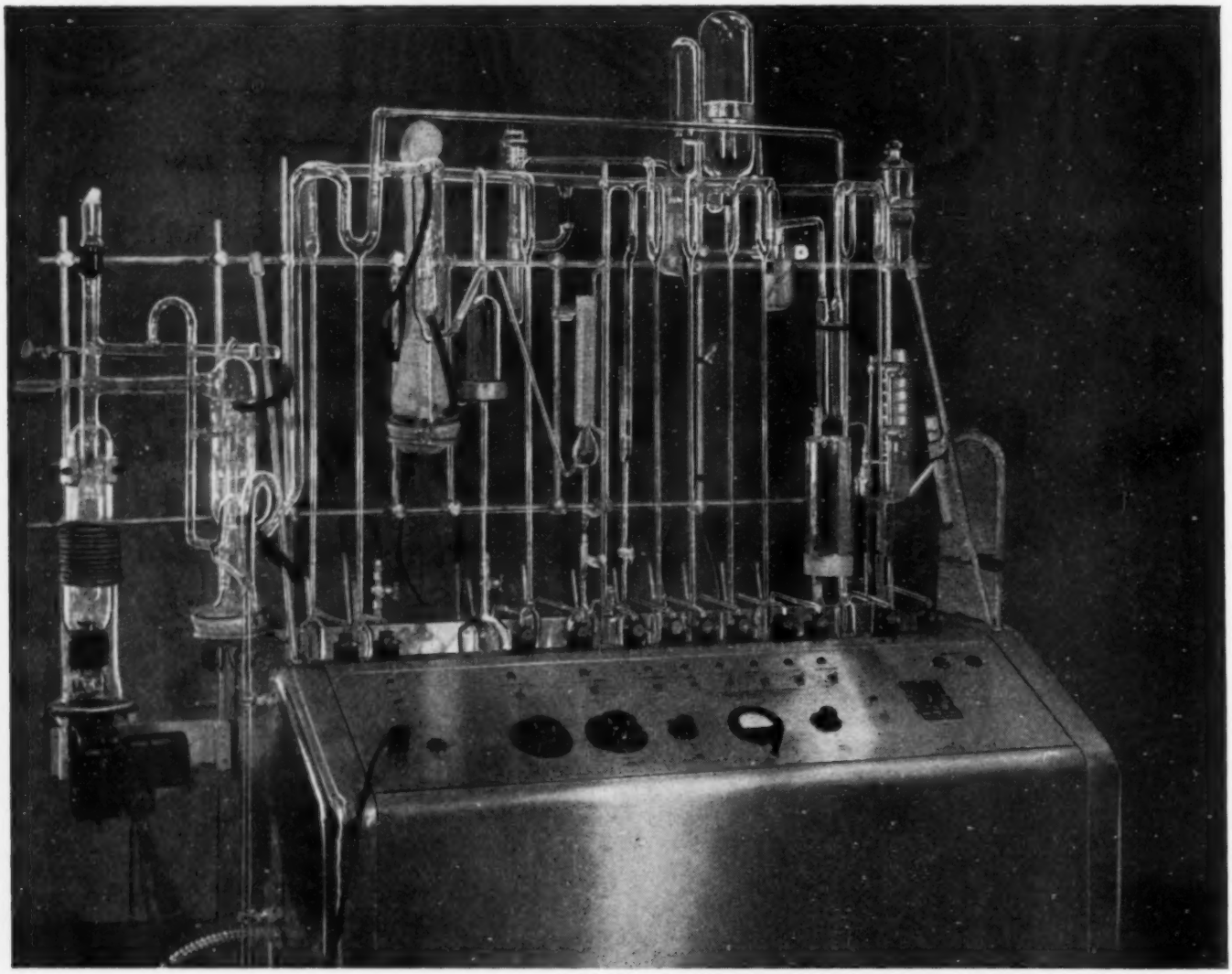

A packaged unit to determine the content of oxygen, nitrogen and hydrogen in metals

A wide variety of metals and alloys, including titanium, can be analyzed to determine the amount of oxygen, nitrogen and hydrogen contained either as combined or dissolved gas, in the range from one per cent to approximately 10^{-4} per cent by weight.

Total gas contents of titanium are reported within approximately the same range as for other metals, through the use of certain special techniques.

The apparatus incorporates the best features and techniques reported in the literature or known to our laboratory and has been employed for some time in connection with our own metallurgical research activities.

Operating procedure is relatively simple and can be readily mastered. Installation and final testing is performed by one of our trained analysts.

Write for details of Type 09-1240 Vacuum Fusion Gas Analysis Apparatus.

INDUSTRIAL RESEARCH • PROCESS DEVELOPMENT
HIGH VACUUM ENGINEERING AND EQUIPMENT

METALLURGY • DEHYDRATION • DISTILLATION
COATING • APPLIED PHYSICS

National Research Corporation

EQUIPMENT DIVISION

Seventy Memorial Drive, Cambridge, Massachusetts

In the United Kingdom: BRITISH-AMERICAN RESEARCH, LTD., London S. W. 7 — Wishaw, Lanarkshire

This electronic nose sniffs out leaks

Starting electronic nose on its way. It is pulled from pole to pole by line extending toward the ground. Previously workmen had to paint the cable with soap solution, so bubbles would disclose leaks.

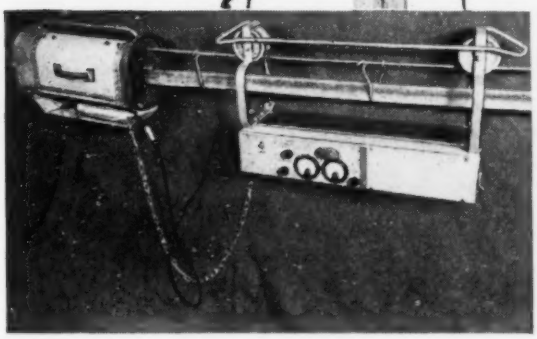

For test, the cable is cleared of protective nitrogen or air, and filled with Freon gas. Case at left collects escaping gas which operates Freon-sensitive detector underneath. At points where Freon escapes through sheath cracks, the box at right—a combined control unit and power supply—rings a bell. Workmen mark the point of leak for later repair.

AFTER years of buffeting by the wind, even tough telephone cable sometimes shows its age. Here and there the lead sheath may crack from fatigue or wear through at support points. Before moisture can enter to damage vital insulation, leaks must be located and sealed.

To speed detection, scientists at Bell Laboratories constructed an electronic nose which *sniffs* out the leaks. Using an electrically operated element developed by the General Electric Company, the device detects leaks of as little as 1/100 cubic foot per day. Sheath inspection can be stepped up to 120 feet per minute.

Thus Bell scientists add findings in other fields to their own original research in ways to make your telephone system serve you better. On the other hand their discoveries are often used by other industries. Sharing of scientific information adds greatly to the over-all scientific and technological strength of America.

BELL TELEPHONE LABORATORIES

Improving telephone service for America provides careers for creative men in scientific and technical fields

IMPORTANT ANNOUNCEMENT

Of general interest to users of radioactive materials is the recent incorporation of the

COMMERCIAL PRODUCTS DIVISION
ELDORADO MINING AND REFINING (1944) LIMITED

as a division of

ATOMIC ENERGY OF CANADA LIMITED

This transfer is made solely to provide a more comprehensive and efficient service for our customers. No changes in personnel, established agents or business routine are involved.

New applications of radioelements for research, medical and industrial uses, and new mechanical devices, will be announced from time to time.

Your requirements for pile-produced isotopes, radium, accessory equipment or consulting services will be satisfied completely by writing to:

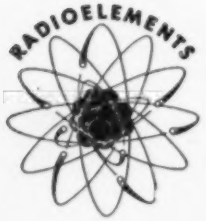

ATOMIC ENERGY OF CANADA LIMITED
COMMERCIAL PRODUCTS DIVISION
P.O. Box 93—Ottawa, Canada

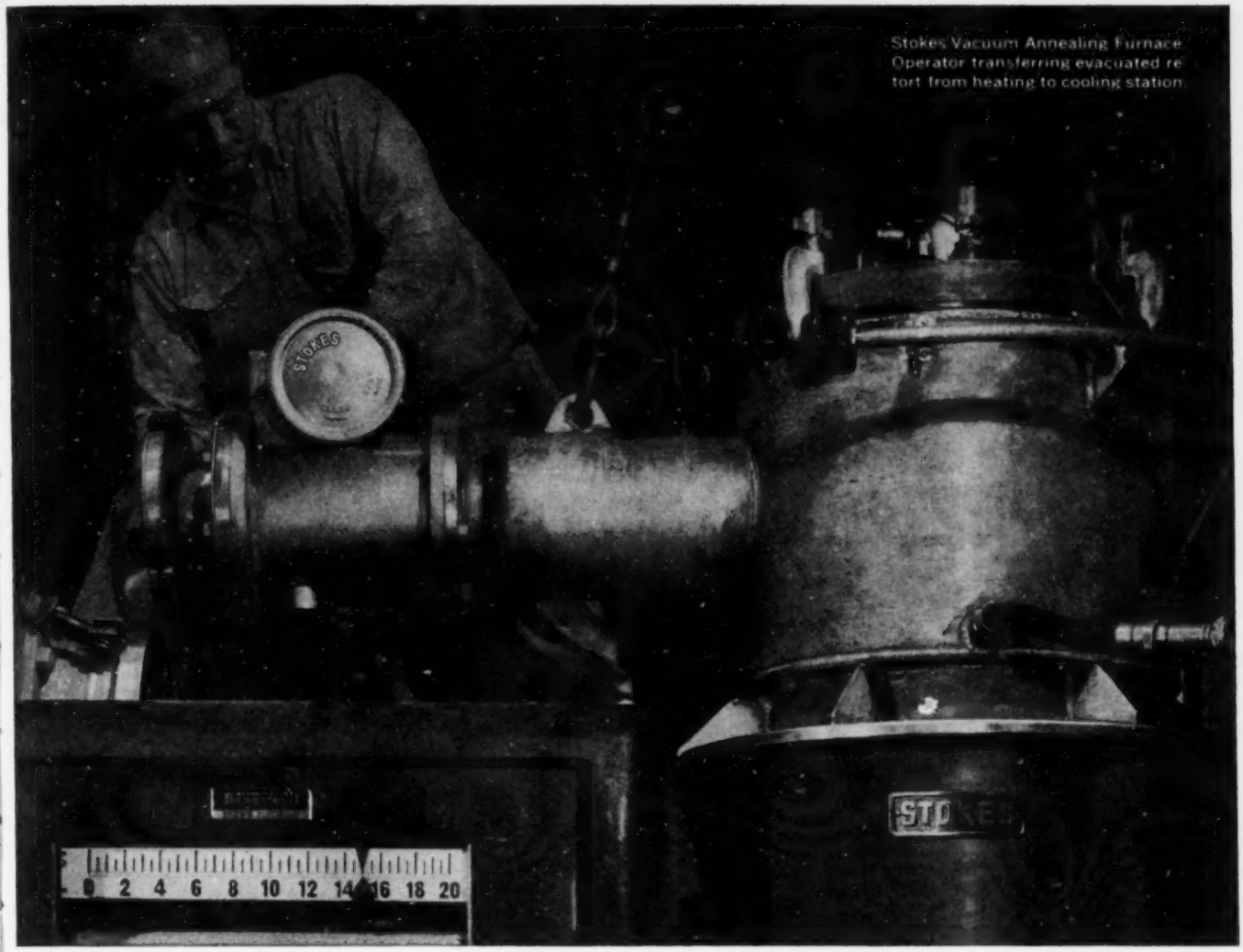

Stokes Vacuum Annealing Furnace. Operator transferring evacuated retort from heating to cooling station.

Make the step...from laboratory to production with Stokes High-Vacuum equipment

For processing titanium, zirconium, hafnium, and other metals . . . for low-cost melting, annealing and sintering of metals which must be processed under vacuum, Stokes makes the vacuum furnaces.

For the production of all high-vacuum processing equipment, Stokes has the largest and most diverse manufacturing facilities.

We build to customers' requirements, with a sure knowledge of what *is* and what is *not* practical.

Stokes techniques of building vacuum processing equipment which *works* and *produces in bulk* at low cost have been developed during fifty years of experience with vacuum and high vacuum.

Visit the Stokes plant and see for yourself that Stokes is first in Vacuum . . . first in the manufacture of vacuum processing equipment which takes you over the gap between the laboratory and commercial production.

F. J. STOKES MACHINE COMPANY,
PHILADELPHIA 20, PA.

STOKES

STOKES MAKES Plastics Molding Presses / Industrial Tabletting and Powder Metal Presses / Pharmaceutical Equipment / Vacuum Equipment / High Vacuum Pumps and Gages / Special Machinery

FOR MAXIMUM FLEXIBILITY IN WAVEFORM TIMING

The Browning Model GL-22A Sweep Calibrator is designed to free its users from limitations encountered in the use of crystal calibrators.

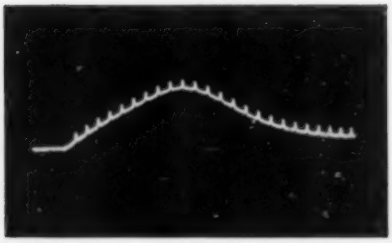

Positive pulse with markers to provide deflection – modulated display.

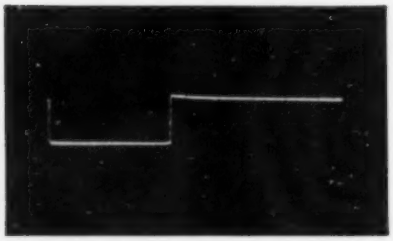

Negative gate pulse.

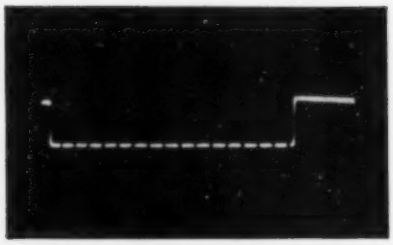

Negative pulse with markers used to blank sweep.

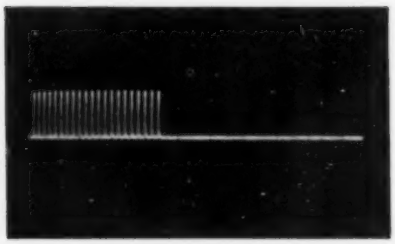

Positive marker output.

here are its advantages

It can be used as the triggering source, or can be triggered externally by the output of the device to be calibrated. The external trigger may be recurrent, up to 100 KC, random, or "one shot".

Using the internal trigger, the interval between successive markers is wholly independent of the trigger rate. The internal trigger is continuously variable from 200 to 5000 pulses per second.

The markers are produced through the keying action of a continuously variable gate, and thus can be restricted to the desired portion of an observed waveform. The gate pulse itself is also available as a useful output, of either polarity, and known duration.

The output markers, at 0.1, 1.0, 10, or 100 microseconds, accurate to $\pm 1\%$, of either polarity, can be continuously varied to 50 volts amplitude — sufficient for either intensity or deflection modulation use. The available intervals, in conjunction with the customary ruled screens, permit accurate measurement of intervals from 0.01 microsecond to several thousand microseconds.

Send for data sheet giving full details.

ENGINEERED FOR ENGINEERS

BROWNING
Laboratories, Inc.
Winchester, Mass.

Sanborn two-channel instruments for the simultaneous recording of two physiological phenomena*

* Phonocardiogram of DIAGNOSTIC quality WITH High-deflection-speed electrocardiogram

OR, two other physiological phenomena in combination.

PHOTOGRAPHIC *Twin-Beam*

CARDIETTE

Equipped with one ECG amplifier and one heart sound amplifier. Both are *removable* and *interchangeable.* Additional ECG amplifier available if recording of 'cardiograms and/or other physiological phenomena in combination is desired. Paper speeds 2.5, 25 and 75 mm/sec. AC power operated. 6cm. bromide paper.

* Electrocardiogram WITH one other physiological phenomenon

OR, two other physiological phenomena in combination.

DIRECT WRITING *Twin-Viso*

CARDIETTE

Each of the two channels may include *either* a Carrier Type or General Purpose Amplifier, or the latter in combination with either ECG or DC Preamplifiers. Amplifiers and preamplifiers *interchangeable.* Five dual sets of speeds —5 and 0.5, 10 and 1, 25 and 2.5, 50 and 5, 100 and 10 mm/sec. 5 inch recording Permapaper.

For further information on either or both of these instruments, address

Sanborn Company CAMBRIDGE 39, MASSACHUSETTS

PUT YOUR FINGER ON THE RIGHT PULSE NETWORK

Hundreds of combinations for the right size...voltage... pulse shape

Whatever your needs in pulse-forming networks—whatever your requirements for size, voltage, number of meshes, pulse lengths, or pulse repetition rates—Sprague has the right answer for that need.

Providing the right network for each application has been a Sprague specialty since Sprague made the very first networks for radar during World War II. Literally hundreds of pulse-forming networks have been designed and built by Sprague since then. Among these standard types can usually be found the solution to a specific requirement. If not, you'll find Sprague ready, willing, and able to manufacture networks to your exact order.

For details, write for our special bulletin "Pulse-Forming Networks."

SPRAGUE ELECTRIC COMPANY
257 Marshall Street • North Adams, Mass.

SPRAGUE

PIONEERS IN ELECTRIC AND ELECTRONIC DEVELOPMENT

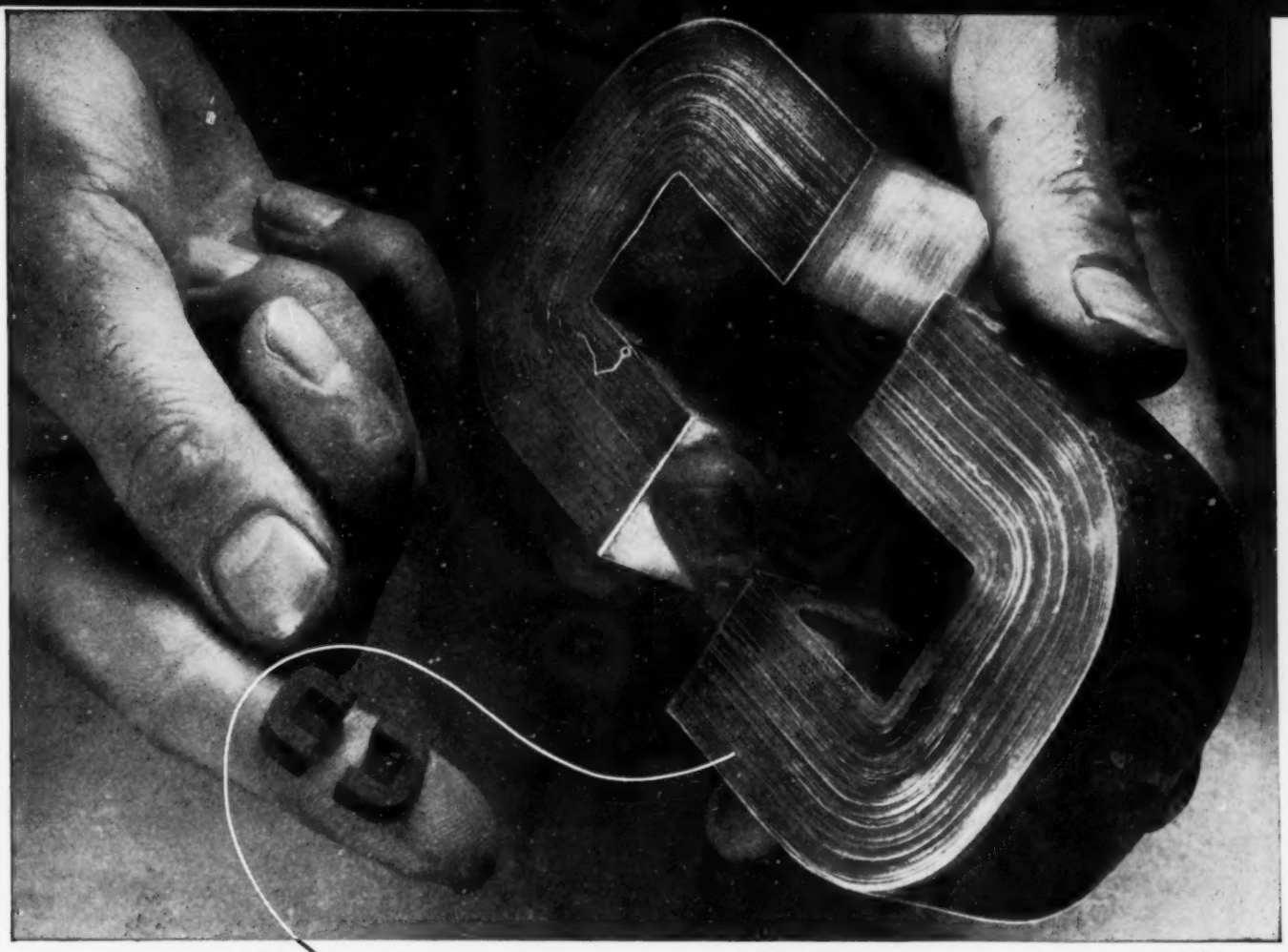

SILECTRON C-CORES...BIG or LITTLE

...any quantity and any size

Wound from precision rolled oriented silicon steel strip as thin as .00025"

For users operating on government schedules, Arnold is now producing C-Cores wound from ¼, ½, 1, 2, 4 and 12-mil Silectron strip. The ultra-thin oriented silicon steel strip is rolled to exacting tolerances in our own plant on precision cold-reducing equipment of the most modern type. Winding of cores, processing of butt joints, etc. are carefully controlled, assuring the lowest possible core losses, and freedom from short-circuiting of the laminations.

We can offer prompt delivery in production quantities—*and size is no object, from a fraction of an ounce to C-Cores of 200 pounds or more.* Rigid standard tests—and special electrical tests where required—give you assurance of the highest quality in all gauges. ● *Your inquiries are invited.*

WSD 4363

THE ARNOLD ENGINEERING COMPANY

SUBSIDIARY OF ALLEGHENY LUDLUM STEEL CORPORATION

General Office & Plant: Marengo, Illinois

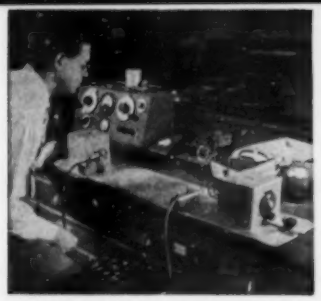

LABORATORIES: Experimental and development work requires extremely close voltage control for accurate and dependable results.

MANUFACTURING: To achieve maximum rated performance of electrically powered equipment, the input nameplate voltage must be maintained.

TESTING: Constant voltage must be maintained when testing or inspecting your product to obtain a valid check.

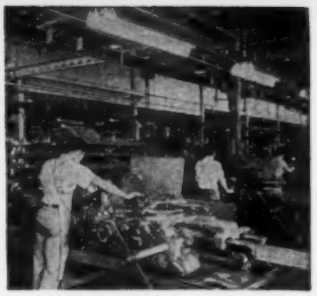

MAINTENANCE: By maintaining constant voltage to lamp loads and electrically operated equipment, productive life is increased and maintenance costs reduced.

ELECTRICAL OPERATIONS IN *Your Plant* REQUIRE

STABILINE

Automatic

VOLTAGE REGULATORS

TYPE EM4115

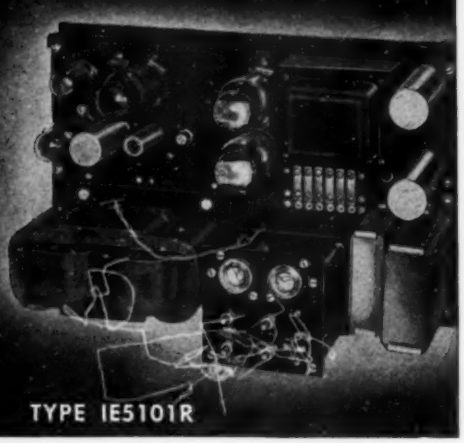

TYPE IE5101R

THERE IS NO BETTER WAY TO MAINTAIN CONSTANT OUTPUT VOLTAGE *Automatically*

TYPE **IE**

INSTANTANEOUS ELECTRONIC

Completely electronic automatic voltage regulators with no moving parts. Offer instantaneous correction . . . excellent stabilization and regulation. Waveform distortion does not exceed 3%. Particularly adapted for use in laboratories . . . test lines and for all other applications where the most exacting voltage regulation is necessary.

TYPE **EM**

ELECTRO MECHANICAL

Consists basically of a very sensitive detector controlling a motor-driven POWERSTAT variable transformer and auxiliary transformer. Correction is not instantaneous but is faster than most automatic voltage regulators. Features zero waveform distortion and high efficiency. Ideally suited for controlling large industrial loads.

FOR YOUR ELECTRICAL OPERATIONS . . .

. . . there is a STABILINE Automatic Voltage Regulator right for the job . . . to maintain constant voltage regardless of line or load changes.
Send today for complete information.

WRITE TO — 611 THURE AVENUE, BRISTOL, CONNECTICUT
ASK FOR — SECO BULLETIN S351

THE SUPERIOR ELECTRIC CO.
BRISTOL, CONNECTICUT

- STABILINE AUTOMATIC VOLTAGE REGULATORS
- POWERSTAT VARIABLE TRANSFORMERS
- VARICELL D-C POWER SUPPLIES
- VOLTBOX A-C POWER SUPPLIES
- SUPERIOR 5-WAY BINDING POSTS
- POWERSTAT LIGHT DIMMING EQUIPMENT

LINEAR AMPLIFIERS

In research problems where small pulses must be greatly amplified for oscillographic examination, or counting with scaler or rate meter, Atomic's Linear Amplifiers assure reliable results. Located in each amplifier section is an inverse feedback providing the amplifier with exceptional stability. Other features are:

Pulse Response: Choice of input time constant from 0.16 microsec. to 16 microsec. in seven steps . . . rise time can be varied from 0.2 microsec. to 2 microsec. in five steps.

Amplification: The voltage amplification varies between 1600 X and 9000 X depending upon the choice of input time constant and rise time. Gain control effected by attenuator having range from 0 to 30 db in 6 db steps.

Input Voltage: Operates on pulses of either positive or negative polarity . . . minimum usable input signal varies from about 200 microvolts to 1 millivolt depending on bandwidth. (2000 ohm input impedance.) Where high impedance input is required, use one of Atomic's preamplifiers—write for descriptions.

Amplifier Outputs: Low Level output gives a maximum signal of about 5 volts at 150 ohms . . . high level output gives a maximum signal of about 100 volts positive without appreciable amplitude distortion.

Noise: Maximum noise output, including AC hum, less than 1 volt from high level putput at maximum gain for all rise times.

Discriminator: A pulse amplitude discriminator operates from the high level output of the amplifier . . . pulses above predetermined level cause the discriminator to give a 10 volt positive pulse of 0.4 microsec. duration . . . discrimination level is dial calibrated for output pulses from 0 to 100 volts.

Model 204B

—another popular Linear Amplifier

Similar to the 204C but with choice of 3 rise times . . . 5 microsec., 0.1 Mc.; 0.8 microsec., 0.5 Mc.; 0.2 microsec., 2 Mc. Maximum voltage amplification 15,000, 10,000 and 3,000. Gain control by coarse and fine attenuators.

Plate and heater voltages for preamplifiers are available from a power connector at the rear. Write for data sheet R204.

Now ATOMIC'S 20 CHANNEL Differential Pulse Height Analyzer

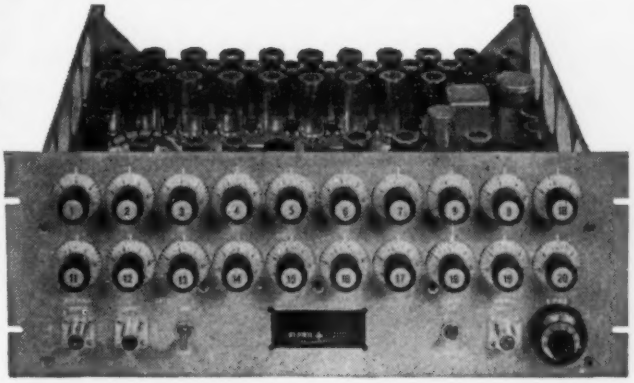

PULSE SORTER UNIT

. . . For the accurate determination (and simultaneous cataloging) of pulse amplitude distribution.

The new Atomic Model 520 - Twenty Channel Differential Pulse Height Analyzer facilitates the compilation of accurate data on the amplitude spectrum of electrical pulses having random amplitude and time distribution.

Specially designed for precision analysis of the energy spectra of radioactive materials, this equipment permits faster, and more accurate gathering of data and minimized decay corrections for short lived isotopes.

Other random distribution studies of radar signal amplitude, fog particle size, thermal noise effects, etc. are greatly facilitated by the use of this twenty channel analyzer.

The Model 520 is a *complete* analyzer for direct operation from nearly any pulse source. Its input linear amplifier permits full discrimination with signals having a maximum of less than 1 millivolts while the stability of the pulse sorter ensures accurate and reproducible results.

CHECK THESE OUTSTANDING FEATURES

Twenty Analysis Channels — Each with Scale of 16 and register — 15 microsecond resolution — up to 320 counts per second (regularly spaced).

Total and Surplus Count Channels — Each with Scale of 256 and register — 2 microsecond resolution.

Electrical Reset — Simultaneous electrical reset of all recording channels for speed and accuracy.

System Resolution — Better than 2.5 microseconds — up to 15,000 random input pulses per second.

Pulse Shaping — Built in linear amplifier to supply up to 70 volt 1 microsecond delay line shaped pulses to pulse sorter with 1 millivolt system input.

Pulse Calibrator — Special built in precision pulse generator for set up and calibration.

Power Supplies — Conservatively designed self contained regulated supplies for continuing reliability.

Unitized Construction — For maximum flexibility — complete in a single enclosed forced ventilated six foot cabinet.

Multiple Installations — 100 Channels or more without cumulative errors by interconnecting standard equipments.

Write or phone today for full information on this new Atomic Model 520 twenty channel differential pulse height analyzer and the Model 510 single channel pulse height analyzer.

Linear Amplifiers, Scalers, High Voltage Supplies, Scintillation Counters, Count Rate Meters, Coincidence and Anticoincidence Instruments, Accessories, Differential Pulse Height Analyzers

ATOMIC INSTRUMENT COMPANY

84 MASSACHUSETTS AVE. CAMBRIDGE 39, MASS.

SALES AND SERVICE REPRESENTATIVES

RESEARCH EQUIPMENT & SERVICE
8654 Woodlawn Avenue
Chicago 37, Ill.

CANADIAN MARCONI CO.
Montreal, Canada

HAROLD A. KITTLESON CO.
7614 Melrose Ave.
Los Angeles 46, Calif.

Engineering hours turn into minutes

when you speed up

You can do it yourself with these Telecomputing Instruments

THIS WAY

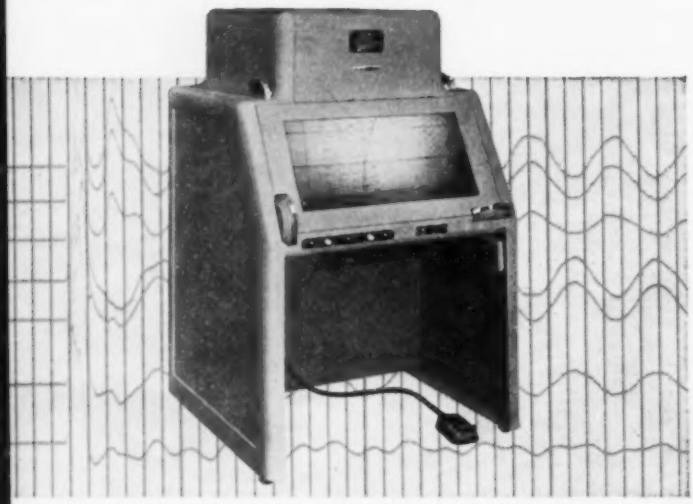

Today you can reduce and analyze film and oscillograph data faster than ever before. Telecomputing Instruments, in conjunction with electronic computing equipment, have made this possible.

The following sequence of automatic data analysis is typical:

The Universal Telereader measures records ranging from 16 and 35 mm film to 12" oscillograph records. Speed: up to 50 measurements per minute.

The Telecordex records the Telereader measurements in decimal form electronically on its own electric typewriter, transmits the data to an IBM Summary Punch for card punching.

The IBM card punch receives the data from the Telecordex, punches it and continues the cycle.

All necessary calculations, including linear and non-linear calibrations, are performed on IBM or other electronic computers.

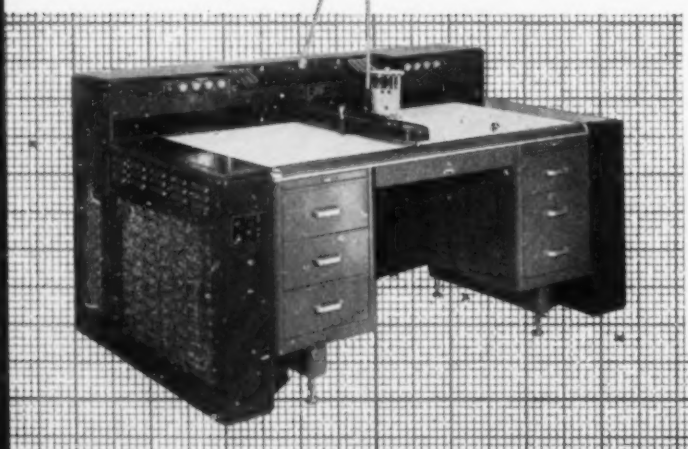

The Teleplotter plots the data electronically from IBM cards or a manual keyboard. Speed: up to 70 points per minute.

...p your data analysis

...WAY OR THIS WAY **Let Telecomputing do it for you in its Computing Division**

Your computing problems, large or small, can be handled quickly and efficiently by Telecomputing's staff of computing specialists.

A trained staff of engineers, physicists and mathematicians can process your problems on a round-the-clock basis, using IBM, Telecomputing and other electronic equipment.

The Computing Division handles data reduction problems from all types of record sources, as well as engineering and scientific mathematical problems of the widest scope.

Clients include major research and industrial organizations and technical government activities throughout the country.

Time and cost estimates will be presented if you will send information defining your computing and data reduction problems.

The coupon below is for your convenience in requesting information on the Computing Division and the Telecomputing Instruments shown at left.

Mr. Preston W. Simms, Engineering, Dept. JAP-11
Telecomputing Corporation, Burbank, California.

Dear Sir: Please send me:

- ☐ Universal Telereader Technical Bulletin TC 101
- ☐ Telecordex Technical Bulletin TC 102
- ☐ Teleplotter Technical Bulletin TC 103
- ☐ Information on your Computing Service
  (In requesting information on the Computing Service, you are invited to send information defining your data reduction and computing problems.)

Name _____

Company _____

Street Address _____

City and State _____

TELECOMPUTING
CORPORATION, BURBANK, CALIFORNIA

❶ Unexcelled Heat Dissipation
❷ Smooth Fine Adjustment
❸ Rugged Construction
Welch AIR-FLOW SLIDE-WIRE RHEOSTATS

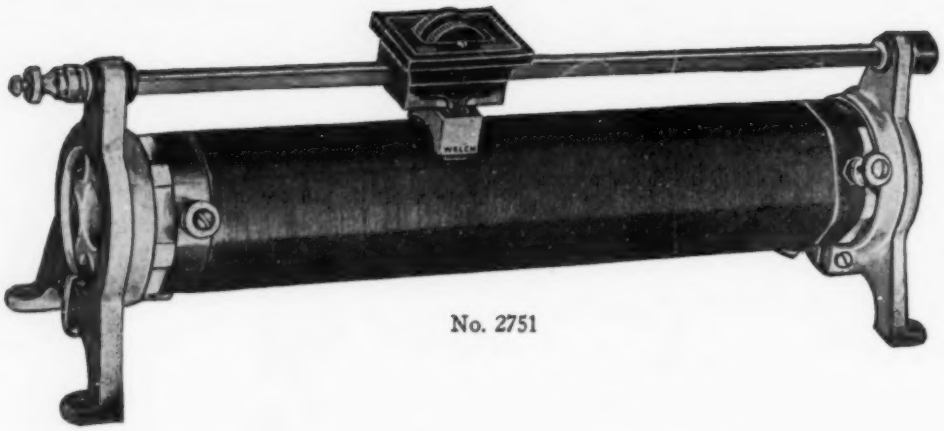

No. 2751

Available with the following nominal ratings:

Ohms	Amperes
2.5	13
5	9.2
10	6.5
20	4.5
40	3.2
85	2.2
170	1.6
340	1.12
680	.80
1300	.57
2600	.40
3800	.34
5500	.30

Welch AIR-FLOW Rheostats allow cool air to flow freely along the under surface of the wire, thereby achieving a cooling effect which permits considerable overloading without damage. The wire is wound on a thick-walled Coors porcelain tube with a deeply grooved outer surface to form the air ducts. Where still greater dissipation is needed, faster convection can be obtained by mounting the rheostat with the axis vertical.

Use of a non-magnetic core reduces disturbing magnetic effects on nearby unshielded equipment, reduces D.C. arcing, and lowers the reactance in A.C. circuits.

Two graphite-copper brushes with large surface area give easy motion and smooth, current control with less wear. A heavily oxidized resistance wire of nickel-chromium-iron alloy is used.

The slider moves the full length of the rheostat, moves rapidly with ease, and has a freely turning fine adjustment at the center.

$16.00 EACH

W. M. WELCH SCIENTIFIC COMPANY

DIVISION OF W M WELCH MANUFACTURING COMPANY

Established 1880

1515 SEDGWICK STREET. DEPT. C-1 CHICAGO 10, ILLINOIS. U.S.A.

Journal
of
Applied Physics

Volume 23, Number 11 November, 1952

Temperature Rise in a Heat-Producing Solid behind a Surface Defect*

WILLIAM KARUSH
The University of Chicago, Chicago, Illinois

AND

GALE YOUNG
Nuclear Development Associates, Inc., White Plains, New York

(Received June 16, 1952)

Simple expressions are obtained, in certain cases, for the temperature increase in a heat-producing body when the normal heat flow from the body is blocked by defective cooling on portions of the surface of the body. Defective areas in the shape of long strips and round spots are considered.

I. INTRODUCTION

CONSIDER a semi-infinite solid $z \geq 0$ in which heat is being produced and is leaving the solid through the boundary $z=0$ at a rate g per unit area which is independent of time and position[1] on the boundary. Suppose now that the temperature field is disturbed by introducing an insulating region R at the boundary. The region R causes the lines of heat flow to diverge around the region R and produces an increase in temperature in its neighborhood. We assume that the appearance of the insulating region does not affect the heat production in the solid; accordingly, the steady-state increment temperature T, i.e., the departure from the undisturbed temperature field, is a space-dependent harmonic function. We assume further that no change in temperature occurs at the surface outside of the region R. Under these circumstances we wish to determine the function T.

We shall solve the proposed problem for the following cases—(a) R is an infinite strip, and (b) R is the interior of a circle. For case (a) the solution is obtained by conformal mapping; using this result the solution for case (b) is obtained by analogy and then verified.[2]

The mathematical problem treated here arose in an application dealing with a heat-producing solid which is coated by a metal of high conductivity, the heat in the solid being carried across the coating into a cooling stream which flows past the coating. The question considered was that of determining the temperature rise caused by a thermal defect forming in the coating at any point between its two boundaries. A brief discussion of the application to this problem will be given in the final section.

II. INFINITE STRIP

Let the insulating strip be given by $-a \leq x \leq a$, $-\infty < y < \infty$. Then our problem is to determine a function $T(x, z)$ harmonic in the domain $-\infty < x < \infty$, $0 < z$, approaching zero for large z, and satisfying the boundary conditions

$$\begin{aligned} -k\frac{\partial T}{\partial z} &= g \quad \text{for} \quad x^2 < a^2, \; z=0, \\ T &= 0 \quad \text{for} \quad x^2 > a^2, \; z=0. \end{aligned} \tag{1}$$

(k is the thermal conductivity.) The first of these boundary conditions asserts that the strip is insulating, i.e., that the flow through the strip for the final temperature field (original field plus increment T) is zero, and the second asserts that the original surface temperature is undisturbed away from the strip.

* This paper is based on work done at the Metallurgical Laboratory, the wartime atomic energy project at the University of Chicago. The project report number is CP-1317.

[1] Actually, it is not necessary for g to be constant spacewise outside that portion R of the boundary where the defect is to be introduced.

[2] An alternative method of solution for case (ii) is given by Titchmarsh, *Introduction to the Theory of Fourier Integrals* (Oxford University Press, London, 1937), pp. 337–339. The solution is obtained there as a particular case of a general method employing Mellin transforms.

To determine $T(x, z)$ we introduce the complex variable

$$u=x+iz$$

and transform the u-plane conformally into the v-plane ($v=r+is$) by means of the equation

$$v=(u^2-a^2)^{\frac{1}{2}}.$$

This transformation carries the successive real line segments $(-\infty, -a)$, $(-a, 0)$, $(0, a)$, (a, ∞) into the respective line segments $(-\infty, 0)$, $(0, ia)$, $(ia, 0)$, $(0, \infty)$ in the v-plane. The imaginary part of v, namely, $s(x, z)$, is a harmonic function since it is the imaginary part of an analytic function. The isothermal lines of $s(x, z)$ are the inverse images in the u-plane of the horizontal lines in the v-plane, and the lines of flow are the inverse images of the vertical lines. From this it immediately follows that at $z=0$,

$$s=0 \quad \text{for} \quad x^2>a^2,$$

$$\frac{\partial s}{\partial z}=0 \quad \text{for} \quad x^2<a^2.$$

We may now show that the desired solution is given by

$$T(x, z)=\frac{g}{k}[s(x, z)-z].$$

Obviously this is an harmonic function which satisfies the boundary conditions (1). To see that T vanishes for large z we write

$$T(x, z)=\frac{g}{k}\,\mathrm{Imag}[(u^2-a^2)^{\frac{1}{2}}-u]$$

$$=\frac{g}{k}\,\mathrm{Imag}\left[u\left(-\tfrac{1}{2}\frac{a^2}{u^2}+\cdots\right)\right].$$

Thus, $T(x, z)\to 0$ as $z\to\infty$. At the surface we have

$$T(x, 0)=\frac{ga}{k}\left(1-\frac{x^2}{a^2}\right)^{\frac{1}{2}} \quad \text{for} \quad x^2<a^2. \tag{2}$$

We may verify the above solution by another method. The function T has the form

$$T(x, z)=\int_0^\infty f(t)\cos(tx)e^{-tz}dt,$$

with flow in the z direction given by

$$F(x, z)\equiv -k\frac{\partial T}{\partial z}=k\int_0^\infty tf(t)\cos(tx)e^{-tz}dt.$$

Keeping in mind the second equation of (1) and Eq. (2) let us determine f by means of

$$T(x, 0)=\int_0^\infty f(t)\cos txdt$$

$$=\begin{cases}\dfrac{ga}{k}\left(1-\dfrac{x^2}{a^2}\right)^{\frac{1}{2}} & \text{for} \quad x^2<a^2,\\ 0 & \text{for} \quad x^2>a^2.\end{cases} \tag{3}$$

By the Fourier transformation we obtain

$$f(t)=\frac{2ga}{\pi k}\int_0^a\left(1-\frac{x^2}{a^2}\right)^{\frac{1}{2}}\cos txdx=\frac{ga}{k}\cdot\frac{J_1(ta)}{t},$$

J, as usual, denoting a Bessel function. Thus,[3]

$$F(x, 0)=ga\int_0^\infty J_1(ta)\cos txdt$$

$$=\begin{cases}g & \text{for} \quad x^2<a^2,\\ -g\left\langle\dfrac{x}{a}-\left(\dfrac{x^2}{a^2}-1\right)^{\frac{1}{2}}\right\rangle\Big/\left(\dfrac{x^2}{a^2}-1\right)^{\frac{1}{2}} & \text{for} \quad x^2>a^2.\end{cases}$$

III. CIRCULAR REGION

In this case we let the variable r denote radial distance from the center of the region R in the (x, y)—plane and attempt to determine a harmonic function $T(r, z)$ satisfying the boundary conditions

$$-k\frac{\partial T}{\partial z}=g \quad \text{for} \quad 0\le r<a, \quad z=0,$$

$$T=0 \quad \text{for} \quad a<r, \quad z=0, \tag{4}$$

a being the radius of R. We proceed as in the second method of solution in the last section. We represent T in the form

$$T(r, z)=\int_0^\infty f(t)J_0(tr)e^{-tz}dt,$$

where the unknown function f is to be determined by (4). We have

$$F(r, z)\equiv -k\frac{\partial T}{\partial z}=k\int_0^\infty tf(t)J_0(tr)e^{-tz}dt.$$

By analogy with (3) we attempt the following surface distribution,

$$T(r, 0)=\int_0^\infty f(t)J_0(tr)dt=\begin{cases}C\left(1-\dfrac{r^2}{a^2}\right)^{\frac{1}{2}} & \text{for} \quad 0\le r<a,\\ 0 & \text{for} \quad a<r,\end{cases}$$

[3] Watson, *Bessel Functions* (Cambridge University Press, Cambridge, 1945), p. 405. We refer to this book as Watson henceforth.

where the constant C is to be determined. By the Fourier-Bessel transformation (Watson, p. 453; also p. 373)

$$f(t)=Ct\int_0^a rJ_0(tr)\left(1-\frac{r^2}{a^2}\right)^{\frac{1}{2}}dr$$

$$=\frac{C}{t}\left(\frac{\sin ta}{ta}-\cos ta\right).$$

Thus (Watson, p. 405)

$$F(r,0)=Ck\int_0^\infty\left(\frac{\sin ta}{ta}-\cos ta\right)J_0(tr)\,dt$$

$$=Ck\begin{cases}\dfrac{\pi}{2a} & \text{for } 0\leq r<a,\\[2ex] \dfrac{1}{a}\arcsin\dfrac{a}{r}-\dfrac{1}{(r^2-a^2)^{\frac{1}{2}}} & \text{for } a<r.\end{cases}$$

Thus if we choose $C=2ga/\pi k$, the boundary conditions (4) are satisfied and the solution is complete.

IV. APPLICATION

Consider now a heat-producing solid from which heat flows into a thin surface coating of high conductivity and thence into a cooling stream (see Fig. 1). Consider a circular defect of radius a located at a distance b from the boundary of the solid. We do not suppose that the defect is necessarily insulating; let it have a conductance h. We wish to estimate the temperature rise behind the center of defect caused by the introduction of the defect.

To obtain an estimate we suppose first of all that the temperature rise T vanishes for $r>a$ at the boundary $z=0$. Let S denote the circular disk of height b and radius a bounded by the defect and the boundary of the solid. We now think of the original flux g, which flowed into S when no defect was present, as flowing out of S when the defect is present via three paths which act as if they were in parallel; first, directly across the defect; second, back into the interior; third, radially. If each of these paths is assumed to be operating alone with the other two not functioning, we obtain, respectively, for the temperature rise T_0 at $r=z=0$,

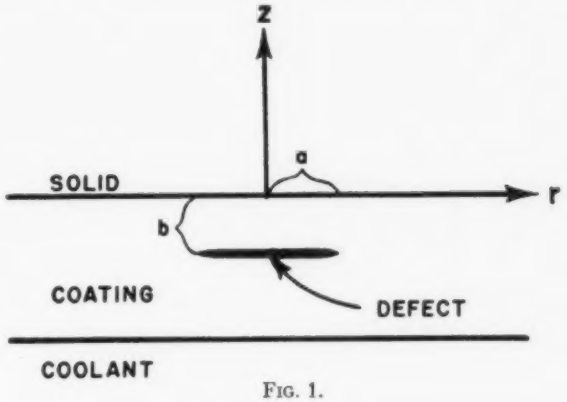

FIG. 1.

$$T_0=\frac{g}{h}$$

$$T_0=\frac{2ga}{\pi k}$$

$$T_0=\frac{ga^2}{4Kb}.$$

(K is the thermal conductivity of the coating.) The equations require justification. The first follows from the fact that the conductance of the defect is h and that we neglect the temperature change in the coating region between the defect and the coolant. The second equation follows from the solution in the preceding section. The third may be derived as follows. The heat conservation condition in S is

$$\frac{d^2T}{dr^2}+\frac{1}{r}\frac{dt}{dr}+\frac{g}{Kb}=0.$$

We wish a regular solution which vanishes at $r=a$. This solution is

$$T(r)=\frac{ga^2}{4Kb}\left(1-\frac{r^2}{a^2}\right),$$

leading to the stated result for $r=0$.

The reciprocal of the coefficient of g in each of the three expressions for T_0 may be regarded as an "effective" conductance for the corresponding path. From this point of view the conductance when the three paths are operating in parallel is the sum of the separate conductances. In this way we obtain the final estimate,

$$T_0=\frac{g}{h+\dfrac{\pi k}{2a}+\dfrac{4Kb}{a^2}}.$$

Mechanism for Self-Diffusion in Graphite*

G. J. DIENES†
Brookhaven National Laboratory, Upton, New York
(Received April 30, 1952)

The mechanism for self-diffusion in single crystals of graphite has been examined theoretically. Calculations for vacancy and direct interchange mechanisms are based on atomic interactions within the graphite hexagonal layers. These interactions are obtained from the known systematic change of carbon-carbon bond strength with interatomic distance. In order to be able to calculate the energy of formation of an interstitial carbon atom, a potential function has been devised to account for interaction between the planes. This potential function consists of two terms, a van der Waals' attraction and an exponential type repulsion. The adjustable constants have been evaluated from known physical data. The interplanar cohesive energy of graphite is calculated to be 4.36 kcal/mole.

Comparison of the total activation energies for self-diffusion via vacancies, direct interchange, and interstitial atoms indicates that direct interchange is the preferred mechanism. The activation energy for self-diffusion by means of direct interchange is estimated to be 90 kcal/mole. The present theoretical treatment is not applicable to diffusion along grain boundaries or pores.

I. INTRODUCTION

THREE possible mechanisms are usually seriously considered in studying self-diffusion, namely, direct interchange of neighboring atoms, diffusion by means of interstitial atoms, and diffusion by means of vacancies. The likelihood of each of these processes has been carefully examined for ionic crystals.[1] It is generally agreed that diffusion by means of vacancies is most probable in ionic crystals with rare gas configurations, while interstitial atoms may play an important role both in crystals of low coordination number and in highly coordinated crystals in which the metal ion contains a newly closed *d*-shell.

Huntington and Seitz carried out a careful theoretical study for the mechanism of self-diffusion in metallic copper.[2,3] They came to the conclusion that the vacancy mechanism is clearly favored over direct interchange or the interstitial mechanism. It should be noted that, according to their work, the energies of activation for moving already existing vacancies or interstitials are of the same order of magnitude. The total activation energy for diffusion is the sum of the energy required to create a mobile unity and the activation energy for moving this unit. It is because of the very high energy of formation of interstitials that this mechanism is eliminated.

Zener[4] suggested recently a cooperative mechanism for diffusion via the motion of rings of atoms. This represents a generalization of the direct interchange mechanism. Seitz[5] reanalyzed the situation and came to the conclusion that on the whole the theoretical and experimental evidence supports the vacancy mechanism. Recent experiments by Nowick[6] also point in this direction.

At the present time, therefore, for the theoretical study of self-diffusion in any material, it should be general enough to consider only the three main mechanisms, namely, vacancy diffusion, interstitial diffusion, and direct interchange.

The purpose of this paper is to describe some theoretical calculations carried out for graphite and designed to indicate which diffusion mechanism is expected to predominate. The nature and magnitude of the interatomic forces for such a material as graphite are not nearly as well known as for ionic crystals or simple metals. Nor are sufficient experimental data available, such as precise elastic constants, from which interatomic potential functions can be calculated. Some of the elastic constants have been estimated by Nelson and Riley[7,8] from thermal expansion data, and full use will be made of these results in calculating the interatomic interactions between the hexagonal planes in graphite. Enough is known, however, about the general

TABLE I. Characteristics of carbon-carbon bonds. (Data from Pauling[a])

Bond	Equilibrium carbon-carbon distance, r_0 in A	Bond strength, D, in kcal/mole
C−C	1.54	58.6
Benzene	1.39	86.0
C=C	1.33	100.0
C≡C	1.20	123.0

[a] L. Pauling, *The Nature of the Chemical Bond* (Cornell University Press, Ithaca, 1944), pp. 53, 131.

* This work was supported by AEC under Contract AT-11-1-GEN-8.

† A considerable portion of this work was done at North American Aviation, Inc. while the author was on the staff of the Atomic Energy Research Department. This paper supersedes the earlier unclassified AEC report NAA-SR-159 which unfortunately contained some computational errors.

[1] W. Jost, *Diffusion und Chemische Reaktionen in Festen Stoffen* (Steinkopf, 1937); N. F. Mott and M. J. Littleton, Trans. Faraday Soc. **34**, 485 (1938).

[2] H. B. Huntington and F. Seitz, Phys. Rev. **61**, 315 (1942); **76**, 1728 (1949).

[3] H. B. Huntington, Phys. Rev. **61**, 325 (1942).

[4] C. Zener, Acta Cryst. **3**, 346 (1950).

[5] F. Seitz, Acta Cryst. **3**, 355 (1950).

[6] A. S. Nowick, Phys. Rev. **82**, 551 (1951).

[7] J. B. Nelson and D. P. Riley, Proc. Phys. Soc. (London) **57**, 477 (1945).

[8] D. P. Riley, Proc. Phys. Soc. (London) **57**, 486 (1945).

nature of carbon-carbon bonds as a function of interatomic distance and about the structure of graphite to permit one to carry out reasonably reliable theoretical calculations.

Graphite is known to be a layer structure of hexagonal planes weakly held together by van der Waals' forces. The bonds within the planes are very strong covalent bonds corresponding to a C—C distance of 1.42A. The forces between the planes are very weak and correspond to an interplanar distance of 3.37A. The structure may, therefore, be pictured, to a good approximation, as a stack of rigid layers. This picture is fully in accord with the highly anisotropic thermal expansion measured by Nelson and Riley.[7,8] As an important consequence of this physical picture, theoretical treatment needs to take into account, to a very good approximation, only the bonds in the hexagonal planes in evaluating such quantities as the total activation energy for vacancy or interchange mechanism. When interstitials are present, the forces between the planes must be evaluated. However, in this case, the motion of the interstitials will be essentially independent of the bonds within the planes. Thus, in both cases, the problem may be handled essentially as a two-dimensional one.

The theoretical treatment is based primarily on carbon-carbon bond strengths and their systematic variation with carbon-carbon equilibrium distance. The pertinent data are listed in Table I. The bond strengths are plotted against the equilibrium interatomic distance in Fig. 1. Except for the C≡C bond the relation between bond strength D and equilibrium interatomic distance r_0 is very adequately described by a semilogarithmic relation

$$\log_{10}D=-1.105r_0+3.470. \quad (1)$$

The systematic decrease in bond strength with increasing bond distance as expressed by Eq. (1), forms the basis of the present theoretical study. It is assumed

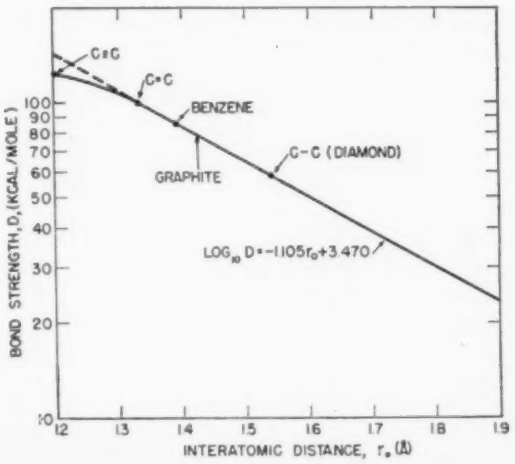

FIG. 1. Bond strength *vs* interatomic distance for carbon-carbon bonds.

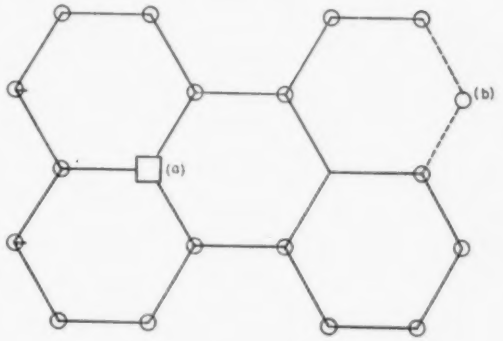

FIG. 2. Vacancy formation in graphite.

that a potential function can be written for carbon-carbon interatomic interactions as a function of interatomic distance which is equivalent to the observed relation expressed in Eq. (1). Various quantities pertinent to the diffusion process can then be calculated.

The bond strength of the carbon-carbon bond in graphite is obtained by interpolation along the line of Fig. 1 to an interatomic distance of 1.42A. The corresponding value for D is 79.6 kcal/mole.[9] This figure will be used throughout for the normal C—C bond within the graphite hexagonal planes. Nearest neighbor approximation will be used for all calculations within the graphite planes. For strong covalent bonds this approximation should be quite satisfactory. Interactions between the graphite planes are treated separately.

II. ACTIVATION ENERGY FOR VACANCY DIFFUSION

The activation energy for self-diffusion via the vacancy mechanism is the sum of two terms: the energy required to form a vacancy, and the activation energy for moving a vacancy. First, the energy required to create a vacancy is calculated as follows: an atom is taken out of the lattice and moved to the surface. In Fig. 2 this is represented by moving an atom from point (a) to point (b), leaving a vacancy at point (a). Three bonds are broken in removing an atom, requiring an expenditure of energy of 238.8 kcal/mole. In placing an atom on the surface, 3/2 bonds are formed, on the average, resulting in an energy gain of 119.4 kcal/mole.

The energy required to form a vacancy, ΔE_f^v, is therefore estimated to be

$$\Delta E_f^v=(-119.4+238.8)=119.4 \text{ kcal/mole}.$$

Consider now the motion of an atom at (c) toward the vacancy as illustrated in Fig. 3. Because of symmetry, the saddle point will be at the half-way point on the line from lattice point (c) to the vacancy. In terms of $r_0(=1.42\text{A})$ and taking the origin at point (c) the saddle

[9] Bond strengths derived from spectroscopic data are taken to be directly applicable to crystals. Further, temperature dependence of the various energy quantities is neglected throughout. The corresponding uncertainties are quite small (see footnote a, Table I). Note that a reasonable value of 118 kcal/mole is obtained for the heat of sublimation of a diamond from Fig. 1.

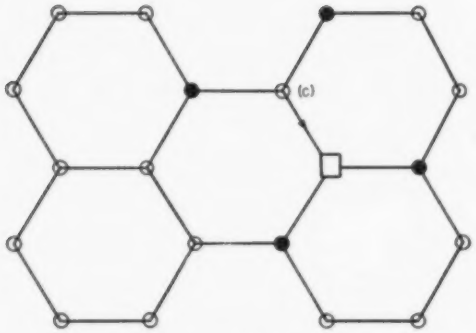

FIG. 3. Vacancy diffusion in graphite

point has the coordinates (0.25, −0.433). After the jump has taken place the configuration is exactly the same as the starting configuration. The activation energy for moving a vacancy is then given by the difference in the potential energy of the saddle point configuration and the starting configuration. Four atoms, symmetrically located around the saddle point, have been taken into account. These atoms are denoted by solid circles in Fig. 3. The energies corresponding to changing bond lengths are as follows:

Starting configuration	*E in kcal/mole*
2 bonds at r_0	$-159.2(79.6\times2)$
Saddle point configuration	
4 bonds at $1.323\,r_0$	$-\ 99.2(34.8\times4)$

The activation energy for motion of a vacancy due to altered bond lengths is, therefore,

$$\Delta E_a{}^v = 60.0 \text{ kcal/mole.}$$

In addition to the stretching of the bonds the original valence angles are distorted in forming the saddle point configuration. Two angles are distorted by 19° and one by 38°. Following Mark and Tobolsky,[10] it is estimated that the energy of bond angle distortion is about 1.5 kcal/mole per 10° distortion. The corresponding component of the activation energy is then 11.4 kcal/mole. The total activation energy for motion of a vacancy is, therefore,

$$\Delta E_a{}^v = 71.4 \text{ kcal/mole.}$$

The activation energy for self-diffusion by means of the vacancy mechanism is given by

$$\Delta E_a{}^d = \Delta E_f{}^v + \Delta E_a{}^v = 119.4 + 71.4 = 190.8 \text{ kcal/mole.}$$

The absolute magnitude of this value is subject to considerable doubt. The whole treatment is based on the assumption that Eq. (1) is an adequate description of the variation of potential energy as a function of distance for the motion of atoms in the hexagonal graphite planes. It is difficult to judge the validity of this approximation. However, a comparison among various mechanisms, based on the same fundamental approximation, should be fairly reliable even though the absolute magnitudes may be considerably in error.

The possible relaxation of atoms around a vacancy, which may decrease slightly the activation energy, was not taken into account. This effect is not likely to be large and its evaluation, which is straightforward but laborious, was not deemed necessary at this time.

III. ACTIVATION ENERGY FOR DIFFUSION BY MEANS OF DIRECT INTERCHANGE

The picture suggested for direct interchange of carbon atoms within the hexagonal planes is illustrated in Fig. 4. The geometry of the lattice indicates that the saddle point is probably at the half-way point with the two moving atoms still essentially r_0 apart. The energy change for this configuration is easily calculated by means of the potential field postulated in Eq. (1) and by means of the empirical value of 1.5 kcal/mole per 10° of valence angle distortion.

First, the activation energy corresponding to the configuration of Fig. 4 was calculated assuming that the moving atoms remain $r_0(r_0=1.42\text{A})$ apart. Four normal bonds are broken and four new bonds are created at a distance of $1.0649\ r_0$ (interaction with the four solid circles of Fig. 4) in forming this saddle point configuration. The bond strength corresponding to $1.0649\ r_0$ is 62.97 kcal/mole. Consequently, the activation energy due to altered bond lengths, $\Delta E_a{}^b$, is

$$\Delta E_a{}^b = 4(79.60) - 4(62.97) = 66.52 \text{ kcal/mole.}$$

This configuration corresponds to the following valence angle distortions. Around each moving atom one angle is distorted very closely by 20° and the other two by 10° each. The valence angle of the nearest neighbors is distorted by 40°. The total valence angle distortion is, therefore,

$$2(20)+4(10)+4(40)=240°,$$

and the corresponding activation energy, $\Delta E_a{}^d$, at 1.5 kcal/mole per 10° distortion is

$$\Delta E_a{}^d = 36 \text{ kcal/mole.}$$

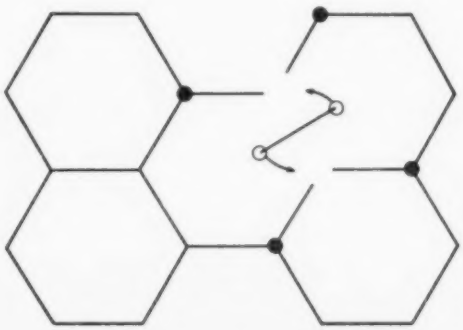

FIG. 4. Diffusion via direct interchange in graphite.

[10] H. Mark and A. U. Tobolsky *Physical Chemistry of High Polymeric Systems* (Interscience Publishers, New York, 1950), p. 21.

The total activation energy for self-diffusion is, then,

$$\Delta E_a = \Delta E_a{}^b + \Delta E_a{}^d = 102.5 \text{ kcal/mole.}$$

The possible relaxation of the atoms at the saddle point configuration was investigated next. It was found that contraction of the bond between the moving atoms decreases the activation energy. Physically this contraction can proceed until the distance between the moving atoms corresponds to a C=C bond of length 1.33A = 0.9366 r_0 which is equivalent to a contraction of 0.0317 r_0 at both ends. The distance to the four nearest neighbors is now 1.0761 r_0 = 1.528A, which is still slightly less than a normal single bond distance. The corresponding activation energies are

(1) contribution from altered bond lengths (4 bonds at 1.528A, 1 bond at 1.33A *vs* starting configuration of 5 bonds at 1.42A),

$$\Delta E_a{}^b = (398.0 - 341.8) = 56.2 \text{ kcal/mole;}$$

(2) contribution from valence angle distortion (2 angles by 18°, 4 angles by 9°, and 4 angles by 39°),

$$\Delta E_a{}^d = 34.2 \text{ kcal/mole:}$$

(3) total activation energy,

$$\Delta E_a = 90.4 \text{ kcal/mole.}$$

According to these results, self-diffusion by means of direct interchange requires an activation energy of 90.4 kcal/mole and proceeds via the saddle point configuration shown in Fig. 5. The following characteristics of this saddle point configuration are of interest. The average number of bonds per atom remains the same as in normal graphite. The double bond distribution of a normal graphite lattice can also be maintained. Further, direct exchange of the atoms involves no distortion of the surrounding atoms in the open graphite structure. Physically the situation is, therefore, quite different from that in metals where the surrounding atoms have to be pushed aside to permit the passage of the moving atoms. In metals, therefore, a large part of the activation energy arises from the increased repulsive interactions. In graphite, the above saddle point configuration involves essentially only a loss of attractive energy. Consequently, it appears physically reasonable that the activation energy for direct interchange is considerably less than for the vacany mechanism.

IV. ACTIVATION ENERGY FOR INTERSTITIAL DIFFUSION

The basic mechanism of self-diffusion by means of interstitial atoms is the following. Interstitial atoms are formed thermally by moving an atom from the surface of the crystal into an interstitial position. In the case of graphite the interstitial carbon atoms will lodge in the relatively open spaces between the layers. The interstitial atoms can diffuse between the planes with their own characteristic activation energy. The activation

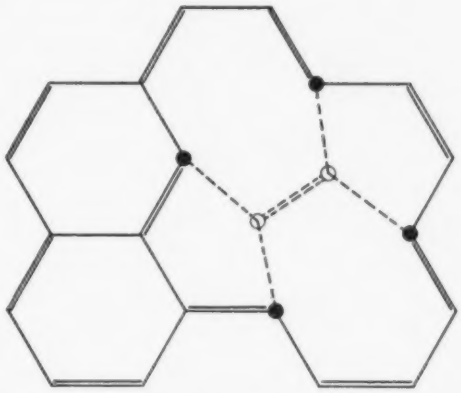

FIG. 5. Saddle point configuration for direct interchange.

energy for self-diffusion is, analagous to the vacancy mechanism, the sum of the energy required to form an interstitial, $\Delta E_f{}^i$, and the activation energy required to move an interstitial, $\Delta E_a{}^i$.

It is clear from the physical discussion given in the introduction that, in order to calculate these quantities, the first task is to construct a potential function for the interplanar interactions in graphite.

A. Interplanar Potential Function for Graphite

The hexagonal layers of molecules in graphite are separated by such a large distance, 3.37A, that there can be no covalent bonds between them. The superimposed large layer molecules are held together by van der Waals' forces which balance the repulsive forces between carbon atoms. The form of these functions is known. The van der Waals' attractive potential varies as the inverse sixth power of the distance, and the repulsive potential may be taken to be an exponential one. Thus, the interplanar potential energy as a function of interatomic distance may be written

$$U_i = -\frac{C}{r^6} + De^{-\alpha(r-r_e)}. \tag{2}$$

This function contains three adjustable constants which must be evaluated. The following procedure was adopted as the most satisfactory in view of the currently available experimental data. The coefficient of the repulsive term, D, is estimated by extrapolating the bond strength *vs* r relation to r_e = 3.37A [Eq. (1), Fig. 1]. This step is equivalent to the assumption that the repulsive potential is approximately given as the repulsive part of a Morse function around r_e. This is probably a fair approximation. Furthermore, the potential energy of an interstitial as well as the interplanar cohesive energy turn out to be quite insensitive to D, but depend strongly on α. The above described extrapolation to r_e = 3.37A gives

$$D = 0.024 \text{ ev/atom.}$$

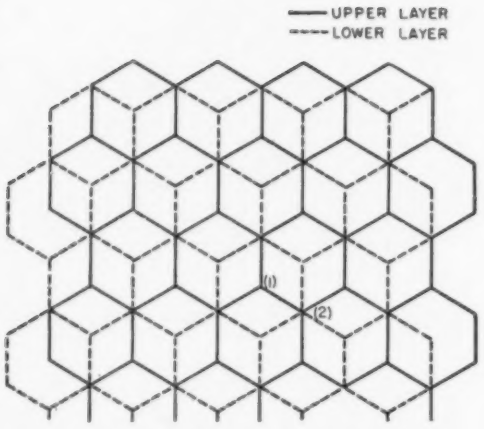

FIG. 6. Graphite lattice in simple *ab* packing.

The two other constants in Eq. (2), C and α, can be determined from the condition that the interplanar potential energy must be a minimum at $r=r_e$ and from the elastic modulus for strain parallel to the c axis. These quantities are calculable from the first and second derivatives of the potential energy as a function of distance summed over as many neighbors in the c direction as necessary. Since we are only concerned here with interplanar interactions, no summation within the planes is required. Simple *ab* packing is assumed throughout these calculations as shown for two superimposed hexagonal planes in Fig. 6. The z direction (which is also the c axis direction) is perpendicular to the plane of the paper. Two kinds of atoms, indicated as (1) and (2) in Fig. 6, must be considered in the summation since their neighbors are differently arranged. The average number of contacts per atom is the arithmetic average for the two kinds of atoms. Simple calculations showed that it is necessary to take into account 5 shells of atoms around any given atom. The 5 shells of atoms around any given atom are listed in Table II. In the equations given below for calculating cohesive energy and elastic constant, the summations indicate sums over the neighbors given in Table II.

The minimum in the potential energy is given by the relation

$$\frac{\partial \sum U}{\partial r}\Big)_{r=r_e}=0, \tag{3}$$

where U is given by Eq. (2) for any particular interaction. The above condition establishes one relation between the two constants C and α.

Riley[8] gives the following values for the elastic constants of graphite at 18°C:

$$s_{11}+s_{12}=1.8\times10^{-13}\ \text{cm}^2/\text{dyne},$$
$$s_{13}=-4.3\times10^{-13}\ \text{cm}^2/\text{dyne},$$
$$s_{33}=58.5\times10^{-13}\ \text{cm}^2/\text{dyne}.$$

From these values the elastic modulus in the c direction c_{33}, corresponding to a stretch in the c direction, is obtainable from the equation

$$c_{33}=(s_{11}+s_{12})/s,$$

where

$$s=s_{33}(s_{11}+s_{12})-2s_{13}^2. \tag{4}$$

The value for c_{33} turns out to be 2.635×10^{11} dynes/cm^2.

A theoretical expression for c_{33} can now be set up as follows. According to Fuchs[11] and some earlier papers by the writer,[12] c_{33} is calculable from the interatomic potential energy function by the relation

$$c_{33}=\frac{1}{\Omega_0}\frac{1}{2}\sum\left(\frac{\partial^2 U}{\partial\epsilon_z^2}\right)_{\epsilon_z=0}, \tag{5}$$

where Ω_0 = volume per atom $=8.80\times10^{-24}$ cm^3 for graphite. ϵ_z = strain in the z direction.

The potential function U is given in terms of r by Eq. (2), but is easily expressed in terms of ϵ_z as follows. If the interplanar distance r_e is increased by Δr, then

$$\epsilon_z=\Delta r/r_e. \tag{6}$$

r is given by

$$r=(z^2+x^2+y^2)^{\frac{1}{2}},$$

or in terms of the strain ϵ_z,

$$r=(r_e^2(1+\epsilon_z)^2+x^2+y^2)^{\frac{1}{2}}, \tag{7}$$

and x and y are, of course, fixed numbers for any neighboring atom.

With this transformation the differentiation and summation indicated in Eq. (5) and tabulated in Table II are easily carried out. The final expression gives a functional relation between C and α. Equations (3) and (5) are, therefore, two relations to be solved simultaneously for the two unknowns C and α. This is best accomplished graphically by calculating the values of C from Eqs. (3) and (5) for various given values of α. The correct value of α is determined by the condition that the values of C calculated from the two equations be identical. This procedure gave the following values:

$$\alpha=3.15\text{A}^{-1},$$
$$C=36.3\ \text{(ev/atom) (A}^6\text{)},$$
$$=58.2\times10^{-60}\ \text{ergs cm}^6.$$

TABLE II. Average number of atoms and their distances surrounding any given atom for interplanar interaction in graphite

Shell	Average number of contacts	Distance in A
1	1	3.37
2	9	3.657
3	6	4.172
4	9	4.407
5	18	5.047

[11] K. Fuchs, Proc. Roy. Soc. (London) **A151**, 585 (1935); **A153**, 622 (1936).

[12] G. J. Dienes (to be published). See also unclassified reports NAA-Sr-80, −125, −144.

The constants of the interplanar potential function, Eq. (2), have now been established. A rough check may be obtained on the suitability of this technique from polarizabilities. The van der Waals' interaction depends essentially on the polarizabilities of the molecules and C may be estimated from the relation[13]

$$C=\tfrac{3}{4}h\nu_i a^2, \tag{8}$$

where a = polarizability and $h\nu_i$ = ionization potential.

For carbon atoms $h\nu_i$ may be taken to be 13.5 ev. The value of a for saturated carbon atoms is 1.0×10^{-24} cm^3. For saturated carbon atoms then,

$$C=16.3\times10^{-60}\text{ ergs cm}^6.$$

Graphite, however, has a considerably higher polarizability because of the approximately one-third double bond character. Assuming one-third double bond character, molar refractivities[13] indicate that a should be 1.8×10^{-24} cm^3. The corresponding C is $C=53\times10^{-60}$ ergs cm^6, which is very close to the value deduced for C by the technique described above.

It appears, therefore, that the constants of the proposed potential function, Eq. (2), have been evaluated in a suitable manner, and Eq. (2) may be used with some confidence.

B. Interplanar Cohesive Energy of Graphite

The interplanar cohesive energy of graphite can now be calculated from the potential function given by Eq. (2). This energy is

$$U_{\text{total interplanar}}=-\tfrac{1}{2}\textstyle\sum_{\text{neighbors}}U,$$

evaluated at $r=r_e$. The summation is over the neighbors listed in Table II. This calculation gave 0.19 ev/atom for the interplanar cohesive energy. This is 4.36 kcal/mole and is seen to be a very reasonable number since van der Waals' interactions usually contribute only a few percent to the total cohesive energy.

Brennan has recently calculated, by quantum-mechanical methods, the repulsive energy between layers of the graphite crystal.[14] The corresponding van der Waals attractive term was found by setting the energy minimum at 3.37A. Brennan calculates the interlayer binding energy to be 3.99 kcal/mole, which is in very satisfactory agreement with the value calculated in this paper. The agreement probably indicates that the exponential function is not a bad approximation of the repulsive potential between layers.

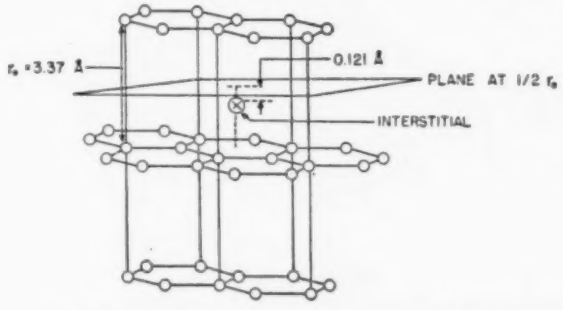

FIG. 7. Equilibrium position of an interstitial atom in the graphite lattice.

TABLE III. Numbers of interactions and their distances around an interstitial.

Number of interactions	Distances in A
1	1.806
6	2.112
3	2.295

C. The Energy Required to Form an Interstitial Atom

In order to form an interstitial atom it is necessary to move a surface atom into an interstitial position. The energy of formation is the difference in the potential energy of the final and the initial configurations. The potential energy of a surface atom was estimated in Sec. II to be -119.4 kcal/mole.

By means of the interplanar potential function one can estimate the potential energy of an interstitial atom. Let an atom be placed somewhere about half-way between the graphite planes. It is easily shown that, because of the exponential nature of the repulsive potential, the attractive potential energy at these relatively close distances is entirely negligible compared to the potential energy arising from repulsion, and it is sufficient to take into account the repulsive interactions only. Ten interactions of the interstitial with neighboring atoms were taken into account. The number of interactions and their distances are listed in Table III. The distances in Table III are measured from the equilibrium position of the interstitial. This equilibrium position was determined by finding the interplanar position of minimum potential energy taking into account ten surrounding neighbors. This position turned out to be directly above (or below) the center of a hexagon and 0.121A below (or above) the median plane of $\frac{1}{2}r_e$. The position of the interstitial is illustrated in Fig. 7.

From Eq. (2) the potential energy of an interstitial is now easily calculated by summing over the distribution given in Table III. A value of

$$U_{\text{interstitial}}=12.94\text{ ev/atom}=297.6\text{ kcal/mole}$$

was obtained.[15] The total energy required to form an interstitial atom is given by

$$\Delta E_f{}^i=297.6-(-119.4)=417.0\text{ kcal/mole},$$

[13] See, for example, S. Glasstone, *Textbook of Physical Chemistry* (D. Van Nostrand Company, Inc., New York, 1940), pp. 291, 528.

[14] R. O. Brennan, J. Chem. Phys. **20**, 40 (1952).

[15] Relaxation around an interstitial may decrease the value of $U_{\text{interstitial}}$ calculated here. This effect cannot be large enough to change the conclusions.

where −119.4 kcal/mole is the potential energy of a surface atom. According to the present calculation, therefore, self-diffusion by means of interstitial atoms is a very unlikely process because of the very high energy required to create interstitial atoms. The total activation energy for self-diffusion, of course, will be even higher than the energy of formation.

V. DISCUSSION

The theoretical treatment presented in the previous sections indicates that the direct interchange mechanism is the preferred one for self-diffusion in graphite. The total activation energy for self-diffusion via the direct interchange mechanism is estimated to be 90 kcal/mole. On the basis of the physical discussion presented in Sec. III, it is concluded that the open hexagonal structure of the graphite crystal is primarily responsible for the relative ease of direct atomic interchange.

It is to be emphasized that the theoretical treatment is applicable only to volume diffusion since a single perfect graphite crystal is assumed throughout the calculations. In a polycrystalline piece of graphite, which contains many grain boundaries and is also porous, self-diffusion may proceed, and almost certainly does in some temperatures ranges, by mechanisms other than volume diffusion. The theory outlined in this paper is not applicable to grain boundary diffusion or to diffusion on the surface of pores or across pores. It does provide, however, a theoretical value for the activation energy with which experimental activation energies can be compared, when they become available.

The author is indebted to Dr. F. J. Ewing, consultant to the Atomic Energy Research Department of North American Aviation, for many helpful suggestions and stimulating discussions and to Miss E. Stratton for performing many of the calculations.

JOURNAL OF APPLIED PHYSICS VOLUME 23, NUMBER 11 NOVEMBER, 1952

Studies of Self-Diffusion in Graphite Using C-14 Tracer*

M. H. Feldman, W. V. Goeddel, G. J. Dienes,† and W. Gossen
Atomic Energy Research Department, North American Aviation, Inc., Downey, California
(Received June 5, 1952)

Self-diffusion in graphite was measured over the temperature range from 1835°C to 2370°C by observing the penetration of C-14 tracer initially applied to one end of a graphite rod.

The experimental data were found to be in agreement with a diffusion mechanism consisting of concurrent volume and grain boundary processes. Activation energies for both processes (E_V and E_B) could not be uniquely obtained from the data, however. An independent determination of either is required in order to evaluate the other. On the basis of recent theoretical work, E_V may be taken to be 90 kcal/mole. From the present experiments and the above value of E_V, the activation energy for grain boundary diffusion, E_B, is calculated to be 75.4 kcal/mole.

I. INTRODUCTION

REACTIONS in the solid state are believed to depend on diffusion processes for their over-all rates.[1] This applies to both chemical reactions and "physical" processes and, furthermore, there is some reason to believe that diffusion processes are among the controlling steps in radiation effects on solids.[2] Measurement of the self-diffusion coefficient and the associated activation energy is of fundamental importance for interpreting many diverse solid-state phenomena. The purpose of the present paper is to describe some experiments on self-diffusion in polycrystalline artificial graphite using C^{14} as a tracer.

II. EXPERIMENTAL TECHNIQUES

1. Materials and Equipment

AUF graphite‡ was chosen for the present study based on the idea that, at least for the first experiment, a graphite of reasonably uniform fine grain, particle size, and density was desirable. Furthermore, AUF graphite was readily available and in pieces large enough to supply many samples from one piece.

Such diffusion experiments have been done with a rod of metal which had been plated on one end with radioactive tracer, annealed, and then had thin slices machined off the end for counting.[3] The sectioning is usually carried out on a lathe. For graphite, sectioning

* Based on studies conducted for the Atomic Energy Commission under Contract AT-11-1-GEN-8.

† Now at Brookhaven National Laboratory, Upton, Long Island, New York.

[1] W. Jost, *Diffusion und Chemische Reaktion in Festen Stoffen* (Theodor Steinkopf, Verlag., Dresden, 1937).

[2] F. Seitz, Disc. Faraday Soc. No. 5, 271 (1949).

‡ A product of the National Carbon Company, AUF has an apparent density of 1.67 g/cm³, a pore volume of about 30 percent, and grain sizes ranging from 1 to 10×10^{-3} millimeter.

[3] See, for example, W. A. Johnson, Trans. Am. Inst. Mining Met. Engrs. **143**, 107 (1941).

where −119.4 kcal/mole is the potential energy of a surface atom. According to the present calculation, therefore, self-diffusion by means of interstitial atoms is a very unlikely process because of the very high energy required to create interstitial atoms. The total activation energy for self-diffusion, of course, will be even higher than the energy of formation.

V. DISCUSSION

The theoretical treatment presented in the previous sections indicates that the direct interchange mechanism is the preferred one for self-diffusion in graphite. The total activation energy for self-diffusion via the direct interchange mechanism is estimated to be 90 kcal/mole. On the basis of the physical discussion presented in Sec. III, it is concluded that the open hexagonal structure of the graphite crystal is primarily responsible for the relative ease of direct atomic interchange.

It is to be emphasized that the theoretical treatment is applicable only to volume diffusion since a single perfect graphite crystal is assumed throughout the calculations. In a polycrystalline piece of graphite, which contains many grain boundaries and is also porous, self-diffusion may proceed, and almost certainly does in some temperatures ranges, by mechanisms other than volume diffusion. The theory outlined in this paper is not applicable to grain boundary diffusion or to diffusion on the surface of pores or across pores. It does provide, however, a theoretical value for the activation energy with which experimental activation energies can be compared, when they become available.

The author is indebted to Dr. F. J. Ewing, consultant to the Atomic Energy Research Department of North American Aviation, for many helpful suggestions and stimulating discussions and to Miss E. Stratton for performing many of the calculations.

JOURNAL OF APPLIED PHYSICS VOLUME 23, NUMBER 11 NOVEMBER, 1952

Studies of Self-Diffusion in Graphite Using C-14 Tracer*

M. H. Feldman, W. V. Goeddel, G. J. Dienes,† and W. Gossen
Atomic Energy Research Department, North American Aviation, Inc., Downey, California

(Received June 5, 1952)

Self-diffusion in graphite was measured over the temperature range from 1835°C to 2370°C by observing the penetration of C-14 tracer initially applied to one end of a graphite rod.

The experimental data were found to be in agreement with a diffusion mechanism consisting of concurrent volume and grain boundary processes. Activation energies for both processes (E_V and E_B) could not be uniquely obtained from the data, however. An independent determination of either is required in order to evaluate the other. On the basis of recent theoretical work, E_V may be taken to be 90 kcal/mole. From the present experiments and the above value of E_V, the activation energy for grain boundary diffusion, E_B, is calculated to be 75.4 kcal/mole.

I. INTRODUCTION

REACTIONS in the solid state are believed to depend on diffusion processes for their over-all rates.[1] This applies to both chemical reactions and "physical" processes and, furthermore, there is some reason to believe that diffusion processes are among the controlling steps in radiation effects on solids.[2] Measurement of the self-diffusion coefficient and the associated activation energy is of fundamental importance for interpreting many diverse solid-state phenomena. The purpose of the present paper is to describe some experiments on self-diffusion in polycrystalline artificial graphite using C^{14} as a tracer.

II. EXPERIMENTAL TECHNIQUES

1. Materials and Equipment

AUF graphite‡ was chosen for the present study based on the idea that, at least for the first experiment, a graphite of reasonably uniform fine grain, particle size, and density was desirable. Furthermore, AUF graphite was readily available and in pieces large enough to supply many samples from one piece.

Such diffusion experiments have been done with a rod of metal which had been plated on one end with radioactive tracer, annealed, and then had thin slices machined off the end for counting.[3] The sectioning is usually carried out on a lathe. For graphite, sectioning

* Based on studies conducted for the Atomic Energy Commission under Contract AT-11-1-GEN-8.

† Now at Brookhaven National Laboratory, Upton, Long Island, New York.

[1] W. Jost, *Diffusion und Chemische Reaktion in Festen Stoffen* (Theodor Steinkopf, Verlag., Dresden, 1937).

[2] F. Seitz, Disc. Faraday Soc. No. 5, 271 (1949).

‡ A product of the National Carbon Company, AUF has an apparent density of 1.67 g/cm³, a pore volume of about 30 percent, and grain sizes ranging from 1 to 10×10^{-3} millimeter.

[3] See, for example, W. A. Johnson, Trans. Am. Inst. Mining Met. Engrs. **143**, 107 (1941).

by means of a microtome§ has been found to be very satisfactory.

The tracer species to be used for self-diffusion experiment in graphite could be chosen from C^{11}, C^{13}, or C^{14}. Twenty-minute C^{11} was useless for an experiment in which many (up to 116) hours were required for anneals. C^{13} would probably have been usable if a mass spectrometer had been available. Finally, C^{14} was chosen because of its radioactivity, availability in fairly high specific activities and long half-life. No account was taken, in this work, of possible "isotope effects," although perhaps C^{12} and C^{14} would have different diffusion rates in AUF graphite.

Graphite containing C^{14} has to be handled with some care from the health physics standpoint. The size of particles of graphite was 4×10^{-4} centimeter in at least one dimension due to the setting of the microtome. This was checked by microscopic examination. Particles of this size probably do not represent an inhalation danger. However, every precaution was taken to ensure safety in a health physics sense. All operations in which the graphite was fragmented were carried out in a gloved box.|| The samples, when necessary, were removed from the box in closed aluminum boxes. Lucite boxes were quite unusable due to build up of electrostatic charge, resulting in obvious dispersion of the graphite particles.

The vacuum furnance used up to about 2400°C has been adequately described.[4] The heating coil in the present experiments was of somewhat larger internal diameter than that of reference 4, but no important differences existed.

Temperature measurement was by means of a Leeds and Northrup Optical Pyrometer (Type 8622-C) calibrated at this laboratory against Bureau of Standards "Standard Lamp." A temperature correction based on Bureau of Standards recommendations was used.[5] It amounted to +75°C at 2325°C (apparent), and decreased linearly to +50°C at 1800°C (apparent). The correction allows for emissivity of graphite and for absorption in the glass shell of the furnace. It does not take into account the possible lens effect if the particular section of glass through which the pyrometer sighted were faulty (i.e., the inner and outer surfaces not parallel). However, this lens effect was avoided by careful selection of a flawless area of the glass shell for pyrometer sighting.

2. Experimental Procedures

One millicurie of C^{14}, in the form of amorphous carbon,¶ was placed in a small agate mortar and a small amount of Aquadag** added. This mixture was carefully ground for several hours, water being slowly added during the process until the consistency was approximately that of a 50 percent water–50 percent glycerine solution. Microscopic examination of this slurry indicated that the C^{14} was in small, very uniform particles of less than 5×10^{-4} centimeter diameter. The size of the diluent Aquadag graphite particles was fairly uniform at about 1×10^{-4} centimeter diameter.

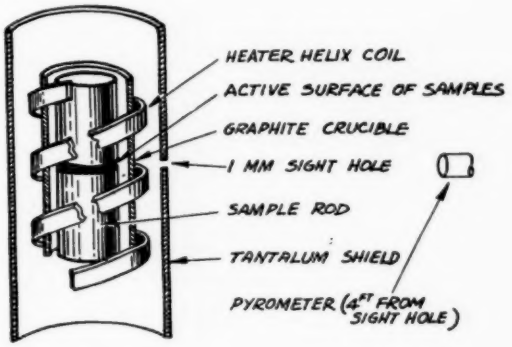

FIG. 1. Furnace—sample arrangement.

Graphite rods $\frac{5}{16}$ inch in diameter and $\frac{1}{2}$ inch long were machined from type AUF graphite. These rods were taken from the center of the stock material with their axes parallel to the grain of the graphite.

Prior to depositing the C^{14}, the rods were placed in the microtome and the ends cut parallel to the blade. An identifying mark was placed on each rod so that it could subsequently be put back in the microtome with its face aligned parallel to the blade.

The specimens were supported upright with the squared end exposed. Using the end of a $\frac{1}{2}$ millimeter wooden rod, a drop of the slurry was picked up and deposited onto the end of the graphite rod. It was possible to spread the drop of slurry fairly evenly over the surface of the graphite by suitable manipulation of the wooden stick as subsequent microscopic examination showed. The surface tension of the water prevented the material from running over the edge and down the side of the graphite but, as a safeguard, 10 thousands of an inch were machined from the radius of each rod after allowing the plated slurry to air dry. About 75,000 –100,000 counts/min were placed on each rod. The average thickness of this active layer was $2.5\pm1\times10^{-4}$ centimeter as determined from 10 samples by difference in weight.

The experimental arrangement for carrying out the diffusion anneal is shown schematically in Fig. 1. Two samples were placed, active faces together, in a small graphite crucible which was supported in the center of the carbon helix of the vacuum furnace.

§ Rotary Model No. 821, manufactured by the American Optical Company of Buffalo, New York.

|| Berkeley design, obtained from Microchemical Specialties, Berkeley, California.

[4] C. A. Smith, NAA-SR-109 (March 5, 1951).

[5] P. Foote *et al.* Bur. Stand. Tech. Paper 170 (1921).

¶ Obtained from Tracerlab, Inc., 130 High Street, Boston 10, Massachusetts.

** Aquadag is an aqueous colloidal suspension of graphite, obtained from the Acheson Colloid Company, Port Huron, Michigan.

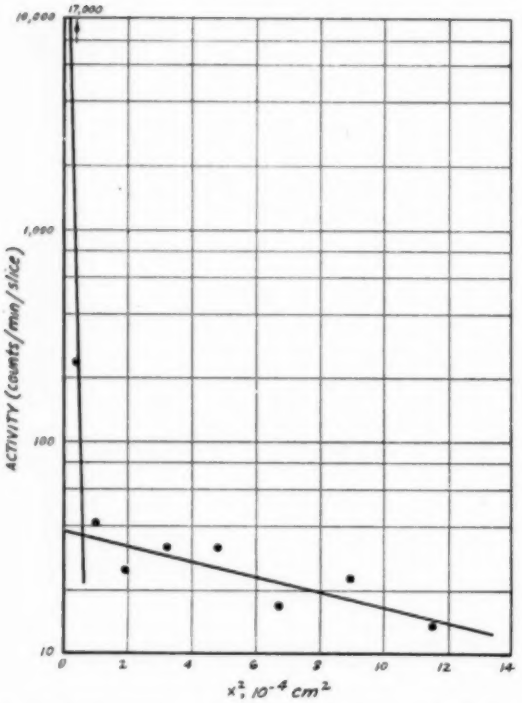

FIG. 2. Blank run (Sample 21). Two mils turned off side. The use of X^2 plot emphasizes the absence of penetration of the principal activity.

Once a pressure of less than 5×10^{-3} millimeter Hg had been obtained in the vacuum system, the deposited layers were baked onto the rods by heating for two hours at each of the following temperatures: 300°, 800°, and 1400°C.

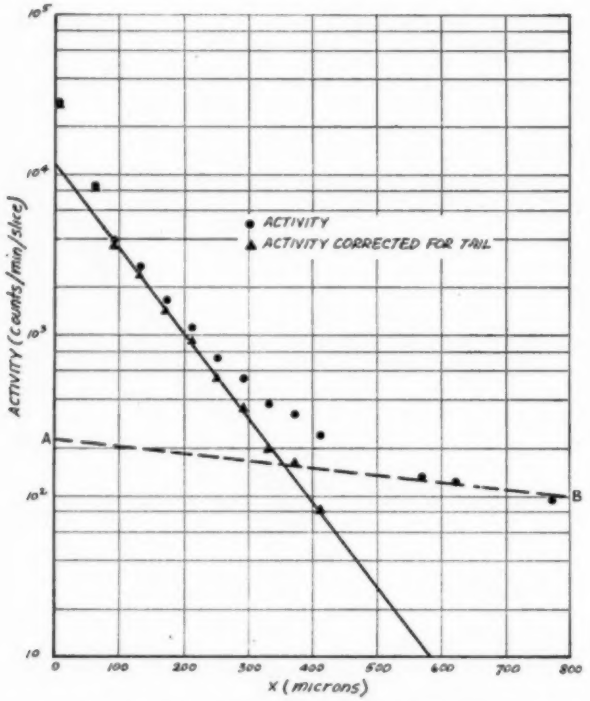

FIG. 3. Data of Sample No. 41; log activity *vs* distance of penetration ($T=2190$°C).

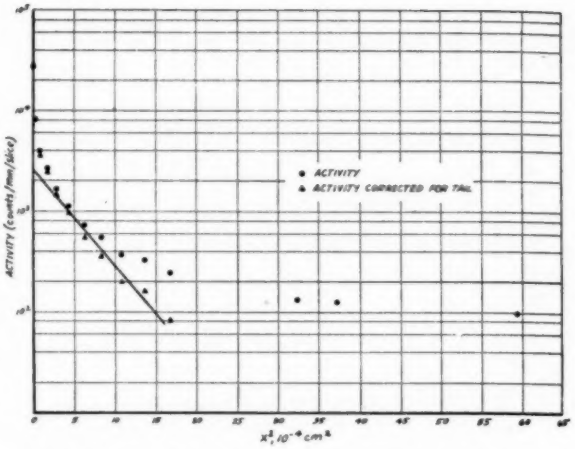

FIG. 4. Data of Sample No. 41; log activity *vs* distance of penetration, squared.

The temperature was then raised to the desired value for the diffusion anneal. Temperature readings were made with the optical pyrometer two to four times an hour during the runs. The pyrometer was mounted 4 feet from the furnace and the readings were made by sighting into a 1 millimeter hole drilled through the tantalum shield. This hole coincided with an opening in the graphite heater helix so that the crucible containing the samples was in direct view (see Fig. 1). The pressure during the runs was of the order of 1×10^{-3} millimeter Hg.

Obscuring of the glass shell of the vacuum furnace by vaporized carbon or tantalum was prevented by an internal soft iron shutter. This was magnetically controlled from outside to protect the sighting area, except during actual pyrometer readings.

No evidence of surface attack on the sample was ever observed. This may be due to the enclosure of the sample in a graphite crucible which did occasionally have spots which appeared eroded.

The individual samples were turned down 0.010 inch on the radius before the anneal and after the anneal using a jeweler's lathe. Test runs indicated the reality of the need for a precaution of this kind. In Fig. 2

TABLE I. Diffusion anneal data.

Sample No.	Temp.[a] (°C)	Time (hr)
27	1835	116.1
28	1835	116.1
19	1940	33.8
26	1940	33.8
40	2190	38.3
41	2190	38.3
44	2370	35.7
45	2370	35.7

[a] These are corrected temperatures. All temperatures indicated are corrected temperatures.

TABLE II.

Slice No.	X^a (Microns)	X^2 ($\times 10^{-4}$ cm^2)	Activity (counts/min/slice)	Activity corrected for tail
		Sample No. 19		
1	15	0.02	31,500	31,400
2	50	0.25	3190	3120
3	90	0.81	663	594
4	130	1.69	327	259
5	170	2.89	157	90
6	210	4.41	133	68
7	250	6.25	82	19
8	290	8.41	85	24
9	330	10.89	44	...
10	370	13.69	53	...
15	570	32.49	41	...
		Sample No. 26		
1	15	0.02	39,400	39,300
2	50	0.25	3980	3870
3	90	0.81	960	848
4	130	1.69	505	394
5	170	2.89	295	185
6	210	4.41	230	122
7	250	6.25	122	17
8	290	8.41	88	...
9	330	10.89	96	...
10	370	13.69	95	...
15	570	32.49	70	...
		Sample No. 27		
1	25	0.06	22,700	22,550
2	70	0.49	3140	3000
3	110	1.21	880	737
4	150	2.25	436	294
5	190	3.61	327	186
6	230	5.29	256	116
7	270	7.29	260	122
8	310	9.61	155	20
9	350	12.25	149	18
10	390	15.21	135	5
11	430	18.49	134	7
12	470	22.09	130	8
14	550	30.25	108	...
15	590	34.81	90	...
17	670	44.89	104	...
18	710	50.41	93	...
		Sample No. 28		
1	15	0.02	46,300	46,200
2	50	0.25	8260	8120
3	90	0.81	2730	2590
4	130	1.69	794	655
5	170	2.89	479	341
6	210	4.41	351	214
7	250	6.25	283	148
8	290	8.41	211	81
9	330	10.89	180	50
10	370	13.69	168	42
11	410	16.81	139	17
15	570	32.49	107	...
		Sample No. 40		
1	20	0.04	26,400	26,300
2	50	0.25	22,400	22,300
3	80	0.64	10,300	10,200
4	120	1.44	2880	2750
5	160	2.56	1525	1390
6	200	4.00	922	790
7	240	5.76	527	400
8	280	7.84	394	270
9	320	10.24	283	163
10	360	12.96	220	104
11	400	16.00	182	70
15	560	31.36	93	...

TABLE II—*Continued.*

Slice No.	X^a (Microns)	X^2 ($\times 10^{-4}$ cm^2)	Activity (counts/min/slice)	Activity corrected for tail
		Sample No. 41		
1	15	0.02	27,900	27,700
2	50	0.25	8320	8120
3	90	0.81	3870	3670
4	130	1.69	2660	2460
5	170	2.89	1640	1450
6	210	4.41	1145	960
7	250	6.25	730	550
8	290	8.41	541	360
9	330	10.89	373	200
10	370	13.69	330	162
11	410	16.81	243	82
15	570	32.49	134	...
16	610	37.21	127	...
20	770	59.29	97	...
		Sample No. 44		
1	15	0.02	3360	3200
2	50	0.25	2390	2230
3	90	0.81	2420	2260
4	130	1.69	2020	1860
5	170	2.89	1650	1500
6	210	4.41	1340	1190
7	250	6.25	970	825
8	290	8.41	742	600
9	330	10.89	627	490
10	370	13.69	468	336
11	410	16.81	350	225
12	450	20.25	259	141
13	490	25.01	225	113
14	530	28.09	151	46
15	570	32.49	139	42
18	690	47.61	77	...
19	730	53.29	70	...
20	770	59.29	65	...
		Sample No. 45		
1	20	0.04	23,100	22,900
2	55	0.30	20,300	20,100
3	90	0.81	10,800	10,600
4	130	1.69	3810	3600
5	170	2.89	2900	2700
6	210	4.41	2140	1940
7	250	6.25	1250	1060
8	290	8.41	1030	850
9	330	10.89	775	608
10	370	13.69	508	353
11	410	16.81	375	232
12	450	20.25	276	146
13	490	24.01	212	94
14	530	28.09	146	40
15	570	32.49	113	19
19	730	53.29	55	...
20	770	59.29	47	...

[a] Calculated as of the center of the cut.

are shown the results of a blank run in which the sample was turned down 0.002 inch. Figure 2 shows the absence of penetration in the absence of the anneal. The tail activity is discussed in later sections.

A separate small camel's-hair brush was used for each slice of the sample, in order to clean up the microtome and to ensure quantitative accumulation of the approximately 0.04 millimeter×0.30 millimeter×0.60 millimeter particles of each slice into the counting pans.

Tests were made of this procedure by weighing the individual cuts in 18 successive cuts and in a second test 8 successive cuts were weighed. The results of these tests indicated reproducible weights per cut (average deviation ±1.7 percent). The total error in length of 10 cuts taken successively could not be detected with a micrometer accurate to ±0.0001 inch; and, therefore, for a 0.002-inch slice, the possible error is ±5 percent on the average. This demonstrated that the procedures used should give reliably quantitative slicing and measuring. The brush technique ensured quantitative accumulation of the pieces of graphite. The procedures resulted in smooth curves as seen in Figs. 3 and 4 and afford an additional proof of the reliability of the microtome procedure for AUF graphite.

Slices 40×10^{-4} centimeter thick were taken. Each slice was caught in an aluminum counting pan held directly under the microtome blade. Any loose graphite remaining on the end of the graphite rod or on the blade was carefully brushed into the pan. A new brush was used for each slice, because of indications that the brushes became contaminated. The loss of a particle or two from any one slice was not serious because of the large number present; but if a particle from a slice near the front of the rod was introduced into a subsequent slice, a serious error could arise due to the rapid drop in activity with penetration. The slices were stored in closed aluminum trays until they were counted.

Crumbling of the thin sections of graphite during cutting produced particles of dimensions 0.04 millimeter ×0.3 millimeter×0.6 millimeter on average, which are easily visible to the eye. They lay flat in the aluminum counting pans on their 0.3×0.6 millimeter surfaces (determined by microscopic examination), giving an actual absorbing layer of 40×10^{-4} centimeter for the betas. The count of the samples was almost always taken to a minimum number of 10,000 counts, or 20 minutes of counting time, and the data given in Figs. 2, 3, 4, and Tables I, II, and III are the actual data, i.e., not normalized.

The slices were counted in reverse order (highest activity last) using a Nuclear Instrument and Chemical Corporation Model 162 scaling circuit in conjunction with a Tracerlab model TGC–2 end window tube which had a window thickness of about 1.5 mg/cm². The background count was about 30 counts/min during most of the determinations.

The reproducibility of these counts was ensured in the following way. Previous tests had shown that if the count was taken at least twice with intermediate jostling and stirring of the particles in the pan, the count was reproducible. Jostling ensured against piling up of the particles and subsequent low count rate of the soft C^{14} beta. If there was reason to believe such piling up had occurred, the procedure was repeated until statistically equal counts were obtained.

Blanks were also taken to check on the possible flow of the C^{14} slurry down the pores of the graphite rod. It was found that a smaller number of counts (approximately 50 to 200/min, but depending on the total activity deposited on the front of the sample) could be picked up in each slice out to distances about three or four times the diffusion region. The slope of this tail activity as a function of penetration distance was quite small. The tail was subtracted, of course, by using actual data taken in each sample for the particular correction of that sample. Blank runs (see Fig. 2) showed that for samples prepared and handled identically to the diffusion samples except for no anneal, only the first cut or the first two cuts had any significant activity. After that, the count fell down to the small tail value which could be traced all the way out to the distances found in actual runs. All the runs were made using the same batch of samples, the same setting of the glass furnace shell, the same microtome setting, and for any given pair of runs, the same counting set-up. Actually, runs 19, 26, 27, 28, 40, 41, 44, and 45 were all made with the identical counting set-up. Since such measurements need only be relative in any given sample, the counting procedure was quite adequate. The latter cuts (lower activity) were counted first to minimize the possibility of a single particle of high activity adhering by electrostatic attraction to the window of the Geiger tube and thus invalidating the subsequent counts. In addition, frequent counts of the background; i.e., between successive counts, were taken as a precaution.

TABLE III.

Sample	1000/T°K	Time	Time (sec)$^{\frac{1}{2}}$	Slope log act/cm	$St^{\frac{1}{2}}$
27	0.474	116.1 hr	25.4	69.68	1772
28	0.474	116.1 hr	25.4	56.74	1443
19	0.452	33.8 hr	18.7	83.95	1568
26	0.452	33.8 hr	18.7	77.06	1439
40	0.406	38.3 hr	19.3	57.51	1108
41	0.406	38.3 hr	19.3	52.21	1006
44	0.376	35.7 hr	18.9	43.15	817
45	0.378	35.7 hr	18.9	44.33	839

3. Experimental Uncertainties

The first cut taken may be in error by as much as 10×10^{-4} centimeter out of the 40×10^{-4} centimeter for which the machine is set. This arises from the fact that the knife cannot be previously manually set to give a 40×10^{-4} centimeter cut on the first cut. However, visual estimates of the first cut as being $\frac{3}{4}$, $\frac{1}{4}$, or $\frac{1}{3}$ or $\frac{1}{4}$ of a cut were quite easy to make, and if the error in this estimate was as much as 50 percent on a cut estimated as $\frac{1}{2}$ a cut, this would lead to a possible error of only 10×10^{-4} centimeter. It is believed that the actual estimate is good to 5×10^{-4} centimeter or better.

Although the counting was done to 10,000 counts in almost all slices, there were a few slices at the outer ends of some samples which were so little above background that an inordinate amount of time would have been required to go to 10,000 or more counts. In these few instances, counted to 20 minutes, slightly more scatter is apparent in the end points of curves where the tail correction is made.

Since a correction was applied for the tail described above, it should be noted that this correction was almost equal to the observed count of the later slices where diffusion counts were low. Although the correction was quite well established, in each run, some uncertainty necessarily attaches to this procedure. On the other hand, this uncertainty effectively vanishes for the earlier slices which have a higher count rate.

III. RESULTS AND DISCUSSION

In Tables I and II are given all the experimental data. The sample numbers represent the numbers assigned to individual samples in the large batch of samples with which all the experimental work was done. The sample numbers not represented in the tables are those of samples used up in blanks, tests, and practice work. Some samples done in another furnace and in a flowing He atmosphere (probably with some oxygen impurity) are not reported, although the results are close to those obtained in the vacuum furnace. In Figs. 3 and 4 are plotted as examples the data of run No. 41, in one case as log (activity) *vs* X and in the other as log (activity) *vs* X^2, where X is the penetration distance.

It is clear from the data that diffusion has occurred and that more diffusion has occurred at the higher temperatures. A comparison of Figs. 3 and 4 shows that a straight line fits the data better in the log activity *vs* X plot than in the X^2 plot. It is to be noted that all but the first two points, which are usually high in a diffusion experiment employing any kind of plating technique, fit well onto a straight line in the X plot of Fig. 3.

The fact that these experiments were carried out on fine grain polycrystalline samples and that the data are better described as a linear penetration suggests that combined grain boundary and volume diffusion has occurred. It is probable that the available cross section for (pore) surface diffusion is considerably smaller than the cross section for grain boundary diffusion. In addition, a surface diffusion would follow an (X^2) law.[6] Either pure volume or pure grain boundary diffusion would obey Fick's law for a line source, i.e., be described by a linear log (activity) *vs* X^2 relation. As pointed out by Fisher[7] and by Hoffman and Turnbull,[8] combined grain boundary and volume diffusion results in a linear log (activity) *vs* X relation. Further, if the penetration data arising from such a united diffusion are forced into an X^2 dependence, the activation energy associated with the diffusion coefficient D, calculated from the X^2 relation may be very much in error.

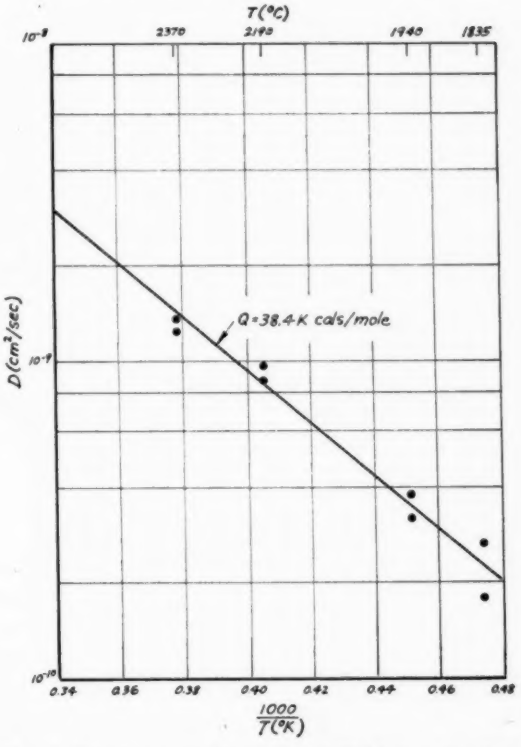

FIG. 5. Temperature dependence of Fick's law D values (from log activity *vs* X^2 plots).

In the present case it has been found that D values calculated from the X^2 plots (Fig. 4) show the usual dependence on temperature and lead to an activation energy of 38.4 kcal/mole (Fig. 5). This is an unreasonably low value for a diffusion process which is not observable below about 1800°C. In view of this and in view of the arguments given above, it is reasonably certain that combined grain boundary and volume diffusion have occurred and the data will be analyzed accordingly.

Fisher[7] has analyzed the mixed grain boundary and volume diffusion process and found that such a process will result in linear penetration. The slope of the linear penetration curve, i.e., the slope of the straight line of Fig. 3, is given by

$$S=\frac{d\log a}{dX}=\frac{-(2)^{\frac{1}{2}}(D_V/D_B\delta)^{\frac{1}{2}}\log_{10}e}{(\pi D_V T)^{\frac{1}{4}}}, \qquad (1)$$

where S = slope of the log activity *vs* x plot (see Fig. 3); X = distance of penetration of the radioactive isotope normal to the plated surface (centimeters); t = time of diffusion (seconds); δ = thickness of grain boundary (centimeters); D_V = self-diffusion coefficient for volume diffusion; D_B = self-diffusion coefficient for grain boundary diffusion; e = base of natural logarithms.

[6] R. A. Nickerson and E. R. Parker, Trans. Am. Soc. Metals 42, 376 (1950).
[7] J. C. Fisher, J. Appl. Phys. 22, 74 (1951).
[8] R. E. Hoffman, and D. Turnbull, J. Appl. Phys. 22, 634 (1951).

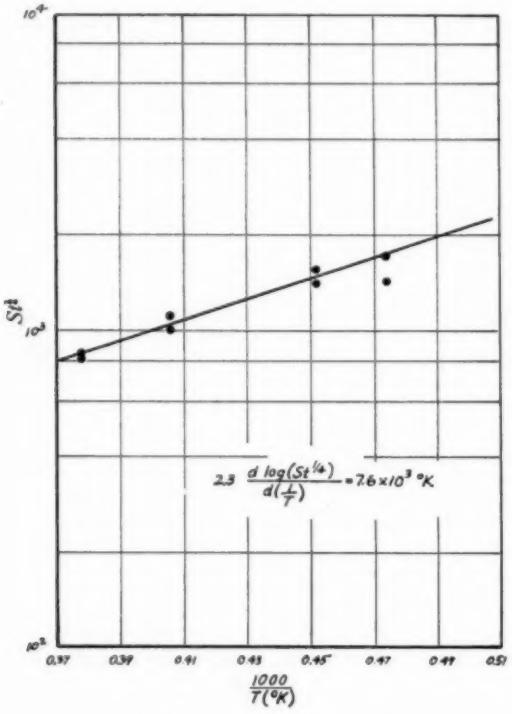

FIG. 6. Plot of $(St^{\frac{1}{4}})$ *vs* $(1/T)$.

The value of D_B cannot be derived from the experiments unless D_V is known. No experimental values are as yet available for the volume self-diffusion coefficient of graphite. By a simple extension of Fisher's analysis, however, one can obtain considerable information about the activation energies involved. If we assume δ to be insensitive to temperature[8] and substitute the usual temperature dependence for the D_V and D_B,

$$D = D_V^{\circ} e^{-E_V/RT}, \tag{2}$$

$$D' = D_B^{\circ} e^{-E_B/RT}, \tag{3}$$

there results

$$St^{\frac{1}{4}} = \text{const}(e^{-E_V/4RT + E_B/2RT}). \tag{4}$$

In the Eqs. (2)–(4), E_V = activation energy for volume diffusion (kcal/mole); E_B = activation energy for grain boundary diffusion; (kcal/mole); T = temperature (°K), and the constant is equal to

$$\frac{-(2)^{\frac{1}{4}} \log_{10} e}{\delta^{\frac{1}{2}} \pi^{\frac{1}{4}}} \cdot \frac{(D_V^{\circ})^{\frac{1}{4}}}{(D_B^{\circ})^{\frac{1}{2}}}.$$

According to Eq. (4), an effective activation energy E_{eff} is derivable from the experimental data by plotting $\log_e(St^{\frac{1}{4}})$ *vs* $(1/T)$. This plot is linear, with a slope equal to $(-E_V/4R + E_B/2R)$, if the experimental conditions satisfy the theoretical requirements underlying Fisher's analysis. It is seen that E_{eff} is a linear combination of E_V and E_B, given (in kcal/mole) by

$$E_{\text{eff}} = -\tfrac{1}{4}E_V + \tfrac{1}{2}E_B, \tag{5}$$

E_{eff} may be positive, negative, or zero depending on the relative magnitudes of E_V and E_B. Equation (4) and (5) are an algebraic extension of Fisher's analysis, and are valid under the same conditions.

In Table III are given the data for the plot of $(St^{\frac{1}{4}})$ *vs* $(1/T)$ shown in Fig. 6. The slope of the straight line drawn through the experimental points in Fig. 6 has the value 7.6×10^3, so that

$$7.6\times10^3 R = E_{\text{eff}} = -\tfrac{1}{4}E_V + \tfrac{1}{2}E_B. \tag{6}$$

The present experiments prove immediately that

$$\tfrac{1}{2}E_V < E_B \text{ and it is known}^{7,8}$$

that $E_V > E_B$, but E_B cannot be evaluated without a knowledge of E_V. A recent calculation[9] gave a value of $E_V = 90$ kcal/mole. If 90 kcal/mole is taken as the correct value of E_V then (by Eq. (6)), the value for E_B is 75.4 kcal/mole. This value of E_B is, of course, subject to revision when an experimental value is obtained for E_V. An energy of activation of about 75.4 kcal/mole is reasonable for a process for which it is necessary to go above 1800°C to produce a measurable rate. It is believed that the 75.4 kcal/mole figure is quite reliable since E_B is not very sensitive to changes in E_V.

IV. SUMMARY

1. Diffusion of C^{14} atoms in AUF type polycrystalline graphite has been observed by following the penetration of the tracer initially applied to one end of a graphite rod. The diffusion anneal was carried out at four temperatures between 1835°C and 2370°C.

2. The activity-penetration curves are best interpreted on the basis of mixed volume and grain boundary diffusion. Essentially linear penetration was observed as required by the theory of such diffusion processes.

3. An energy of activation has been deduced for grain boundary diffusion. Assuming a value of $E_V = 90$ kcal/mole for volume diffusion and using an extension of Fisher's analysis, the calculated activation energy for the grain boundary diffusion of C^{14} atoms in AUF graphite is 75.4 kcal/mole.

[9] G. J. Dienes, J. Appl. Phys. (to be published).

A New Permanent Magnet from Powdered Manganese Bismuthide*

EDMOND ADAMS, WILLIAM M. HUBBARD, AND ALBERT M. SYELES
Naval Ordnance Laboratory,
White Oak, Silver Spring, Maryland

(Received June 23, 1952)

Permanent magnets in present use consist chiefly of alloys containing cobalt or nickel, or both. Because these elements are currently scarce, possible substitute materials were examined. The intermetallic compound manganese bismuthide was chosen for this investigation because it has the highest recorded magnetic crystal anisotropy. The new permanent magnet was prepared by hot pressing finely pulverized MnBi in the presence of a strong magnetic field to facilitate particle alignment. Some of these compacts showed a maximum energy product $(BH)_{max}$ as high as 4.3×10^6 gauss-oersteds, a coercive force (H_c) of 3400 oersteds and a residual flux density (B_r) of 4300 gauss. This preliminary work shows that aside from its possibilities as a substitute for magnets requiring cobalt, this new magnet material has a value which exceeds present materials for special applications where a high coercive force is desirable, e.g., where one cannot use a magnet that is long compared to the air gap required. There is also theoretical possibility of further improvement in maximum energy product.

INTRODUCTION

BECAUSE the present demand for cobalt and nickel greatly exceeds their availability, there has been an increasing interest, in both this country and abroad, in the development of permanent magnets not containing these elements. Among the most promising materials investigated have been ultrafine anisotropic ferromagnetic powders. The material chosen for this investigation is the finely powdered intermetallic compound manganese bismuthide, MnBi.

That small particles would behave as elementary magnets was noted by many observers, notably Gottschalk[1] and Dean and Davis[2] in this country and by Frenkel and Dorfman[3] in Europe. This phenomenon was quantitatively examined by Néel,[4] Stoner and Wohlfarth,[5] and Kittel,[6,7] who derived expressions for the evaluation of the various energies involved. They showed that the effective internal energy of the small particles will be high if (1) the magnetic crystal anisotropy is high, (2) the particle is elongated, or (3) a severe strain is present in an anisotropic manner. The applied external field necessary to overcome this internal energy is called the coercive force H_c.

SELECTION OF MATERIAL

From the theoretical considerations, as presented by these workers, it became evident that in order to make a practical magnet from fine particles of domain size, one should select a material with a high anisotropy energy. In addition, the material should have a relatively large magnetic saturation moment and a high Curie temperature.

Magnets of ultrafine iron powder have been produced by the French,[8] at the Naval Ordnance Laboratory,[9] and others,[10] utilizing chiefly the crystal anisotropy of the iron. Efforts to increase the coercive force by taking advantage of the large shape anisotropy of iron have been unsuccessful, because present thermal methods of preparation yield essentially spherical particles.

Most of the high crystal anisotropy materials contain cobalt. Nesbitt and Heidenreich[11] report for Alnico 5 a value of 0.96×10^6 ergs/cm^3 for the crystal anisotropy constant. Cobalt itself has a reported K_1 value of 4.3×10^6 ergs/cm^3. At least one other known material has a crystal anisotropy which exceeds these values. It is an intermetallic compound, manganese bismuthide. Guillaud[12, 13] reports that this material has a crystal anisotropy K_1 of 11.6×10^6 ergs/cm^3 at 25°C, a saturation magnetization I_s at 27°C of 600 gauss and a Curie temperature of 340-360°C. According to Guillaud, if one could compact the powdered MnBi into a magnet with all the particles aligned in their preferred direction of magnetization to 100 percent density, the maximum energy product should be 18×10^6 gauss-oersteds. Because of these considerations, MnBi was selected for this investigation, although practical difficulties prevented Guillaud from making a quality magnet.

HISTORICAL

The ferromagnetic nature of manganese-bismuth alloys was first reported by Heusler[14] about 1904. This

* The process and product, bismanol, described herein is a development of the Naval Ordnance Laboratory and is the property of the United States Government. Application for license under a pending U. S. patent application may be made to the Chief of Naval Research, Washington 25, D. C.

[1] V. H. Gottschalk, Bureau of Mines R. I. 3268, 83 (1935).
[2] R. Dean and F. Davis, U. S. Patent 2,239,144 (1941).
[3] J. Frenkel and J. Dorfman, Nature **126**, 274 (1930).
[4] L. Néel, Compt. rend. **24**, 1550 (1947); **24**, 1488 (1947).
[5] E. C. Stoner and E. P. Wohlfarth, Trans. Roy. Soc. (London) **240**, 599 (1948).
[6] C. Kittel, Phys. Rev. **73**, 810 (1948).
[7] C. Kittel, Revs. Modern Phys. **21**, 541 (1949).
[8] L. Néel, U. S. Patent 2,497,268 (1950).
[9] NavOrd Report 1826, April 1951.
[10] B. Kopelman, Elec. Eng. **71**, 447 (1952).
[11] E. A. Nesbitt and R. D. Heidenreich, J. Appl. Phys. **23**, 352 (1952).
[12] C. Guillaud, thesis, University of Strasbourg (Strasbourg, France) 1943.
[13] C. Guillaud, U. S. Patent 2,576,679 (1951).
[14] F. Heusler, Z. angew. Chem. **17**, 260 (1904).

TABLE I. Chemical and physical analysis of manganese and bismuth powders.[a]

	Manganese	Bismuth
Apparent density	4.14 g/cc	2.75 g/cc
Plus 200 mesh	Trace	Trace
Plus 325 mesh	13.3 percent	8.0 percent
Minus 325 mesh	87.7 percent	91.7 percent
Hydrogen loss (max)	0.25 percent	0.50 percent
Purity (min)	99.5 percent	99.0 percent

[a] Material and analysis supplied by Metals Disintegrating Company, Elizabeth, New Jersey.

was confirmed by Arrivaut[15] in 1905 and others at about this same period. Bekier,[16] in 1914, considered the formation of a phase MnBi as probable; this phase resulting from a peritectic reaction at 450°C between pure manganese and the melted alloy containing 9 percent manganese. Siebe[17] concluded that the phase rich in MnBi is produced at 445°C by the reaction of a sort of a "crystalline X," formed at 597°C out of the molten alloy. Parravano and Perret[18] established the phase diagram for this system and isolated (but did not describe) crystals containing 19.9 percent manganese, which they considered to be the MnBi phase. Wedekind and Veit[19] earlier reached the same conclusion. They also reported octahedral crystals of MnBi. Hilpert and Dieckmann[20] also noted the strong ferromagnetism of these alloys and placed the Curie temperature at around 360–380°C. Fürst and Halla[21] concluded from x-ray studies that a single compound was present with the structure Mn_2Bi. Montignie,[22] however, showed that MnBi represented the only stable compound. In further studies by Halla and Montignie[23] the same results were obtained.

Guillaud thoroughly investigated this system and, in addition to measuring the saturation moment, magnetic crystal anisotropy, and Curie temperature, established experimentally the fact that the coercive force of the material increased with the reduction of particle size. For an average particle diameter of 3.3 microns, he obtained an intrinsic coercive force on the loose powder of 12,000 oersteds. He also concluded that a single phase, MnBi, was responsible for the ferromagnetic character of the alloy. Approximately the same results were arrived at by Kondo,[24] who made additional measurements of some of the physical properties of this material. Thielman[25] also reported similar data and, in addition, determined the hysteresis loops on capsules of sintered powdered manganese and bismuth, but since the purity and density of these compacts were low, the magnetic properties were poor.

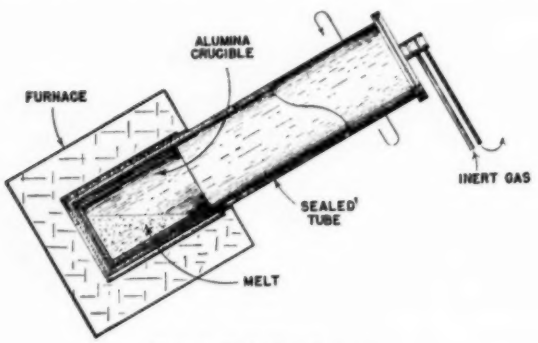

FIG. 1. Rotating furnace.

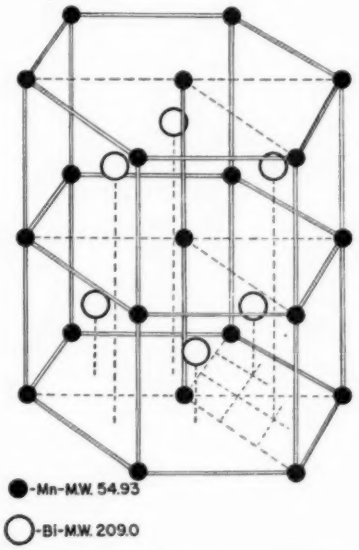

FIG. 2. Crystal structure of MnBi.

EXPERIMENTAL

Preparation of Manganese Bismuthide

The preparation of this compound is complicated by the fact that it is of the peritectic type. The formation of the magnetic phase MnBi never proceeds to completion regardless of the initial proportions of manganese and bismuth present. When the initial charge consists of manganese and bismuth in equal atomic proportion according to the compound MnBi, the melt always consists of MnBi plus unreacted manganese in a matrix of bismuth. The procedure finally adopted to provide an alloy richest in the ferromagnetic phase is outlined below:

(1) Finely pulverized manganese and bismuth powders were mixed in the proportions of 16.65 percent manganese to 83.35 percent bismuth by weight and placed in an alumina crucible. The chemical and physical analysis of these powders is shown in Table I.

[15] C. R. Arrivaut, Soc. Sci. Phys. Nat., Bordeux, June 8, 1905.
[16] E. Bekier, Intern. Z. Metallographie **7**, 83 (1914).
[17] Z. Siebe, Z. anorg. u. allgem. Chem. **108**, 161 (1919).
[18] N. Parravano and U. Perret, Gazz. Chem. ital. **451**, 390 (1915).
[19] E. Wedekind and T. Veit, Ber. deut. chem. Ges. **44**, 2263 (1911).
[20] S. Hilpert and T. Dieckmann, Ber. deut. chem. Ges. **44**, 2831 (1911).
[21] U. Fürst and F. Halla, Z. physik Chem. **B40**, 285 (1938).
[22] E. Montignie, Bull. soc. chim. **5**, 343 (1938).
[23] F. Halla and E. Montignie, Z. physik Chem. **B42**, 153 (1939).
[24] K. Kondo, J. Phys. Soc. (Japan) **5**, 26 (1950).
[25] K. Thielman, Ann. Physik **37**, 41 (1940).

(2) The crucible was then positioned in a stainless steel rotating furnace, illustrated in Fig. 1, and heated to 700°C under a protective atmosphere of helium. This temperature was maintained for five hours with the furnace rotating at approximately 20 rpm. At the end of this period the temperature was lowered, at approximately 65°C/hr, to 440°C. At this temperature, the rotation of the furnace was discontinued and the melt held at 440°C for sixteen hours.

(3) The melt was then cooled to 320°C at the rate of 40°C/hr. At this time the furnace was rotated 180 degrees in order to place the semi-solid mass in the upper part of the crucible. This allowed any unreacted bismuth (which was added in excess for this reason) to drain out to the lower part of the crucible. This condition was maintained for eight hours.

(4) The furnace was allowed to cool to room temperature and the fused melt was removed by machining or breaking away from the crucible.

Due to the large difference in their respective densities and melting points, the powdered manganese tends to float on the molten bismuth. This provides only a small contact surface for the constituents to combine. Rotating the furnace at a 45-degree angle speeded up the reaction considerably. The long aging period at 440°C allowed time for the small MnBi crystals to increase in size. Some of the early workers reported visible crystals of MnBi but did not sufficiently describe them for definite identification. By following the general method of preparation, we have been able to grow crystals, as large as one cm long, of apparently the hexagonal structure of MnBi, as shown in Fig. 2. This crystal structure is derived as a result of x-ray studies by Hocart and Guillaud.[26] A cluster of almost perfect hexagonal MnBi crystals imbedded in the melt is illustrated in Fig. 3. The value for the hexagonal axis from x-ray analysis of these crystals agrees by interpolation with recent values of Guillaud,[27] as shown in Table II.

PULVERIZATION AND SEPARATION

In order to prepare a permanent magnet from manganese bismuthide, it is necessary to pulverize it into fine particles approaching domain size. According to Weil,[28] because of the high crystal anisotropy of MnBi, this critical dimension is as large as 8000A even if the width of the Bloch wall is only about 200A. The intrinsic coercive force ($H_{ci}=2K/I_s$) calculated for oriented loose particles of this size would be about 35,000 oersteds; the exact value being dependent on the temperature. This large dimension for single domain behavior of MnBi permits the use of mechanical grinding to provide the necessary powder. For low crystal anisotropy materials, such as iron, this critical dimension is

[26] R. Hocart and C. Guillaud, Compt. rend. **209**, 443 (1939).
[27] C. Guillaud, J. phys. et radium **12**, 143 (1951).
[28] L. Weil, J. phys. et radium **12**, 440 (1951).

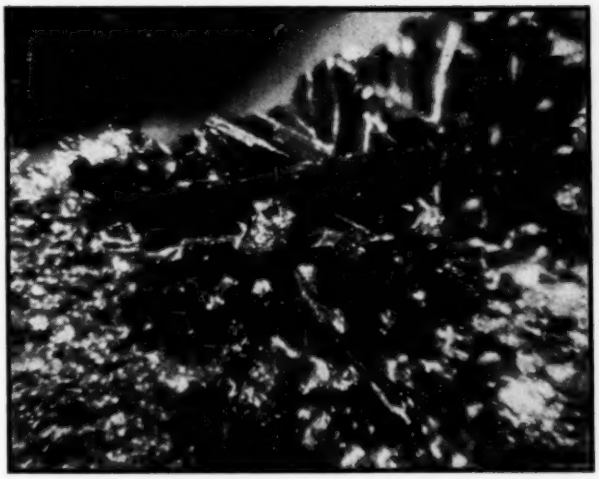

FIG. 3. Hexagonal crystals of the compound MnBi imbedded in the melt. 4×

of the order of 160A, obtainable only by chemical or thermal means.

The melt was pulverized in a high speed hammer mill in a helium atmosphere to prevent oxidation. The resulting powder was found to be irregular in shape and extremely pyrophoric. The particles tended to form clusters due to their permanent magnet nature. These factors made the quantitative determination of their size very difficult. The average particle diameter was found to be 8 microns by means of an air classifier.

Even the most enriched melt consists of MnBi plus some unreacted manganese and bismuth. To obtain a material that was relatively pure, it was necessary to devise a method for further enrichment. Therefore, a magnetic separator of a type shown in Fig. 4 was constructed for the purpose. The determination of the percentage of MnBi in the magnetically separated fraction was made by a combination of chemical and magnetic analysis. By chemical analysis, the relative percentages of manganese and bismuth were determined. The magnetic analysis determined the percentage of magnetic material in the test samples by comparing their saturation magnetization I_s with that reported for the pure material. A preliminary analysis by this method showed that the magnetically separated portion contained about 90 percent MnBi, 4 percent uncombined manganese, and 6 percent bismuth.

TABLE II. X-ray data of MnBi.

Sample	Length of unit cell along hexagonal axis
NOL−3[a] (quenched from 320°C)	5.87±0.02A
Guillaud (quenched from 400°C)	5.83A
Guillaud (slow cool to room temp.)	6.11A

[a] X-ray measurements were made by Miss Selma Greenwald of the Research Department, Naval Ordnance Laboratory.

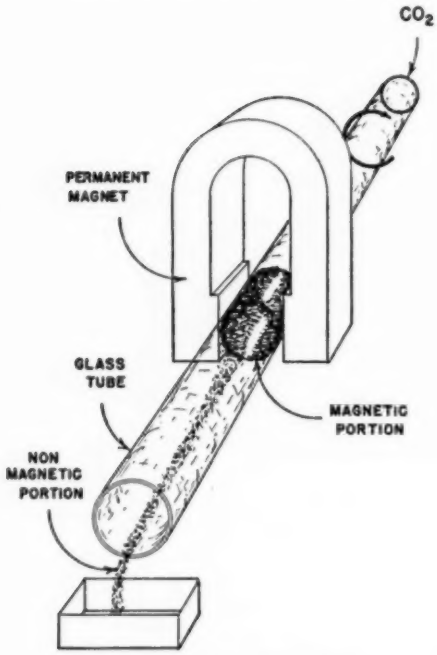

FIG. 4. Magnetic separator.

COMPACTION INTO MAGNETS

The magnetically separated powder was compacted using low pressures (not exceeding 3000 psi), at approximately 300°C in an electrically heated cylindrical die with double acting rams. To protect the powder from oxidation, it was loaded into the die in an inert atmosphere. During compaction a pulsating magnetic field parallel to the direction of pressing was applied to the powder by means of a water-cooled solenoid. The purpose of the field (up to 20,000 oersteds) was to align the particles with their easy direction of magnetization parallel to the direction of testing.

The compacting was performed in a heated die in order that a relatively high density would be obtained at low pressures. In this respect, it is probably desirable to have a small amount of free bismuth present in the powder. This provides a fluid medium at 300°C to facilitate particle alignment and after solidification, upon cooling, effectively separates and immobilizes the particles.

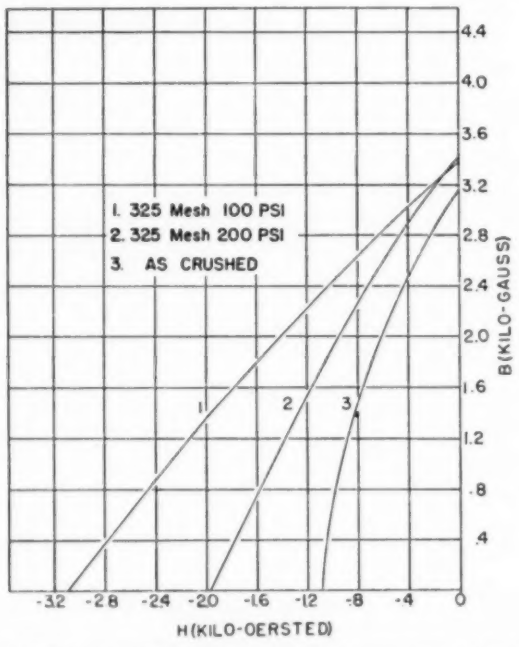

FIG. 5. Effect of particle size on coercive force: samples 1 and 3. Effect of compacting pressure: samples 1 and 2.

DISCUSSION OF TEST RESULTS

In order to prepare the best possible permanent magnet from MnBi, it was first necessary to determine the optimum conditions for producing the material and for its subsequent compaction. A discussion of the four most important factors follows:

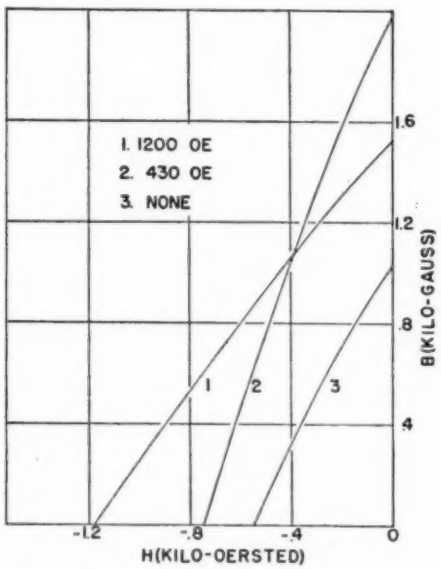

FIG. 6. Effect of magnetic field on particle alignment of same material. Sample 1 aligned in paraffin. Samples 2 and 3 cold pressed at 200 psi.

(1) Enriched material. After trying various methods of preparation, the procedure of fusion, enrichment and magnetic separation provided a material of sufficiently high MnBi content.

(2) Particle size. Initial attempts at pulverization of the melt were made in a ball mill. This proved impractical, because during ball milling the soft bismuth matrix caked on the walls of the jar. Best results were obtained by pulverizing the melt in a high speed hammer mill in an inert atmosphere. To further reduce the size of the particles, the material was sieved through a 325 mesh screen. The coercive force was determined on two samples of the powder, each compacted in the same manner, before and after sieving. The increase in the coercive force of sample 1 over sample 3, shown in Fig. 5, is indicative of its smaller particle size.

(3) Particle alignment. The effect of particle alignment on the magnetic properties is illustrated in Fig. 6. Sample 2 was compacted in a magnetic field of 430 oersteds, while sample 3 was compacted without an applied field. Subsequent experiments have shown that a field of 430 oersteds is insufficient to provide complete alignment, but even this partial alignment improves the coercive force H_c and residual flux density B_r. Sample 1 of Fig. 6 represents a sample that had been made by suspending MnBi powder in molten paraffin, aligning the particles in a field of 1200 oersteds and, after solidification, machining out a cylindrical test specimen. The density of this sample 1 was only 2.6 g/cm³, but since the alignment was excellent, it proved to have a very high B_r. This indicates that if better alignment could be obtained at higher densities, the values of B_r and H_c would be increased considerably.

(4) Compacting pressure. That the amount of pressure used in compaction of the MnBi magnets greatly influences their magnetic properties was observed in the early stages of the investigation. To illustrate this, two samples of the same material were compacted in the same manner, varying only the pressure. Samples 1 of Fig. 5 was compacted at a pressure of approximately 100 psi to a density of 6.6 g/cm³, while sample 2 was compacted at a pressure of 200 psi to a density of 7.5 g/cm³. The large increase in the coercive force of sample 1 is a result of better alignment and, more important, less sintering of the individual particles at the lower pressure. Despite the differences in density, the value of B_r of the samples remained essentially the same. This effect was probably due to the better alignment of the particles, resulting from less opposition to the field by the compacting pressure.

EVALUATION OF THE MAGNETS

The evaluation of the MnBi magnets with respect to stability under various operating conditions is at present incomplete. There are indications that at a high relative humidity some protective coating may be necessary to prevent deterioration by oxidation.

TABLE III. Magnets of MnBi compared with other permanent magnets.

Magnet	Density	B_r	H_c	H_{ci}	$(BH)_{max} \times 10^{-6}$
MnBi-4	7.0	3160	1110	1240	1.3
MnBi-7	7.5	3400	1995	4650	1.9
MnBi-11	6.6	3375	3100	7740	2.9
Bismanol[a]	8.1	4300	3400	7000	4.3
Alnico II	7.1	7200	540	540	1.6
Alnico V	7.3	12,000	580	580	4.5
Pt-Fe	10.0	5800	1570	1700	3.0
Pt-Co	11.0	4500	2600	3600	3.8
Silmanal	9.0	550	550	6000	0.08

[a] Typical values of MnBi magnets prepared by essentially the same process as described except that the MnBi content was increased by improved separation.

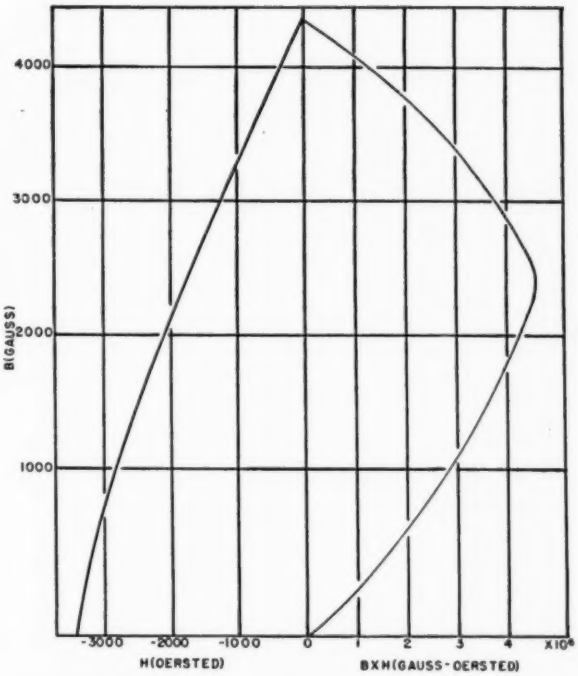

FIG. 7. Typical demagnetization curve of a MnBi magnet.

At lower temperatures there is a decrease in the coercive force due to the lower crystal anisotropy of MnBi[12]. At minus 45°C a 40 percent decrease in the H_c value was measured. After remagnetization at room temperature one obtains the original value of H_c. Upon heating to 100°C, no change in remanence was noted.

COMPARISON WITH PRESENT MAGNETS

The magnetic properties for some of these new magnets are shown in Table III, along with data[29] for other magnets for reference.

A typical demagnetization loop of the new magnet prepared from MnBi is shown in Fig. 7.

CONCLUSION

A new class of permanent magnets has been prepared utilizing powder metallurgy techniques. These magnets exhibit a coercive force (H_c) exceeded by no other known practical magnets. They can be used for practically all present applications of permanent magnets; however, in short lengths where a high resistance to demagnetization is important, these MnBi magnets exceed most commercial permanent magnets in flux density.

The authors wish to express their thanks to Dr. G. W. Elmen, both for suggesting this investigation and for his encouragement and counsel during its progress.

[29] R. M. Bozorth, *Ferromagnetism* (D. Van Nostrand Company, Inc., New York, 1951), p. 872.

The Polarization of Acoustic Waves in Cubic Crystals*

A. E. Fein and Charles S. Smith
Case Institute of Technology, Cleveland, Ohio
(Received June 23, 1952)

The directions of particle motion associated with acoustic waves have been computed and are displayed graphically, for each of the three waves, as a function of propagation direction. The numerical example used is cubic nickel and the maximum polarization angle found is 11½ degrees.

In order to give a quantitative description to the character of the ultrasonic waves in single cubic crystals of various orientations, the angles of polarization for the longitudinal and two transverse waves were calculated from the Christoffel equations of motion for an anisotropic medium.[1] The calculations were carried through using the elastic constants of nickel as a typical example.

The curves in Fig. 1 are a contour map of the angle α, between the direction of particle displacement (eigenvector) associated with the longitudinal wave and the direction of propagation. This angle, which may be considered to be an "angle of polarization," is shown as a function of crystal orientation. The plot was made on specially prepared polar coordinate paper and uses the customary spherical coordinates θ and ϕ to designate the orientation of the nickel crystal. At the three corners ([100], [110], and [111]) the longitudinal wave is "pure", i.e., the direction of particle displacement is coincident with the direction of propagation. Moving from the corners to the center of the unit triangle, the value of α increases rapidly and linearly at first, reaching a comparatively flat region near the center. Here the angle varies slowly between 10° and 11½°.

The curves in Fig. 2 give the angle of polarization, $|90-\beta|$ for the high velocity transverse wave, i.e., the difference between 90° and the angle β between the eigenvector associated with the transverse wave and the direction of propagation. It may be seen that the higher transverse velocity wave is always nearly pure, $|90-\beta|$ never exceeding 4°. Thus this wave should be easily excited alone.

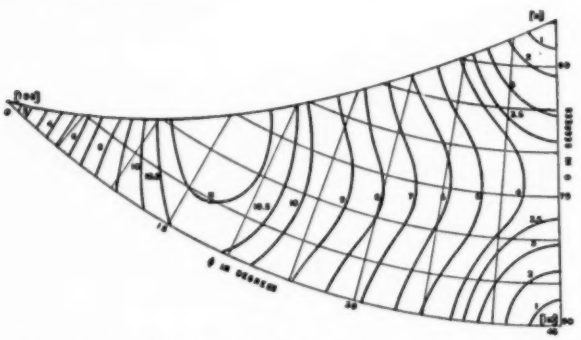

Fig. 1. The polarization angle α for the longitudinal wave.

In a similar manner Fig. 3 shows the polarization angle $|90-\gamma|$ for the low velocity transverse wave. The values of $|90-\gamma|$ for this wave are approximately those of α for the longitudinal wave.

For directions of propagation lying in the plane containing [100] and [110] the polarization angle $|90-\beta|$ of the high velocity transverse wave is zero. It is easily derivable from the equations of motion governing wave propagation[1] that the particle displacement in this wave is normal to the plane named, and it follows from the orthogonality of the three particle displacements that those for the other two waves lie in the plane. The same situation prevails in the plane containing [100] and [111]; a similar one occurs in the plane containing [100] and [111] but with the role of the high and low velocity transverse waves interchanged.

These three sets of curves demonstrate that the three waves set up in the crystal by ultrasonic vibrations are never far from pure waves, even in regions close to the center of the unit triangle. Thus, the pulsed ultrasonic method of determining the elastic constants of cubic cystals should encounter no serious difficulty in any crystal regardless of its orientation. The method of determining the elastic constants in the region of high polarization by applying perturbation corrections has been outlined previously by Neighbours and Smith,[2] and applied to nickel.[3]

The polarization angles for cubic crystals other than nickel can be inferred qualitatively from the present

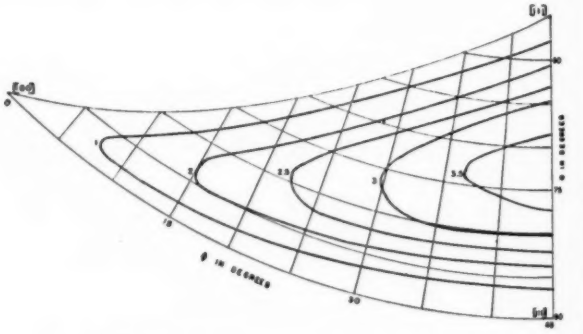

Fig. 2. The polarization angle $|90-\beta|$ for the high velocity transverse wave.

* This work was supported by the ONR.
[1] I. Koga, Physics 3, 70 (1932).
[2] J. R. Neighbours and Charles S. Smith, J. Appl. Phys. **21**, 1338 (1950).
[3] Neighbours, Bratten, and Smith, J. Appl. Phys. **23**, 389 (1952).

results. The elastic constant $C=(C_{11}-C_{12}-2C_{44})$ is a measure of the anisotropy of the crystal; if C is zero all polarization angles are zero. Further, for directions of propagation in the plane containing [100] and [110] the slope of the α *versus* ϕ curve is $C(C_{11}-C_{44})^{-1}$ at [100] and $-C(C_{44}+C_{12})^{-1}$ at [110]. The numerical values of the elastic constants can be introduced in these expressions to estimate the polarization angles to be expected for any other substance. Thus, for nearly isotropic aluminum, and for the alkali halides the general picture will be similar to that for nickel but with a much reduced scale. Copper, gold, silver, and iron will all be very similar in character and magnitude to nickel. The case of the highly anisotropic alkali metals and beta-brass is more difficult to analyze, but it is certain that the initial slopes at least will be much larger than for nickel.

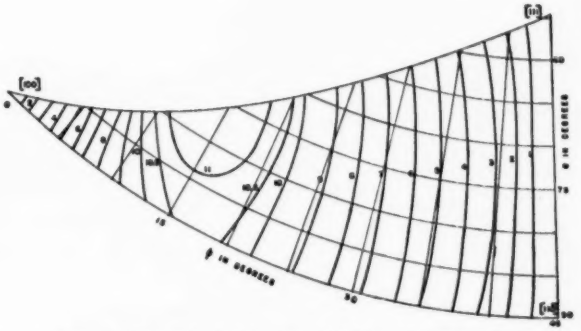

FIG. 3. The polarization angle $|90-\gamma|$ for the low velocity transverse wave.

JOURNAL OF APPLIED PHYSICS VOLUME 23, NUMBER 11 NOVEMBER, 1952

The Use of Radioactive Material for the Generation of High Voltage

E. G. LINDER AND S. M. CHRISTIAN
RCA Laboratories Division, Radio Corporation of America, Princeton, New Jersey

(Received May 19, 1952)

An investigation has been made of the use of beta-emissive radioisotopes for generating high voltages. Voltage was obtained by supporting a beta-emitter on an insulated electrode in a low-pressure gas and allowing it to charge itself by virtue of its electron emission. This method represents a direct conversion of nuclear energy into electrical energy. The apparatus is described. Data on insulation breakdown, the effect of gas pressure, and the electrode material are given. The maximum voltage was obtained at a pressure of 10^{-3} mm of Hg. The electrical characteristics of such a generator are discussed. Using an emitter containing 0.25 curie of strontium 90, a voltage of 365 kilovolts was obtained.

INTRODUCTION

THIS paper describes a method of generating electrical energy directly from the radiation of charged-particle-emitting materials. The materials used were radioactive isotopes emitting beta-rays; however, in principle, any charged particle radiation might be used. Basically the method comprises charging a condenser by means of charged particles moving from one electrode to another, and using the energy thus stored.

In using practical quantities of radioisotopes in such a manner, the power available is quite minute, being only a few milliwatts per curie. Most materials are now obtainable in only millicurie amounts. Hence it would appear that at the present time, this type of device would be useful only where power requirements are very small. Nevertheless, there is reason to believe that in the future suitable materials will be available in much large quantities and at much lower prices.

Brief notices of the present work have been published.[1,2] These publications include several references to related work by other investigators.

[1] E. G. Linder, Phys. Rev. **71**, 129 (1947).
[2] E. G. Linder and S. M. Christian, Phys. Rev. **83**, 233 (1951).

APPARATUS

A diagram of the apparatus is shown in Fig. 1. Here K is the emitter. It consists of a nickel foil cylinder containing a layer of strontium nitrate on its inner surface. At its ends are two field-reducing spheres. A metal shaft B supports the emitter, and connects it to a spherical electrode A. This entire assembly is supported on a fused quartz insulator D, which rests upon the collector C. A vacuum pump is connected at F. The resistance of the load is represented at R.

Strontium 90 was used as the energy source. This substance is a pure beta-emitter, although in the present case some gamma-radiation was present due to impurities. It has a half-life of about 30 years, decaying into yttrium 90 with the emission of a 0.65-Mev electron. The yttrium has a half-life of 62 hours, and emits a 2.16 Mev electron, decaying to stable zirconium 90. Strontium 90 in equilibrium with these disintegration products, appears to be the most suitable presently available material for such a voltage generator. It can be obtained in comparatively large quantities, it is relatively low priced, it has a long half-life, it has no gamma-emission (when pure), it emits high energy

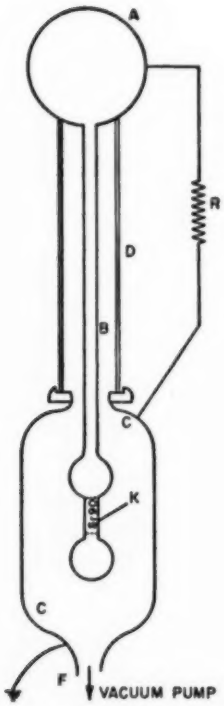

FIG. 1. Simplified diagram of generator.

electrons, it has no gaseous products, it is obtainable with relatively high specific activity, it emits two electrons per original strontium atom, and it is readily manipulated chemically.

The emitter consisted of a cylindrical, seamless, nickel shell, 0.0008 in. thick, 0.80 in. in diameter and 1.50 in. long. This was strengthened by an internal supporting rib structure. The strontium 90 was introduced in the form of an aqueous solution of strontium nitrate and evaporated to dryness during rotation of the cylinder. The total beta-ray absorption of this emitter was computed to be 15 percent.

Nominally, 250 millicures of Sr 90 were used, but no accurate determination of the amount was made. By direct measurement the current to the collector at zero voltage was 1.05×10^{-9} ampere.

The collector, which served also as the vacuum envelope, consisted of a metal shell completely surrounding the emitter except for the exit opening for the emitter support, and the vacuum pump connection. It was made of such a size as to minimize voltage gradients, and sufficiently thick to reduce gamma-radiation below the tolerance level. It was made of copper, and was lined with aluminum to reduce secondary electron emission and bremsstrahlung.

A fused silica insulator was used. The surface resistance at 25 percent relative humidity was measured to be 2×10^{15} ohms.

A photograph of the complete generator and vacuum pump is shown in Fig. 2.

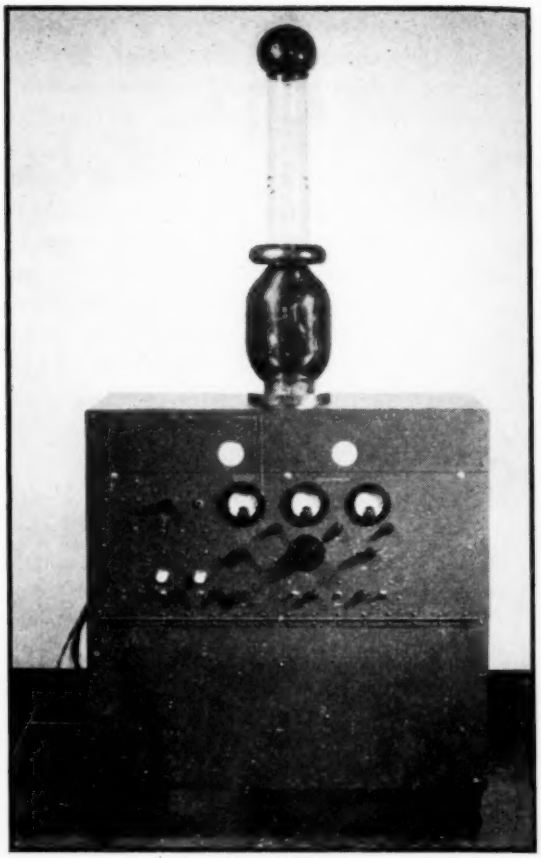

FIG. 2. Generator and vacuum pump.

The voltage was measured by several different methods: (1) sphere gaps, (2) fiber voltmeter, and (3) attracted-disk voltmeter. The first of these is well known. The second consisted of a metal fiber deflected by the electric field, the deflection being measured and calibrated in terms of voltage. The third consisted of a metal disk suspended flush with the internal collector wall. The electrical attraction was balanced with a magnetic force supplied by an electromagnet. The magnet current was calibrated in terms of generator potential. The fiber voltmeter was not usable over 115 kv due to corona from the fiber. The disk voltmeter was enclosed in the vacuum and was usable to the highest voltages generated.

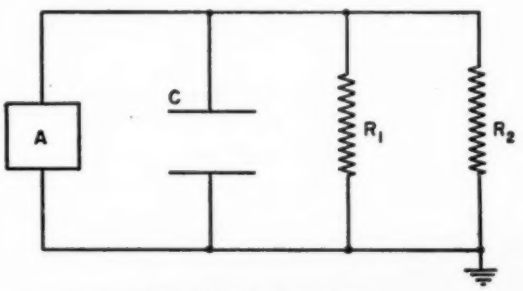

FIG. 3. Equivalent circuit.

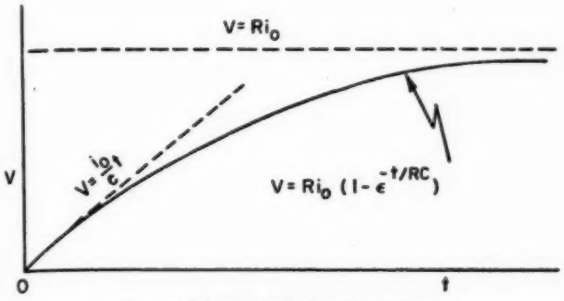

FIG. 4. Theoretical charging curve.

THEORY

The equivalent circuit of this type of generator is shown in Fig. 3. Here the active material is represented by a current generator A, which produces a current i_0 at small voltages, but a smaller current at high voltages when the retarding field repels lower energy beta-particles. The emitter and collector are represented by a capacitor C, which is charged by the beta-ray current. The resistance R_1 is the internal resistance of the generator, and R_2 is the load resistance.

The voltage attained by the above described circuit is given by

$$V = Ri_0(1-\epsilon^{-t/RC}), \qquad (1)$$

if i_0, R, and C are considered constant, t is measured from the instant at which charging commences, and R is the total resistance.

For the case where the final voltage is small compared to the equivalent average voltage of the emitted particles, this expression is quite accurate. It is represented by the graph of Fig. 4, where voltage is plotted against charging time. At the beginning of charging, $t \ll RC$ and

$$V = i_0 t/C.$$

Thus the initial charging is linear. At the final equilibrium voltage, $t \gg RC$, and

$$V = Ri_0.$$

These represent the two limiting cases for constant charging current.

Over a large voltage range, however, the charging current is not constant, but decreases as the voltage increases, since a retarding field for the beta-particles is created. If a potential drop V_1 exists across the generator, the current is that contributed by the electrons to the right of V_1 in Fig. 5, which shows the beta-spectrum of Sr 90—Y 90. Electrons to the left of V_1 are turned back to the emitter by the retarding field. By integration, Fig. 6 is obtained showing the resultant current at various voltages. A load line representing 2×10^{15} ohms, the insulator resistance, is included. The intersection shows that the generator should charge to 0.8 Mev, if there were no current leakage. The approximately linear drop of current up to 0.4 Mev also is shown. For such a linearly decreasing current the charging characteristic is still of the same general form as given by Eq. (1), the initial slope is still i_0/C, and the final voltage is Ri, but $i<i_0$.

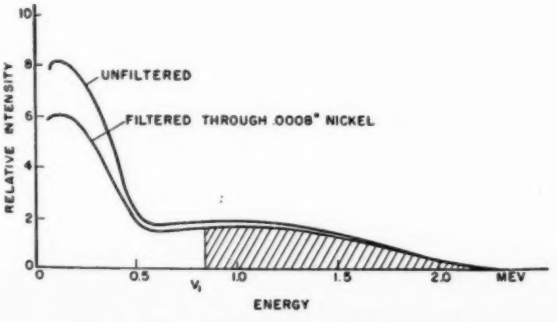

FIG. 5. Beta-ray spectrum of Sr 90—Y 90.

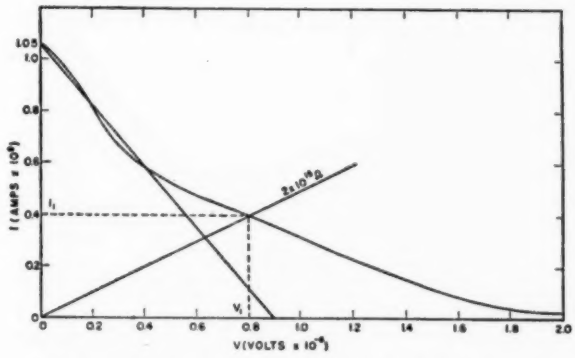

FIG. 6. Current-voltage characteristic derived from spectrum of Fig. 5.

EXPERIMENTAL DATA

Experimental data are shown in Fig. 7, along with a computed curve. The curve, indicated by the solid line, is based on a measured resistance of 2×10^{15} ohms and an initial current of 1.05×10^{-9} ampere, which decreased linearly as determined approximately from the Sr 90—Y 90 spectrum. The points in the figure were obtained by setting the voltage-measuring spark gap at a fixed distance and then allowing the apparatus to

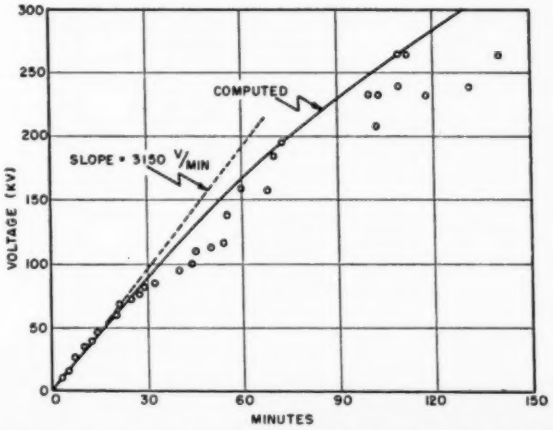

FIG. 7. Theoretical charging curve with experimental points.

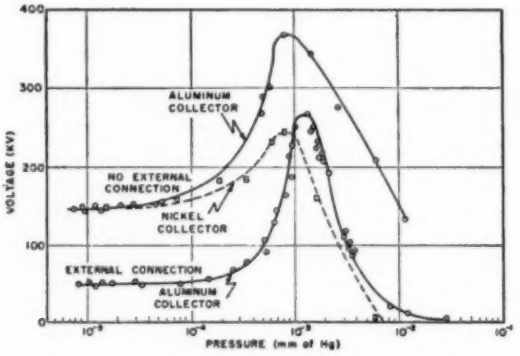

FIG. 8. Variation of maximum voltage with gas pressure and electrode material.

charge until a discharge occurred across the gap. The scattering is due mainly to erratic charging at the higher voltages due to current leakage. When the voltage was monitored continuously with the fiber voltmeter or attracted-disk voltmeter a smooth curve was usually obtained initially but charging became erratic as the upper limit was approached. The initial slope agrees with the i_0/C value obtained directly from the measured values of i_0 and C.

A modified form of this generator also was tested in which the emitter was suspended in a vacuum with no connection to any outside electrode. This eliminated corona losses and external leakage over the insulator, and also increased the minimum spacing of the internal electrodes. This apparatus yielded a maximum voltage of 365 kv.

The computed upper voltage limit for the generator was 800 kv, as is seen from Fig. 6. The failure to reach this is attributed to internal breakdown through the vacuum in the space between collector and emitter. This breakdown appeared to be of the type described by Trump and Van de Graaff[3] in which secondary electrons are emitted from the anode by ion bombardment, and positive ions are given off from the emitter by electron bombardment. Under certain conditions this process results in a build-up of current which discharges the device. In the present apparatus the discharge pulses could be observed with an oscilloscope. Their polarity was in accordance with this explanation. Furthermore, the limiting voltage was found to depend upon the electrode material, and the gas pressure, as is shown in Fig. 8. The left-hand, horizontal portions of the curves represent the high vacuum voltage limits. The peaks probably correspond to a surface condition in which secondary electron and ion emission are somewhat inhibited. The drop at the right-hand side is due to ionization of the gas.

[3] J. G. Trump and R. J. Van de Graaff, J. Appl. Phys. **18**, 327 (1947).

DISCUSSION

This work is regarded as a preliminary investigation, the main purpose of which was to estimate some limitations and future possibilities of radioactive charging devices.

It was shown that the insulation problem is the chief limitation in obtaining both a high and a stable voltage. To obtain higher and stabler voltages further study of insulation breakdown in a vacuum, or at low pressures, and in the presence of radioactive radiation, would no doubt be helpful. However, although this type of generator is capable of producing high voltages, it may be used also at low voltages. In this case the insulation problem is greatly simplified.

The insulation problem was augmented by the small charging current. This was of the same order of magnitude as the leakage current over the voltage range mostly studied. Fluctuations of leakage current therefore showed up as large fluctuations of voltage. Obviously greater quantities of radioactive material would result in both a stabler and higher output.

A second limitation, in so far as applications are concerned, is the small power available. For a typical beta-emitter, this is of the order of 5 milliwatts per curie, thus to obtain 1 watt would require about 200 curies. At the present time this would be considered a large and costly amount of material.

It would thus seem that as of this date, and disregarding for the moment what the future may bring, this type of generator does not represent a low cost method of producing power. Its present advantages lie rather in other aspects, such as being a self-contained, long-life source independent of external connections. Possible smallness of size and weight may also be an advantage, since it is estimated that an activity equivalent to about 100 curies could be obtained per square centimeter, this limit being determined by the self-absorption of the material. Such a density of activity would generate about 0.5 watt per square centimeter for a typical beta-emitter.

All of the limitations which have been mentioned arise from the use of a small amount of radioactive material. At the present time the available quantities are quite limited and costly. However, the picture may be greatly changed in the future. When radioactive materials become plentiful and really of low cost, radioactive chargers, such as we have described, should have considerable use as sources of energy.

Application of Fluorescence X-Rays to Metallurgical Microradiography*

H. R. SPLETTSTOSSER AND H. E. SEEMANN
Eastman Kodak Company, Rochester, New York

(Received May 21, 1952)

Fluorescence x-rays may be more useful analytically in metallurgical microradiography than the line emission from a tube target because of the greater homogeneity of the former radiation. Although the intensity of fluorescence is very low, exposure times are not prohibitive for some applications. In the present report, the method and apparatus are described and illustrative examples are shown.

CONSIDERABLE work has been done in microradiography using continuous-spectrum x-rays and in the metallurgical field, the use of line-emission x-rays has proved advantageous. The abrupt and considerable change in x-ray absorption at the K discontinuity and the fact that the location of this absorption edge depends upon the atomic number, has made possible the more or less successful identification of an element using suitably chosen wavelengths for making microradiographs. Most commonly, the application has been made using the characteristic emission of an element as the target of an x-ray tube, this radiation being accompanied, however, by the continuous-spectrum background. Clark and his co-workers[1] and Maddigan[2] have applied this procedure and have presented the theory of the method, assuming the radiation to be homogeneous. Several other workers have also applied the method.[3] So far as we are aware, Dershem[4] was the first to use the fluorescence x-rays from a secondary target to obtain a desired wavelength for making the radiograph. He used scandium K radiation to obtain high absorption in the calcium of a biological section but, in order to avoid excessive air absorption, he enclosed the secondary radiator, specimen, and film in a vacuum chamber. Other biological and chemical extensions of this work have recently been made.[5]

The principal advantage in using radiation generated within an x-ray tube is that of intensity, but it seems to us that the disadvantages, namely, the need for either a large number of different x-ray tubes or a demountable tube, are serious drawbacks to economical application of this principle. Furthermore, the continuous-spectrum background which is associated with the characteristic emission may cause experimental results to fall short of those to be expected from the theory.

The advantage of x-ray fluorescence excited by the continuous spectrum, preferably from a beryllium window tube, is that it is more homogeneous than can be obtained by any other means except diffraction by a crystal.[6] It is convenient to arrange a small piece of an element in a holder located as close as possible to the tube target. A selection of elements can be acquired at low cost and it is a simple matter to change from one to the other, thereby having a wide variety of wavelengths conveniently available. It is not necessary that the element whose fluorescence radiation is desired shall be in the form of the chemical element; it may be

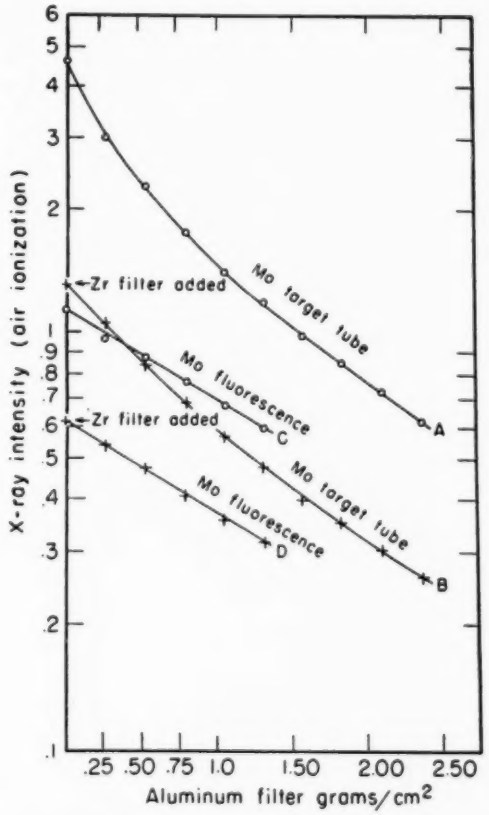

FIG. 1. Absorption curves of x-rays from a molybdenum target x-ray tube and from a molybdenum secondary radiator. (X-ray intensity from the tube cannot be compared with that from the fluorescence radiator on this graph.)

* Communication No. 1490 from the Kodak Research Laboratories.

[1] G. L. Clark and W. M. Shafer, Trans. Am. Soc. Metals **29**, 732 (1941); G. L. Clark and S. T. Gross, Ind. Eng. Chem., Anal. Ed. **14**, 676 (1942).

[2] S. E. Maddigan, J. Appl. Phys. **15**, 43 (1944); S. E. Maddigan, Ind. Radiography **4**, 22 (1946).

[3] For example, (a) J. J. Trillat, Rev. Sci. **78**, 212 (1940). (b) E. Cohen, Metallurgia **41**, 227 (1950). (c) W. Betteridge and R. S. Sharpe, J. Iron and Steel Inst. **158**, 185, Part 2 (1948). (d) Smoluchowski, Lucht, and Hurd, J. Appl. Phys. **17**, 864 (1946).

[4] E. Dershem, J. Opt. Soc. Am. **29**, 41 (1939).

[5] T. H. Rogers and W. B. Lurie, Cathode Press **7**, 6, No. 4 (1950). Marinelli, Ferlazzo, Fitzgerald, and Foote, Reported at Annual Meeting Am. Assoc. Pathol. and Bact., Boston, April, 1949. A. Engström, Acta Radiol. Supp. **63**, 1 (1946).

[6] A. H. Compton and S. K. Allison, *X-Rays in Theory and Experiment* (D. Van Nostrand Company, Inc., New York, 1935), p. 516.

a compound such as the oxide or the carbonate, in which the other elements are of low atomic number and therefore do not introduce characteristic wavelengths near those of the major element. The disadvantage of this system is the low intensity of x-ray fluorescence. It is our purpose to show what may be done by this method and to show that even with low intensity, exposures need not be too long for application to many research problems.

As an example of the difference in homogeneity of radiation emitted by the target of an x-ray tube and that emitted by a fluorescence radiator of the same element as the target, aluminum absorption curves are shown in Fig. 1. In one case, a molybdenum target x-ray tube was operated at 30 kilovolts, constant potential. (The K radiation of molybdenum requires a minimum of 20 kilovolts for excitation.) The departure of curve A from a straight line indicates considerable inhomogeneity of the radiation. In curve B, a zirconium filter, 0.0291 gram/cm^2, was placed in the beam and made some improvement, but if the radiation had consisted only of the $K\alpha$ and $K\beta$ lines, the initial intensity would have been reduced in the ratio of 1.9:1 instead of 3.5:1, the value obtained. It was assumed in the calculation that the relative intensities of the $K\alpha$ and $K\beta$ lines are the same in fluorescence spectra as when generated in an x-ray tube.[7]

The data obtained for molybdenum K fluorescence radiation from a secondary target in curve C justify the drawing of a straight line. Introduction of the zirconium filter reduced the initial intensity in the ratio 1.8:1, which is much nearer the value to be expected from zirconium absorption of Mo K radiation, as mentioned in the preceding paragraph.

The wavelengths calculated from the absorption data of curves C and D are 0.697 A and 0.715 A, respectively. Although we do not claim the accuracy implied by expressing wavelengths to three significant figures, their difference is in the direction to be expected from the effect of the zirconium filter which absorbs the Mo $K\beta$ radiation, the shorter wavelength, preferentially. The linear absorption curve, though not an extremely sensitive test for homogeneity, indicates that the fluorescence is sufficiently homogeneous for microradiographic applications since the theory assumes no more than constancy of the absorption coefficient for a given material with a particular radiation. Absorption tests of the secondary x-rays from a copper target irradiated with continuous-spectrum x-rays excited at 20 kilovolts and at 40 kilovolts showed good homogeneity in both cases. Other tests carried out in the course of another investigation[8] were equally satisfactory, except in the case of tungsten and platinum radiators. For heavy element radiators, it may be that there would be improvement if the continuous-spectrum x-rays were filtered to remove some of the longer wavelengths which do not excite the K lines but do undergo scattering.

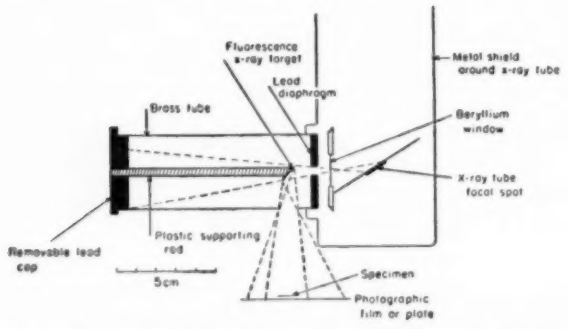

FIG. 2. Schematic diagram of apparatus for generating fluorescence x-rays in a secondary radiator for microradiography.

Metallurgical specimens for microradiographic examination must be made quite thin in order that they will transmit the x-rays in sufficient intensity to be photographically recorded in a reasonable length of time. Furthermore, a thin specimen will, in general, give a sharper outline of its parts than will a thick specimen, because the projection of boundaries, other than those perpendicular to the plane of the film, will be much narrower. It is conceivable that boundary images may be disturbed by diffraction effects from individual crystals.[3d]

Figure 2 is a schematic diagram showing the arrangement of a fluorescence target as it is attached to one of the well-known x-ray tubes—in this case, the Machlett AEG 50T. The design of this tube permits the secondary target to be placed fairly near the focal spot of the tube, thus obtaining relatively high intensity. The removable lead cap of the attachment supports a slender plastic rod on which is mounted a small piece of the element whose fluorescence is desired. This secondary target is approximately elliptical in shape, with the major axis about 1.4 times the minor axis, thus giving a circular focal-spot projection when the major axis is set at 45°. It is stuck to the supporting rod with a bit of wax and is easily changed. We favor this type of secondary target because it gives a better defined focal spot than if the beam from the x-ray tube is diaphragmed near the tube and the primary radiation allowed to fall on a large sheet of secondary radiator element.† Furthermore, in this latter case, off-focus radiation from the tube is poorly diaphragmed, resulting in off-focus radiation from the fluorescence radiator as well. Primary radiation which does not strike the secondary target is trapped in the far end of the brass tube.

The use of thin specimens contributes to geometrical sharpness of the image but the value of thinness may be lost if the specimen does not everywhere make in-

[7] See reference 6, p. 637.

[8] H. E. Seemann, Rev. Sci. Instr. **21**, 314 (1950).

† In his vacuum apparatus, Dershem (see reference 4) provided for a well-defined focal spot by diaphragming the *fluorescence* radiation, the opening thus becoming the effective focal spot. Our method is particularly convenient if the amount of radiator substance is limited and, for a system used in air, it provides the minimum air path with a given focal-spot size.

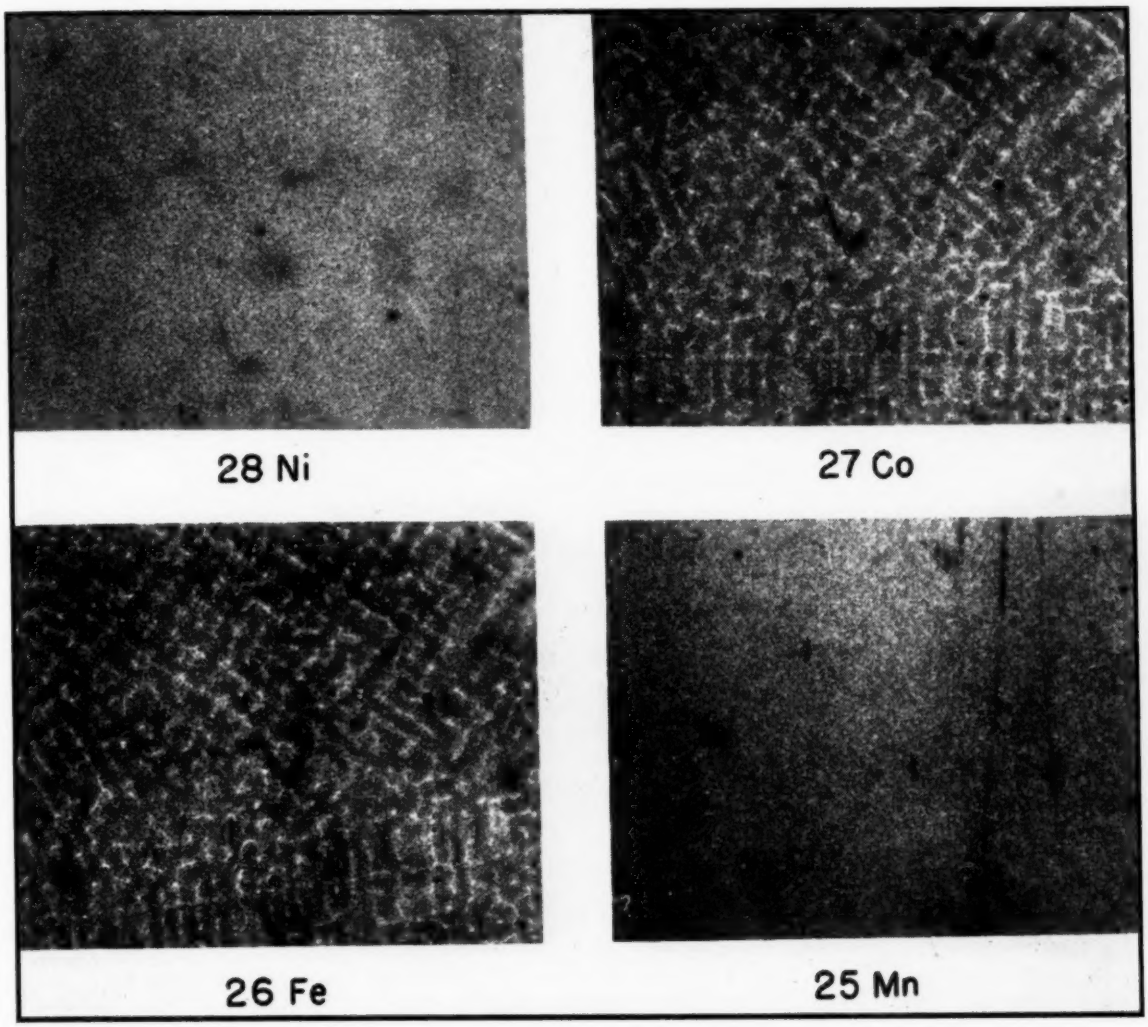

FIG. 3. Microradiographs 35×. Specimen: 74 percent Fe, 8 percent Ni, 18 percent Cr. Thickness, 0.003 cm. Radiations: *K* fluorescence from 28 Ni, 27 Co, 26 Fe, 25 Mn. X-ray tube excited at 35 kvcp and 30 ma. Exposure times: 25, 10, 10, and 12 minutes, respectively. Focal-spot diameter, projected: 0.63 cm. Target-to-film distance: 7.5 cm. Photographic plate: Kodak Spectroscopic Plate, Type V-O, developed 5 minutes in Kodak Rapid X-Ray Developer at 68°F.

timate contact with the photographic emulsion. For assuring good contact, a vacuum cassette has been used.[9]

The geometrical sharpness of radiographic images is governed by a simple relation in which the width of the penumbral shadow of an opaque part is called the "geometrical unsharpness," U_g. The relation is $U_g = Ft/d$, where F is the projected diameter of the focal spot, t is the thickness of the specimen or the maximum distance from any part of it to the film, and d is the distance from the focal spot to the specimen. In microradiography, where t is very small compared to d, the latter may be taken as the focus-film distance. For a given specimen thickness, t, a certain maximum value of U_g is permissible and is determined experimentally[10] by the limits found for F and d, these limits being those beyond which no appreciable improvement in image sharpness is seen. (If the radiograph is enlarged n times, the geometrical unsharpness becomes nU_g.) Thus, for a given specimen thickness, U_g depends only on the ratio, F/d.

The intensity of the fluorescence radiation at the film is proportional to the area of the secondary radiator and inversely to the square of the distance, or $I = kF^2/d^2$. Thus, the intensity and hence the exposure time is determined by the same ratio as the unsharpness. Once an acceptable value for U_g is decided on, nothing can be done to the system, geometrically considered, to increase the intensity. In radiography with long-wavelength x-rays, however, the absorption in the air path may reduce the intensity by a significant amount, thus increasing the exposure time. Very high air absorption necessitates the use of a vacuum chamber, and the geometrical argument is perfectly valid.

[9] H. F. Sherwood, Rev. Sci. Instr. **18**, 80 (1947).
[10] H. E. Seemann, Non-Dest. Testing **7**, 12 (1949).

If air absorption is appreciable, but not sufficient to warrant the inconvenience of a vacuum system, the distance d should be made as small as possible, with a proportionate reduction in F.

Figure 3 shows a series of microradiographs of a specimen of stainless steel having the following composition: 26 Fe—74 percent, 28 Ni—8 percent, 24 Cr—18 percent. Beginning at the upper left, the secondary radiators used were: 28 Ni, 27 Co, 26 Fe, and 25 Mn. It will be seen from this illustration that no structure is shown with the first wavelength; the second and third wavelengths show structure with good contrast, and structure has again disappeared using the fourth wavelength. We interpret this to mean that the specimen has no localized concentration of 28 Ni, for such areas would be dark because of the high transparency of an element for its own radiation. The next two wavelengths from 27 Co and 26 Fe, respectively, are absorbed strongly by 24 Cr and weakly by 26 Fe. The lighter areas therefore indicate the chromium-rich regions, and the darker areas the iron-rich regions. All of the constituents are fairly transparent to 25 Mn radiation, so no structure is brought out. Attempts to show structure in this specimen with several different-kilovoltage continuous spectra were unsuccessful.

In Fig. 4 is shown a series of microradiographs of a specimen containing 11-13 percent of 24 Cr, 2.0-2.4 percent 6 C, and the balance 25 Fe. The radiation from 28 Ni is absorbed about the same in 24 Cr and 26 Fe; hence the uniform appearance of the first radiograph. The radiations from 27 Co and 26 Fe bring out a structure in which the lighter parts must represent chromium or a chromium-rich phase. Iron and chromium are about equally transparent to 25 Mn and 24 Cr radiation, and

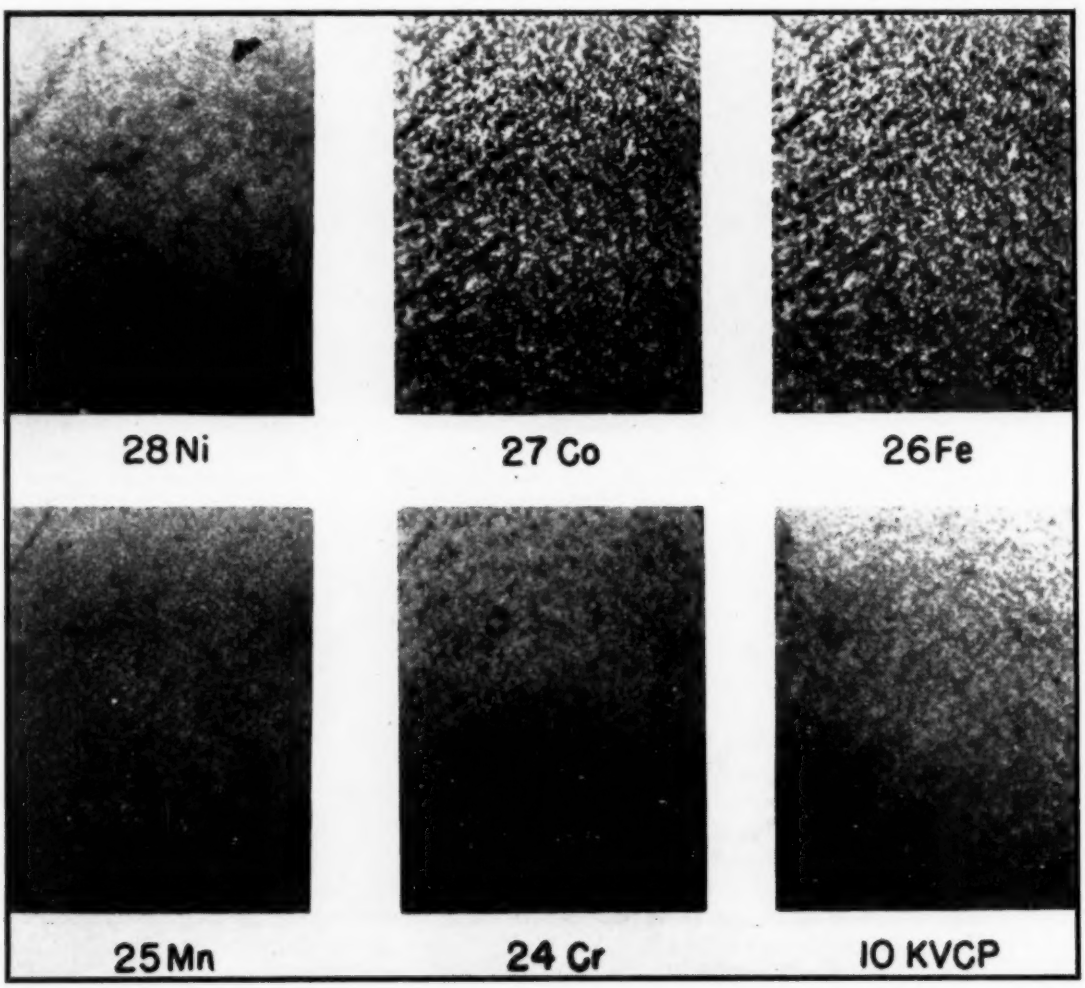

FIG. 4. Microradiographs 35×. Specimen: 11-13 percent Cr, 2.0-2.4 percent C, balance Fe. Thickness, 0.004 cm. Radiations: K fluorescence from 28 Ni, 27 Co, 26 Fe, 25 Mn, 24 Cr. Also 10 kvcp, tungsten target tube. X-ray tube excited at 35 kvcp and 30 ma. Exposure times: 20, 5, 4, 4, 4, 0.5 minutes, respectively. Focal spot, same as in Fig. 3, except 0.5 cm. for 10 kvcp. Target-film distance; 6.3 cm, except 15 cm for 10 kvcp. Photographic film: Kodak Industrial X-Ray Film, Type M, one emulsion developed, 5 minutes Kodak Rapid X-Ray Developer at 68°F. (Type M has emulsion on both sides of the base. Waterproof fabric adhesive tape should be applied to the "back" emulsion before development and removed during fixation. In this special procedure, the white lights must not be turned on until the back emulsion has cleared.)

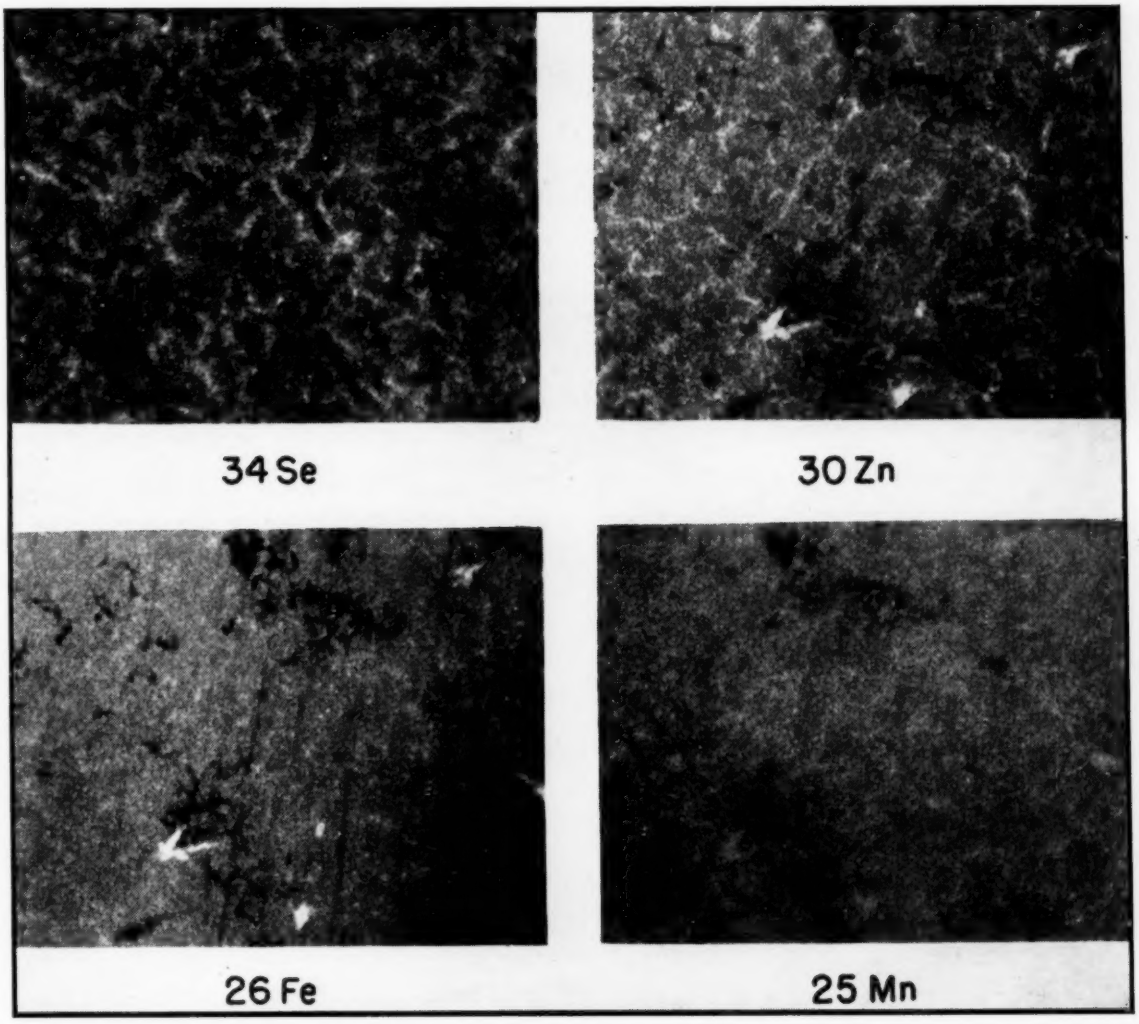

FIG. 5. Microradiographs 35×. Specimen: 93 percent Al, 5.5 percent Zn, 0.55 percent Mg, 0.5 percent Cr, 0.2 percent Ti. Thickness, 0.015 cm. Radiations: *K* fluorescence from 34 Se, 30 Zn, 26 Fe, 25 Mn. X-ray tube excited at 35 kvcp and 30 ma. Exposure times: 3, 2, 5, 5 minutes, respectively. Focal spot: same as in Fig. 3. Target-film distance: 6.3 cm. Photographic film: Same as in Fig. 4.

therefore, the structure disappears. The structure is visible to a very limited extent with 10-kilovolt radiation, but this is the best radiograph made with several different potentials from 7 to 14 kilovolts applied to a tungsten target tube with beryllium window.

The specimen radiographed for Fig. 5 consisted of 93 percent of 13 Al, 5.5 percent of 30 Zn, 0.55 percent of 12 Mg, 0.5 percent 24 Cr, and 0.2 percent 22 Ti. Radiation from 34 Se gives a radiograph showing contrast between a zinc-rich phase and the surroundings. With 30 Zn and 26 Fe radiation, four particles of chromium are brought out in white. Since chromium is relatively transparent to 25 Mn radiation, these particles practically disappear. Several black branching areas indicate porosity.

The first two radiographs of the bronze specimen in Fig. 6 show that image sharpness, in a sample having somewhat diffuse boundaries, is practically as good when radiographed at 6.3 centimeters distance as at 38 centimeters, specimen thickness, focal-spot size, and enlargement being those given. Comparing these with the third radiograph, which was made with 29 Cu *K* radiation, it is apparent that, in cases where a heavy element is associated with considerably lighter elements, continuous-spectrum x-rays excited at the proper kilovoltage may be nearly as satisfactory as wavelengths chosen specifically.[11] However, in no case can the continuous spectrum offer the possibilities for identification inherent in the fluorescence radiation procedure. Although emission from certain x-ray tube targets has been demonstrated to be useful, there must, in our opinion, be cases where this method represents a compromise between the fluorescence and the continuous-spectrum techniques and will therefore not be as satis-

[11] See R. C. Woods and V. C. Cetrone, Metals and Alloys **18**, 1320 (1943).

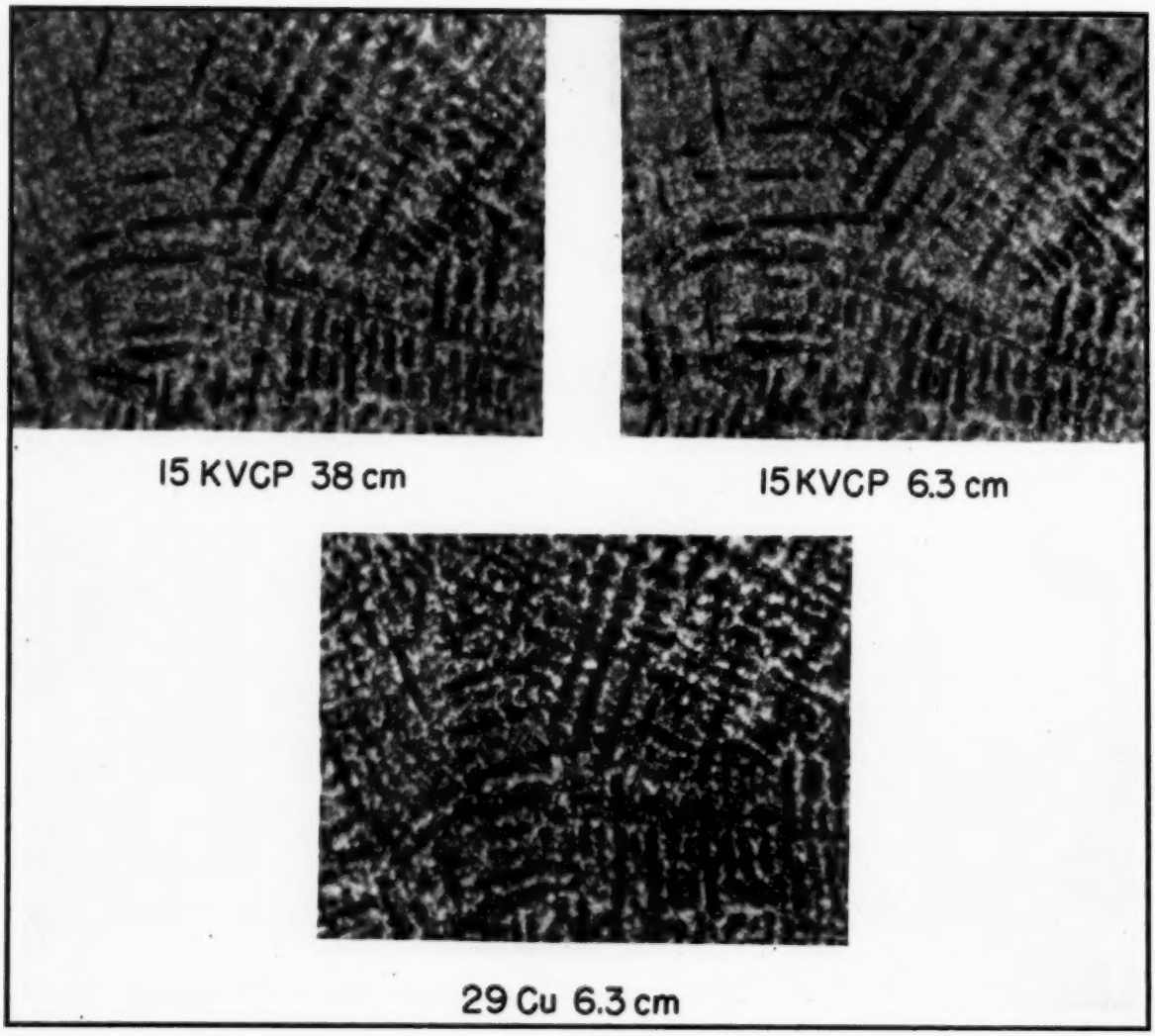

FIG. 6. Microradiographs 75×. Specimen: Bronze, composition unknown, presumably Cu, Zn, and Sn. Thickness, 0.004 cm. Radiations: 15 kvcp tungsten target tube, 25 ma and 10 ma, respectively, and K fluorescence from Cu with x-ray tube excited at 35 kvcp and 30 ma. Exposure times: 1.5, 0.1, and 10 minutes, respectively. Focal spot: 0.5 cm in x-ray tube, 0.63 cm secondary radiator. Target-film distances: 38, 6.3, and 6.3 cm, respectively. Photographic film: Eastman Fine Grain Release Positive Safety Film, developed in Kodak Rapid X-Ray Developer for 8 minutes at 68°F.

factory as the former nor as unsatisfactory as the latter.

The sensitivity of fluorescence radiography for detecting small amounts of an element may not be as great as that calculated from the absorption coefficients. This is due to the fact that fluorescence radiation emitted by the specimen itself is recorded by the photographic emulsion, thus reducing contrast. Fluorescence radiation is not recorded when absorption coefficients are determined. Our tests, using thin specimens of metallic elements, have indeed shown that the fluorescence emission from a strongly absorbing specimen is radiographically appreciable, This is to be expected, since radiation just on the short-wavelength side of the K-absorption edge is very efficient in exciting fluorescence, and the element is relatively transparent to its own fluorescence. This effect was mentioned by Cohen[3b] but he did not observe it.

The experimenter who undertakes problems in fluorescence microradiography will find it very helpful, if not actually essential, to plot the linear absorption *versus* wavelength curves for the elements which may be in his specimens. On the same diagram, the emission lines which occur in this region should also be indicated. Differential absorptions obtained from these curves will facilitate interpretation of the radiographs obtained.

Note: In the interval between submission of our manuscript and arrival of printer's proof, we have seen a paper by T. H. Rogers on "Production of monochromatic x-radiation for microradiography by excitation of fluorescent characteristic radiation," in J. Appl. Phys. **23**, 881–887 (1952), which will be of interest to readers of our paper.

On the Relation between the Conductance and the Noise Power Spectrum of Certain Electronic Streams

J. J. FREEMAN
National Bureau of Standards, Washington, D. C.
(Received May 21, 1952)

The noise power spectrum of a diode with a temperature limited current and also for a diode with a retarding field is shown to be the sum of two parts. One, the "pure" shot effect, is the spectrum which would obtain if the electrons were all emitted with zero velocity, that is, if the cathode were at zero temperature (and still maintained the same emitting properties). The second is the thermal contribution, namely, $4kTg$, where T is the cathode temperature and g is the conductance of the electron stream.

I. INTRODUCTION

ASSOCIATED with every electronic current is its conductance and its noise power spectrum, and the question arises whether there is any relation between the two. To what extent does Nyquist's law[1] ($\langle i^2\rangle = 4kTgdf$ where $\langle i^2\rangle$ is the mean square current fluctuation in the frequency range df in a short-circuited impedor whose conductance is g) hold for the conductance of an electronic current? What is the connection between shot noise and thermal noise in a tube? The following investigation attempts to answer the above questions which have been debated in the literature at various times.[2] Two particularly simple electronic currents are investigated, namely, that in a temperature-limited diode, and that in a diode with a retarding field. For both of these it is shown that the power spectrum may be decomposed into a sum of two parts; one of which, the "pure" shot spectrum, is the spectrum which would obtain if all electrons were emitted with zero initial velocity, that is, if the cathode were at zero temperature (and still maintained the same total emission). The other part is the thermal contribution, namely $4kTg$, where T is the cathode temperature and g is the conductance of the electron stream.

II. THE TEMPERATURE-LIMITED DIODE

A. Computing the Conductance

We proceed to compute the admittance of a temperature-limited diode by computing the current induced by a voltage generator in series with the diode (Fig. 1). It is assumed that cathode and anode consist of two parallel plates sufficiently close so that edge effects may be neglected, and that the plate voltage, V_p, is sufficiently positive so that the potential distribution between cathode and anode is linear.

Consider an electron at a distance x from the cathode traveling with velocity $\dot{x}$. The electron will induce a current[3]

$$i(t) = e\dot{x}/d \tag{1}$$

in the external circuit. The total induced current is simply the sum over all the electrons of the elementary induced currents, and the immediate problem is to calculate the velocity of a typical electron.

If V_p is the dc plate voltage, $V\cos\omega t$ the ac voltage, and $\alpha = V/V_p$, the potential distribution within the diode is

$$V(x) = V_p x/d(1+\alpha\cos\omega t), \tag{2}$$

where d is the plate-cathode separation.

The equation of motion of an electron is

$$\ddot{x} = \beta(1+\alpha\cos\omega t)$$

where

$$\beta = eV_p/md \tag{3}$$

and e and m are, respectively, the charge and mass of the electron.

$$\dot{x} = v_0 + \beta\left[t - t_0 + \frac{\alpha}{\omega}(\sin\omega t - \sin\omega t_0)\right], \tag{4}$$

where t_0 is the time at which the electron was emitted with initial velocity v_0.

The integral of Eq. (4) yields:

$$x = v_0(t-t_0) + \beta\left[\frac{(t-t_0)^2}{2} - \frac{\alpha}{\omega^2}[\cos\omega t - \cos\omega t_0 + \omega(t-t_0)\sin\omega t_0]\right]. \tag{5}$$

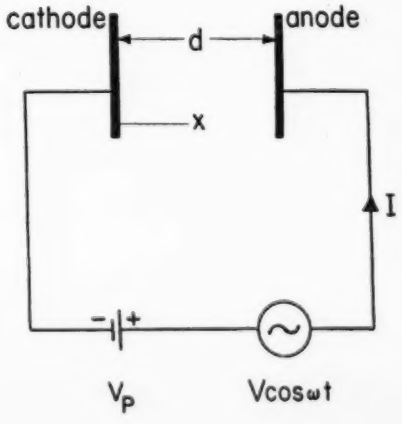

FIG. 1. Schematic of diode.

[1] H. Nyquist, Phys. Rev. **32**, 110 (1928).
[2] Discussion in Proc. Phys. Soc. (London) **59**, 403 (1947). Note comments by D. A. Bell, C. W. Bull, and D. K. C. MacDonald.
[3] W. Shockley, J. Appl. Phys. **19**, 635 (1938).

If an electron leaving the cathode at $t_0=t-\tau$ reaches the plate, $x=d$, at time t, then from Eq. (5):

$$v_0\tau+\frac{\beta\tau^2}{2}=d+\frac{\alpha\beta}{\omega^2}[\cos\omega t-\cos\omega(t-\tau)+\omega\tau\sin\omega(t-\tau)]. \quad (6)$$

Let N equal the number of electrons emitted per second. Of these let $f(v_0)dv_0$ be the fraction having initial velocity v_0. Then, from (1), the total induced current due to all the electrons between cathode and plate is

$$I(t)=\frac{Ne}{d}\int_0^\infty f(v_0)\int_{t-\tau}^{t} v(t,t_0)dt_0dv_0. \quad (7)$$

Substitute (4) in (7), integrate, and utilize the relation in Eq. (6), to obtain

$$I(t)=\frac{Ne}{d}\int_0^\infty f(v_0)\left\{d+\frac{\alpha\beta}{\omega^2}[2\cos\omega t-2\cos\omega(t-\tau)+\omega\tau[\sin\omega t+\sin\omega(t-\tau)]]\right\}dv_0. \quad (8)$$

Now we assume that the ac voltage is small compared to the dc plate voltage, or $\alpha^2=(V/V_p)^2\ll 1$. Further, we assume that the trajectories are continuous functions of plate potential (there is no potential minimum) so that τ may be expanded as a power series in α,

$$\tau=\tau_0+\alpha\tau_1+\alpha^2\tau_2+\cdots. \quad (9)$$

where τ_0, τ_1, etc., depend upon the initial velocity, v_0.

Accordingly, Eq. (8) will be correct to the first order in α if one substitutes therein τ_0 for τ. Thus,

$$I(t)=I_0+\frac{I_0\alpha\beta}{\omega^2 d}\int_0^\infty f(v_0)\{[2(1-\cos\omega\tau_0)-\omega\tau_0\sin\omega\tau_0]\cos\omega t+[\omega\tau_0(1+\cos\omega\tau_0)-2\sin\omega\tau_0]\sin\omega t\}dv_0, \quad (10)$$

where $I_0=Ne$ is the dc plate current; but

$$I-I_0=V[g\cos\omega t-b\sin\omega t], \quad (11)$$

where g is the rf conductance and b the susceptance. Hence, assuming the electrons are emitted with a Maxwellian velocity distribution so that

$$f(v_0)=mv_0/kT\exp(-mv_0^2/2kT) \quad (12)$$

one obtains from (10), (11), and (12),

$$g=\frac{I_0e}{kT\omega^2d^2}\int_0^\infty \exp(-mv_0^2/2kT)\{2(1-\cos\omega\tau_0)-\omega\tau_0\sin\omega\tau_0\}v_0dv_0. \quad (13)$$

B. The Power Spectrum

We compute the power spectrum of the current fluctuations induced in an external short circuit (Fig. 1, with the signal generator absent).

If $i(v_0)$ is the induced current due to electrons with initial velocity v_0, then by Campbell's theorem,[4] assuming the electrons are emitted independently,

$$\langle(i-\bar{i})^2\rangle_{\Delta\nu}=\frac{n(v_0)e^2}{d^2}\int_0^{\tau_0}\dot{x}^2dt=2\frac{n(v_0)e^2}{d^2}\int_0^\infty|F(f)|^2df,$$

where $n(v_0)$ is the average number of electrons emitted per second with initial velocity v_0,

$$(n(v_0)e=mI_0/kT\exp(-mv_0^2/2kT)v_0dv_0)$$

and

$$F(f)=\int_{-\infty}^{\infty}\dot{x}\exp(-j\omega t)dt=\int_0^{\tau_0}\dot{x}\exp(-j\omega t)dt, \quad (14)$$

where $\dot{x}$ is given by Eq. (4) for $\alpha=0$.

After averaging over the entire velocity class, the total current fluctuations are

$$\langle(i-\bar{i})^2\rangle_{\Delta\nu}=\frac{2I_0em}{d^2kT}\int_0^\infty\int_0^\infty \times\exp(-mv_0^2/2kT)|F(f)|^2v_0dv_0df, \quad (15)$$

and $P(f)$, the power spectrum of $\langle(i-\bar{i})^2\rangle_{\Delta\nu}$ is

$$P(f)=\frac{2I_0em}{d^2kT}\int_0^\infty \exp(-mv_0^2/2kT)|F(f)|^2v_0dv_0. \quad (16)$$

Integrating (15) by parts and substituting the explicit value for $F(f)$ obtained from Eq. (14), one obtains

$$P(f)=\frac{2I_0e}{d^2}|F(f)|^2_{v_0=0}+\frac{4I_0e}{d^2\omega^2}\int_0^\infty \times\exp(-mv_0^2/2kT)[2(1-\cos\omega\tau_0)-\omega\tau_0\sin\omega\tau_0]v_0dv_0. \quad (17)$$

Comparing Eqs. (17) and (13),

$$P(f)=\frac{2I_0e}{d^2}|F(f)|^2_{v_0=0}+4kTg. \quad (18)$$

The first term on the right represents the spectrum which would result if all electrons were emitted with zero initial velocity; the second term represents the contribution due to the Maxwellian velocity distribution.

[4] N. R. Campbell and V. J. Francis, J. Inst. Elec. Engrs. **93**, Pt. III, 45 (1946).

III. THE DIODE WITH A RETARDING FIELD

If the plate voltage of the diode is sufficiently negative practically all of the electrons will be returned to the cathode, and the diode may be considered to be in thermal equilibrium provided one can neglect the electrons captured by the plate. For this case, under the assumption of a linear potential distribution, the conductance has been shown to be[5,6]

$$g=\frac{4I_0e}{d^2kT\omega^2}\int_0^\infty v_0\exp(-mv_0^2/2kT)\times[\sin\theta-\theta\cos\theta]\cos\theta dv_0 \quad (19)$$

where $\theta=\omega v_0md/eV_p$.

A calculation similar to the temperature limited case shows that the noise power spectrum, $P(f)$, is here given by

$$P(f)=4kTg. \quad (20)$$

Here the power spectrum vanishes at $T=0$ since electrons with zero initial velocity induce no current.

[5] J. J. Freeman, J. Appl. Phys. **23**, 743 (1952), Eq. (13).
[6] N. Begovich, J. Appl. Phys. **20**, 457 (1949).

IV. CONCLUSION

For the case of a temperature-limited diode and one with a retarding field it has been shown that the noise power spectrum may be resolved into a sum of two components: one is the "pure" shot spectrum one would obtain if the initial velocity of the emitted electrons were zero. The other arises from the initial velocity distribution, which may be considered as thermal noise, and is related to the conductance by Nyquist's law. The above method of calculation assumes that the trajectories of the electrons are continuous functions of the initial velocity. Hence no potential minimum is permitted. Also, it assumes that the random variations in trajectories due to fluctuations in the potential distribution may be neglected, so that the electrons may be considered to describe their trajectories independently.

Although not shown explicitly, it would appear from the method of calculation that for any electron stream satisfying the above two assumptions a resolution of the noise spectrum into "thermal" noise (satisfying Nyquist's law) plus "pure" shot noise, neglecting the initial velocity distribution, can be made.

JOURNAL OF APPLIED PHYSICS VOLUME 23, NUMBER 11 NOVEMBER, 1952

Electric Potential Produced by Two Point Current Sources in a Homogeneous Conducting Sphere*

ERNEST FRANK
Moore School of Electrical Engineering, University of Pennsylvania, Philadelphia, Pennsylvania and the Edward B. Robinette Foundation, Medical Clinic, Hospital of the University of Pennsylvania
(Received May 26, 1952)

The electric potential produced by positive and negative point current sources located in a homogeneous conducting sphere, a problem of interest in the field of electrocardiography, is obtained for arbitrary source locations and separations. Certain special cases of the general solution that are of particular value in both experimental and theoretical electrocardiographic research are also presented.

INTRODUCTION

IT has been well established[1] that human heart action is accompanied by a current field in the conducting tissues, fluids, and organs of the body. These currents, largely confined to the torso, produce at the surface of the skin electric potentials which can be measured by a recording voltmeter called the electrocardiograph, indirectly enabling certain heart ailments to be diagnosed when properly analyzed and interpreted. In much of the theoretical work in this field, the body is assumed to be a homogeneous, isotropic, resistive medium of spherical shape, and the heart is frequently represented by an equivalent current generator; in special cases a current dipole.[2] Also, electrocardiographic experimentation on live animals, cadavers, and models sometimes involves a study of the potentials produced by two current electrodes that are inserted in the medium.

Consequently, it becomes pertinent to investigate the potentials produced by a current generator in a homogeneous conducting sphere, particularly at the boundary, and this has been done by others for special cases such as a dipole at the center of a sphere,[3] a dipole at the center of a circular lamina,[4] and a dipole anywhere

* This investigation was supported in part by grants of the National Heart Institute, United States Public Health Service.
[1] R. Ashman and E. Hull, *Essentials of Electrocardiography* (The Macmillan Company, New York, 1945).

[2] A dipole is defined as a special case of a current generator in which the separation between the positive current source and the negative current source approaches zero, maintaining constant the product of source strength times the separation between sources.
[3] R. Canfield, Heart **14**, 102 (1927).
[4] Wilson, MacLeod, and Barker, "The distribution of the currents of action and of injury displayed by heart muscle and

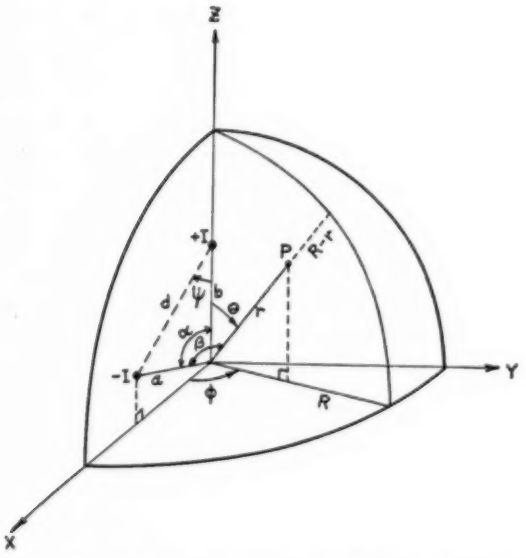

FIG. 1. Two point current sources arbitrarily located in a homogeneous conducting sphere, one octant of which is shown. The two sources and the sphere origin always define an equatorial plane which has been taken as the $\phi=0$ plane for convenience. The angle ψ is useful for describing the orientation of a current dipole, one of the special cases presented.

in a sphere.[5] The general solution presented here contains all other previous solutions as well as certain additional cases of special importance.

GENERAL SOLUTION

An expression for the electric potential is desired at the perfectly insulating wall of a homogeneous conducting sphere of conductivity γ and radius R resulting from a current generator whose output terminals are arbitrarily located within the sphere. The method of solution which is well known requires that the potential satisfy Laplace's equation $\nabla^2 V=0$ as well as boundary conditions. In this case the normal derivative of the potential must be zero at the boundary $r=R$.

By taking the origin of coordinates at the center of the sphere in Fig. 1 it is possible, with no loss in generality, to pass the z-axis through one of the sources (a distance $b<R$ from the origin) and to orient the $\phi=0$ plane so that it contains the other source (a distance $a\lessgtr b$ from the origin). The distance between sources is $d=(a^2+b^2-2ab\cos\alpha)^{\frac{1}{2}}$ where α is the angle between line a and the z-axis. The line r to an arbitrary point $P(r,\theta,\phi)$ within the sphere makes an angle θ with b and an angle β with a, where

$$\cos\beta=\sin\alpha\sin\theta\cos\phi+\cos\alpha\cos\theta. \tag{1}$$

A strong clue to the solution is given by examining V_∞, the potential in an unbounded medium, which can be formulated in terms of the inverse distances from the sources to P.[6]

$$V_\infty=\frac{I}{4\pi\gamma}\left(\frac{1}{r_b}-\frac{1}{r_a}\right), \tag{2}$$

where[7]

$$\frac{1}{r_b}=(r^2+b^2-2rb\cos\theta)^{-\frac{1}{2}}=\frac{1}{r}+\frac{1}{r}\sum_{n=1}^{\infty}\left(\frac{b}{r}\right)^n P_n(\cos\theta), \quad r>b, \tag{3}$$

and

$$\frac{1}{r_a}=(r^2+a^2-2ra\cos\beta)^{-\frac{1}{2}}=\frac{1}{r}+\frac{1}{r}\sum_{n=1}^{\infty}\left(\frac{a}{r}\right)^n P_n(\cos\beta), \quad r>a. \tag{4}$$

Moreover,

$$P_n(\cos\beta)=\sum_{m=0}^{m=n}(2-\delta_m{}^0)\frac{(n-m)!}{(n+m)!}\times P_n{}^m(\cos\alpha)P_n{}^m(\cos\theta)\cos m\phi, \tag{5}$$

where $\delta_m{}^0=1$ when $m=0$ and $\delta_m{}^0=0$ when $m\neq 0$, and $P_n{}^m$ is the associated Legendre function of the first kind. Consequently,

$$V_\infty=\frac{I}{4\pi\gamma}\sum_{n=1}^{\infty}\sum_{m=0}^{m=n}\frac{1}{r^{n+1}}S_{mn}(\theta,\phi), \quad r>b, \tag{6}$$

where $S_{mn}(\theta,\phi)$ signifies the surface harmonics,

$$S_{mn}(\theta,\phi)=b^n P_n(\cos\theta)-a^n(2-\delta_m{}^0)\frac{(n-m)!}{(n+m)!}\times P_n{}^m(\cos\alpha)P_n{}^m(\cos\theta)\cos m\phi. \tag{7}$$

The current may be confined to the sphere of radius R by adding to (6) a solution of Laplace's equation which has no poles in the region $r<R$ and makes $\partial V/\partial r$ zero at $r=R$. The result is evidently (8) which can be seen by inspection to satisfy these conditions.

$$V=\frac{I}{4\pi\gamma}\sum_{n=1}^{\infty}\sum_{m=0}^{m=n}\left(\frac{n+1}{n}\frac{r^n}{R^{2n+1}}+\frac{1}{r^{n+1}}\right)S_{mn}(\theta,\phi), \quad r>b. \tag{8}$$

This also may be written, using (4)

$$V=\frac{I}{4\pi\gamma}\sum_{n=1}^{\infty}\left(\frac{n+1}{n}\frac{r^n}{R^{2n+1}}+\frac{1}{r^{n+1}}\right)\times\left[b^n P_n(\cos\theta)-a^n P_n(\cos\beta)\right], \quad r>b. \tag{9}$$

other excitable tissues," University of Michigan Studies, Scientific Series (University of Michigan Press, Ann Arbor, 1933), Vol. X.

[5] F. N. Wilson and R. H. Bayley, Circulation 1, 84 (1950).

[6] S. A. Schelkunoff, *Electromagnetic Waves* (D. Van Nostrand Company, Inc., New York, 1943), p. 129.

[7] For this and other Legendre function relations and definitions used in this paper, see E. W. Hobson, *The Theory of Spherical and Ellipsoidal Harmonics* (Cambridge University Press, Cambridge, 1931).

At the sphere boundary, $r=R$,

$$V_R=\frac{I}{4\pi\gamma}\sum_{n=1}^{\infty}\sum_{m=0}^{m=n}\frac{2n+1}{nR^{n+1}}S_{mn}(\theta,\phi). \tag{10}$$

This is the general solution for the boundary potential.

These general results may also be expressed in closed form. Let r_{bi} be the distance from the field point P to the image point $r=R^2/b$, $\theta=0$ of the source at $r=b$, $\theta=0$. Then, as with (3),

$$\frac{1}{r_{bi}}=\frac{b}{R^2}+\frac{b}{R^2}\sum_{n=1}^{\infty}\left(\frac{r}{R^2/b}\right)^n P_n(\cos\theta).$$

Also, in (9) it is observed that

$$\frac{n+1}{n}\,\frac{b^n r^n}{R^{2n+1}}=\frac{r^n}{R}\left[\left(\frac{b}{R^2}\right)^n+\int_0^b\frac{b^{n-1}db}{R^{2n}}\right].$$

Thus,

$$\sum_{n=1}^{\infty}\frac{n+1}{n}\,\frac{r^n b^n}{R^{2n+1}}P_n(\cos\theta)=\frac{R}{br_{bi}}-\frac{1}{R}+R\int_0^b\frac{db}{b^2 r_{bi}}-\int_0^b\frac{db}{bR}.$$

But $br_{bi}=(R^4+r^2b^2-2R^2rb\cos\theta)^{\frac{1}{2}}$ so that the integrals become

$$-\frac{1}{R}\ln\frac{br_{bi}+R^2-rb\cos\theta}{2R^2}.$$

In exactly the same way the terms involving a lead to

$$-\frac{R}{ar_{ai}}+\frac{1}{R}+\frac{1}{R}\ln\frac{ar_{ai}+R^2-ra\cos\beta}{2R^2}.$$

Adding yields (9) in closed form

$$V=\frac{I}{4\pi\gamma}\left[\frac{1}{r_b}-\frac{1}{r_a}+\frac{R}{br_{bi}}-\frac{R}{ar_{ai}}+\frac{1}{R}\ln\frac{ar_{ai}+R^2-ra\cos\beta}{br_{bi}+R^2-rb\cos\theta}\right]. \tag{11}$$

At the sphere boundary, $ar_{ai}=Rr_a$ and $br_{bi}=Rr_b$ so the closed-form solution corresponding to (10) becomes, from (11),

$$V_R=\frac{I}{4\pi\gamma}\left[\frac{2}{r_b}-\frac{2}{r_a}+\frac{1}{R}\ln\frac{r_a+R-a\cos\beta}{r_b+R-b\cos\theta}\right]. \tag{12}$$

SOME SPECIAL CASES

General Dipole

A number of cases of special interest may be extracted from the general results, one of the important ones being the dipole defined by $d\to 0$ with the product Id finite. A dipole may be formed at $z=b$ by allowing d to approach zero along the line in the $\phi=0$ plane which intersects the z-axis at an angle ψ. For *any* d, $\sin\alpha=d\sin\psi/a$. Hence, $P_n^m(\cos\alpha)$ can be written

$$P_n^m(\cos\alpha)=(-1)^m\binom{d}{a}^m(-\sin\psi)^m\frac{d^mP_n(\cos\alpha)}{d(\cos\alpha)^m}. \tag{13}$$

To retain only first-order terms in d, it can be seen from (13) that $m=0$ and $m=1$ are the only surviving terms in the m-summation of (10). Therefore, (10) becomes

$$V_R=\frac{I}{4\pi\gamma}\sum_{n=1}^{\infty}\frac{2n+1}{nR^{n+1}}\left\{[b^n-a^nP_n(\cos\alpha)]P_n(\cos\theta)-2a^n\frac{(n-1)!}{(n+1)!}P_n^1(\cos\alpha)P_n^1(\cos\theta)\cos\phi\right\}. \tag{14}$$

Now, as $d\to 0$ with Id finite, $\cos\alpha\to 1$, $d\cos\psi=b-a\cos\alpha\to b-a$, and $a\to b$. Consequently, in (14) $P_n(\cos\alpha)\to 1$ and the following difference appears:

$$b^n-a^n=(b-a)(b^{n-1}+b^{n-2}a+\cdots+a^{n-1})\to nb^{n-1}d\cos\psi. \tag{15}$$

Moreover, with $m=1$ and $\cos\alpha\to 1$ the derivative in (13) becomes

$$\left.\frac{dP_n(\cos\alpha)}{d(\cos\alpha)}\right]_{\cos\alpha=+1}=\frac{(n+1)!}{2(n-1)!},\quad n\neq 0.$$

Incorporating the foregoing limiting values into (14) yields the dipole solution

$$V_{R_{\text{dipole}}}=\frac{p}{4\pi\gamma}\sum_{n=1}^{\infty}\frac{(2n+1)b^{n-1}}{nR^{n+1}}[n\cos\psi P_n(\cos\theta)+\sin\psi\cos\phi P_n^1(\cos\theta)] \tag{16}$$

where $p=Id$ is the dipole moment. The corresponding closed-form result in (17) can be shown to agree with Wilson's[5] which contains numerous terms involving an assortment of ten different direction cosines.

$$V_{R_{\text{dipole}}}=\frac{p}{4\pi\gamma Rb}\left\{\cos\psi\left[\frac{1-f^2}{(1+f^2-2f\mu)^{\frac{3}{2}}}-1\right]-\frac{\sin\psi\cos\phi}{\sin\theta}\left[\frac{3f-3f^2\mu+f^3-\mu}{(1+f^2-2f\mu)^{\frac{3}{2}}}+\mu\right]\right\}, \tag{17}$$

where $\mu=\cos\theta$ and $f=b/R$.

Equatorial Plane of Sources

The measurement of potentials at various points within the sphere poses serious experimental difficulties caused by distortion of the field owing to the pick-up devices used. However, the equatorial plane containing the current sources may be explored (and

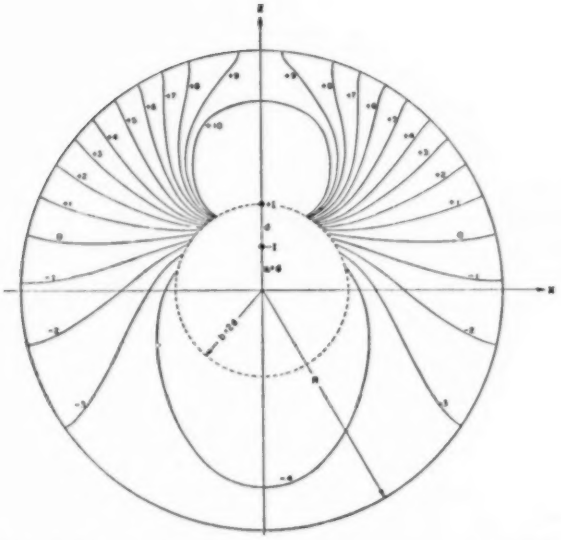

FIG. 2. Illustration of equipotentials in an equatorial plane for the special case of eccentric current sources when the line joining the sources passes through the sphere origin for $a=d=0.172R$ and $b=2d$. The area between the sphere boundary $r=R$ and the dotted circle $r=b$ through $+I$ represents the region of convergence of the series solution. The units of potential are arbitrary.

excited) conveniently by taking advantage of the property that no current lines pierce this plane in the general case, and hence, half of the sphere may be removed without altering the field except for a factor of two in magnitude. This permits probing of the equatorial plane with negligible disturbance of the field. Therefore, solutions in the plane $\phi=0$ are of special interest. A convenient form for computation purposes is obtained by recognizing from (1) that with $\phi=0$, $\cos\beta=\cos(\theta-\alpha)$, so (9) may be written

$$V_{\text{equat.}}=\frac{I}{4\pi\gamma}\sum_{n=1}^{\infty}\left(\frac{n+1}{n}\,\frac{r^n}{R^{2n+1}}+\frac{1}{r^{n+1}}\right)\times[b^nP_n(\cos\theta)-a^nP_n(\cos[\theta-\alpha])],\quad r>b. \tag{18}$$

The potential at the boundary is obtained simply by replacing the function of r in (18) by $(2n+1)/nR^{n+1}$, while the dipole result is available in (16) or (17) by setting $\cos\phi=1$.

Solutions with ϕ-Symmetry

When the line joining the sources passes through the sphere origin, the potential is symmetrical with respect to ϕ, i.e., $\partial V/\partial\phi=0$. Also, $\psi=0$ and $\alpha=0$ or π. There are three cases of interest called eccentric ($a>0$, $b>0$, $\alpha=0$), semi-centric ($a=0$, $b=d$) and centric ($a=b$, $\alpha=\pi$). In all of these cases the potential distribution is the same in any equatorial plane containing the sources.

For eccentric cases, (10) yields

$$V_R=\frac{I}{4\pi\gamma}\sum_{n=1}^{\infty}\frac{2n+1}{nR^{n+1}}(b^n-a^n)P_n(\cos\theta), \tag{19}$$

since $P_n^m(\cos\alpha)=0$ when $m\neq0$ with $\alpha=0$. An example of equipotentials is given in Fig. 2 for an eccentric case. For $a\to b$ the eccentric dipole result may be obtained using (16) and $\cos\psi=1$.

$$V_R=\frac{p}{4\pi\gamma R^2}\sum_{n=1}^{\infty}(2n+1)\left(\frac{b}{R}\right)^{n-1}P_n(\cos\theta), \tag{20}$$

or from (17) the closed-form expression becomes

$$V_R=\frac{p}{4\pi\gamma Rb}\left[\frac{1-f^2}{(1+f^2-2f\mu)^{\frac{1}{2}}}-1\right]. \tag{21}$$

For the semi-centric case, $a=0$ and $b=d$ may be inserted in (19) to obtain

$$V_R=\frac{I}{4\pi\gamma}\sum_{n=1}^{\infty}\frac{2n+1}{nR^{n+1}}d^nP_n(\cos\theta), \tag{22}$$

which becomes, for a dipole, discarding all terms in d^2 and higher order

$$V_R=\frac{3p\cos\theta}{4\pi\gamma R^2} \tag{23}$$

which is really a centric result.

The more general centric result can be obtained from (18) by setting $\alpha=\pi$, $a=b=d/2$ and using the relation $P_n(-\cos\theta)=(-1)^nP_n(\cos\theta)$ which leads to cancellation of all terms with n even and results in

$$V=\frac{I}{2\pi\gamma}\sum_{n=1}^{\infty}{}^{\text{odd}}\left(\frac{n+1}{n}\,\frac{r^n}{R^{2n+1}}+\frac{1}{r^{n+1}}\right)\left(\frac{d}{2}\right)^nP_n(\cos\theta),\quad r>\frac{d}{2}. \tag{24}$$

When $d\to0$ in (24) the only surviving term is $n=1$ and (23) is obtained by setting $r=R$.

The equations presented here have been directly useful in both theoretical and experimental investigations in the field of electrocardiography, and have also enabled a better understanding of the behavior of current fields in volume conductors in non-idealized cases. Equipotentials for the case given in Fig. 2 have been measured experimentally in a water-filled hemisphere to within an accuracy of about 5 percent, the departures from theory being attributable to errors inherent in the experimental equipment.

The author expresses appreciation for the helpful manuscript criticisms offered by Dr. J. G. Brainerd and Mr. D. F. Hunt.

JOURNAL OF APPLIED PHYSICS VOLUME 23, NUMBER 11 NOVEMBER, 1952

Scabbing of Metals under Explosive Attack: Multiple Scabbing*

JOHN S. RINEHART
U. S. Naval Ordnance Test Station, Inyokern, China Lake, California
(Received May 5, 1952)

Further quantitative data bearing on the scabbing of metals under explosive attack are presented in this paper. In particular, the mechanics of the generation of multiple scabs is established. Experimental data have been obtained that show that multiple scabbing will occur whenever the maximum stress σ_0 in the transient wave that impinges on a free surface is more than double the critical normal fracture stress σ_c of the material. The number of scabs that will be formed will be equal to the first whole number smaller than the quotient σ_0/σ_c. The thickness of each scab is governed by the shape of the stress wave.

INTRODUCTION

IT is well known that the high intensity transient stresses induced in a metal by an exploding charge can cause fracturing (or scabbing) near a free surface as the result of interference between the incident wave and the reflected wave. Considerable quantitative data bearing on the scabbing of metals under explosive attack were presented in an earlier paper.[1]

An extremely interesting aspect of scabbing—and one not discussed in that paper—is multiple scabbing. The term "multiple scabbing" is used to describe the situation in which several juxtaposed and parallel scabs are generated within a single plate. An excellent example of multiple scabbing is shown in Fig. 1. This figure is a photograph of a section cut from a 3-in. thick mild steel plate that had been acted upon by a cylinder of explosive which was detonated on the top surface of the plate. Close scrutiny of the plate itself disclosed six separate and distinct scabs. Only that area of the plate which lies close to an extension of the axis of the charge is considered here and in the discussions that follow.

Multiple scabbing has been observed to occur in many cases. It always appears to be associated with waves of very high stress levels. Its occurrence is not limited to mild steel. Under suitable conditions copper, brass, 24ST aluminum alloy, and other metals exhibit multiple scabbing. It is not governed to any appreciable degree by direction of rolling texture.

An attempt is made in this paper to establish the mechanics of the generation of these multiple scabs. Experimentally obtained stress data are used as the basis for the discussion.

MECHANICS OF MULTIPLE SCABBING

It was established in the earlier paper[1] that scabbing is governed principally by the spatial distribution of stress within the transient wave and by a critical normal fracture stress that is characteristic of the material under attack. The latter may be influenced by the conditions of loading and the state of stress in the body. An extension of the geometrical considerations, presented in the earlier paper, indicate that multiple scabbing might be expected to occur when the level of stress within the wave that reaches the free surface is more than double the critical normal fracture stress of the material.

Consider the following situation. A high intensity transient compressional stress wave of the form shown in Fig. 2 is moving to the right through a laterally infinite slab of perfectly elastic material and is shortly to impinge upon a free surface as indicated in Fig. 3(A). When the stress wave strikes the free boundary of the plate, it will be reflected as a tension wave. Interference between the incident compression wave and the reflected tension wave causes the plate to scab provided the maximum level of stress is greater than the critical normal fracture stress, σ_c. The thickness, δ_1, of the scab will be given by

$$\delta_1 = x_1/2$$

where x_1 has such a value that

$$\sigma_0 - \sigma(x_1) = \sigma_c$$

i.e., the thickness of the scab will be equal to one-half of the distance within the wave that corresponds to a decrease in stress equal to σ_c. Assume that the fracture is generated instantaneously. The remainder of the wave, i.e., the part of the wave to the right of x_1 in Fig. 2, will suddenly find itself impinging on a freshly created free boundary surface. The result will be the formation of another scab. Conditions leading to forma-

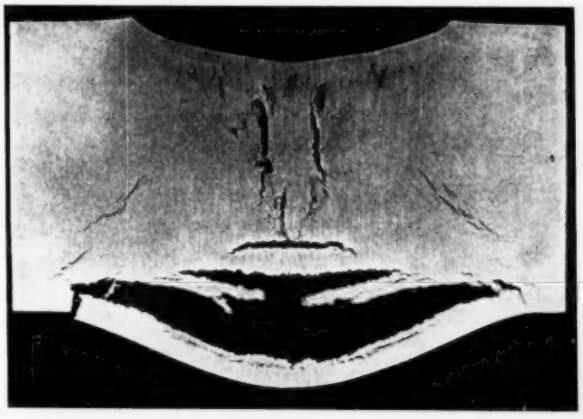

FIG. 1. Photograph of example of multiple scabbing in steel.

* Work supported by Armament Branch, ONR.
[1] J. S. Rinehart, J. Appl. Phys. **22**, 555 (1951).

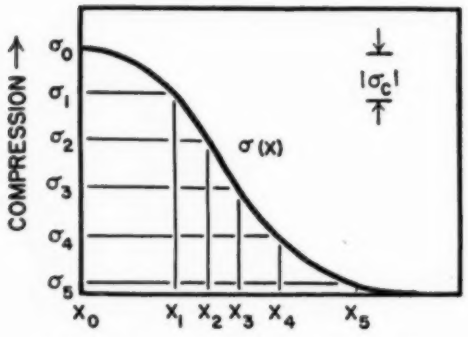

FIG. 2. General form of stress distribution.

tion of the second and third scabs are indicated in the last two drawings of Fig. 3. The thickness, δ_2, of the second scab will be

$$\delta_2=(x_2-x_1)/2$$

where

$$\sigma(x_1)-\sigma(x_2)=\sigma_c.$$

The foregoing process will repeat itself until the stress level of the wave has been reduced to a value less than σ_c. The number of scabs that will be formed will be equal to the first whole number smaller than the quotient σ_0/σ_c.

The relative thicknesses of the several scabs will be governed by the shape of the stress wave, if σ_c is assumed constant. For example, the stress wave shown in Fig. 2 will generate five scabs. The first three are indicated in Figs. 3(A)–(C). The first scab is thick; the next two are thin, and of about the same thickness. The fourth, not shown in the figure, would be relatively thick, and the fifth would be still thicker. It is assumed, of course, that the critical normal fracture stress is not influenced by state of stress. Any effect that state of stress might have on σ_c would modify the picture somewhat.

Quantitative verification of the foregoing suggestions was achieved by experimentally determining stress waves and relating the shapes and intensities of these waves to observed scab thicknesses.

SCHEME FOR OBTAINING STRESS WAVE

The method that has been employed to obtain stress information is similar in principle to that used in previous scabbing studies. The spatial distribution of particle velocities is obtained by observing the velocities with which pellets are impelled from a plate that has been explosively attacked. The stress wave is then constructed from the distribution of particle velocities through use of the relationship

$$\sigma=\rho c v \qquad (1)$$

where σ is the stress at a point in the wave, v is the particle velocity at that point, c is the velocity of the wave, and ρ is the density of the material.

In the previous tests, a small cylinder of explosive was placed on one face of a heavy metal plate and a small pellet of the same material placed on the opposite or rear face in line with the charge. The charge was detonated and velocity of the pellet measured. This procedure was repeated with pellets of different lengths. A new charge and plate were used each time. Usually, the firing of pellets of five different thicknesses provided data sufficient to construct a single stress distribution.

The above method will yield good results provided the intensity of the stress wave is not excessively high. If the intensity of the stress wave is high, the pellet itself may scab. It may also flow plastically since lateral motion is not prohibited. Moreover, the scheme does not permit the determination of the particle velocity (or stress) at the precise place within the plate where scabbing occurs. Rather, the pellet measures the average stress level in an increment of the stress wave as it impinges on the rear face of the plate. This stress is substantially, but not exactly, the same as the spatial distribution of stress within the plate. The difference will not be significant for a low intensity wave which usually decays slowly. The discrepancy will be serious, however, when the decay is rapid as might be the case with a high intensity wave.

The several aforementioned shortcomings were either eliminated or their troublesomeness greatly reduced by modification of the previous experimental arrangement. The modified arrangement is shown schematically in Fig. 4. In the former arrangement, a single pellet was placed on the surface of the rear face of the plate; in the present arrangement, a hole is bored in the rear face of the plate and several pellets are placed in it. It is then assumed that, as far as propagation of the longitudinal compressional stress wave is concerned, the

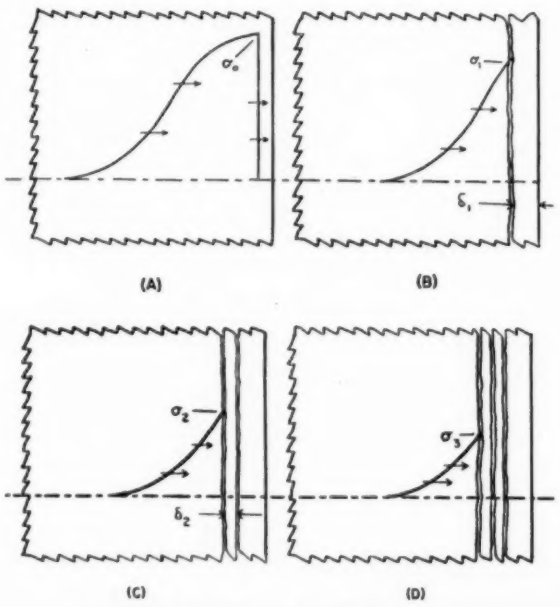

FIG. 3. Multiple scab generation process.

pellets act as though they were integral with the plate. That this assumption appears to be justified was demonstrated experimentally by boring holes to different depths and by using various combinations of pellet thicknesses. In each case, the locations of the respective scabs were not changed. For example, when a single long pellet was placed into a deep hole, the pellet scabbed exactly as though it were part of the plate. It is also to be noted that the hole constrains the pellets so that no lateral motion takes place.

Scabbing of the pellets can be avoided, then, simply through judicious selection of their respective thicknesses. It is only necessary that the pellets be stacked in the hole in such a way that the faces of two pellets will always be in contact at the place where fracturing is expected.

With the arrangement shown in Fig. 4, a single shot can be made to yield data sufficient for the construction of a complete stress or particle velocity distribution. This will be true provided the stress wave has a sharp front that is followed by a monotonous decrease in stress level. Assume that the explosive charge in Fig. 4 has been detonated and that such a compressional stress wave is traveling through the plate toward the group of pellets. Specifically, assume that the spatial distribution of particle velocity, $v(x)$, has the form shown in Fig. 5. The several pellets will remain in contact with one another until the front of the wave is reflected from the right-hand face of pellet No. 1 and returns to the interface between pellets Nos. 1 and 2. At the instant the front of the wave reaches the interface, the velocity of the left-hand face of pellet No. 1 will be equal to the sum, $v(x_0)+v(x_1)$, and, hence, will be greater than the velocity of the right-hand face of pellet No. 2, whose velocity at this instant is only equal to $v(x_1)$. Here, x_1 is equal to twice the thickness of pellet No. 1. The faces will separate because of this velocity differential. The velocity, V_1, with which pellet No. 1 leaves the plate will

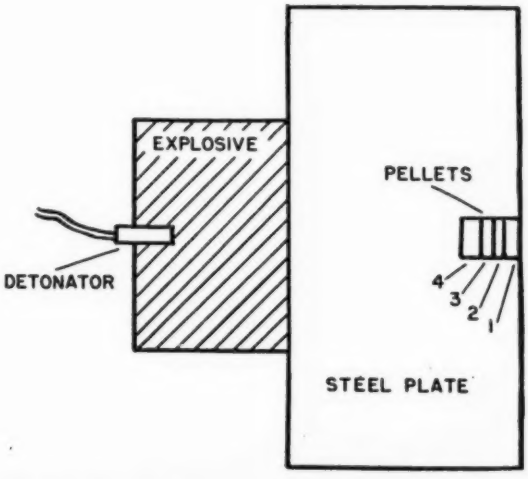

FIG. 4. Experimental arrangement used to obtain stress wave.

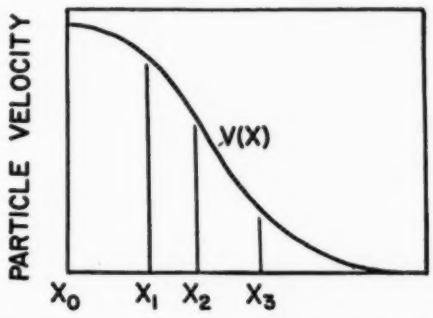

FIG. 5. Assumed spatial distribution of particle velocity.

be given by

$$V_1=\frac{2\int_{x_0}^{x_1} v(x)dx}{x_1-x_0}.$$

By use of similar reasoning, it follows that the velocity of the ith pellet will be

$$V_i=\frac{2\int_{x_{i-1}}^{x_i} v(x)dx}{x_i-x_{i-1}}$$

where x_i is equal to twice the total thickness of all the pellets up to and including the ith pellet. If $v(x)$ is a monotonously decreasing function of x, the velocity of the ith pellet will always be less than that of the $(i-1)$th pellet. The average value of the particle velocity over the interval (x_i-x_{i-1}) will be equal to $\frac{1}{2}V_i$. Thus, if the respective velocities of the several pellets from a single firing are measured, a histogram can be constructed that will approximate rather closely the true spatial distribution of particle velocities in the wave. The front of the stress wave is assumed to be plane and parallel to the faces of the pellets. This condition is reasonably well fulfilled provided the diameter of the pellet is small.

TESTS

Several histograms have been obtained experimentally. An annealed 1020 steel plate 6 in. in diameter and 3 in. thick was used in each test. The diameter and length of the explosive charge were 3 in. and 2 in., respectively. The hole in the rear face of the plate was $\frac{1}{2}$ in. in diameter and about $\frac{3}{4}$ in. deep. The diameter of each pellet was machined to a sliding fit. Pellet thicknesses ranged from 20/64 in. to 5/64 in. In one series of tests, a group of five pellets was fired each time. Their respective thicknesses were 0.218, 0.077, 0.093, 0.109, and 0.312 in. In another series, a group of eight identical pellets, each 0.094 in. thick, were fired. The velocity of each pellet was measured close to the plate over

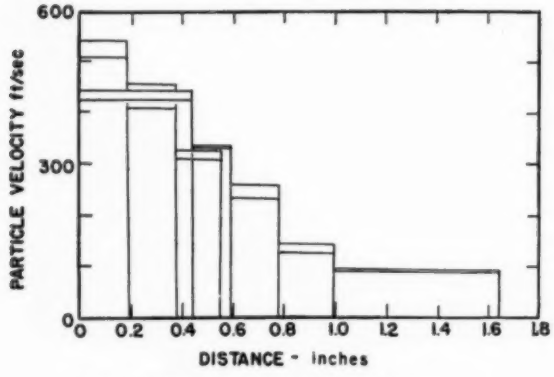

FIG. 6. Experimentally obtained histograms.

about a 3-ft interval by means of special multiflash photography.[2]

Parts of four individual histograms are plotted in Fig. 6 in order to indicate the character of the data that are obtained. Reproducibility from round to round is seen to be good. The increased definition, which results from use of thinner pellets, is particularly evident in the figure. It is also reassuring that the measured velocity of the first thick pellet is close to the velocity that would be predicted by averaging the velocities of the first three thin pellets.

RELATION BETWEEN SCABS AND STRESS WAVES

The spatial distribution of stress within the plate and the thicknesses of the scabs are the experimental data that are needed to determine whether the mechanics of multiple scab formation advanced earlier in this paper are physically realistic. These data will now be examined.

The stress wave, deduced from histographs of the type shown in Fig. 6, is drawn as a smooth curve in Fig. 7. Equation (1) was used to convert particle velocity to stress. The general velocity of sound for waves of dilatation in steel has been found[3] recently to be 234,000 in./sec. This value was used for c in Eq. (1).

The shape of the wave and the magnitudes of the stresses reached in it are such that multiple scabbing is to be expected. The stress rises suddenly and then decays rapidly. The total effective length of the wave as far as scabbing is concerned is about $1\frac{1}{2}$ in. The maximum stress reached is 1,080,000 lb/in.^{2}, a value some five to six times the critical normal fracture stress for steel, and, hence, of about the proper intensity to generate the six scabs that were observed.

The measured thicknesses of the respective scabs agree well with those that would be predicted from the stress wave. Arrows have been placed on Fig. 7 to indicate this agreement. The distance between two successive arrows is equal to twice the thickness of the scab that was generated by the portion of the stress wave contained between the two arrows. It is interesting and significant to note that the scabs are thick in the regions where the slope of the curve is small and are thin in the region where the slope is large.

The difference in stress that corresponds to the distance between successive arrows ought to be equal to the critical normal fracture stress. The following six values of σ_c are obtained from the curve: 220,000, 100,000, 160,000, 160,000, 170,000, and 170,000 lb/in.^{2}. These values, except perhaps for the first two, are in excellent agreement. In fact, in much better agreement than might be expected since the uncertainty in determination of scab thickness could easily introduce an uncertainty of 50,000 lb/in.^{2} in the determination of the critical normal fracture stress from any one scab.

The first value appears to be significantly somewhat higher than the others and the reason for this is not immediately apparent. If, as suggested previously, the critical normal fracture stress is strongly dependent on the state of stress, the effect ought to be apparent in the other values. An inspection of Fig. 7 does not indicate that any strong dependence exists.

A reliable average value for σ_c is obtained by dividing by six the difference between the stress level at the front of the wave and the stress level at the place where the last scab occurred. The value of σ_c found in this way is 160,000 lb/in.^{2}. This value compares favorably with the previous value[1] which ranged from 130,000 lb/in.^{2} to 230,000 lb/in.^{2}.

FURTHER DEMONSTRATION OF VALIDITY OF SCABBING MECHANICS

A rather convincing further demonstration of the general correctness of the foregoing concepts regarding the mechanics of scabbing has been achieved by using a backing plate to reduce the intensity of the reflected stress wave.

The backing plate was simply a solid cylinder of 24S–T4 aluminum alloy of the same diameter as the steel plate. The contact surfaces of the steel and backing

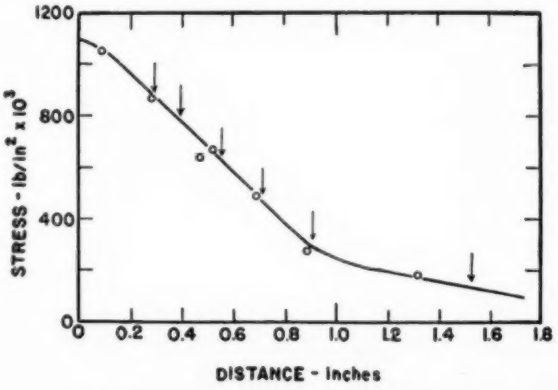

FIG. 7. Stress wave deduced from Fig. 6.

[2] E. C. Barkofsky, "Multiple-image silhouette photography for aeroballistics research," presented at 70th Semi-annual Convention, Society of Motion Picture and Television Engineers, Hollywood, October, 1951.

[3] R. D. Fay and O. V. Fortier, J. Acoust. Soc. Am. 23, 339 (1951).

plate were both ground flat and covered with a light film of oil before being put together in order to insure an acoustically good joint.

The influence of the backing plate on the formation of scabs can be best illustrated by means of a few fairly elementary considerations. Consider a sharp-fronted triangular stress wave, of length λ and maximum amplitude σ_0, that is advancing through the steel toward the backing plate as shown in Fig. 8. As the wave arrives at the boundary, between the two plates, *mn* in Fig. 8, two waves will be generated. One will move toward the left from the boundary and, hence, back into the steel plate, and the other will move into the backing plate. The boundary conditions that must be satisfied during this transformation are (1) continuity of stress and (2) continuity of particle velocity. These conditions must hold for every point on the incident wave. The phase and magnitude of the reflected stress will be governed by the relative values of the specific acoustic resistances, i.e., density times velocity of sound, of the steel plate and the backing plate. If the specific acoustic resistance of the steel plate is greater than that of the backing plate, a compressive stress will be reflected as a tension. This is the only case that will be considered here. The absolute intensity of the reflected stress will, in general, be less than that of the incident stress. The amount of reduction is readily expressible[4] in terms of the respective densities and sound velocities of the steel and backing plate. If σ_I is the stress at a particular point on the incident wave and σ_R the stress at the corresponding point on the reflected wave, the two will be related by the equation

$$\sigma_R = \frac{\rho_S c_S - \rho_B c_B}{\rho_S c_S + \rho_B c_B} \sigma_I$$

where ρ_S and c_S are the density and velocity of sound, respectively, in the steel plate and ρ_B and c_B are those of the backing plate. The velocity of the dilatation wave is the appropriate one to use here. In the present case, the ratio, σ_R/σ_I was calculated to be 0.46.

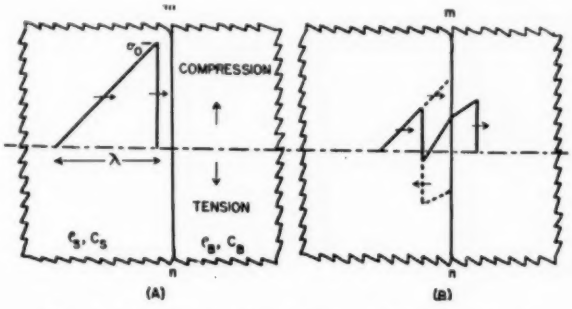

FIG. 8. Diagram showing influence of backing plate.

[4] J. S. Rinehart, Am. J. Phys. **18**, 546 (1950).

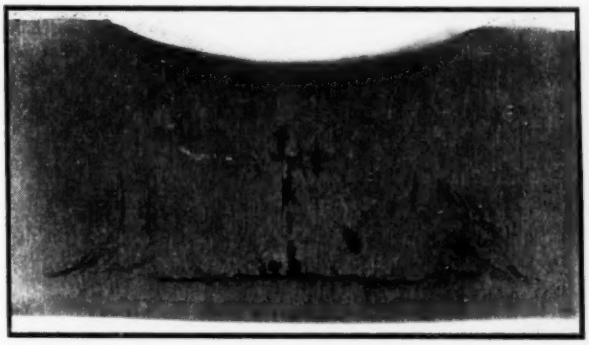

FIG. 9. Photograph of section of steel plate backed by aluminum alloy backing plate.

The backing plate reduces the intensity of the reflected wave. The wave must now travel further back into the steel plate before the plate will scab than would have been the case had no backing plate been used. For the triangular stress wave illustrated in Fig. 8, the thickness of the first scab will be simply increased by the factor σ_I/σ_R. In practice, the stress waves are usually not triangular and the effect of the backing plate must be studied graphically. The first scab will occur at the place in the plate where the difference, $(\sigma_R/\sigma_I)\sigma_0 - \sigma(x_1)$, is equal to σ_c.

Once the first scab has formed, the locations and thicknesses of additional scabs will not, of course, be further influenced by the backing plate.

The foregoing suggestions concerning the probable effect of a backing plate on scabbing have been substantiated experimentally. The influence of the aluminum alloy backing plate is illustrated in Fig. 9. Only two instead of six scabs were formed. The predicted locations of the two scabs agree within accuracy of measurement to observed locations.

CONCLUSIONS

The mechanics of the generation of multiple scabs by very high intensity transient compressional stress waves has been treated in this paper. Specifically, it has been demonstrated that multiple scabbing will occur whenever the maximum level of stress, σ_0, within the wave is more than twice the critical normal fracture stress, σ_c, of the material. The number of scabs that will be formed will be equal to the first whole number smaller than the quotient σ_0/σ_c. The relative thicknesses of the several scabs is found to be governed by the shape of the stress wave.

In conclusion, the author wishes to acknowledge the help of Mr. J. Craig McLaughlin who conducted the tests. Mr. John Pearson reviewed the manuscript and made numerous helpful suggestions.

Thermal Stresses in a Partially Clamped Elastic Half-Plane

J. H. HUTH
The Rand Corporation, Santa Monica, California
(Received June 9, 1952)

Numerical methods, such as those of Southwell, have made amenable to approximate analysis a large class of problems in the theory of elasticity. However, certain loadings must occasionally be considered which may give rise to theoretical stress singularities. In such cases an analytical study, at least in the immediate neighborhood of the singularities, would appear to be mandatory.

One such problem is that of determining the thermal stresses in a partially clamped elastic half-plane. The solution given in this paper assumes self-equilibrating tractions over the clamped portion of boundary so that the results apply approximately also to large finite areas.

I. INTRODUCTION

MODERN numerical methods[1] have proven to be extremely useful in treating a large class of problems in plane stress and strain. However, whenever stress singularities may be present an analytical investigation is highly desirable, at least to serve as a guide for the numerical work. Knein[2] and Sadowsky,[3] among others, have treated problems of this type.

One further problem in plane strain which exhibits such singularities, and which is worthy of considerable attention, is that of determining the thermal stresses in a partially clamped elastic half-plane. Practically, the semi-infinite half-plane may be replaced by a large homogeneous mass with a relatively rigid plate welded to a portion of the boundary.

II. ANALYTICAL FORMULATION

Consider the partially-clamped lower half-plane as shown in Fig. 1, and set the problem to be one of plane strain. A perfectly rigid plate is attached to the boundary as illustrated. This attachment is assumed free to move up and down, but prevents any lateral contraction or expansion along the juncture. Under these conditions a uniform change in temperature of the elastic media will result in the following boundary conditions: (They may be derived by first considering the elastic half-plane to be free to expand, and then imposing suitable displacements to permit re-attachment of the plate)

$$\left.\begin{aligned} u&=\epsilon x \\ v&=C \end{aligned}\right\} \quad |x|\leq| \quad y=0, \qquad (1)$$

$$\sigma_y=\tau_{xy}=0 \quad |x|>| \quad y=0.$$

Of course ϵ is proportional to the temperature increment.

Complex stress functions may be introduced in the usual fashion as follows:[4]

$$\begin{aligned} &\sigma_x+\sigma_y=2[\Phi(Z)+\overline{\Phi(Z)}] \\ &\sigma_y-\sigma_x+2i\tau_{xy}=2[\bar{Z}\Phi'(Z)+\Psi(Z)] \end{aligned} \qquad (2)$$

$$2\mu(u+iv)=K\varphi(Z)-Z\overline{\varphi'(Z)}-\overline{\psi(Z)},$$

where

$$\varphi(Z)=\int\Phi(Z)dZ \quad \text{and} \quad \psi(Z)=\int\Psi(Z)dZ.$$

Following Muskhelishvili,[5] the stress function Φ will be extended to the upper half-plane by means of the equation:

$$\Phi(Z)=-\overline{\Phi(\bar{Z})}-Z\overline{\Phi'(\bar{Z})}-\overline{\psi(\bar{Z})} \quad Z(S^+. \qquad (3)$$

Then $\Psi(Z)$ may be expressed in terms of $\Phi(Z)$ defined in the entire plane.

$$\Psi(Z)=-\Phi(Z)-\overline{\Phi(\bar{Z})}-Z\Phi'(Z) \quad Z(S^-. \qquad (4)$$

The components of stress and displacement may now be expressed in terms of a single stress function. In

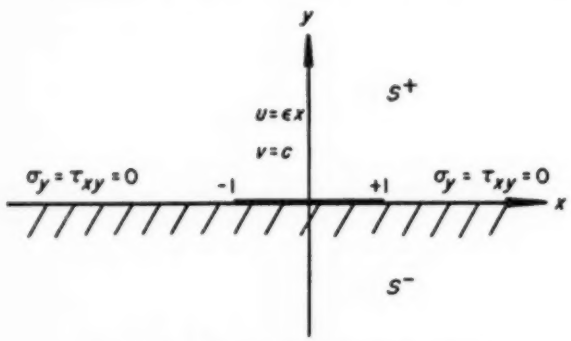

FIG. 1. Coordinate system used in analysis.

[1] J. H. Huth, "Net-point methods in solid and fluid mechanics," Ph.D. dissertation (Stanford University, June, 1950).
[2] M. Knein, "Zur Theorie des Druckversuchs," Abhandlung aus dem Aerodynamischen Institut an der Technischen Hochschule Aachen 7, 43–62 (1927).
[3] M. Sadowsky, Z. Angew. Math. Mech. 8, 107–121 (1928).
[4] J. A. Joseph and J. S. Brock, J. Appl. Mech. 17, 353–358 (1950).
[5] N. I. Muskhelishvili, "Singular integral equations," (Tiflis, U. S. S. R., 1946), second edition. [Commonwealth of Australia, Department of Supply and Development, Aeronautical Research Laboratories, Translation No. 12, February 1949.]

particular:

$$\sigma_y - i\tau_{xy} = \Phi(Z) - \Phi(\bar{Z}) + (Z-\bar{Z})\overline{\Phi'(Z)}$$
$$2\mu\left(\frac{\partial u}{\partial x} + i\frac{\partial v}{\partial x}\right) = K\Phi(Z) + \Phi(\bar{Z}) - (Z-\bar{Z})\overline{\Phi'(Z)}. \quad (5)$$

The reason for the form of Eq. (3) is now clear. It represents an analytical continuation of Φ across the unstressed portions of the x axis. Consequently the problem reduces to finding a function Φ which is analytic in the entire plane cut along the x-axis from -1 to $+1$. The "cut" condition becomes:

$$\Phi^+ + K\Phi^- = 2\mu\epsilon \quad y=0 \quad -1 \leq x \leq +1. \quad (6)$$

If it is required that all stresses and rotations vanish at infinity, and further that the surface tractions on the plate be self-equilibrating, then it can be shown that Φ must be of the order of $1/Z^2$ for very large Z. This fact, together with Eq. (6), determines Φ.

III. SOLUTION

It is convenient to first find a nontrivial solution of the following homogeneous problem: (For convenience in the following, Poisson's ratio is taken $=\frac{1}{4}$)

$$X^+ + 2X^- = 0 \quad y=0 \quad -1 \leq x \leq +1. \quad (7)$$

This may be done in the following steps:

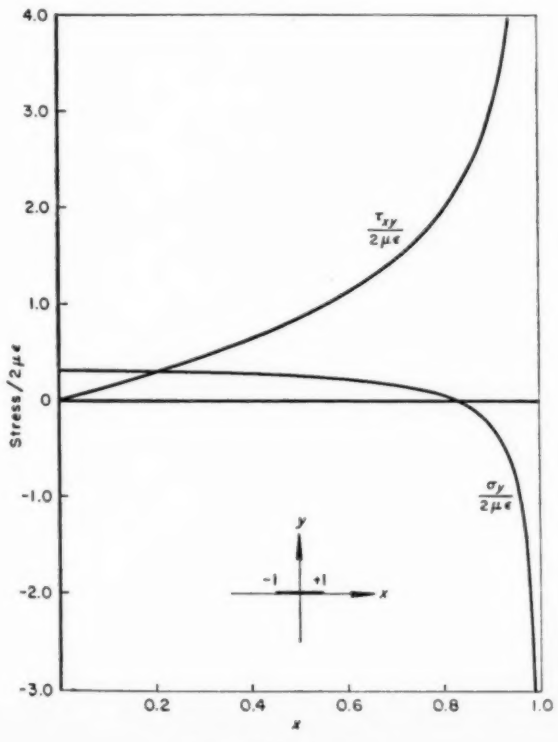

FIG. 2. Plate stresses.

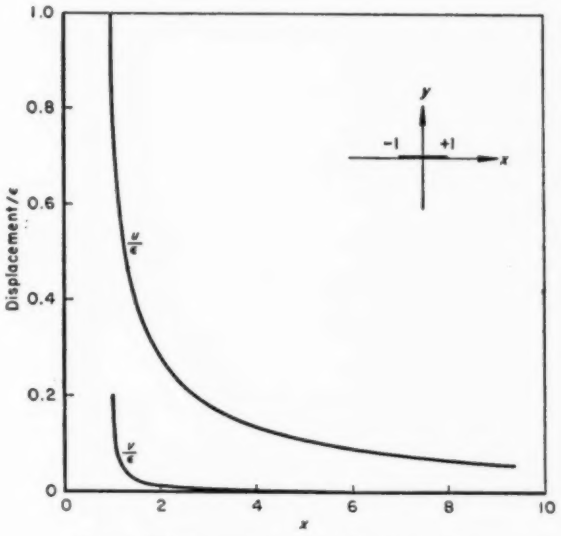

FIG. 3. Displacements of the free boundary.

1. $[\ln X]^+ - [\ln X]^- = \ln(-2)$;

2. By use of the Plemelj formula (see either Muskhelishvili[5] or Kellog[6]),

$$\ln X = \frac{1}{2\pi i}\int_{+1}^{-1} \frac{\ln(-2)dt}{(t-Z)}.$$

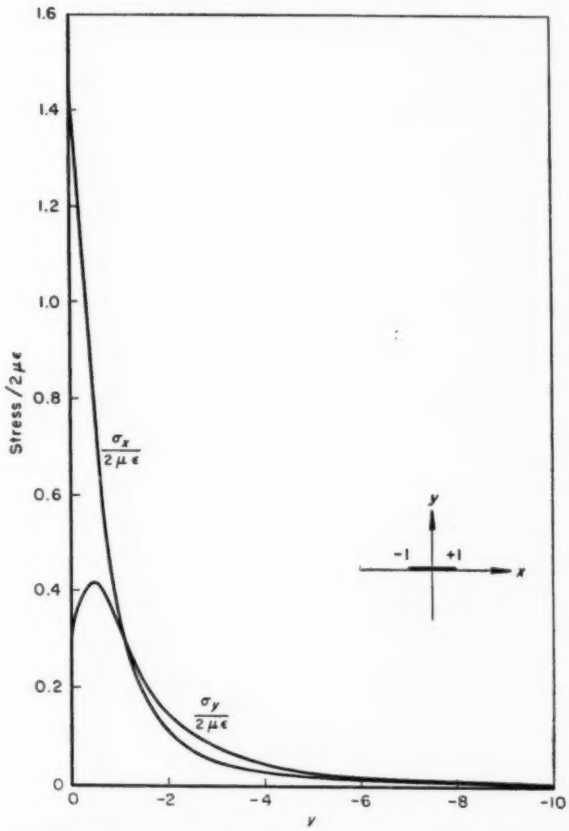

FIG. 4. Stress in the half-plane as a function of depth.

[6] O. D. Kellogg, *Foundations of Potential Theory* (Ungar Publishing Company, New York, 1929), pp. 160–168.

The line integral may be evaluated by relating it to a contour integral taken clockwise around the cut, and then suitably deforming the path. The resulting function vanishing at infinity will be called the fundamental solution, and is given by:

$$X=\frac{[(Z+1)/(Z-1)]^{\ln 2/2\pi i}}{(Z^2-1)^{\frac{1}{2}}}. \tag{8}$$

The inhomogeneous problem [Eq. (6)] can now be treated quite simply. The procedure is as follows:

1. Since $X^+ + 2X^- = 0 \quad 2 = -X^+/X^-$.
2. Therefore $(\Phi/X)^+ - (\Phi/X)^- = 2\mu\epsilon/X^+$.
3. Again, using the Plemelj formula,

$$\Phi=\frac{\mu\epsilon}{\pi i}\frac{[(Z+1)/(Z-1)]^{\ln 2/2\pi i}}{(Z^2-1)^{\frac{1}{2}}}\times\int_{+1}^{-1}\frac{(t^2-1)^{\frac{1}{2}}dt}{(t-Z)[(t+1)/(t-1)]^{\ln 2/2\pi i}}+\frac{C_0[(Z+1)/(Z-1)]^{\ln 2/2\pi i}}{(Z^2-1)^{\frac{1}{2}}}.$$

The integral occuring in step 3 may be evaluated by relating it to a contour integral as indicated previously. The functions $[(Z+1)/(Z-1)]^{\ln 2/2\pi i}$ and $(Z^2-1)^{\frac{1}{2}}$ are assumed to approach 1 and Z, respectively, as Z becomes large, and care must be taken to remain at all times on the proper Riemann surface.

Finally Φ is given by the expression:

$$\Phi=\left\{C_0+\frac{\mu\epsilon\ln 2}{3\pi i}\right\}\frac{[(Z+1)/(Z-1)]^{\ln 2/2\pi i}}{(Z^2-1)^{\frac{1}{2}}}+\frac{2\mu\epsilon}{3}\left\{1-\frac{Z}{(Z^2-1)^{\frac{1}{2}}}\left(\frac{Z+1}{Z-1}\right)^{\ln 2/2\pi i}\right\}. \tag{9}$$

The constant C_0 may be evaluated from the restriction on the behavior of Φ near infinity, and will be found to be equal to $\mu\epsilon\ln 2/2\pi i$.

Consequently, displacements and tractions of interest may now be found by substituting (9) into (2). The results are summarized by the following formulas and Figs. 2–4 (Poisson's ratio $=\frac{1}{4}$).

$$-1\le x\le 1,\ y=0:\quad \sigma_y=+2\mu\epsilon\left(\frac{2}{1-x^2}\right)^{\frac{1}{2}}\left\{\frac{\ln 2}{\pi}\cos\ln\left(\frac{1+x}{1-x}\right)^{\ln 2/2\pi}-x\sin\ln\left(\frac{1+x}{1-x}\right)^{\ln 2/2\pi}\right\}$$

$$\tau_{xy}=-2\mu\epsilon\left(\frac{2}{1-x^2}\right)^{\frac{1}{2}}\left\{x\cos\ln\left(\frac{1+x}{1-x}\right)^{\ln 2/2\pi}+\frac{\ln 2}{\pi}\sin\ln\left(\frac{1+x}{1-x}\right)^{\ln 2/2\pi}\right\}$$

$$1\le x\le\infty,\ y=0:\quad u=\epsilon\left[x-(x^2-1)^{\frac{1}{2}}\cos\ln\left(\frac{x+1}{x-1}\right)^{\ln 2/2\pi}\right]$$

$$v=\epsilon\left\{(x^2-1)^{\frac{1}{2}}\sin\ln\left(\frac{x+1}{x-1}\right)^{\ln 2/2\pi}-\frac{\ln 2}{\pi}\right\}$$

$$x=0,\ -\infty\le y\le 0:\quad \sigma_y=\frac{-2\mu\epsilon}{3}\left\{\frac{2y}{(y^2+1)^{\frac{1}{2}}}\frac{1}{2^{\beta/2\pi}}\left[\frac{1+(\ln 2/\pi)^2}{y^2+1}\right]+\frac{1}{2^{(1/2\pi)(\beta+4\alpha)}}\left[\frac{y}{(y^2+1)^{\frac{1}{2}}}(2^{2\alpha/\pi}-2)-\frac{\ln 2}{\pi}\frac{1}{(y^2+1)^{\frac{1}{2}}}(2^{2\alpha/\pi}+2)\right]\right\} \tag{10}$$

$$\sigma_x=\frac{8\mu\epsilon}{3}\left\{1+\frac{y}{y^2+1}\frac{1}{2^{\beta/2\pi}}+\frac{\ln 2}{\pi}\frac{1}{(y^2+1)^{\frac{1}{2}}}\frac{1}{2^{\beta/2\pi}}\right\}-\sigma_y$$

$$\tau_{xy}=0 \qquad \beta=\tan^{-1}\frac{2y}{y^2-1} \qquad \alpha=-\tan^{-1}y.$$

IV. CONCLUSIONS

Of particular interest are the essential singularities resulting at the tips of the plate, and also the vertical deflection of the plate given by $\epsilon\ln 2/\pi$. It would seem that the results also hold approximately for finite square cross sections providing that the sides are at least of the order of ten times the width of the plate.

The values of σ_y and σ_x along the line of symmetry are, of course, of the order of $1/y^2$ for large depths.

It is worth noting that the results shown in Fig. 2

are in general agreement with a purely numerical solution of a very similar problem treated earlier by the author.[1]

The author wishes to express his appreciation to the Rand Corporation for assistance in preparing the manuscript and graphs, and to Dr. J. N. Goodier for several helpful criticisms of the manuscript.

SYMBOLS

u, v	Components of displacement in x and y directions, respectively.
C	Constant.
ϵ	Constant of proportionality between temperature and displacement.
σ_x, σ_y	Normal stresses in the x and y directions, respectively.
τ_{xy}	Shearing stress.
Z	Complex variable $Z=x+iy$.
$\Psi, \Phi, \varphi, \psi$	Complex stress functions.
K	$(\lambda+3\mu)/(\lambda+\mu)$.
λ, μ	Lame's constants.
S	Designates upper or lower half-plane depending on superscript.
x, y	Cartesian coordinates.
X	Fundamental solution.
t	Variable running along the x axis from $+1$ to -1.

SUPERSCRIPTS

$+$	Upper half-plane.
$-$	Lower half-plane.
$\overline{\quad}$	Complex conjugate.
$'$	Differentiation with respect to the independent variable.

JOURNAL OF APPLIED PHYSICS VOLUME 23, NUMBER 11 NOVEMBER, 1952

Development of Porosity during Diffusion in Substitutional Solid Solutions*

R. W. Balluffi and B. H. Alexander†
Atomic Energy Division, Sylvania Electric Products Inc., Bayside, New York

(Received May 5, 1952)

A metallographic study was made of the diffusion zones present in copper-α-brass, copper-nickel, and gold-silver diffusion couples. Usual sandwich type couples and also vapor-solid type couples in which the higher vapor pressure component was diffused either into or out of the couple through the vapor phase were investigated. Significant porosity was always generated by diffusion in the sandwich couples and also in the vapor-solid couples when the higher vapor pressure component was diffused out of solid solution. Upon inward diffusion from the vapor porosity formed in the gold-silver couples but not in the copper-α-brass or copper-nickel couples.

It is concluded that porosity may form in any alloy system when the components diffuse at different rates and that it may cause appreciable error in the measurement of diffusion coefficients if ignored.

INTRODUCTION

WHEN zinc is removed from brass by heating it in vacuum, a porous structure results. When zinc is removed from brass by diffusion into pure copper, a porous structure also results. This latter fact has been largely overlooked in diffusion studies and no one has considered it important enough to affect diffusion measurements.‡

Smigelskas and Kirkendall[1] note a tendency for pitting to occur in the diffusion zone of copper-α-brass couples, and daSilva and Mehl[2] report slight porosity in this system and also in copper-aluminum diffusion couples. They suggest a possible degeneracy of the structure. In the present work we demonstrate the reality of the porosity that develops during diffusion in various alloy systems and in various types of samples. We conclude that it is a general effect and that it cannot be overlooked in the exact analysis of diffusion data.

The experiments described below fall into three different groups. In the first we have made a quantitative study of the rate of porosity formation in alpha-brass during dezincification. Our purpose here was to show that the diffusion coefficients calculated from such data are the same as those obtained in the customary manner using sandwich type diffusion couples, and furthermore, it was desired to see what fraction of the zinc that left the brass resulted in the formation of porosity.

In another group of experiments we made a metallographic study of the porosity that develops in sandwich type diffusion couples in order to demonstrate that it is the same in amount and appearance (after the same degree of diffusion) as that found in the dezincification experiments.

In the third group of experiments we made a metallographic study of the diffusion zone after diffusing various metals from the vapor phase into the solid

* This work was sponsored by the AEC and was done under Contract AT-30-1 GEN-367.

† Now at Boston Electronics Division, Sylvania Electric Products Inc., Boston, Massachusetts.

‡ Since the completion of this manuscript Buckle and Blin[10] have described such porosity in Cu/brass and 7 percent Al-93 percent Cu/Cu couples. Their work directly confirms a number of conclusions of the present paper.

[10] H. Buckle and J. Blin, J. Inst. Metals **80**, 385 (1952).
[1] A. Smigelskas and E. Kirkendall, Trans. Am. Inst. Mining Engrs. **171**, 130 (1947).
[2] L. C. C. daSilva and R. F. Mehl, J. of Metals **191**, 155 (1951).

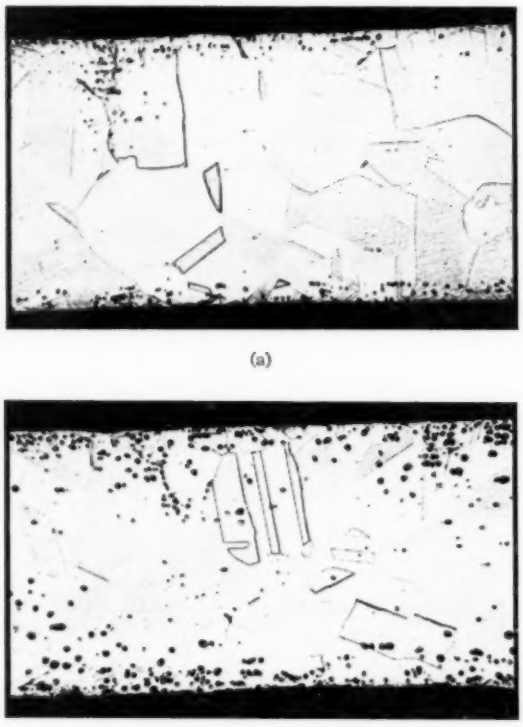

(a)

(b)

FIG. 1. Porosity developed by dezincifying α-brass in vacuum (specimens etched—55×). (a) dezincified 5 hr at 700°C. (b) dezincified 20 hr at 700°C.

phase. In this case we were trying to determine whether any porosity at all occurred.

EXPERIMENTAL

A. Porosity Developed by Evaporation of One Metal from a Solid Alloy

A series of polycrystalline 0.025-in. thick, high purity 70/30 brass sheet specimens were dezincified in a vacuum of 10^{-4} mm of mercury at 700°, 800°, and 900°C for various times. Typical structures after treatment at 700°C are shown in Figs. 1 and 2. As diffusion proceeds, the porous region extends further into the specimen while individual holes increase in size. The holes (shown in the unetched condition in Fig. 2) initially form as polyhedra which eventually round off.

A number of single crystal α-brass specimens were similarly dezincified in vacuum, and metallographic examination showed that the resulting porosity was very similar to the porosity generated in the polycrystalline material. Some preferential formation of pores occurred at a very few grain boundaries in the polycrystalline material but it was estimated that this phenomenon could not have had any significant effect upon the rate of zinc loss from the sheets.

The weight loss from polycrystalline sheets was measured as a function of time at three different temperatures, Fig. 3, and the curves are parabolic, as

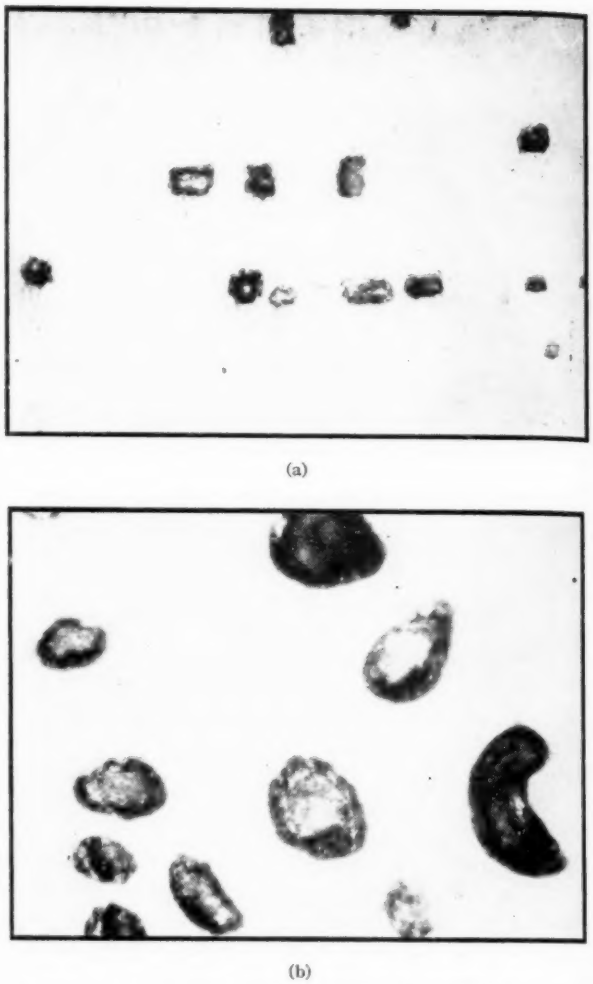

(a)

(b)

FIG. 2. Porosity developed in α-brass dezincified in vacuum (specimens not etched—800×). (a) dezincified 5 hr at 700°C. (b) dezincified 64 hr at 700°C.

expected, but deviate at high weight losses due to depletion of zinc throughout the sheets. In these experiments loss of copper by evaporation was found to be negligible. The chemical diffusion coefficient

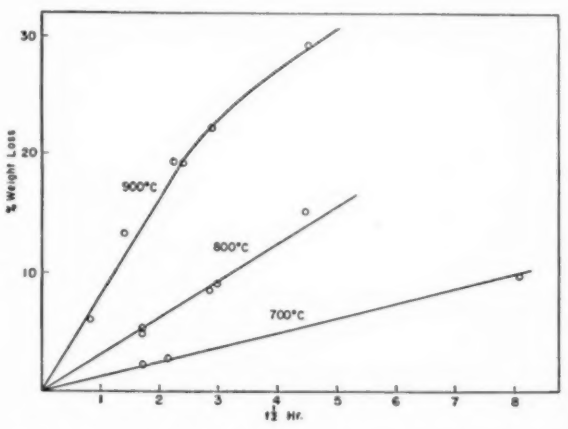

FIG. 3. Percent weight loss *vs* (time)$^{\frac{1}{2}}$ during dezincification of α-brass in vacuum at 700°, 800°, and 900°C.

TABLE I. Chemical diffusion coefficients for alpha-brass.

	700°C	800°C	900°C
D(cm²/sec) This investigation	4×10^{-10}	2×10^{-9}	1×10^{-8}
D(cm²/sec) Average value from reference 4	5×10^{-10}	2×10^{-9}	6×10^{-9}

at each temperature was calculated from these data by assuming that the diffusion coefficient does not depend upon concentration and by using the method described in detail by Jenkins.[3] These values are given in Table I and agree reasonably well with values obtained by other investigators and recently reviewed by Kubaschewski.[4]

The evaporation method for measuring diffusion coefficients has been previously criticized because of possible effects of surface contamination and excessive zinc loss by surface diffusion or vapor transport along any holes or cracks present.[3–5] However, the most recent data obtained by evaporation methods for the case of brass (Jenkins[3] and the present work) agree quite well with data obtained from solid couples. The correlation is taken as evidence that loss of zinc during vacuum dezincification occurs by diffusion.

The average porosity in the dezincified specimens was calculated from density measurements and in Fig. 4 we show the porosity plotted against the weight loss. For comparison we have calculated the maximum porosity that could be obtained assuming that all of the zinc which was removed resulted in the formation of porosity and that the volume of the pores was equal to the volume of zinc removed; this is the upper curve in Fig. 4. The difference between the two curves represents either the volume of pores that were filled by the counter diffusion of copper or, if no copper diffused, the volume of pores that were removed by a sintering process. Figure 4 illustrates the important

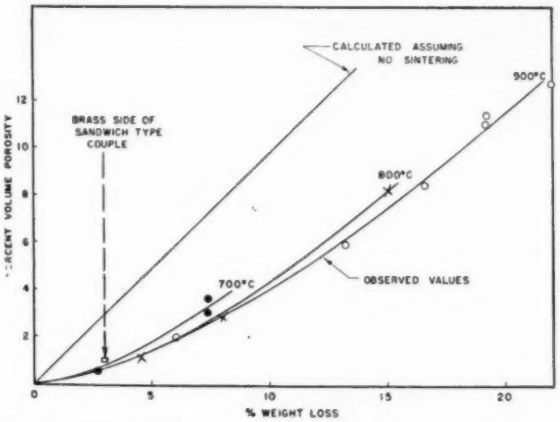

FIG. 4. Percent porosity *vs* percent weight loss during dezincification of α-brass in vacuum at 700°, 800°, and 900°C.

[3] I. Jenkins, J. Inst. Metals **73**, 641 (1947).
[4] O. Kubaschewski, Trans Faraday Soc. **46**, 713 (1950).
[5] R. F. Mehl, Trans. Am. Inst. Mining Engrs. **122**, 11 (1936).

(a)

(b)

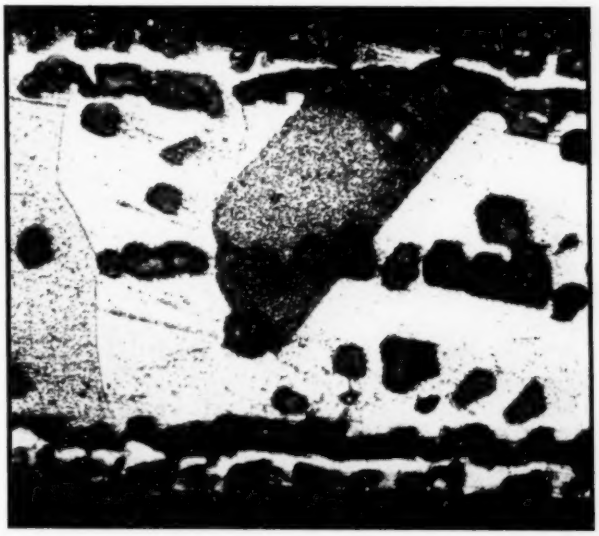

(c)

FIG. 5. (a) 50–50 weight percent silver-palladium foil desilverized in vacuum 60 hr at 1100°C (400×), (b) Surface region of 50–50 wieght percent copper-nickel alloy heated in vacuum 19 hr at 1075°C (150×), (c) 75 weight percent silver gold-silver foil desilverized in vacuum 2 hr at 940°C (250×).

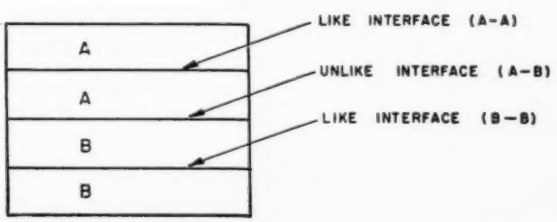

FIG. 6. Schematic diagram of multiple sandwich-type couples made of two different metals, *A* and *B*.

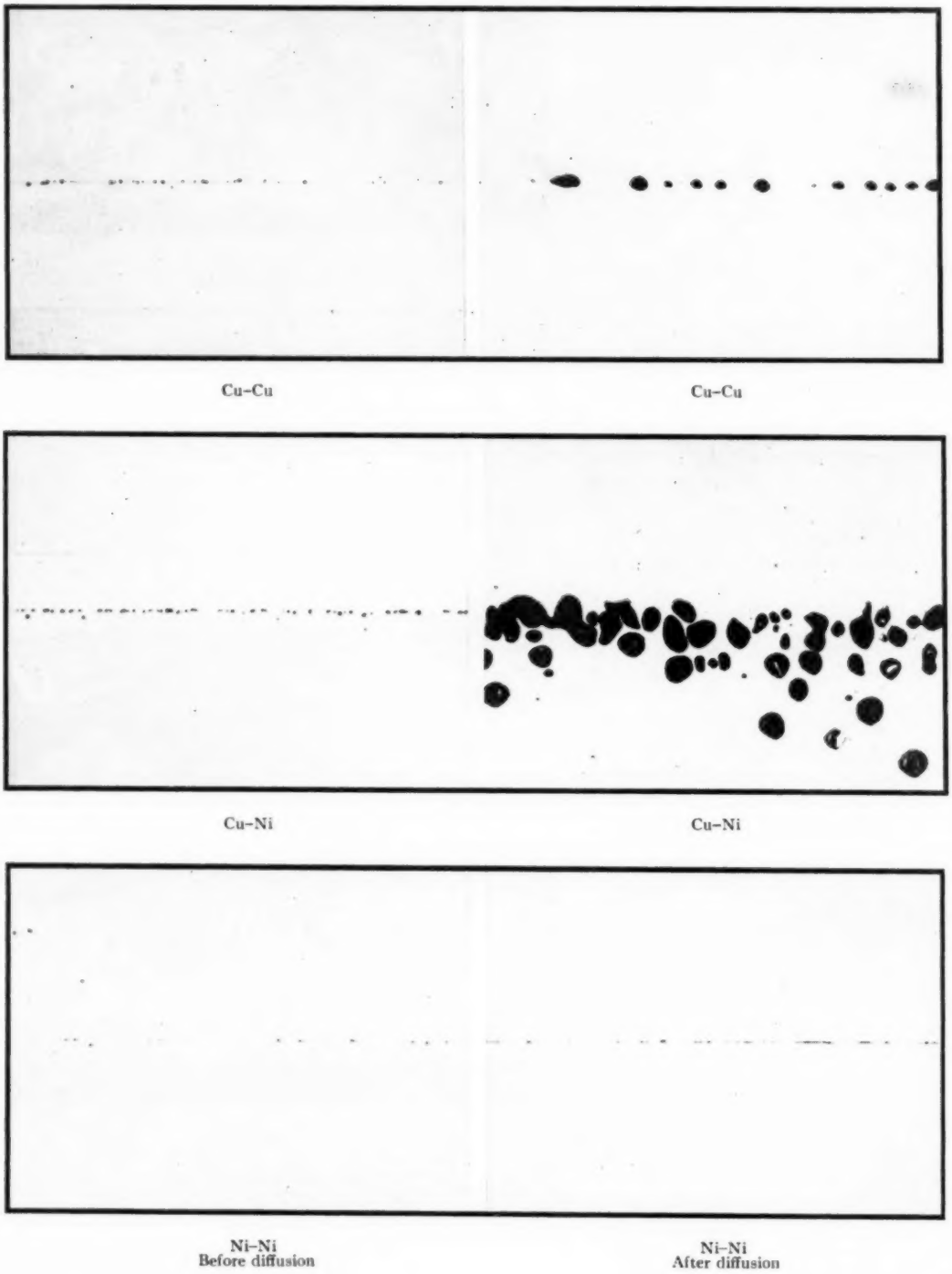

FIG. 7. Structures developed at copper-copper, copper-nickel, and nickel-nickel interfaces before and after diffusion for 239 hr at 1055°C in hydrogen (unetched—80×). At the unlike interfaces the copper is shown at the bottom of the photomicrograph.

fact that a relatively large portion of the maximum possible porosity actually remains in the brass. For instance, at 10 percent weight loss of zinc about 40 percent of the maximum possible porosity remained in the specimen.

Porosity was observed qualitatively in other systems by evaporating copper from solution in a copper-nickel alloy, silver from solution in a silver-gold alloy, and silver from solution in a silver-palladium alloy in vacuum. Figure 5 shows the porosity resulting from these treatments.

B. Porosity Developed in Sandwich Type Diffusion Couples

Sandwich type Cu-α-brass, Cu-Ni, and Ag-Au diffusion couples were prepared by welding approximately $\frac{1}{4}$-in. thick and 1-in. diameter disks together under

pressure at elevated temperatures. In the case of Cu-Ni and Ag-Au multiple sandwiches were made containing *A–A*, *A–B*, and *B–B* interfaces, as shown in Fig. 6.

Multiple interfaces were made so that porosity developed directly by the diffusion process could be distinguished from any possible porosity arising from other causes (e.g., poor bonding, the gas atmosphere, etc.). If porosity appears only in the diffusion zone at unlike interfaces it is safe to attribute the porosity to diffusional effects alone. High purity materials were used and provision was made for preheating and welding the disks in hydrogen, thus insuring clean oxide-free interfaces. After pressure welding, a portion of each sandwich was removed for metallographic examination of the welded interfaces, and the remainder was diffusion-annealed. After diffusion, all specimens were again sectioned and the annealed interfaces were examined metallographically. Diamond dust was used as an abrasive in order to reduce smearing of the surface during polishing, and the structures were examined both before and after etching to eliminate any possibility of etch pitting or preferential etching at the welded interface.

The three interfaces in the Cu-Ni sandwich are shown both after welding and after diffusion in Fig. 7. Considerable porosity has obviously been generated in the Cu-rich side of the diffusion zone. Diffusion sufficient to produce slight porosity has already occurred during the pressure-welding operation (15 min at 1040°C). At the like interfaces, the only effect of the diffusion anneal was to spheroidize and slightly enlarge the fine pores which were present along the joint after pressure-welding these sandwiches. Since appreciable porosity is only generated at the unlike interface such porosity must be a direct result of diffusion.

The porosity developed in the Cu-Ni diffusion zone is shown etched in Fig. 8. The holes are undoubtedly present in the structure and are not a result of etch-pitting or other surface phenomena.

Similar structures were obtained before and after diffusion in the Au-Ag system. The series of interfaces in these sandwiches after welding and also after diffusion are shown in the etched condition in Fig. 9. Again in this case, noticeable diffusion occurred during the welding operation and some porosity developed before the diffusion anneal. A Cu-α-brass interface after diffusion is shown etched in Fig. 10. In all of these couples the porosity formed only on one side of the boundary between the two halves of the couple. This, of course, is the interface which would be defined by inert markers originally placed at the original join and which we have termed the "original moving Kirkendall interface."

The porosity is undoubtedly generated within the diffusion zone and does not depend upon the presence of nearby surfaces, since a sandwich type Cu-α-brass couple only 0.055-in. thick showed the same amount of porosity as a 0.750-in. thick couple after the same amount of diffusion.

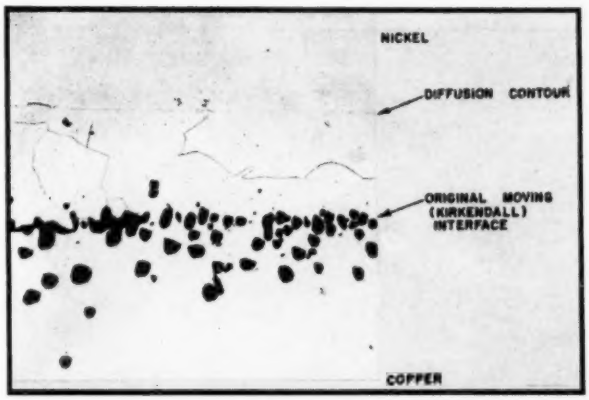

FIG. 8. Porosity developed in copper side of solid copper-nickel couple after diffusion for 239 hr at 1055°C in hydrogen (about 46×).

The average volume percent of porosity remaining in the brass side of the diffusion zone of the couple shown in Fig. 10 was found to be about 1 percent by lineal analysis. Since about 3 percent of the zinc was removed from this volume by diffusion into the Cu side, the remaining porosity was equivalent in volume to about one-third of the zinc lost by diffusion. This one result can be compared to the experimental curve of Fig. 4, and it can be seen that the porosity was approximately the same in the dezincified samples as it was in the sandwich type diffusion couples after the same percentage of zinc was removed.

It can be seen above that porosity appears in α-brass when zinc is removed either by evaporation into vacuum or by diffusion into copper. No matter where the zinc goes, it apparently moves out of the brass by diffusion and leaves voids behind. One is tempted to say that this is a direct result of the unequal diffusion rates of copper and zinc in α-brass and that zinc atoms which diffuse outward are replaced not by copper atoms but by lattice vacancies which may precipitate to form microscopic voids. These voids may subsequently be removed by a sintering process, but presumably the sintering process is slower than the diffusional process of forming voids. There is a slight temperature effect, however, as can be seen from the curves in Fig. 4 where the lower the temperature the greater the porosity for a given weight loss.

C. Inward Diffusion in Solid-Vapor Couples

Polycrystalline and single-crystal copper specimens $\frac{1}{4}$-in. thick and 1-in. diameter were zincified with zinc vapor from a large reservoir of fine α-brass chips. A concentration of approximately 26 weight percent zinc was maintained on the specimen surface during diffusion. After diffusion no porosity was found in any part of the diffusion zone (Fig. 11(a)). Nickel was similarly exposed to copper vapor from a source of pure

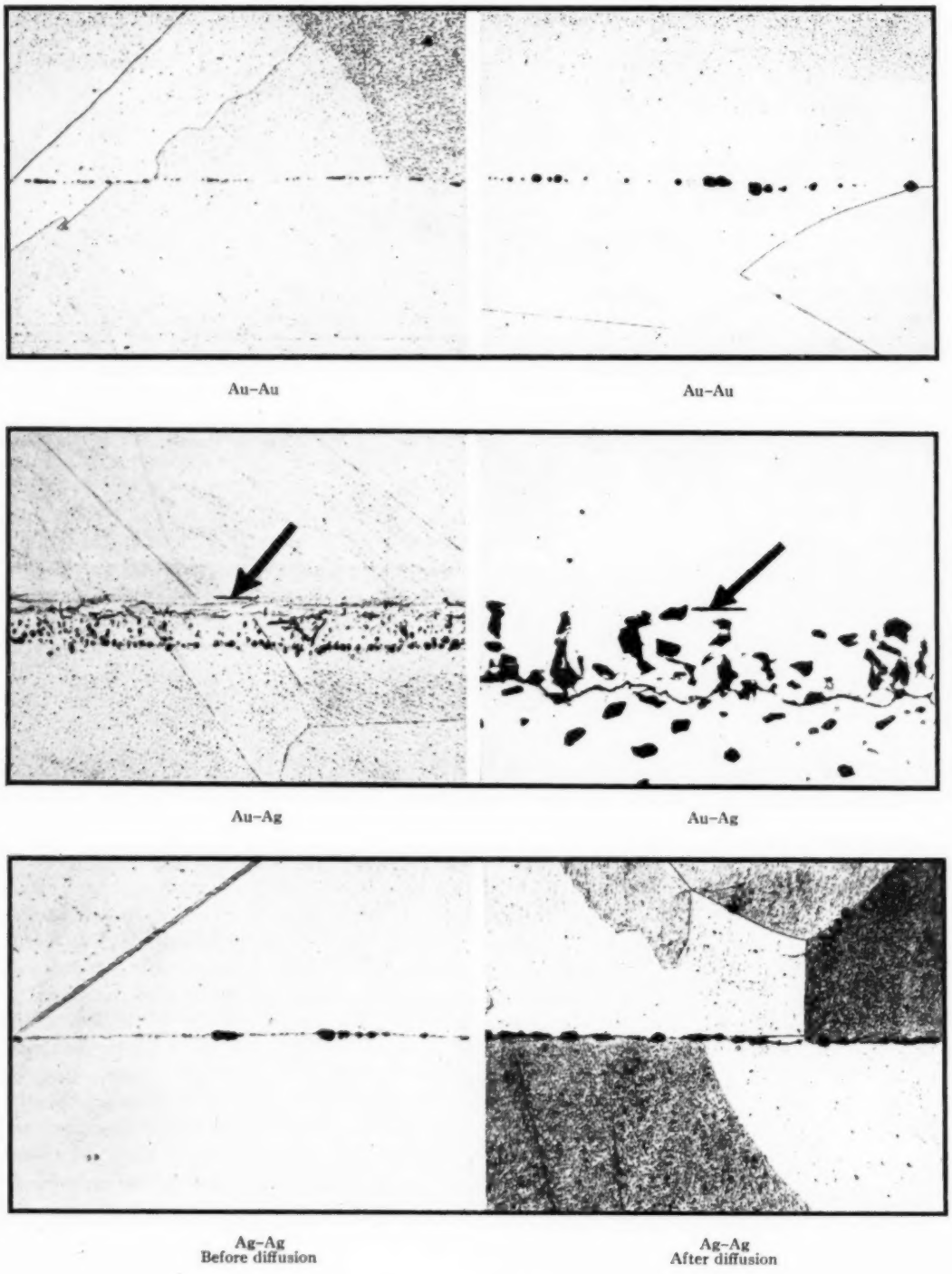

FIG. 9. Structures developed at gold-gold, gold-silver, and silver-silver interfaces after diffusion at 920°C for 44 hr in argon (etched—160×). At the unlike interfaces the silver is shown at the bottom of the photomicrograph. The arrows indicate the position of the original moving (Kirkendall) interface.

copper, and a surface concentration of approximately 80 percent copper was maintained during the inward diffusion of copper. No porosity was developed by this treatment (Fig. 11(b)).

In the case of diffusion of silver into gold from the vapor phase, a surface concentration of about 92 weight percent silver was maintained. A band of holes was always found a small distance from the specimen surface (Fig. 12). This porous region appeared after using both single crystal and polycrystalline gold exposed to silver vapor from reservoirs of both single crystal and polycrystalline silver. This experiment indicates that the porosity could not be caused by unequal rates of silver evaporation between the reservoir and specimen brought about by grain size differences.[6]

[6] W. Rosenhain and D. Ewen, J. Metals 3, 1949 (1912).

The diffusion penetration curve obtained by chemical analysis exhibited no abnormality near the porous region.

DISCUSSION OF RESULTS

The experiments described above bring out the following facts that are in want of explanation:

1. The porosity generated during the vacuum dezincification of α-brass is the same in amount and appearance to the porosity generated in the brass side of a sandwich type copper-α-brass diffusion couple after the same amount of diffusion.
2. A significant amount of porosity develops in the diffusion zone of Cu-Ni, Ag-Au, and Cu-α-brass sandwich type diffusion couples.
3. The porosity that develops in sandwich type couples is not distributed evenly throughout the diffusion zone, but is concentrated entirely on one side of this zone.
4. Upon the inward diffusion of a metal from the vapor phase, porosity was developed in the case of Ag-Au, but not in the case of Cu-Zn or Cu-Ni systems.

The first statement indicates that there is no essential difference between the vacuum dezincification process and the process that occurs in a sandwich type diffusion couple between copper and alpha-brass. The diffusion coefficients measured by either method are in good agreement. Although it has been known that vacuum dezincification of brass results in porosity, and while others have shown that the measured diffusion coefficients are comparable, the porosity that develops in the sandwich type couple has always been neglected or considered of minor importance.

We believe, however, that sufficient porosity is often developed in sandwich couples to cause a significant error in diffusion coefficients calculated by usual methods. This is particularly the case with complete solid solubility couples such as copper-nickel and gold-silver which may develop more than 50 percent volume porosity near the moving Kirkendall interface. Standard solutions of the diffusion equation assume that equal numbers of lattice points are conserved on adjacent planes and, of course, that all atom transport occurs by diffusion. Actually, lattice points are not conserved and an appreciable fraction of the higher mobility atom transport probably occurs through the vapor phase by evaporation and condensation. In every case studied the higher mobility atoms possessed an appreciable vapor pressure which was in turn considerably higher than the vapor pressure of the slower diffusing atoms. However, since we have no means of estimating changes in the number of lattice sites and the relative rates of transport through the bulk material and across the pores, the effect of porosity upon the "diffusion coefficient" of porous structures cannot be determined quantitatively at present.

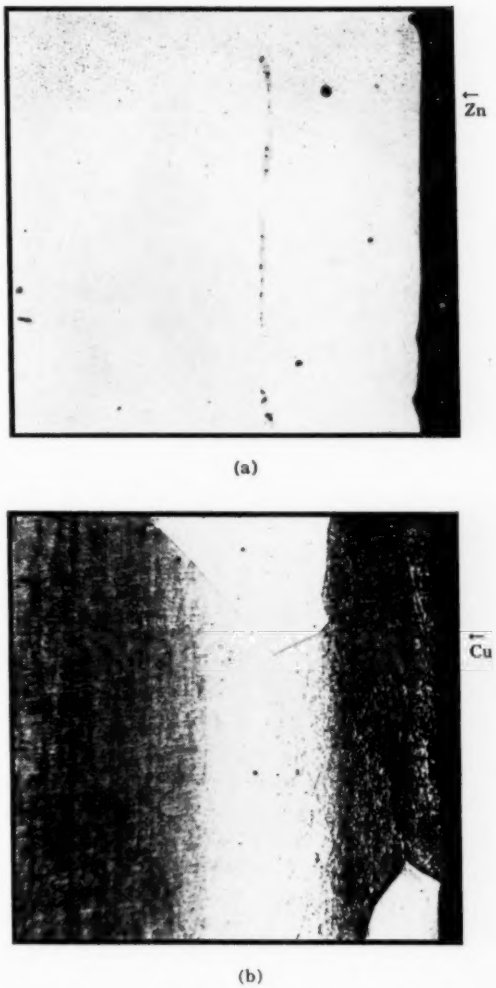

FIG. 11. (a) Copper single crystal exposed to zinc vapor from α-brass 167 hr at 890°C (400×). (b) Polycrystalline nickel exposed to copper vapor 336 hr at 1065°C (160×).

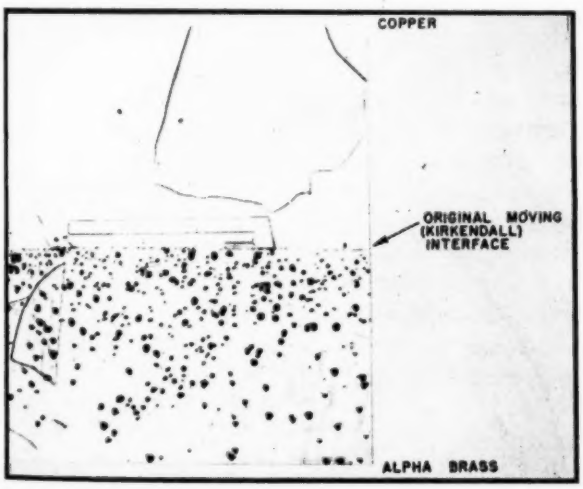

FIG. 10. Porosity developed in brass side of solid copper-α-brass couple after diffusion for 88 hr at 880°C in hydrogen (25×).

FIG. 12. Polycrystalline gold exposed to silver vapor 93 hr at 940°C (80×).

It seems likely that the development of porosity is intimately related to the Kirkendall effect. Kirkendall demonstrated quite conclusively that the two different kinds of atoms in a substitutional solid solution do not diffuse at the same rate, and that this results in a dimensional change with respect to fiducial markers Using the Cu-α-brass system as an example, we can describe the facts as follows: Zinc diffuses out of the α-brass more rapidly than copper diffuses into it. As a result the α-brass side of the diffusion couple loses mass and may shrink while the copper side gains mass and is enlarged. If fiducial markers are placed at the initial junctions of a diffusion couple consisting of α-brass sandwiched between copper, they will be displaced toward the α-brass as a result of this unequal diffusion. Now the results of the present studies show that part of the zinc which diffuses out of the alpha-brass leaves vacancies behind which may precipitate in the form of microscopic pores. Our measurements show that approximately $\frac{1}{3}$ of the zinc which leaves the brass is replaced by porosity. Obviously the movement of fiducial makers is less in this case than if this remaining porosity were eliminated by sintering.

The observation that porosity developed in silver-gold couples but not in copper-α-brass or copper-nickel couples upon inward diffusion from the vapor phase cannot be satisfactorily explained at present. We believe that the composition does not change considerably in the porous region during diffusion. An investigation of this phenomenon is continuing.

The mechanism by which the faster moving atoms diffuse away and leave vacancies behind is not established at present. Bardeen and Herring[7] and Seitz[8] have discussed a vacancy mechanism explaining unequal diffusion and the Kirkendall effect by assuming substitutional exchange of vacancies and atoms. If one type of atom has a higher probability of exchanging places with vacancies than the other unequal diffusion results. An over-all current of diffusing atoms is established in one direction which is balanced by a flow of vacancies in the opposite direction. If it is assumed that the vacancies are maintained everywhere in local thermal equilibrium, Darken's equations[9] relating the two different diffusion coefficients in binary systems with the resulting Kirkendall marker movement follow. Vacancies are continuously "pumped" into the side of the couple which loses the higher mobility atoms by this process. Dislocations within the diffusion zone possessing Taylor-Orowan character are possible sources and sinks for the required vacancies. Our results indicate that if the above model is correct the sinks actually present are not capable of maintaining the vacancies near equilibrium values, since sufficient supersaturation occurs in the side of the couple gaining vacancies to cause the vacancies to precipitate there as holes.

Although the results can be explained according to the above mechanism involving only vacancies, we think an equally acceptable picture of what is happening can be obtained by postulating that Frenkel defects are involved. We may distinguish initially between two types of Frenkel defects in a substitutional lattice consisting of A and B atoms. One type consists of a vacancy and an interstitial A atom and the other of a vacancy and an interstitial B atom. If there are always many more defects of one type present in equilibrium than the other, and/or one type of interstitial atom diffuses interstitially more rapidly than the other we have the possibility of unequal diffusion and porosity formation. We may explain our results by saying that if one of the above conditions hold, a larger number of atoms may diffuse interstitially out of one side of a couple than will diffuse in. The vacancies left behind in this side will reach a state of supersaturation and so will precipitate as holes. The interstitial atoms can always be incorporated back into the lattice at sinks such as dislocations.

The writers wish to acknowledge the help of Mr. A. Timper and Miss A. Hamilton of the Sylvania Metallurgical Laboratories in carrying out the experimental and metallographic phases of this work.

[7] J. Bardeen and C. Herring, Trans. Am. Soc. Metals **43A**, 87 (1951).
[8] F. Seitz, Acta Cryst. **3**, 355 (1950).
[9] L. S. Darken, Trans. Am. Inst. Mining Engrs. **175**, 184 (1948).

JOURNAL OF APPLIED PHYSICS VOLUME 23, NUMBER 11 NOVEMBER, 1952

The Effect of Cyclotron Bombardment on Self-Diffusion in Silver*

R. D. JOHNSON† AND A. B. MARTIN
North American Aviation, Inc., Atomic Energy Research Department, Downey, California

(Received June 16, 1952)

Radioactive tracer techniques have been employed to measure the rate of self-diffusion in silver in polycrystalline and single crystal solvents over a wide range of temperatures, and to investigate the effect of bombardment with 10-Mev protons on this diffusion process. A least squares fit of the data from laboratory control experiments with both single crystal and polycrystalline solvents in the temperature range 903°C to 640°C has yielded the diffusion constants $Q=40{,}800\pm700$ cal/mole and $D_0=0.11\pm0.05$ cm²/sec for the volume diffusion process. No effect of intense proton bombardment ranging from 0.5 to 5μa/cm² has been detected on the volume self-diffusion process in silver specimens which were simultaneously irradiated in the cyclotron target box and annealed at temperatures ranging from 852°C to 555°C. These results are, at least semiquantitatively, in accord with both the elastic collision model and the thermal spike model of radiation damage. Cyclotron techniques and apparatus are described in some detail.

I. INTRODUCTION

WITH the known variation of the diffusion coefficient with temperature and the accepted vacancy mechanism for diffusion in close-packed metals, a qualitative picture would suggest that diffusion rates might be increased significantly by intense proton bombardment, which produces additional lattice vacancies and possibly thermal spikes, i.e., localized regions of high temperature.[1] A knowledge of the effect of radiation on the process of atomic diffusion would add considerably to our present understanding of basic kinetic phenomena which occur in solids. This knowledge would be of fundamental importance in both metallurgy and solid-state physics in determining how radiation affects the properties of solids, especially with respect to the behavior of materials in nuclear reactors. Hence, this investigation was undertaken to determine the effect of intense proton bombardment on the rate of self-diffusion in silver under well-controlled experimental conditions.

Self-diffusion is the most interesting case of diffusion in metals, especially from a theoretical viewpoint, since it lends itself to interpretation more readily than does intermetallic diffusion. This stems from the fact that the self-diffusion coefficient is a function of temperature alone and is not dependent on the concentrations of the solute and the solvent atoms. Neither is it affected by solubility characteristics, phase phenomena, compound formation, or differences in atomic size, valence, and melting point, as may well be the case in intermetallic diffusion. The problem may be restricted further to the process of volume diffusion by using single crystal solvents, especially in the temperature range where grain-boundary diffusion is appreciable.

The radioactive tracer method was employed, since it is a precise method of measuring absolute D values. Also, it appeared to be the most suitable technique to study the effect of cyclotron bombardment on self-diffusion in silver. The size of the specimens was chosen to conform to restrictions imposed by the area of the cyclotron beam obtainable.

A complete set of control experiments was carried out in the laboratory to develop the experimental techniques involved in preparing and processing the diffusion specimens, and to aid in designing the more costly experiments carried out in the presence of cyclotron irradiation. These were in addition to the control specimens which were incorporated in each bombardment.

II. EXPERIMENTAL PROCEDURE

A. Materials and Preparation

The radioactive tracer material used for the solute in these experiments was Ag^{110}, the 270-day[2] half-life isotope of silver, obtained from the Isotopes Division of the Atomic Energy Commission. This sample had a specific activity of 182 millicuries per gram and a radiochemical purity greater than 99.9 percent. The polycrystalline solvent material used in this investigation was Johnson and Matthey 99.999 percent pure silver, in the form of rods 7 millimeters in diameter. The single crystals of silver were cut from a long specimen obtained from R. E. Hoffman of the General Electric Research Laboratory. It was prepared from Handy and Harmon 99.97 percent pure silver by the Bridgman technique.

The polycrystalline specimens, cut in $\frac{1}{4}$-inch lengths from the silver rods, were sealed off in evacuated quartz tubes and given a 48-hour anneal at 850°C to stabilize the mean linear dimension of the grains at about 0.3 millimeter. The single crystals, after being cut to size, were sealed in an evacuated Pyrex tube and given a recovery treatment that consisted of 1 hour at 250°C, 1 hour at 350°C, and 2 or more hours at 450°C, after which they were allowed to cool slowly. These crystals

* This paper is based on studies conducted for the AEC under Contract AT-11-1-Gen-8.
† Now at Battelle Memorial Institute, Columbus, Ohio.
[1] J. C. Slater, J. Appl. Phys. **22**, 237 (1951).
[2] National Bureau of Standards, NBS Circular **499**, p. 122 (1950).

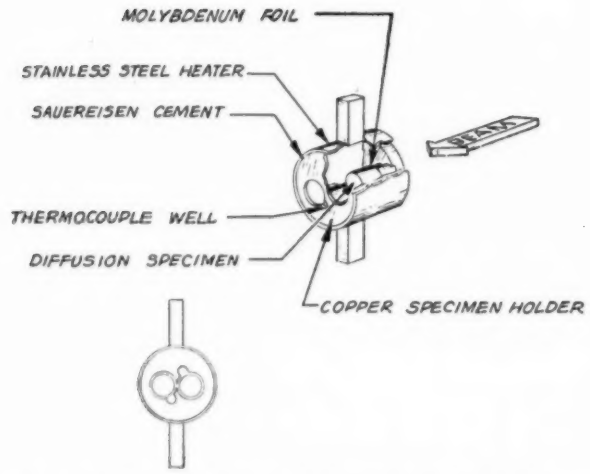

FIG. 1. Heater assembly for cyclotron irradiation-diffusion experiment. The 0.020-inch stainless steel cylindrical shell is a resistance heater. Two ¼-inch long diffusion specimens are mounted side by side in the solid copper block.

were then etched heavily with potassium cyanide to remove most of the cold-worked surfaces which remained after the recovery treatment. In preparation for electroplating, the specimens were mounted in Lucite disks, polished on emery paper and on a wet polishing wheel, and cleaned with sulfuric acid and distilled water.

The radioactive silver was plated from a cyanide solution onto the polished end of the silver rod in a shielded apparatus. The specimens were plated to an activity of approximately 75 mr/hr at 1 centimeter as read on a calibrated ionization chamber. This activity corresponded to a deposit about 0.01 mil (10^{-5} inch) thick. A double-ended plating cell was also utilized to prepare specimens with radioactive silver platings on both ends of the silver rod.

B. Description of the Experiment

This experiment was designed to measure the rate of self-diffusion in silver specimens which were simultaneously annealed and bombarded with an intense proton beam, and to compare this rate with the rate determined from specimens given the same time-temperature treatment without the presence of radiation, i.e., control specimens. For this purpose a diffusion heater (see Fig. 1) was designed which would enable the simultaneous bombardment of two diffusion samples, one plated on both ends and one plated only on the back end, that is, the end away from the cyclotron beam. This arrangement provided two plated ends away from the beam to serve as control specimens for the plated end which was irradiated. The relatively short range of 10-Mev protons (9 mils in silver) made it possible to make control measurements, beyond the range of the protons, on the same specimen in which the effects of irradiation were being studied. The unplated irradiated end served as a means to determine the amount and distribution of radioactivity induced in the silver by the proton beam.

In addition to the specific controls on each bombardment, a complete set of laboratory control experiments was performed. These diffusion specimens, sealed in evacuated quartz or Vycor tubes, were annealed in a small potentiometrically controlled furnace in which the temperature was measured to within ±1C°. The time t used in each anneal was calculated to yield approximately the same slope, s, on a $\ln c$ *vs* x^2 plot by using the value of the diffusion coefficient,

$$D=0.895e^{-45,950/RT},$$

reported by W. A. Johnson[3] and the relation, $D=-1/4st$, which will be discussed in Sec. III. The anneals in the furnace control experiments were designed to produce a decrease in the concentration of the solute by a factor of about 20 from the first to the fifth of five 2-mil sections of the solvent. It has been observed in this laboratory, in silver self-diffusion and in the intermetallic diffusion of gold into copper,[4] that more consistent results are obtained over a wide range of temperatures if the slope of the $\ln c$ *vs* x^2 curve is approximately the same in each case.

After the diffusion anneal, a section a few mils in thickness was trimmed off the cylindrical periphery of the diffusion specimens, and they were sectioned in a jeweler's lathe by taking 6 to 8 cuts of 2 mils or less in thickness. The cuttings from each section were collected, weighed, and dissolved in nitric acid in preparation for determining the concentration of solute in each section of the solvent by means of an immersion-type geiger counter. The solution counting method had the important advantage that counting rates of widely different activities, as encountered here, could be adjusted to approximately the same counting rate by the method of aliquoting.

C. Cyclotron Techniques and Apparatus

The diffusion heater developed for these experiments is shown in Fig. 1. The copper specimen holder, used to increase the thermal capacity of the specimens for temperature control purposes, was electrically insulated from the stainless steel heated by a 10-mil coating of sauereisen cement, which was baked for an hour or more above 1000°C after application. The specimens were force fitted into the two holes in the copper block, after being wrapped with 1-mil molybdenum foil to prevent fusion of the silver specimens into the copper holder. A thermocouple, protected from the beam by sauereisen, was inserted in each of the thermocouple wells along the specimens.

The heater was spring clamped into position in a water-cooled mounting bracket assembly on the back

[3] W. A. Johnson, Trans. Am. Inst. Mining Met. Engrs. **143**, 107 (1941).

[4] A. B. Martin and Frank Asaro, "The diffusion of gold into copper," NAA-SR-83 (June 27, 1950).

plate of the hot target box as shown in Fig. 2. This back plate with the diffusion heater target could easily be attached to the target box (see Fig. 3), which was already in position, just prior to bombardment. A flow of helium at room temperature was maintained through the target box to aid in temperature control and to cool the specimen after the power was shut off. Resistance heating was employed, and power could be supplied by currents as high as 300 amperes at a maximum of 10 volts dc. The power was regulated by a dynalog recorder-controller connected to the control thermocouple. A similar dynalog, connected to the second thermocouple, was used to monitor the temperature at another point in the target during bombardment.

The 60-inch cyclotron at the University of California is ideally suited for this investigation. Under normal operating conditions a 5 microampere beam of singly ionized hydrogen molecules (equivalent to 10 microamperes of 10-Mev protons) can be held quite steady on the target for at least eighty to ninety percent of the bombardment time (see Table II). When the target is oscillated during bombardment, the resulting beam profile is quite uniform over an area approximately $\frac{5}{8}$-inch wide by $\frac{3}{8}$ inch in the vertical direction, although it extends over a total area of dimensions $\frac{3}{4}$ inch by $\frac{5}{8}$ inch. For proton beams as high as 2 microamperes, an oscillated target can be used to get a uniform bombardment of both diffusion specimens in the heater while controlling the temperature of the specimens to within $\pm 5C°$ of the heater temperature while the beam sweeps back and forth across the target. For higher beams, which result in larger energy dissipation in the target, the variation in the temperature of the specimens becomes prohibitive (as high as $\pm 25C°$ for a 10 microampere beam of protons) for a well-controlled diffusion experiment, since it is possible to control the temperature at only one point in the target during bombardment. For very intense bombardments, a stationary target is required to maintain reasonable temperature control. Bombardment of a stationary target produces a fairly uniform irradiation over a somewhat smaller area than is obtained when the target is oscillated. However, bombardment with proton beams as high as 10 microamperes produces temperature gradients in the target which must be taken into account. In order to measure this effect, thermocouples were fused into the the front and back faces of one of the two pieces of silver rod, which were mounted in the diffusion heater in the same manner as the usual diffusion specimens, along with the control thermocouples. These measurements indicated a temperature gradient of 10C° from the front to the back end of the silver rod with a 5 to 6 microampere proton beam, and a gradient of 15C° with an 8 to 10 microampere proton beam. The temperatures of the faces of the diffusion specimens were also determined with respect to the control temperature in the diffusion heater since a gradient existed across the molybdenum foil between the silver specimens and the copper holder during the more intense bombardments.

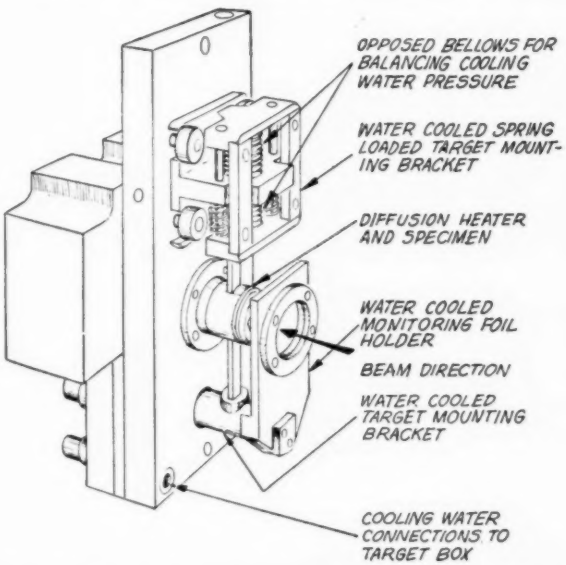
OPPOSED BELLOWS FOR BALANCING COOLING WATER PRESSURE
WATER COOLED SPRING LOADED TARGET MOUNTING BRACKET
DIFFUSION HEATER AND SPECIMEN
WATER COOLED MONITORING FOIL HOLDER
BEAM DIRECTION
WATER COOLED TARGET MOUNTING BRACKET
COOLING WATER CONNECTIONS TO TARGET BOX

FIG. 2. Diffusion heater mounted on back plate of cyclotron target box. The heater is spring clamped into position in a water-cooled mounting bracket assembly which can be quickly attached to the target box.

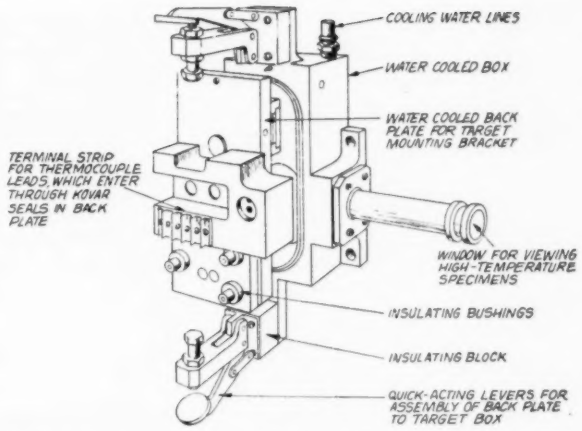
COOLING WATER LINES
WATER COOLED BOX
WATER COOLED BACK PLATE FOR TARGET MOUNTING BRACKET
TERMINAL STRIP FOR THERMOCOUPLE LEADS WHICH ENTER THROUGH KOVAR SEALS IN BACK PLATE
WINDOW FOR VIEWING HIGH-TEMPERATURE SPECIMENS
INSULATING BUSHINGS
INSULATING BLOCK
QUICK-ACTING LEVERS FOR ASSEMBLY OF BACK PLATE TO TARGET BOX

FIG. 3. Cyclotron target box assembly. The water-cooled back plate containing the diffusion heater mounting is shown assembled to the cyclotron target box by means of quick acting toggle clamps.

Beam profiles were determined by counting the activity in a foil placed in front of the target during bombardment. These beam profiles, along with the measurements of the induced activity in the unplated irradiated specimen, provided a means for correcting the activity measurements from the irradiated plated specimen for the proton induced activity. This technique was used on all the bombardments except the one at the lowest temperature, in which the penetration of solute was about 3 mils. In this case a simple chemical separation of cadmium from silver was necessary to remove the high background of induced activity, resulting from the intense 50-hour bombardment, from the solutions containing the diffused Ag^{110} activity in order to obtain reliable measurements at very low penetrations.

TABLE I. Silver self-diffusion data on furnace control specimens.

Sample no.	T (°C)	Time (hours)	D (cm²/sec)
	Volume diffusion data		
14	903	4.0	2.56×10^{-9}
15	903	4.0	2.56×10^{-9}
5	800	20.0	4.65×10^{-10}
7	800	20.0	5.50×10^{-10}
8	722	96.3	1.23×10^{-10}
9	722	96.3	1.08×10^{-10}
38	697	167	7.56×10^{-11}
39	697	167	7.78×10^{-11}
1s[a]	697	167	7.22×10^{-11}
2s	697	167	7.43×10^{-11}
3s	697	167	7.99×10^{-11}
3	677	234	4.43×10^{-11}
4	677	234	3.83×10^{-11}
36	640	1008	1.41×10^{-11}
37	640	1008	1.46×10^{-11}
	Grain-boundary diffusion data		
30	497	401	$D_B=7.7\times10^{-8}$
32	497	401	$D_B=8.2\times10^{-8}$

[a] The suffix "s" denotes a single crystal solvent.

Radioacitivity measurements on a sample containing only the induced activity, presumably from the $Ag^{109}(p, n)\,Cd^{109}$ reaction, resulted in a 99.5 percent removal of the activity from the solution after the first separation of cadmium from silver, and a 100 percent removal after the second separation.

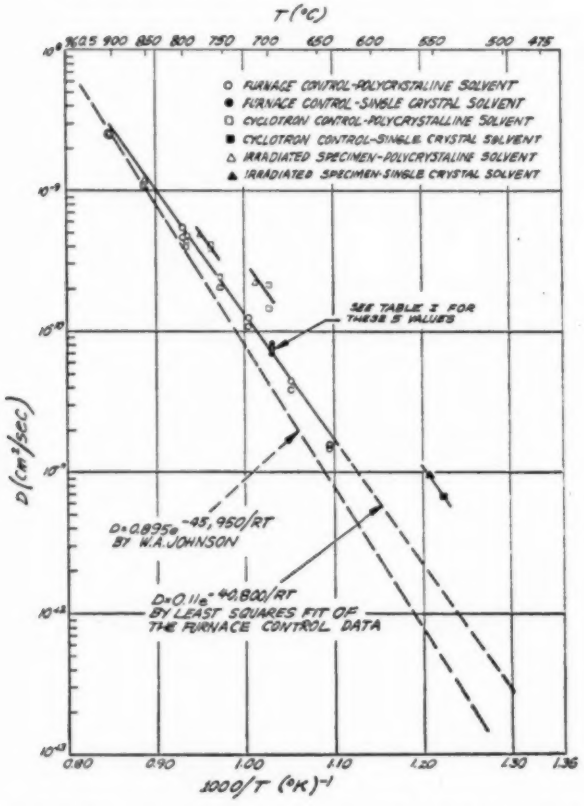
T(°C)
962.5 900 850 800 750 700 650 600 550 500 475
FURNACE CONTROL-POLYCRYSTALLINE SOLVENT
FURNACE CONTROL-SINGLE CRYSTAL SOLVENT
CYCLOTRON CONTROL-POLYCRYSTALLINE SOLVENT
CYCLOTRON CONTROL-SINGLE CRYSTAL SOLVENT
IRRADIATED SPECIMEN-POLYCRYSTALINE SOLVENT
IRRADIATED SPECIMEN-SINGLE CRYSTAL SOLVENT
SEE TABLE I FOR THESE D VALUES
D=0.895e^-45,950/RT BY W.A.JOHNSON
D=0.11e^-40,800/RT BY LEAST SQUARES FIT OF THE FURNACE CONTROL DATA
D (cm²/sec)
0.80 0.90 1.00 1.10 1.20 1.30 1.36
1000/T (°K)⁻¹

FIG. 4. Log$D$ *vs* $1/T$ data for silver self-diffusion. This plot summarizes the data from laboratory control experiments, cyclotron control samples and irradiated specimens. Results are shown for both single crystal and polycrystalline solvents. The solid line is a least squares fit of the data from laboratory control samples. For comparison, the dashed line represents the results obtained by W. A. Johnson for self-diffusion in silver.

III. EXPERIMENTAL RESULTS

The method of analyzing the data has been described adequately elsewhere.[5] Stated briefly, it consists of solving Fick's equation for diffusion in one direction with the boundary conditions implied by a very thin plating of solute on the flat end of a cylindrical rod. The solution for the concentration, c, of the solute at a

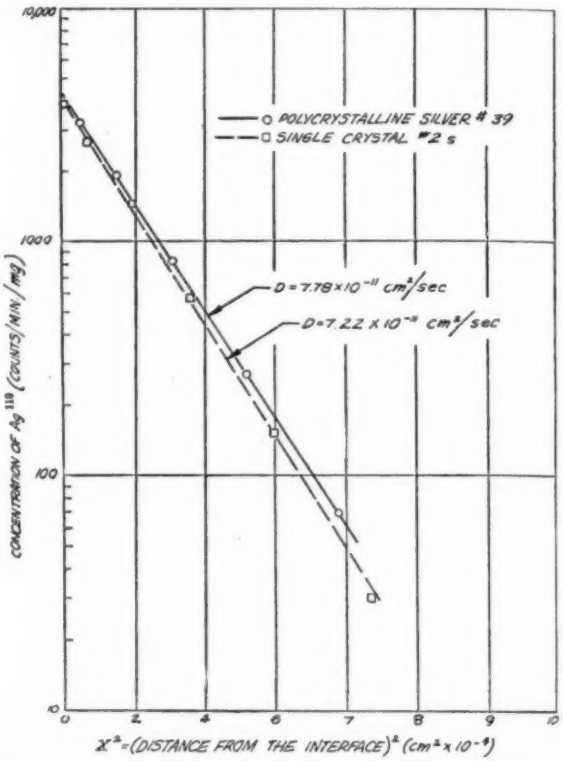

FIG. 5. Plot of log$c$ *vs* x^2 for volume diffusion in (a) polycrystalline sample number 39 (solid line) and (b) single crystal sample number 2*s* (dashed line). The two specimens were annealed simultaneously for 167 hours at 697°C. At this temperature the effect of grain boundary diffusion is apparently not significant.

distance x from the original interface at time t can be written in the form

$$\ln c = -x^2/4Dt + \ln[c_0/2(\pi Dt)^{\frac{1}{2}}], \qquad (1)$$

where c_0 is a constant proportional to the amount of solute plated on the solvent and D is the volume diffusion coefficient at the temperature of the anneal. It is readily seen that if the logarithm of the concentration is plotted against the square of the distance from the original interface, the resulting plot can be represented by a straight line whose slope is $-1/4Dt$. From the measured slope and the time of the anneal, the diffusion coefficient at the temperature of the anneal can be readily computed.

[5] Reference 3, pp. 109–110.

TABLE II. Silver self-diffusion data for the cyclotron irradiated and cyclotron control specimens.

Run no.	Sample no.	T (°C)	Time (hours)	D (cm²/sec)	μahr of protons on target	μa/cm² of protons on specimen[a]	Type target	Hours beam on target
1	10	852	11.0	1.17×10^{-9}	16.7	0.55±5 percent	Oscillated	8.8
	10c[b]	852	11.0	1.09×10^{-9}				
	16c	852	11.0	1.10×10^{-9}				
2	11	795	16.65	4.50×10^{-10}	12.1	0.60±15 percent	Oscillated	15.6
	11c	795	16.65	4.82×10^{-10}				
	18c	795	16.65	4.00×10^{-10}				
3	22	755	40.0	2.10×10^{-10}	72.1	0.75±5 percent	Oscillated	38.4
	22c	755	40.0	2.07×10^{-10}				
	31c	755	40.0	2.42×10^{-10}				
4	24	780	30.0	4.95×10^{-10}	225	4.0±60 percent	Stationary	25.0
	24c	765	30.0	4.10×10^{-10}				
	33c	765	30.0	3.83×10^{-10}				
5	27	715	50.0	2.18×10^{-10}	403.6	5.0±100 percent	Stationary	43.5
	27c	700	50.0	2.12×10^{-10}				
	55c	700	50.0	1.43×10^{-10}				
6	4s	555	50.0	9.52×10^{-12}	255	4.4±100 percent	Stationary	47.7
	4s–c	545	50.0	6.71×10^{-12}				
	5s–c	545	50.0	(3.11×10^{-11})[c]				

[a] The average beam intensity on the diffusion specimen and the percentage variation of the beam intensity across the face of the specimen as determined from the beam profile.
[b] The suffix "c" denotes a cyclotron control specimen; "s" denotes a single crystal solvent.
[c] This result is unreliable because the specimen was not properly aligned in the lathe for sectioning.

The experimental data and the measured D values for the laboratory control experiments are tabulated in Table I. The data presented for single crystal and polycrystalline solvents in the temperature range 903°C to 640°C were fitted to the equation

$$D=D_0e^{-Q/RT} \tag{2}$$

by the least squares method to determine the constants D_0, the atomic mobility, and Q, the activation heat of diffusion, for the volume diffusion process. The values obtained were $D_0=0.11\pm0.05$ cm²/sec and $Q=40{,}800\pm700$ cal/mole where the errors indicated are the probable errors calculated by the least squares method. The experimentally determined points are plotted in Fig. 4 along with the expression obtained from the least squares fit. A plot of log$c$ *vs* x^2 is shown in Fig. 5 for a single crystal and a polycrystalline solvent which were annealed for 167 hours at 697°C. The agreement of the experimental data with the linear log D *vs* $1/T$ plot in Fig. 4, the agreement of the results from single crystal and polycrystalline solvents annealed simultaneously at 697°C (see Fig. 5), and the accurate linearity of the log$c$ *vs* x^2 plots indicate that grain-boundary diffusion has not affected the measured volume diffusion rates in the temperature range 903°C to 640°C. The maximum difference in the D values determined from specimens annealed simultaneously is about 20 percent while the average difference is about 10 to 15 percent.

The data from the two polycrystalline control specimens annealed for 401 hours at 497°C produced a linear plot of log$c$ *vs* x as compared with a linear plot of log$c$ *vs* x^2 which is obtained in volume diffusion. This linear plot of log$c$ *vs* x is attributed to grain-boundary diffusion. These data were analyzed by a method proposed by Fisher,[6] which yields the expression

$$\frac{D}{D_B\delta}=\tfrac{1}{2}(\pi Dt)^{\frac{1}{4}}\left(\frac{d\ \ln c}{dx}\right)^2, \tag{3}$$

where D is the coefficient for volume diffusion at the temperature of the anneal, D_B is the coefficient for grain-boundary diffusion, also at the temperature of the anneal, and δ is the width of the grain-boundary, assumed to be approximately two atomic layers thick, or 5A in the case of silver, and independent of temperature. The symbols t, c, and x have the same meanings as in Eq. (1). With the above analysis, values of 7.7 and 8.2×10^{-8} cm²/sec were obtained for D_B at 497°C. These values compare quite favorably with the value of 9.4×10^{-8} cm²/sec at 497°C determined by Hoffman and Turnbull[7] with the same analysis on the same type silver, but with a slightly smaller grain size.

The results of the six cyclotron bombardments are tabulated in Table II and plotted in Fig. 4. Table II also lists the total integrated beam (μahr) on the target, which consists of the heater and the two diffusion specimens, and the average beam intensity (μa/cm²) on the irradiated plated specimen. The percentage variation of the beam intensity across this plated specimen as determined from the beam profile is given for each bombardment. In the first three bombardments

[6] J. C. Fisher, J. Appl. Phys. **22**, 74 (1951).
[7] R. E. Hoffman and D. Turnbull, J. Appl. Phys. **22**, 634 (1951).

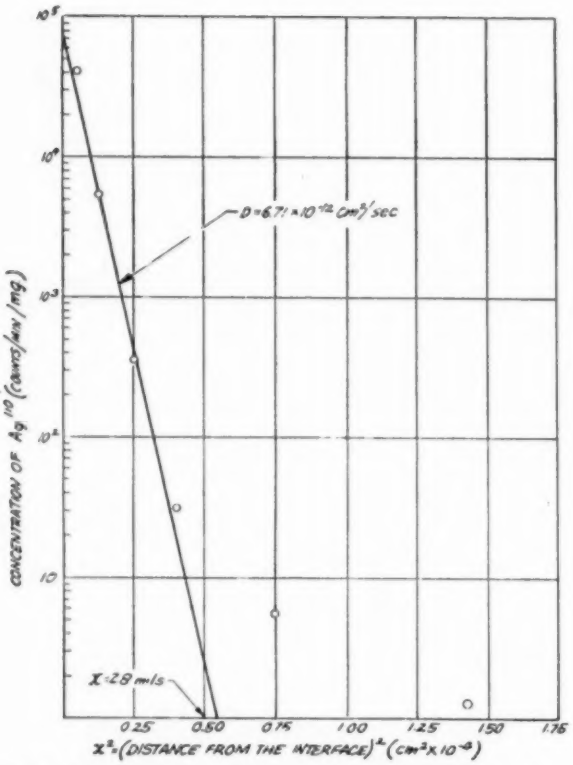

FIG. 6. Log$c$ *vs* x^2 plot for single crystal cyclotron control sample 4s–c (50 hours at 545°C). The penetration to which diffusion measurements could be made was only 0.06 mm.

at temperatures of 852°C, 795°C, and 755°C, the target was oscillated to insure uniform irradiation of the diffusion specimen, the beam was limited to maintain good temperature control, and the annealing times were comparable with those used in the laboratory control experiments at the same temperatures. The results from the cyclotron control specimens are in good agreement with the expression for D obtained in the laboratory control experiments (see Fig. 4). However, no effect of proton bombardment was detected on the rate of self-diffusion so it was deemed necessary to increase the intensity of the bombardments and to decrease the temperature of the anneals while maintaining reasonable annealing times, with a maximum of 50 hours, the latter restriction being imposed primarily by economy with respect to cyclotron time.

In the second set of three bombardments, the target was held stationary, the intensity of the bombardment was increased by a factor of about 10, and the annealing times were short compared to those used in laboratory control experiments at comparable temperatures. The resulting D values from the cyclotron control specimens were high with respect to the expression for D obtained in the laboratory control experiments. This apparent dependence of D on the time of anneal has also been observed in the intermetallic diffusion of gold into copper.[8]

[8] Martin, Johnson, and Asaro (to be published).

The use of higher beam intensities, up to 5μa/cm², with a stationary target resulted in a temperature gradient of 10 to 15C° from the irradiated end to the control end of the specimen. Hence, the measured D value from the irradiated end must be compared with the D value from the control end increased by 10 to 15C° in temperature. This is indicated on the log$D$ *vs* $1/T$ plot in Fig. 4 by plotting the D value from the irradiated ends at a slightly higher temperature than that from the control ends, and drawing a line with slope Q through the average of the measured D values from the two control ends. The ordinate value on this line which corresponds to the temperature of the irradiated specimen is to be compared with the D value from the irradiated specimen. As can be seen in Fig. 4 after making this comparison, no significant effect of intense proton bombardment has been detected on the rate of self-diffusion in silver within the limits of the experimental errors involved in this investigation.

The reason for the omission of the second control value of D at 545°C from the log$D$ *vs* $1/T$ plot is that proper alignment was not obtained before sectioning this end of the single crystal specimen. Since the penetration was only about 3 mils after 50 hours at 545°C, this alignment was extremely critical. A plot of log$c$ *vs* x^2 for the other single crystal control at 545°C is shown in Fig. 6. The linearity of this plot down to an activity of about 30 counts per min per mg indicates that the use of single crystal solvents has restricted the predominant process being studied to volume diffusion.

IV. DISCUSSION OF THE RESULTS

The results of the laboratory control experiments agree quite well with the data of others who have measured self-diffusion in silver by similar or other methods. In Fig. 4, the expression obtained for D by W. A. Johnson,[9] who used sandwich-type diffusion samples and radioactive tracer methods, is plotted for comparison. This expression has been substantiated by the work of Hoffman and Turnbull,[10] who also used tracer methods with diffusion specimens of the same type used here. As can be seen in Fig. 4, the results of the present investigation agree quite well with their work in the high temperature range (around 900°C) but differ slightly at the lower temperatures. The expression obtained for D in this investigation agrees quite well with Kuczynski's determination,[11] $D=0.6e^{-42,000/RT}$, by the sintering of spherical particles to a flat plate. Kuczynski has also obtained[12] $D=0.9e^{-45,700/RT}$, by the sintering of wires to a cylindrical bar. As mentioned previously, the determination of the grain-boundary diffusion coefficient at 497°C agrees quite well with the work of Hoffman and Turnbull.[13]

[9] Reference 3, p. 110.
[10] Reference 7, p. 635.
[11] G. C. Kuczynski, J. Metals **1**, 169 (1949).
[12] G. C. Kuczynski, J. Appl. Phys. **22**, 632 (1950).
[13] Reference 7, p. 638.

The internal consistency of the constants determined for the volume self-diffusion process can be checked by using the empirical relation

$$D_0 = \nu\lambda^2 K e^{Q/RT_m} \quad (4)$$

proposed by Dienes.[14] For the case of silver, the vibrational frequency of the solid, ν, is 4.5×10^{12} per second; the distance between nearest neighbors, λ, is 2.88×10^{-8} centimeter; the empirical constant, K, has the value 10^{-6}, and the melting point, T_m, is 1234°K. R is the universal gas constant and Q is the activation heat of diffusion in the appropriate units. With the measured value of Q, 40,800 cal/mole, the calculated value of D_0 is 0.16 cm²/sec. This value is within the limits of the probable error of the value, $D_0 = 0.11\pm0.05$ cm²/sec, found in this investigation. This empirical relation shows good agreement with several cases of self-diffusion and also many cases of intermetallic diffusion in which the concentration of the solute is quite low.

No large experimental errors are to be expected with the techniques used. The times of anneal are known to within 1 percent. For five samples which were treated simultaneously in the same anneal, the results indicate that the probable error in D arising from the sectioning (including alignment) and counting procedures is about ±3 percent. In the laboratory experiments, the temperatures were measured to ±1C°, however, some uncertainty in these temperatures (±5C° at most) arises from the fact that the themocouples were not calibrated prior to use. The agreement of the controls from the three low intensity bombardments with the expression obtained for D in the laboratory control experiments is indicative of consistent temperature measurements in the furnace and in the cyclotron target box. The more difficult temperature measurements with the high intensity proton beams (as high as 5 μa/cm²) are believed to be correct within about ±5C° because of the agreement obtained in two independent measurements of the temperature gradients in the target during intense bombardment. These experimental errors would indicate that the probable error in a single measurement of D at a given temperature is about 6 to 13 percent.

The results from the specimens simultaneously annealed and bombarded with intense proton beams clearly indicate that there has been no significant effect of irradiation on the rate of volume self-diffusion in silver in the temperature range 852°C to 555°C. Even though the measured D values from the cyclotron control specimens in the last three bombardments, in which the annealing times were too short to yield the same penetration of the solute atoms as was obtained in the laboratory control experiments, were high compared to the values predicted by the expression, $D=0.11e^{-40,800/RT}$, obtained in the laboratory control experiments, nevertheless, these specific controls on each bombardment offer direct evidence that there has been no effect of the intense proton bombardment on the self-diffusion process.

The null effect obtained in these experiments agrees with the results of intermetallic diffusion studies by Pol Duwez,[15] who found no effect of proton bombardment of the same intensity on interdiffusion in CuNi and CuAu powder compacts made up of extremely small particles which were mixed in equal atomic percentages. These irradiation-diffusion studies were performed at 550°C and 600°C in CuNi compacts and at 345°C in a CuAu compact. The experiments were designed to place the control surface of the powder compact in a state of partial diffusion after the anneal, and then to employ x-ray diffraction techniques to measure the progress of diffusion in the control and the irradiated portions of these powder compacts. No differences were found in the progress of diffusion between the irradiated and the control parts of the specimens.

V. THEORY OF RADIATION EFFECTS

Although the effects of nuclear radiations on the physical properties of solids are as yet imperfectly understood, it is of interest to attempt to correlate the null results obtained in the present study of diffusion with the prevailing theories of radiation damage.

In passing through matter, charged particles lose energy in two ways. The greater part of the energy loss is through excitation and ionization of electrons, in which case the kinetic energy of the incident particle is transferred to individual electrons rather than to the atom as a whole. This energy transfer does not make an important contribution to the production of displaced atoms and vacant lattice sites, however, because the exchange of energy between electrons and atomic nuclei is slow compared to the rate at which the energy of excitation is dissipated throughout the lattice by electronic conduction. Thus, the ionization energy along the path of the incident particle is spread throughout the solid very rapidly and is reduced to a low energy per unit volume before an appreciable fraction is transferred to lattice oscillations. Consequently, individual atoms receive only small increments of thermal energy.

A smaller part of the energy loss of the charged particle takes place through elastic collisions in which the incident particle transfers an appreciable fraction of its kinetic energy to the struck atom as a whole. If the energy transfer is greater than the minimum unit displacement energy, usually taken to be 25 ev, the atom is displaced from its normal lattice position and an interstitial and a vacant lattice site result. The recoil atom in turn collides with other atoms along its path, producing secondary and tertiary recoils, until the energy of the final recoil atoms in the chain is below the minimum required to produce displacements. The process continues until all of the energy of the initially displaced atoms is used up in producing displacements,

[14] G. J. Dienes, J. Appl. Phys. **21**, 1141 (1950).

[15] Pol Duwez, private communication.

vacancies, elastic oscillations in the lattice of the solid, and electronic excitation. There are now two ways in which the ultimate effects of this elastic energy transfer may be approached. The statistical, or thermal spike, approach will be discussed later in this section. In the elastic collision, or branching chain, model of radiation damage, attention is fixed on displaced atoms and vacancies resulting from the direct transfer of kinetic energy from the moving particle to initially stationary atoms.

From the analysis outlined by Seitz[16] for treating the energy loss of fast charged particles in matter, the number of vacancies produced per incident proton can be calculated. In the particular case of silver bombarded with 10-Mev protons, approximately 63 atoms are displaced per incident particle, if a displacement energy of 25 ev is assumed. From this number and the beam intensity, the average rate of generation of vacancies can be computed. If vacancies are generated at a uniform rate, q, in a spherical region of radius R whose boundaries are sinks to which the vacancies can diffuse and disappear by recombination, the equilibrium density of vacancies, ρ, resulting only from bombardment is given by the steady-state diffusion equation

$$\frac{1}{r^2}\frac{\partial}{\partial r}\left(D_v r^2 \frac{\partial \rho}{\partial r}\right)+q=0. \tag{5}$$

The diffusion coefficient for vacancies, D_v, is related to the diffusion coefficient for atoms, D, by the relation[17]

$$D=\rho' D_v. \tag{6}$$

D is defined by Eq. (2), and ρ' is the equilibrium concentration of vacant lattice sites due to thermal energy. ρ' can be defined by the expression[18]

$$\rho'=Ce^{-U/RT} \tag{7}$$

where C is a constant and U is the activation energy for creation of a vacancy. U is related to Q, the activation energy for diffusion by the vacancy mechanism, by the equation

$$Q=U+E \tag{8}$$

where E is the activation energy for motion of a vacancy. Combining Eqs. (2), (6), (7), and (8) yields the expression

$$D_v=\frac{D_0}{C}e^{-E/RT}. \tag{9}$$

Integrating Eq. (5) with appropriate boundary conditions gives the expression for the density of vacancies due to bombardment alone,

$$\rho=\frac{q}{6D_v}(R^2-r^2). \tag{10}$$

Integration of this expression over a sphere of radius R yields the average density of vacancies $\bar{\rho}$ resulting in the sphere from bombardment at the temperature of the diffusion anneal. The result is

$$\bar{\rho}=\frac{qR^2}{15D_v}. \tag{11}$$

From Eq. (6), $D_v=D/\rho'$; therefore, the ratio of the average equilibrium density of vacancies due to bombardment to the equilibrium density of vacancies due to thermal energy is just

$$\frac{\bar{\rho}}{\rho'}=\frac{qR^2}{15D}. \tag{12}$$

The fractional increase in density of vacancies resulting from proton bombardment will then be obtained when the pertinent numerical values are substituted in the right-hand member of (12). From (6), the volume diffusion coefficient, D, is directly proportional to the density of vacancies, if the diffusion coefficient for vacancies, D_v, is not altered by the bombardment.

The most pronounced effect of proton bombardment would be expected in diffusion sample number 4*s* (Table II), a single crystal specimen which was irradiated with 4.4 μa/cm^2 of 10-Mev protons for approximately 50 hours, at 555°C. Since no grain-boundary diffusion occurred in this sample, and the amount of volume diffusion due to the thermal treatment at this relatively low temperature was just large enough to be measurable, a change in the rate of volume diffusion resulting from the bombardment should have been clearly indicated. The cyclotron beam intensity employed in this experiment was sufficient to produce vacancies in the 9-mil layer of silver which was irradiated at an average rate of 1.3×10^{-6} displacement per atom per second. If the boundaries of the mosaic block are assumed to represent sinks for the vacancies produced by bombardment, it is reasonable to take R to be of the order of 10^{-4} cm. Using the value of D obtained from this specimen, the ratio $\bar{\rho}/\rho'$ is only 10^{-4}. An increase in the density of vacancies of this magnitude would not be detectable experimentally.

Moreover, these calculations have not taken into account the probability of vacancies being lost by recombination within the mosaic block. This effect is probably quite important in metals as close-packed as silver and would reduce the equilibrium density of vacancies resulting from bombardment below the value calculated above.

In the thermal spike model of radiation damage, the kinetic energy transferred elastically from the incident

[16] F. Seitz, Disc. Faraday Soc. No. 5, 271 (1949).

[17] Smoluchowski, Mayer, and Weyl, editors, *Phase Transformation in Solids* (John Wiley and Sons, Inc., New York, 1951), Chapter 4 by F. Seitz, p. 100.

[18] Reference 17, p. 116.

particle to the atoms of the solid is considered to enhance the thermal energy of the lattice in a small volume surrounding the track of the recoil atoms, giving rise to a localized region of high temperature which is rapidly degraded through the lattice, leading to additional displacements and enhanced lattice oscillations. The maximum temperature attained in the spike and the duration of the thermal pulse depend upon the extent to which the kinetic energy of the incident particle is localized upon a few atoms, and the rate at which the disturbed atoms transfer the excess energy to the surrounding matrix. It is generally assumed that the temperature in the spike exceeds the melting point of the materials, perhaps by a considerable amount, and that the duration of the pulse is of the order of 10^{-10} second.[19]

Following the treatment outlined by Seitz,[20] it is calculated that when silver is bombarded with 10 Mev protons, the fraction of energy going into elastic collisions is one-thousandth of the total energy, or 10^4 ev per particle. The remaining 99.9 percent of the proton energy is dissipated in electron excitation and ionization and, as mentioned above, these processes are believed to make no important contribution to the thermal energy of the lattice nuclei. The bombardment experienced by diffusion sample 4*s*, 220 μa hr/cm^2 of 10 Mev protons, is then equivalent to an elastic energy transfer of 2×10^{24} ev/cc, on the average, or 35 ev per silver atom. We may now consider the possibility of enhanced diffusion rates from this treatment, on the assumption that the silver remains in the solid phase, that is, that the temperature of thermal spikes does not exceed the melting point (960°C). The maximum temperature increase above the temperature of the diffusion anneal is then 405°C, or 0.035 ev, and hence each atom in the solid would, on the average, experience 1000 thermal spikes during the bombardment, each lasting 10^{-10} second. If the pulse duration is assumed to be as long as 10^{-8} second in this case, the total time that the material would spend at the elevated temperature would be only 10^{-5} second. The slope of the log concentration *versus* square of the penetration plot, or essentially the amount of diffusion which takes place, is determined by the product of D, the diffusion coefficient, and t, the time at temperature. For the 555°C sample the amount of diffusion resulting from the thermal anneal would then be proportional to $D_1t_1\doteq10^{-11}\times2\times10^5=2\times10^{-6}$, while the additional diffusion arising from thermal spikes would be proportional to $D_2t_2\doteq10^{-8}\times10^{-5}=10^{-13}$. Under these assumptions, the effect of thermal spikes is apparently negligible.

If the maximum temperature associated with the thermal spikes is considerably above the melting point of the irradiated material, then the number of thermal spikes experienced by each atom in acquiring 35 ev of energy is considerably smaller. Hence, the actual time that each atom spends at an elevated temperature is less. However, since the manner in which D varies with temperature above the melting point is not known, it is only possible to infer that, since the average time spent by each atom at an elevated temperature is quite small, it is improbable that the diffusion coefficient is changed significantly, at least by bombardments of the intensity encountered in this investigation. An order of magnitude calculation, based on the assumption that the diffusion equation holds at least approximately for temperatures above the melting point, indicates that if the duration of the thermal pulse is as long as 10^{-7} second the incremental amount of diffusion resulting from thermal spikes is still inappreciable for temperatures in the spike of the order of 10,000°K.

From these admittedly semiquantitative correlations with the elastic collision and the thermal spike theories of radiation damage it is concluded that any incremental diffusion rate induced by nuclear bombardments of the magnitudes employed here will be only a small fraction of the diffusion rate due to thermal anneal. This conclusion may be valid only for cases in which the temperature of the thermal anneal is sufficiently high to produce an observable amount of diffusion on a macroscopic scale.

VI. CONCLUSIONS

The results of the laboratory control experiments, which yielded the expression $D=0.11e^{-40,800/RT}$ for the volume diffusion process in the temperature range 903°C to 640°C, are in good agreement with the data of other workers who have also studied self-diffusion in silver. The linearity of the log$D$ *vs* $1/T$ plot and the agreement between the D values determined from polycrystalline solvents and those from single crystal solvents, all annealed at 697°C, indicate that the measured diffusion coefficients have not been affected by grain-boundary diffusion in the temperature range investigated. However, measurements on polycrystalline solvents diffused at 497°C indicate that grain-boundary diffusion is the predominant process at this temperature, and single crystal solvents are necessary to study volume diffusion at temperatures in the vicinity of 500°C and below.

Intense proton bombardment, ranging from 0.5 to 5μ a/cm^2, has produced no measurable effect on the rate of self-diffusion in silver in the temperature range 852°C to 555°C. This result is in agreement with the results of experiments in intermetallic diffusion carried out at slightly lower temperatures in powder compacts in the presence of cyclotron irradiation of the same intensity. The null result appears to be in accord with both the thermal spike and the elastic collision models of radiation damage.

VII. ACKNOWLEDGMENTS

It is a pleasure to acknowledge the able assistance of W. V. Goeddel in electroplating the specimens and in

[19] S. Siegel, Phys. Rev. **75**, 1824 (1949).
[20] Reference 16, p. 275.

performing the associated chemical operations, and of W. J. Stephan in conducting the cyclotron bombardments with the cooperation of the staff at Crocker Radiation Laboratory. We would like to thank Pol Duwez, M. M. Mills, G. J. Dienes, and J. A. Brinkman for stimulating discussions held with them, and also the many other workers at North American Aviation, Inc., too numerous to mention, who rendered assistance throughout the course of this work. We are indebted to R. E. Hoffman of the General Electric Research Laboratory for the single crystal of Handy and Harmon silver.

JOURNAL OF APPLIED PHYSICS VOLUME 23, NUMBER 11 NOVEMBER, 1952

Effect of Filament Voltage on the Plate Current of a Diode

HENRY F. IVEY*
Research Department, Westinghouse Electric Corporation, Bloomfield, New Jersey
(Received May 26, 1952)

The effect of the potential drop across the filament of a diode with directly heated emitter on the plate current of the diode is considered. Calculations are made for both space-charge-limited and retarding-field conditions. Filament heating by direct current and by alternating current is considered. The results are given in convenient graphical form.

IT is the purpose of this paper to consider the effect of the potential drop across the filament of a diode with directly heated emitter on the plate current of the diode. For generality the plate voltage is measured from an arbitrary point on the cathode. This condition is met in practice if the plate return is made to a tap on a resistor shunted across the filament.

I. SPACE-CHARGE-LIMITED DIODE

The characteristics of a space-charge-limited diode with equipotential cathode are most conveniently expressed for out purpose as

$$I_0=GV_a^{3/2}, \tag{1}$$

where I_0 is the diode current, G is the perveance, and V_a is the plate voltage relative to the cathode (including contact potential correction). The diode may be planar or cylindrical. We use the subscript on I to indicate the absence of cathode potential drop. Equation (1) assumes that initial velocities of emission are negligible. It will also be assumed below that the voltage varies linearly over the filament. This will not be true if the resistance of the filament is not constant, as will be the case if it is subject to end cooling, or if the plate current is appreciable compared to the filament current.

It will be convenient to introduce the quantity

$$w=V_a/V_f \tag{2}$$

giving the relative magnitude of the plate and filament voltages. It is also convenient to express the effect of the filament voltage drop on the diode characteristic by the function g, where

$$I=gI_0. \tag{3}$$

Thus g is the ratio of the current actually flowing in the diode to that which would flow in the same diode with the same plate voltage if the emitter were equipotential.

A. Filament Heated by Direct Current

Consider a diode with the filament heated by direct current. Let the plate voltage be measured with respect to a point which is located at a distance x from the negative end of the filament, where x is expressed as a fraction of the total filament length. Then the effective plate voltage at a point on the filament at a distance z from the negative end, where z is also expressed as a fraction of the filament length, is given by

$$V=V_a+(x-z)V_f. \tag{4}$$

Combination of the above equations leads to the expression

$$g(w)=\int\left[1+\frac{x-z}{w}\right]^{3/2}dz, \tag{5}$$

where the limits on the integral are to be adjusted so that only the active emitting length of the filament is considered. If $w>(1-x)$ then V, as given by equation (4), will be everywhere positive, so that emission is collected from the entire filament and the appropriate limits are 0 and 1. In this case g becomes[1]

$$g=\tfrac{2}{5}w\left[\left(1+\frac{x}{w}\right)^{5/2}-\left(1-\frac{1-x}{w}\right)^{5/2}\right], \quad (w>1-x). \tag{6}$$

* Present address: Skiatron Electronics and Television Corporation, 30 East 10th Street, New York 3, New York.

[1] Equations (6) and (7) also appear in a paper by K. H. Kingdon and H. M. Mott-Smith, Gen. Elec. Rev. 32; 139 (1929).

This expression may be expanded in series form to give

$$g=1+\tfrac{3}{4}[x^2-(1-x)^2]w^{-1}+\tfrac{1}{8}[x^3+(1-x)^3]w^{-2}$$
$$-\tfrac{1}{64}[x^4-(1-x)^4]w^{-3}+\cdots$$
$$+(-1)^n\frac{3(2n-5)!}{2^{2n-3}(n-3)!(n+1)!}$$
$$\times[x^{n+1}-(x-1)^{n+1}]w^{-n}+\cdots. \quad (7)$$

If $w<(1-x)$ then emission is not collected from the entire length of the filament and the limits on the integral in (5) becomes 0 and $(w+x)$. The result is

$$g=\tfrac{2}{5}w\left(1+\frac{x}{w}\right)^{5/2}, \quad (w<1-x). \quad (8)$$

Values of the function g are plotted in Fig. 1. The dashed line in this figure passes through the points for which $w=1-x$. For larger values of w the entire filament is active; for smaller values of w only a portion of the filament is active. It may be noted that if the plate return is made to the midpoint of the filament ($x=0.5$), g is always greater than unity. This fact is a consequence of the three-halves exponent in the space charge equation. For values of x slightly lower than 0.5, however, the effect of filament voltage on the diode characteristics is minimized. For $x=0.45$, for example, the maximum deviation of g from unity is about four percent for $w>0.45$, while for $x=0.48$, $g=1.002$ for $w=1$ and of course approaches unity even more closely for higher values of w.

B. Filament Heated by Alternating Current

If V_f designates the rms value of the alternating filament voltage, the effective plate voltage at any point z on the filament at any time in the cycle is given by

$$V=V_a+\sqrt{2}V_f(x-z)\sin\theta. \quad (9)$$

Since the two ends of the filament are indistinguishable in this case, x may be measured from either end as long as z is measured from the same end. Only the case $w>\sqrt{2}(1-x)$, where $x<0.5$, will be considered here so that the effective plate voltage for every portion of the filament will be positive during the entire cycle. We consider the average value of the diode current, as read by the usual dc meter.

Under these conditions the expression for g becomes

$$g=\frac{1}{2\pi}\int_0^1\int_0^{2\pi}\left[1+\frac{\sqrt{2}}{w}(x-z)\sin\theta\right]^{3/2}dzd\theta. \quad (10)$$

This integral may be evaluated by expanding the integrand in series form and then integrating term by term. One obtains

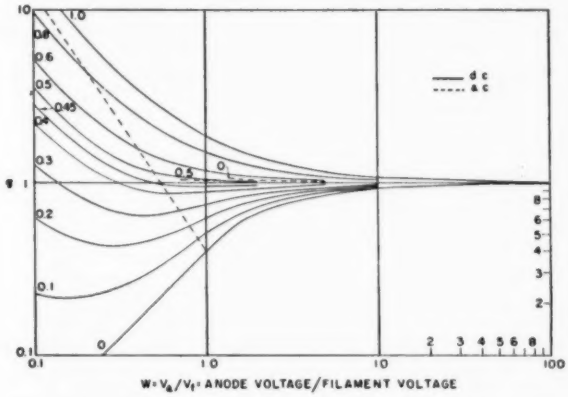

FIG. 1. Effect of filament voltage on plate current of space-charge-limited diode (Parameter = x = position of point on filament from which anode voltage is measured, expressed as a fraction of the filament length and measured from the negative end for dc case).

$$g_a=1+\tfrac{1}{8}[x^3+(1-x)^3]w^{-2}$$
$$+\frac{9}{1280}[x^5+(1-x)^5]w^{-4}+\cdots$$
$$+\frac{3(4n-5)!}{(2n+1)2^{5n-3}(2n-3)!(n!)^2}$$
$$\times[x^{2n+1}+(1-x)^{2n+1}]w^{-2n}+\cdots. \quad (11)$$

All terms of this series are positive and g_a is therefore always greater than unity, i.e., the current is always greater than for an equipotential emitter. This is a result of the presence of the three-halves exponent in the space-charge law. The function g_a is plotted in Fig. 1 for $x=0$ and $x=0.5$ (dashed curves). It is seen that g does not vary rapidly with x and is never much greater than unity. It would be very desirable if values of g_a were available for the case where w is so small that the whole emitter is not active during the entire cycle, but this evaluation has not yet been made.

II. DIODE UNDER RETARDING-FIELD CONDITIONS

Consider first a planar diode with equipotential cathode. Then under retarding-field conditions the anode current will be given by a simple Boltzmann relation,

$$I_0=I_s e^{\epsilon V_a/kT}, \quad (12)$$

where I_s is the saturation value of the cathode emission (we assume negligible space charge), V_a is the plate voltage (which is of course negative) including the correction for contact potential, T is the "electronic temperature" (which we may take as equal to the cathode temperature), ϵ is the electronic charge, and k is Boltzmann's constant. We use the subscript on I to indicate the absence of cathode potential drop. The

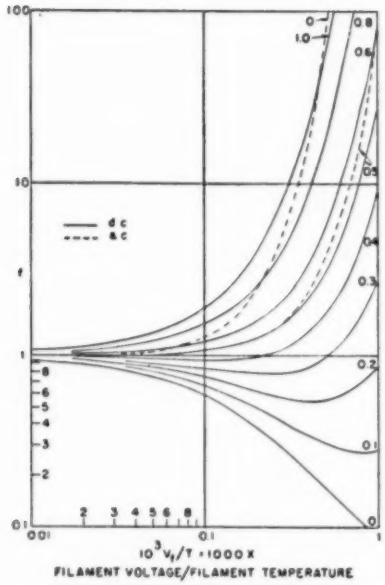

FIG. 2. Effect of filament voltage on plate current of diode under retarding-field conditions (Parameter = x = position of point on filament from which anode voltage is measured, expressed as a fraction of the filament length and measured from the negative end for dc case).

situation for a cylindrical diode is more complicated, but here also if the retarding plate voltage is great enough, a relation of the form of Eq. (12) will apply.[2,3] The discussion below is restricted to this case.

It will be convenient to introduce the quantity

$$v=\epsilon V_f/kT=11{,}606V_f/T. \tag{13}$$

It is also convenient to express the effect of the filament voltage drop on the diode characteristic by the function f, where

$$I=fI_0. \tag{14}$$

Thus f is the ratio of the current actually flowing in the diode to that which would flow in the same diode with the same plate voltage and filament temperature if the emitter were equipotential.

A. Filament Heated by Direct Current

In this case the effective plate voltage is given by Eq. (4). We consider only cases for which $|V_a|>xV_f$ so that the entire length of the filament is in a retarding field. The function f is seen to be given by the relation

$$f=\int_0^1 e^{v(x-z)}dz=e^{xv}(1-e^{-v})/v. \tag{15}$$

Values of f have been plotted in Fig. 2 as a function of x and v (actually the related ratio V_f/T has been used). As in the space-charge-limited case, the effect of the filament voltage drop on the diode characteristic is a minimum for values of x slightly less than 0.5. For $x=0.45$ for example, f is very near unity for $V_f/T<10^{-4}$. For larger values of V_f/T, however, the deviations become quite large. For $x=0.5$, $f=(2/v)\sinh(v/2)$.

B. Filament Heated by Alternating Current

The effective plate voltage for this case is given by Eq. (9). We consider only the case $|V_a|>\sqrt{2}(1-x)V_f$, with $x<0.5$, so that every portion of the filament will be in a retarding field during the entire cycle. The expression for f becomes

$$f_a=\frac{1}{2\pi}\int_0^1\int_0^{2\pi}\exp[-\sqrt{2}v(x-z)\sin\theta]dzd\theta. \tag{16}$$

Upon expanding the integrand in series form and integrating term by term, one obtains

$$f_a=1+\tfrac{1}{6}[x^3+(1-x)^3]v^2+\frac{1}{80}[x^5+(1-x)^5]v^4+\cdots+\frac{v^{2n}}{2^n(2n+1)(n!)^2}[x^{2n+1}+(1-x)^{2n+1}]+\cdots. \tag{17}$$

All terms of this series are positive and f_a is therefore always greater than unity, i.e., the current is always greater than that for an equipotential emitter. The function f_a is plotted in Fig. 2 for $x=0$ and $x=0.5$ (dashed curves). For the same value of x, the value of f increases more rapidly as V_f is increased for ac filament heating than for dc heating.

The foregoing analysis has shown that the effect of filament voltage drop on the retarding potential characteristic of a diode, for either ac or dc filament heating, is determined only by the ratio V_f/T. The conclusion to be drawn from this is that even if the cathode is not unipotential, for a given condition of V_f and T, the plate current is multiplied by a constant factor independent of V_a so that the slope of the retarding-potential characteristic (log I *vs* V_a) is not affected. This conclusion is, of course, subject to the assumption of the simple Boltzmann relation of Eq. (12).

[2] W. Schottky, Ann. Physik **44**, 1011 (1914).
[3] L. H. Germer, Phys. Rev. **25**, 795 (1925).

An X-Ray Diffraction Study of the Hafnium-Hydrogen System

S. S. SIDHU AND J. C. MCGUIRE
Argonne National Laboratory, Chicago, Illinois

(Received May 19, 1952)

The hafnium-hydrogen system at room temperature consists of three phases. The lattice parameters of the hafnium metal used in this investigation and of the three phases are as follows: hafnium, $a_0=3.200$A, $c_0=5.061$A, and $c=1.58$; deformed cubic phase, $a_0=4.702\pm0.012$A, $c_0=4.678\pm0.012$A, and $c=0.995$; face-centered cubic phase, $a_0=4.708\pm0.002$A; and face-centered tetragonal phase, $a_0=4.882\pm0.002$A, $c_0=4.384\pm0.002$A, and $c=0.898$. The deformed cubic phase extends up to $HfH_{1.53}$ and converts into the face-centered cubic phase between $HfH_{1.53}$ and $HfH_{1.70}$. The face-centered cubic phase transforms into the tetragonal phase between $HfH_{1.80}$ and $HfH_{1.87}$. The tetragonal phase extends up to $HfH_{1.98}$.

INTRODUCTION

THIS paper covers the study of the limit of solid solubility of hydrogen in hafnium, the number of hafnium-hydrogen phases formed and their crystalline structures.

EXPERIMENTAL PROCEDURE

The samples were prepared from 1 in.$\times\frac{1}{2}$ in.$\times$11 mil pieces of crystal bar metallic hafnium, with major impurity of zirconium of about 5 atomic percent. Each piece was polished, cleaned, weighed, and then placed in a quartz tube, which was connected by means of stopcocks to a mercury diffusion pump and to a calibrated volume equipped with a monometer, as shown in Fig. 1. Connections were also made so that any gas present in the quartz tube could be returned to the calibrated volume by means of an automatic Toepler pump and measured.

The system was pumped down to approximately 10^{-6} mm Hg pressure and the metal was outgassed for four hours by heating it at 1100°C. The temperature was then lowered to 1000°C and a measured volume of carefully purified hydrogen gas was admitted into the tube at a known pressure. Most of the absorption of hydrogen took place at 700–800°C. The sample was cooled to room temperature at a rate of about 4°C per minute. The gas pressure in the tube at this point was 0.1 mm Hg. The excess hydrogen was pumped back into the calibrated volume and measured.

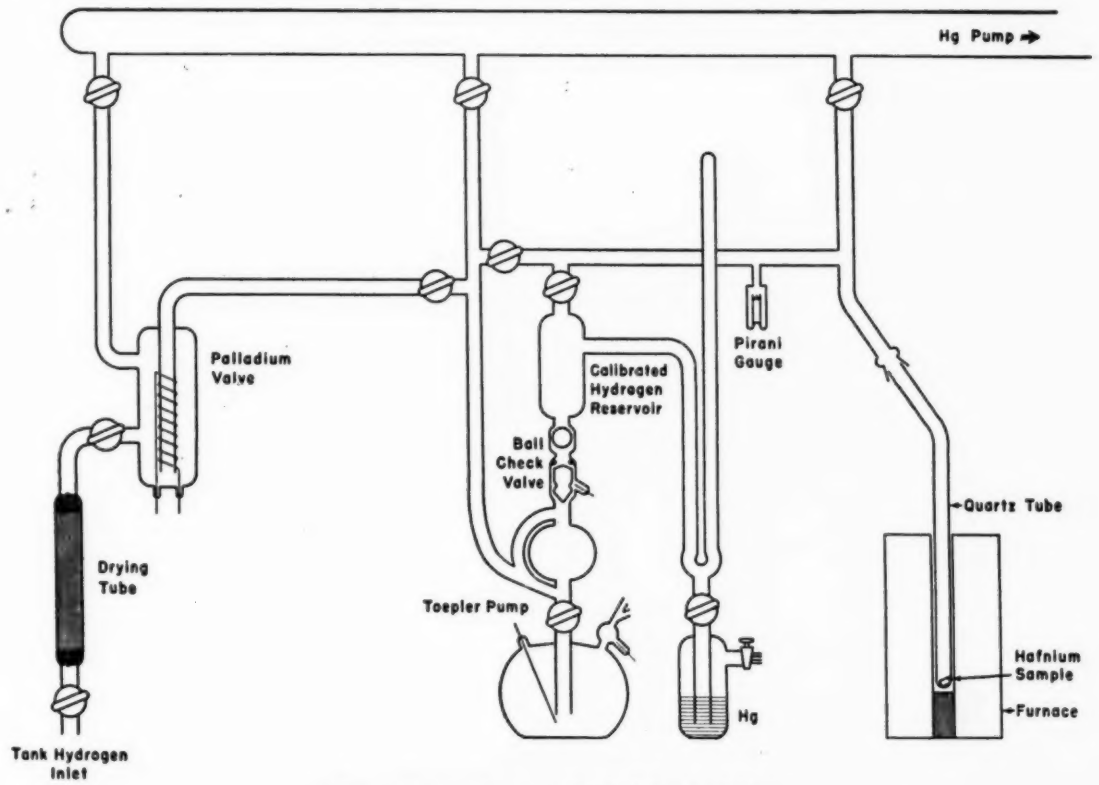

FIG. 1. System for preparing hafnium hydrides.

TABLE I. Interplanar spacings (d), estimated relative intensities (I/I_0) and the Miller indices (hkl) of hafnium.

d(A)	I/I_0*	hkl
2.77	s	100
2.53	s	002
2.43	v.s.	101
1.868	s	102
1.600	s	110
1.443	s	103
1.383	w	200
1.354	s	112
1.337	s	201
1.265	m+	004
1.216	m	202
1.152	m	104
1.065	s	203
1.049	w+	120
1.027	s	121
0.993	s	114
0.968	m	122
0.951	s	105
0.935	m	204
0.924	m	300
0.890	s	123
0.868	m	302
0.844	w	006
0.817	m	205
0.807	m	124, 106

* v = very; s = strong; m = medium; w = weak.

In the preparation of HfH_2 sample where 125.4 cc of H_2 were required for each gram of Hf, the volume of hydrogen admitted into the tube was 300 percent in excess of the theoretical absorption. The sample was cooled to room temperature at a rate of 2.5°C per minute. Hydrogen was then desorbed from the metal by heating and evacuating with the Toepler pump. This cycle was repeated twice to obtain a thoroughly reacted sample.

A few samples of lower composition were made by removing the desired volume of hydrogen from the higher hydrides at about 750°C. Compositions of the samples were calculated from the weight of the metal and the volume of the absorbed hydrogen.

X-ray diffraction data for identification and structure determination of each phase formed were obtained from powder patterns made of annealed representative samples of hydrides. The annealing was done at 350°C for periods over 24 hours. The limit of solubility of hydrogen in hafnium, and the interphase boundaries were determined by employing both the x-ray diffraction and the microscopic techniques.

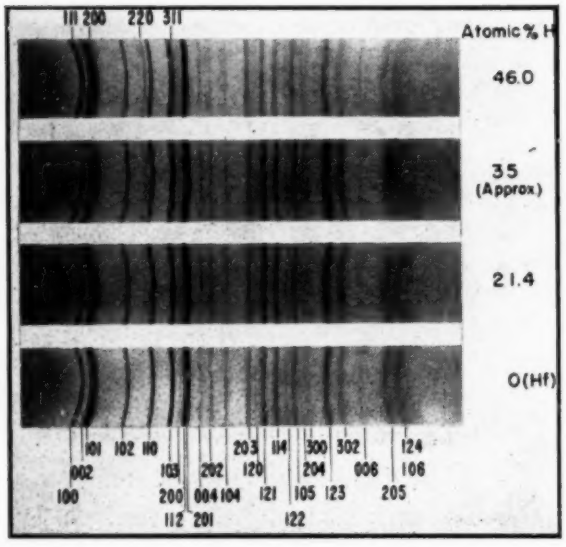

FIG. 2. X-ray diffraction patterns of Hf–H alloys between 0 and 46.0 atomic percent H. (Cu, Kα-radiation, 114.6-mm diameter camera.)

RESULTS

X-ray diffraction data for hafnium metal used in this study are given in Table I. The lattice parameters are: $a_0 = 3.200$A, $c_0 = 5.061$A, and $c = 1.58$. The measured density of the metal was 12.9 g/cc and the calculated density 13.1. These data differ considerably from those given in the literature.[1] The lattice parameters and the density too are different,[1,2] except for some recent values reported by Russell.[3] It is possible that the earlier data were obtained with relatively impure metal.

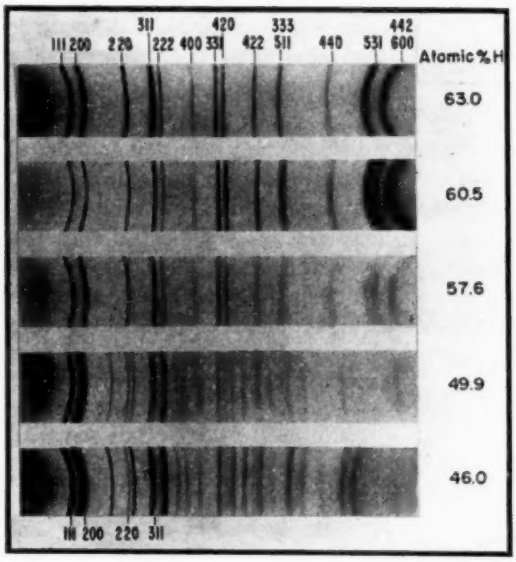

FIG. 3. X-ray diffraction patterns of Hf-H alloys between 46 and 63 atomic percent H. (Cu, Kα-radiation, 114.6-mm diameter camera.)

X-ray diffraction patterns of a series of hafnium samples containing 2.25 to 46.0 atomic percent hydrogen showed that diffraction lines of a hafnium-hydrogen phase began to appear in the pattern of a sample containing 21.4 atomic percent hydrogen. As shown in Fig. 2, no appreciable change was apparent in the diffraction lines of the hafnium metal itself. Photomicrographs of the same series of samples, given

[1] Noethling and Tolkodorf, Z. Krist. **62**, 256 (1925). ASTM Card 2-0885.
[2] A. E. VanArkel, Z. physik. Chem. **130** (1927).
[3] R. B. Russell, MIT-1073 (1951).

TABLE II. Interplanar spacings, estimated relative intensities, and the Miller indices of the cubic phase of hafnium-hydrogen system. Composition: 63.0 atomic percent hydrogen.

d(A)	I/I_0	hkl
2.71	v.s.	111
2.35	s	200
1.665	s	220
1.419	s	311
1.360	m	222
1.177	w	400
1.081	m	331
1.053	m	420
0.962	m	422
0.906	m	(333, 511)
0.832	w	440
0.796	m	531
0.784	m	(442, 600)

below, however, showed that this phase was present in the sample containing as little as 2.25 atomic percent hydrogen, and it increased in amount with the increasing atomic percent of hydrogen until it could be identified by the x-ray diffraction method. It seems, therefore, that the solubility of hydrogen in hafnium must be very small.

Diffraction study of the next series of samples containing 46.0 to 64.8 atomic percent hydrogen revealed that the increase in the hafnium-hydrogen phase continued up to 60.5 atomic percent hydrogen. Between 60.5 and 63.0 atomic percent hydrogen the hafnium metal was completely converted into a single phase hydride. As shown in Fig. 3, this phase extends to 64.8 percent hydrogen. Its diffraction data are given in Table II. It has a face-centered cubic structure with $a_0=4.708\pm0.002$A.

As shown in Fig. 4, the face-centered cubic phase transforms into a face-centered tetragonal phase be-

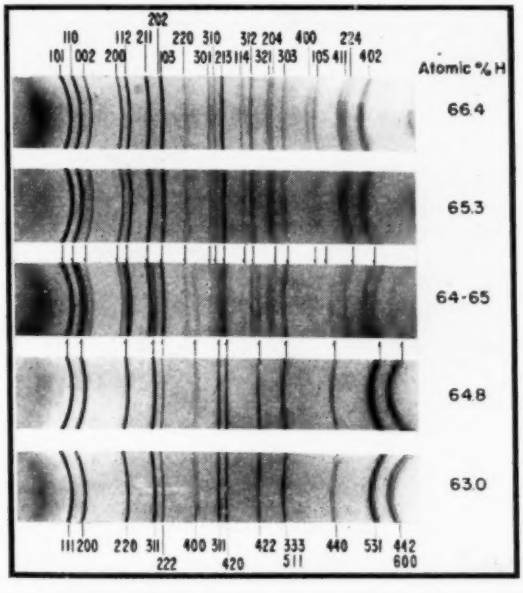

FIG. 4. X-ray diffraction patterns of Hf-H alloys between 63 and 66.4 atomic percent H. (Cu, Kα-radiation, 114.6-mm diameter camera.)

TABLE III. Interplanar spacings, estimated relative intensities, and the Miller indices of the tetragonal phase of hafnium-hydrogen system. Composition: 66.4 atomic percent hydrogen.

d(A)	I/I_0	hkl (F.C.T.)	hkl* (B.C.T.)
2.71	v.s.	111	101
2.44	s	200	110
2.197	m	002	002
1.727	m	220	200
1.631	s	202	112
1.455	s	311	211
1.356	m	222	202
1.348	m	113	103
1.219	w	400	220
1.113	m	331	301
1.091	m−	420	310
1.064	m+	313	213
1.002	w+	204	114
0.977	m−	422	312
0.935	w	511	321
0.928	w	224	204
0.905	w	333	303
0.863	w	440	400
0.853	w	115	105
0.822	m	531	411
0.817	w	404	224
0.802	m−	442	402

* $h_{B.C.T.}=\frac{1}{2}(h+k)_{F.C.T.}$; $k_{B.C.T.}=\frac{1}{2}(h-k)_{F.C.T.}$; $l_{B.C.T.}=l_{F.C.T.}$
(F.C.T.) = face-centered tetragonal, and
(B.C.T.) = body-centered tetragonal.

tween 64 and 65 atomic percent hydrogen with lattice parameters, $a_0=4.882\pm0.002$A, $c_0=4.384\pm0.002$A, and $c=0.898$. The diffraction data for this phase are given in Table III. The phases found at various hydrogen compositions may be summarized as in Table IV.

In working with these hydrides, it was observed that, in general, as the amount of hydrogen increased the ductility of the sample decreased. The sample containing 46.0 atomic percent hydrogen was extremely hard. The hydrides with compositions $HfH_{1.70-1.98}$ were very brittle and could be easily pulverized by crushing in mortar and pestle. Also, the metallic lustre of the hafnium metal in these hydrides was lost and the samples appeared gray-black. However, all the hydrides studied in this investigation were stable at room temperature.

TABLE IV. Hafnium-hydrogen system.

Composition	Atomic % H	Phases and Intensity
$HfH_{0.023}$	2.25	Deformed cubic (v.v.w.)+Hf (s)
$HfH_{0.27}$	21.4	Deformed cubic (v.w.)+Hf (s)
$HfH_{0.55}$	35.0	Deformed cubic (w)+Hf (s)
$HfH_{0.85}$	46.0	Deformed cubic (w+)+Hf (m+)
$HfH_{0.995}$	49.9	Deformed cubic (m)+Hf (m)
$HfH_{1.36}$	57.6	Deformed cubic (s)+Hf (w)
$HfH_{1.53}$	60.5	Deformed cubic (s)+Hf (v.w.)
$HfH_{1.70}$	63.0	Cubic (s)
$HfH_{1.80}$	64.8	Cubic (s)
$HfH_{1.78-1.86}$	64–65	Cubic (m)+tetragonal (m)
$HfH_{1.87}$	65.3	Tetragonal (s)
$HfH_{1.98}$	66.4	Tetragonal (s)

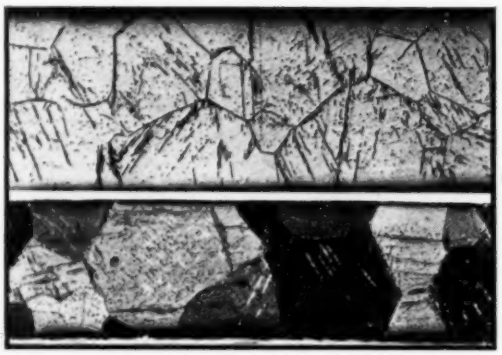

(a)

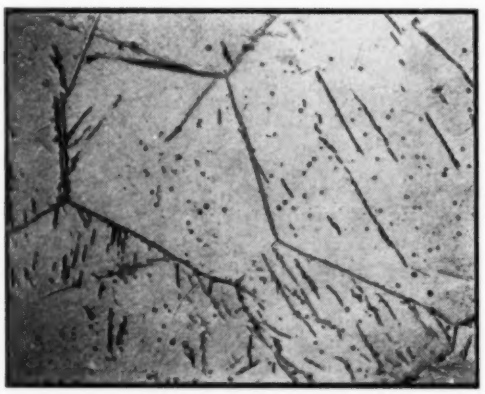

(b)

FIG. 5. Photomicrographs of $HfH_{0.023}$. Magnifications (a) 75, (b) 250.

DISCUSSION

From the results obtained here it is seen that at room temperature hafnium-hydrogen system consists of three phases. The first phase forms at very low concentration of hydrogen, and increases with increasing amount of hydrogen as shown in Figs. 5–7. It coexists with hafnium metal up to a composition of $HfH_{1.53}$. X-ray diffraction patterns of samples between HfH and $HfH_{1.53}$, as seen in Fig. 3, have characteristic appearance of line splitting and groups of lines where single reflection for cubic structure occurs. Diffraction data for $HfH_{1.53}$ sample, as given in Table V, are typical of these samples. The unit cell is slightly deformed and displays a degree of tetragonality with, $a_0=4.702\pm0.012$A, $c_0=4.678\pm0.012$A, and $c=0.995$. However, it approaches a cubic symmetry, and converts to an ideal face-centered cubic structure between $HfH_{1.53}$ and $HfH_{1.7}$.

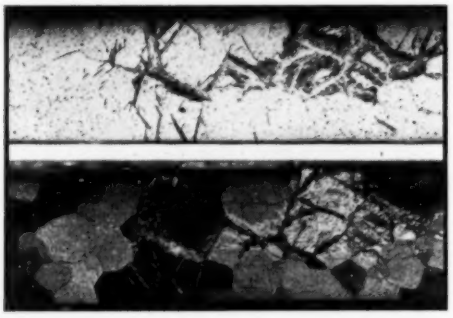

FIG. 6. Photomicrograph of $HfH_{0.27}$. Magnification 75.

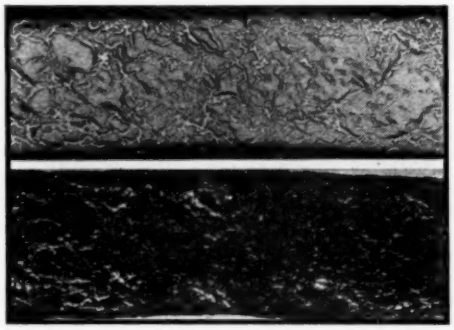

FIG. 7. Photomicrograph of $HfH_{0.55}$. Magnification 75.

The structure of tetragonal phase with composition $HfH_{1.98}$ appears isomorphous with those of ZrH_2[4,5] and ThH_2[5]. For a body-centered tetragonal cell as transformed* from face-centered tetragonal:

$$a_0=3.452\pm0.002\text{A}, \quad c_0=4.384\pm0.002\text{A}, \quad \text{and} \quad c=1.27.$$

The volume of the unit cell is 52.24×10^{-24} cc, density 11.48 grams per cc, and there are 2 HfH_2 per unit cell:

$$\text{Hf}: 000, \tfrac{1}{2}\tfrac{1}{2}\tfrac{1}{2}$$
$$\text{H}: 0\tfrac{1}{2}\tfrac{1}{4}, 0\tfrac{1}{2}\tfrac{3}{4}, \tfrac{1}{2}0\tfrac{1}{4}, \tfrac{1}{2}0\tfrac{3}{4}.$$

The transformation of the tetragonal cell into the face-centered cubic cell at $HfH_{1.8}$ produces only a

TABLE V. X-ray diffraction data for a deformed cubic phase of hafnium-hydrogen system. Composition 60.5 atomic percent hydrogen.

d(A)	I/I_0	hkl
2.716	v.s.	111
2.353	s	200
2.332	s	002
1.664	s	220
1.660	s	202
1.423	s	311
1.411	s	113
1.356	m	222
1.184	w	400
1.175	w	004
1.080	s	331
1.075	s	313
1.054	m	402
1.046	m	204
0.960	m	422
0.956	m	224
0.909	w	511
0.904	m	333
0.898	w	115
0.834	w	440
0.828	w	404
0.796	m	531
0.791	m	513

[4] G. Hägg, Z. Phys. Chem. **B11**, 433 (1930).
[5] Rundle, Shull, and Wallan, Acta. Cryst. **5**, 22 (1952).
* $a_{0(\text{B.C.T.})}=a_0/\sqrt{2}_{(\text{F.C.T.})}$ and $c_{0(\text{B.C.T.})}=c_{0(\text{F.C.T.})}$.

slight contraction in the cell. It seems, therefore, that it may be a second-order transformation. The mechanism of this transformation and the detailed structure of the face-centered cubic cell will be described elsewhere.

Our thanks are due to Mr. Maurice Odie and Dr. H. H. Chiswik for the metallographic examinations of the samples, to Mr. Daniel Zauberis for the x-ray diffraction patterns, and to Dr. Frank G. Foote for helpful discussions.

JOURNAL OF APPLIED PHYSICS VOLUME 23, NUMBER 11 NOVEMBER, 1952

Bariated Tungsten Emitters

RAY C. HUGHES AND PATRICK P. COPPOLA
Philips Laboratories, Inc., Irvington on Hudson, New York
(Received June 9, 1952)

Thermionic emitters consisting of barium oxide dispersed throughout a body of porous tungsten can be successfully made if suitable compounds of barium are employed as the source of the oxide. Compounds such as the carbonate, which can oxidize tungsten and react to form Ba_3WO_6:

$$3BaCO_3+W\rightarrow Ba_3WO_6+3CO,$$

are unsuitable. However, if by various means, BaO is dispersed in tungsten, reaction occurs at operating temperature of the cathode to slowly generate free barium: $6BaO+W\rightarrow Ba_3WO_6+3Ba$, which diffuses to the surface and lowers the work function.

Cathodes consisting of approximately 5 percent of BaO in W are capable of supplying continuous emission in excess of 100 amp/cm², give equivalent dc and pulsed emission, and are highly resistant to damage by arcing, temporary poor vacuum, ion bombardment, and high temperatures.

Emission current of approximately 8 amp/cm² was obtained at an operating temperature of 1000°C from a typical cathode of this type. The life of this cathode, at 1100°C, was in excess of 650 hours. Constants of the Richardson equation for a relatively inactive cathode were $\phi=1.56$ ev, $A=0.6$ amp/cm²/deg².

A SURFACE consisting of a thin film of barium over a thin layer of oxygen on tungsten forms a fairly good emitter of approximately 1.35-ev work function.[1] Recently a successful cathode with emissive surface of this type has been announced.[2] The barium is generated in an internal cavity by reaction between barium oxide and tungsten and diffuses out through a porous tungsten plug, thus constantly replenishing the supply of Ba on the emissive external surface.

A porous tungsten mass throughout which barium oxide is dispersed should function similarly; the tungsten and barium oxide reacting slowly to generate free barium, which diffuses to the surface, maintaining an emissive surface of low work function.

Recent studies[3] have shown barium oxide and tungsten to react as follows:

$$6BaO+W\rightarrow Ba_3WO_6+3Ba.$$

Barium carbonate was shown to react quantitatively in the temperature range 600°–800°C without the formation of any elementary barium:

$$3BaCO_3+W\rightarrow Ba_3WO_6+3CO.$$

Other compounds capable of furnishing an atom of additional oxygen per molecule of barium oxide will also react similarly to produce no free barium.

Since barium oxide is extremely hydroscopic, it is not generally employed as such in cathode work. Rather, the carbonate, hydroxide, or nitrate have been used, and relied upon to disassociate into the oxide. As already indicated, such compounds may react without formation of free barium. This accounts for the failure of prior attempts to produce good emitters from barium compounds dispersed in tungsten; the resulting

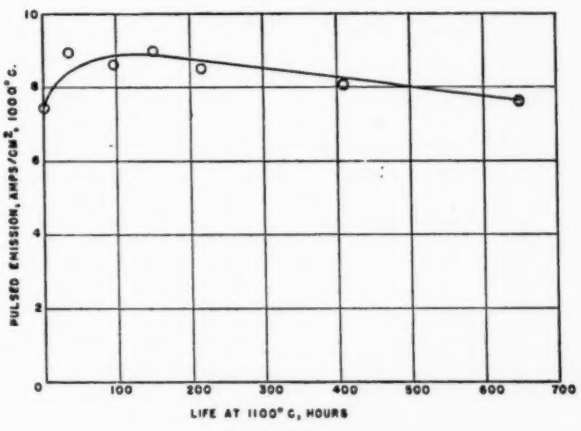

FIG. 1.

[1] A. L. Reimann, *Thermionic Emission* (John Wiley and Sons, Inc., New York, 1934).
[2] Lemmens, Jansen, and Loosjes, Philips Tech. Rev. **11**, 341 (1950).
[3] Hughes, Coppola, and Evans, Phys. Rev. **85**, 388 (1952).

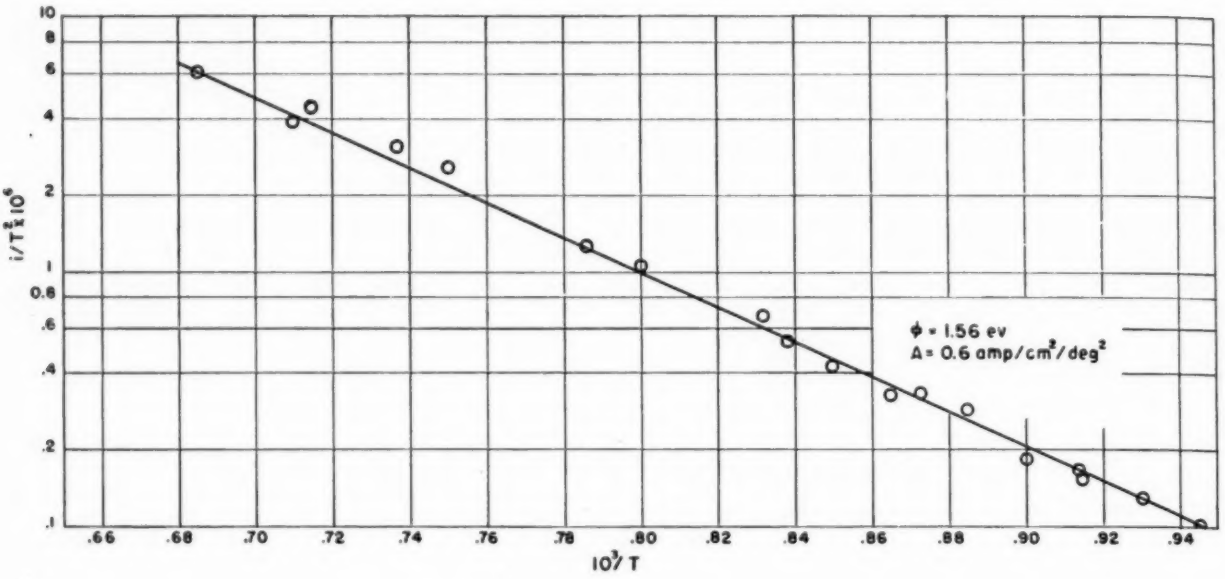

FIG. 2.

cathodes have been successful only as "cold cathodes," not as "hot cathodes."

Barium oxide can be obtained dispersed in tungsten, without simultaneous oxidation of the tungsten, by various expedients, for example:

(a) Formation of BaO and mixing with W rapidly to avoid reversion to hydroxide and carbonate.

(b) Use of two or more barium compounds which react together to form BaO and no by-products capable of oxidizing W. (Example: $Ba(N_3)_2+Ba(COOH)_2 \rightarrow 2BaO+3N_2+2CO+H_2$).

(c) Addition of a reducing agent which reduces $BaCO_3$ (or other Ba compound) to BaO. (Example: $BaCO_3+C \rightarrow BaO+2CO$).

(d) Stabilizing BaO by firing with other oxides, such as Al_2O_3 or SiO_2. The product gives a decreased reaction rate and consequent lower rate of barium evolution.

By these means, cathodes consisting of 5–10 percent by weight of barium oxide dispersed in tungsten have been successfully made.

Figure 1 shows a plot of emission (pulsed, 100 microsecond pulse length, repetition rate 20 per sec) at a cathode temperature of 1000°C as a function of life. This cathode was operated continuously at 1100°C and measured intermittently at 1000°C.

Figure 2 shows a Richardson plot for a cathode of moderate activity. The work function of this cathode is 1.56 ev. Emission densities as high as 15 amperes/cm² were measured for this plot. At higher unmeasured temperatures, an emission density exceeding 100 amps/cm² was continuously obtainable.

From a cathode of slightly higher activity, a direct current emission of 1.5–2 amperes/cm² was obtained at 900°C in a diode structure with 200 volts on the plate. Pulsewise, a similar emission was obtained at the same temperature.

These cathodes, having an emissive surface essentially metallic in character and with continuously replenished barium supply, are not permanently damaged by ion bombardment, temporary poor vacuum, or arcing. Operation at 1300°C also causes no permanent damage.

JOURNAL OF APPLIED PHYSICS VOLUME 23, NUMBER 11 NOVEMBER, 1952

Creep of Copper under Deuteron Bombardment

WARREN F. WITZIG
University of Pittsburgh and Westinghouse Electric Corporation, Pittsburgh, Pennsylvania*
(Received June 18, 1952)

The creep rate of copper under deuteron bombardment has been investigated using the 16-Mev external beam of the University of Pittsburgh cyclotron. Measurements were made of the second stage creep rate of a copper wire under deuteron bombardment at a temperature of 260°C and a loading of 10,000 psi. Within the precision of the experiment ±20 percent, the creep rate during and after bombardments of 10 to 20 hours duration was unchanged from the creep rate preceding bombardment. Theoretical considerations of the type discussed by Slater, predict that with the available deuteron flux of 10^{12} particles per cm^2 per sec there should be no appreciable change in creep rate. The available deuteron flux cannot displace enough atoms from their normal lattice sites to produce a dislocation involving a hundred atoms or more; further, the steady-state density of displaced atoms is not enough to impede the motion of those dislocations present in the crystals. While regions of increased local temperature are produced during bombardment, these also should not affect the creep rate. Thus, apparently the considerations of solid-state theory are confirmed and creep rates should not be expected to increase for all metals under bombardment.

I. INTRODUCTION

A LITERATURE search reveals little experimental information on radiation damage to the physical properties of metals. Andrade,[1] however, describes large increases in the creep rate of cadmium while under alpha-particle bombardment. This has led to considerable concern by those who use metals subjected to particle radiation.

In this work the creep of copper was determined under deuteron bombardment in the University of Pittsburgh Cyclotron. Such bombardment can displace atoms from lattice sites and can produce small regions of higher temperature, "thermal spikes." Slater[2] indicates that the creep rate under particle radiation might be expected to increase or decrease depending upon the relative magnitude of these two effects.

II. EXPERIMENTAL

A. Creep Specimen

The specimen was made of oxygen-free high-conductivity copper in the form of 0.0200 in.±0.0001 diameter wire and was obtained from the North American Phillips Company. Table I lists the impurities as found by a spectrographic analysis. Since the range of deuterons in copper is about 0.0128 in., all the deuterons were stopped in the specimen.[3]

TABLE I. Impurities in OFHC copper.

Element	Percent
Ag	0.0005
Al	0.001[a]
Si	0.008
Ca	0.005[a]
Pb	0.001

[a] Less than. Not detected: As, Au, Be, Cb, Cd, Gd, Ir, Sb, Tl, V, W, Zn, Zr.

The wire was annealed in a vacuum (10^{-5} mm Hg) at 300°C for one hour and furnace cooled. The grain size of the specimen before and after annealing was the same, ASTM No. 9, with an orientation along the wire.

The gauge length of the specimen was fixed on one end by a quadrant of a copper disk soldered to the creep wire. The disk served as an electrical contact for the extensometer. On the other end the gauge length was fixed by allowing the wire at the end of the furnace to operate much below the creep temperature.

B. Creep Apparatus

Figure 1 shows the special creep machine that was designed to maintain the operating temperature and to remotely record the specimen elongation.

It was possible to control the creep furnace temperature to within ±1C° throughout a creep test without bombardment. The entire furnace volume could be made uniform in temperature within ±1C° by adjustment of the power flowing to three furnace windings. The bombardment introduces another source of power into the furnace. It was found by means of 8-mil

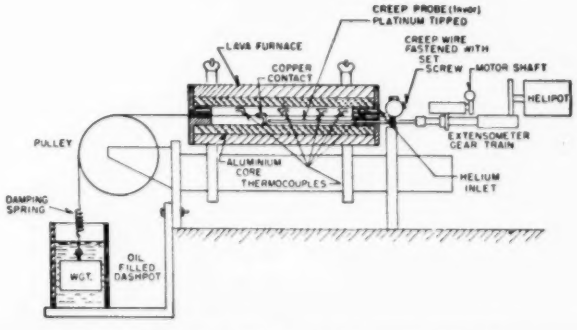

FIG. 1. Schematic sketch of the creep apparatus.

* A portion of a dissertation presented to the University of Pittsburgh in partial fulfillment of the requirements for the degree of Doctor of Philosophy.

[1] E. N. daC. Andrade, Nature **156**, 113 (1945).

[2] J. C. Slater, J. Appl. Phys. **22**, 237 (1951).

[3] *Range Energy Curves*, University of California Research Laboratory Report 121 (1949).

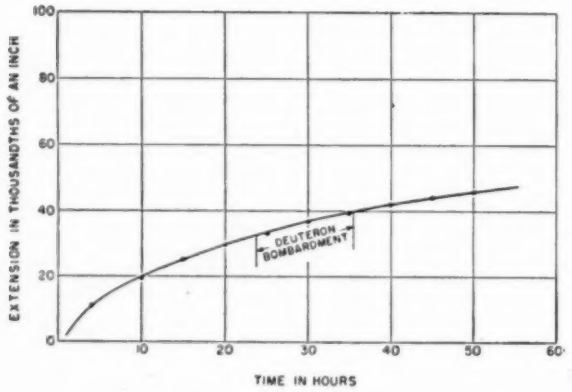

FIG. 2. Extension with deuteron bombardment *versus* time for OFHC copper 10,000 psi stress, 260°C, 3.78 in. gauge length.

Chromel-Alumel thermocouples mounted on the creep wire that: (a) the wire could be held within ±5C° during bombardment, (b) the wire temperature at any thermocouple location was within ±4C° of the average temperature.

1. Stress and Extension

The specimen wire was fastened rigidly at one end; the other end was draped over a pulley and fastened by a spring to a lead weight. The weight rode in an oil-filled cylinder with small tolerances. This combination of dashpot and spring effectively reduced vibration of of the specimen wire. Under load (about 1500 grams) a 5-gram weight was sufficient to produce an acceleration of the pulley and its load. Thus, pulley friction could cause a maximum error of 0.3 percent in the applied stress. The specimen extension was measured by an extensometer, a motor driven probe which continuously hunted the copper disk on the creep wire.[4] The precision of location of this disk was 30 microinches, but when this went through a gear train, helipot and a recorder, the precision dropped to 100 microinches.

2. Creep Tests Without Radiation

To test the creep machine a series of runs without radiation was made. The creep rate in the second stage at 260°C and 10,000 psi was 13 percent/1000 hr (3.7×10^{-8} 1/sec); this is in good agreement with values in the literature for 0.125 in. diameter copper wire.[5]

C. Creep Under Bombardment

During the experiments with radiation the temperature of the specimen was kept near 260°C by suitable adjustment of the currents in the heating coils.

The deuteron beam intensity during the creep tests varied over the gauge length of the specimen, roughly in a parabolic form; the intensity at the disk was twice that at the other end of the gauge length. This was verified by the temperature rise of the creep wire due to the heating caused by the beam and by radioactivity measurements on the creep wire. The intensities given for bombardments are average intensities over the gauge length.

Figure 2 shows the graph of specimen extension *versus* time. In this figure and the following figure, the extension caused by the initial application of stress has not been plotted. The deuteron bombardment was started at the 24th hour and was stopped at the 37th hour. There is no discontinuity at either place. For control purposes, several specimens, identical to the one used in the first experiment were made; extension as a function of time (without radiation) of one of these specimens is shown in Fig. 3. It was found that the creep rate of the control specimens at any given time agreed within ±12 percent, this established the combined precision for the apparatus and specimen history. The creep rates or slopes of these curves were determined mechanically after a method described by Worthing.[6] For this purpose curves were very carefully drawn using a great many more points than are shown here. These creep rates are tabulated in Table II.

III. DISCUSSION

It is generally accepted that the creep of single crystals proceeds by the movement of lattice imperfections called dislocations.[7–9] Polycrystalline material is composed of grains of single crystals; in such material creep may proceed not only by movement of lattice imperfections but by yielding of the material at the grain boundaries. This latter phenomenon is important only at very high temperatures.[10,11] In this work, which was conducted at 260°C, yielding of grain boundaries should be negligible.[12]

The specific questions are: (1) Can the bombarding deuterons produce dislocations? (2) Is the steady state density of displaced atoms reached in the specimen high enough to appreciably impede the motion of the dislocations? (3) Can thermal spikes increase the creep rate?

A. Dislocations

A dislocation is a lattice defect which was first postulated to explain the low yield stress of single crystals[13]; one of its several general forms has been

[4] M. J. Manjoine, Trans. Am. Soc. Mech. Engrs. **67**, 111 (1945).
[5] *Metals Handbook* (ASM Cleveland, 1948), p. 908.
[6] A. G. Worthing and J. Geffner, *Treatment of Experimental Data* (John Wiley and Sons, Inc., New York, 1944).
[7] E. Orowon, Z. Physik **89**, 634 (1943).
[8] M. Polanyi, Z. Physik **89**, 660 (1934).
[9] G. I. Taylor, Proc. Roy. Soc. (London) **145**, 362 (1934).
[10] Nathans, Parker, and Hazlett, "A survey of theories of creep of metals" (University of California Report UCM-2, November, 1949).
[11] E. Orowon, Some problems of creep of metals (Purdue University Creep Seminar, April 12, 1951).
[12] T. S. Ke, "A grain boundary model and the mechanism of viscous intercrystalline slip" *Tenth Quarterly Report to ONR on Deformation on Metals*, N798, p. 55 (1948).
[13] F. Seitz and T. A. Read, J. Appl. Phys. **12**, 100, 170, 470, 538 (1941).

experimentally confirmed in a recent paper by Frank.[14] During creep, dislocations move under the applied stress, allowing the grains of the polycrystal to deform. According to the recovery theory of creep,[15] the density of dislocations in the metal remains constant during the second stage where the strain rate is constant. Under these conditions the rate of annihilation of dislocations is equal to their rate of generation. Dislocations can impede one another's motion; also, impurity atoms, displaced atoms, and lattice defects of other types produce stress fields which can retard dislocations.

TABLE II. Creep rate of copper wire.

Time	Experiment	Control
10 hours	8.9×10^{-8} sec^{-1}	8.0×10^{-8} sec^{-1}
15	7.3	7.0
20	6.4	5.7
25	5.6[a]	4.5
30	5.0[a]	4.0
35	3.9[a]	3.3
40	2.9	3.2
45	2.9	3.2
50	2.9	3.2

[a] Under deuteron bombardment (8×10^{11} deuterons/cm^2 sec). This experiment was repeated a second time with essentially the same results.

B. Radiation Damage

When a charged nuclear particle of high velocity penetrates matter, it interacts with both the electrons in the material and to a smaller extent with the nuclei of the atoms. The rate of energy loss depends on the energy of the bombarding particle. The encounters with electrons result in atomic excitation and ionization; encounters with the nuclei are elastic collisions in general.

If the energy lost in an elastic collision is larger than some value E_d, the atom is ejected from its lattice site. This results in the production of an interstitial atom and a vacant lattice site or hole. Such a combination is labeled a displacement. If the energy lost is less than E_d, the atom is not ejected but oscillates about its lattice site. This lattice vibration degenerates into ordinary thermal motion.

Energy spent ionizing atoms and exciting the electron gas in the metal will quickly spread itself over large areas due to the large mean free path of the electrons. However, excited electrons and lattice vibrations can be considered as resident energy, localized near the path of the nuclear particle. This gives rise to small regions of higher temperature or thermal spikes.

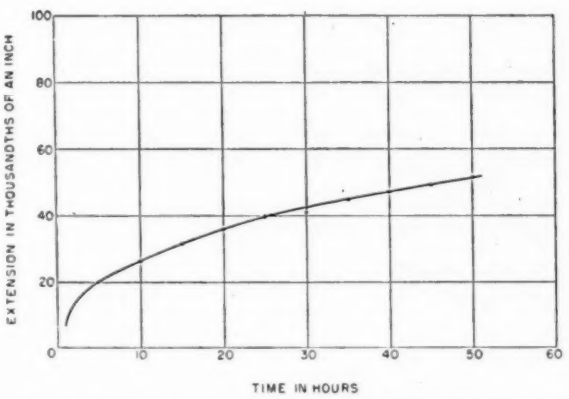

FIG. 3. Extension *versus* time (control) for OFHC copper 10,000 psi stress, 260°C, 4.12 in. gauge length.

1. Displacements

Rough estimates of the number of displacements produced by a deuteron can be made as follows. About 1/1000th of the deuteron energy goes into elastic nuclear collisions and this occurs primarily after ionization has practically ceased. Essentially the cross section for elastic collisions becomes large when the deuteron energy falls below 10^4 electron volts. Of this energy approximately half will be spent on lattice vibrations and half on displacements. If the energy required to displace an atom is 25 ev, the number of displacements will be 200. Following Seitz,[16] a more refined calculation yields about 100 displaced atoms per deuteron.

In a typical experiment the deuteron intensity was of the order of 1×10^{12} deuterons/cm^2 sec. This means one displaced atom for every thousand atoms during a 10-hour bombardment. This is a maximum value as no annealing of displaced atoms is considered.

On the basis of Rutherford scattering, a deuteron might cause at most one displaced atom per five atom planes near the end of its range. Since a dislocation may be considered as involving some 10^3 atoms (number of atoms in a row extending through a mosaic block) it is difficult to picture this type of bombardment as a producer of dislocations.

Another source of lattice disruption is the high energy copper recoils produced at the beginning of the deuteron range. These recoils can produce a continuous chain of displacements but, since their range is much less than the dimensions of a mosaic block, production of a large dislocation (10^3 atoms or more) is not possible. However, at the end of their range, the production of small loop dislocations appear reasonable. Since there are few of these copper recoils, as can be seen by the lack of straggling at the end of the deuteron range, it appears that the production of a large number of dislocations is improbable.

a. Steady-state number of displacements.—While displacements are being produced at some rate, B, they are also annealing because of hole and interstitial encounters. The rate of annealing may be assumed to be proportional to the product of the number density of

[14] F. C. Frank, Phys. Rev. **83**, 874(T) (1951).
[15] E. Orowon, J. Western Scot. Iron and Steel Inst. **22**, 45 (1947).
[16] F. Seitz, Discussions of the Faraday Society, Crystal Growth No. 5, Gurney and Jackson (London 1949), p. 271.

vacancies, N_v, and the number density of interstitials, N_i. Since $N_v=N_i=N$, the annealing is proportional to N^2. At steady-state conditions, where the production rate equals the annealing rate, the number of displacements becomes,

$$N=(B/K)^{\frac{1}{2}}. \quad (1)$$

The annealing constant K can be correlated with the coefficient of self-diffusion, D, on a basis of hole migration for the annealing of interstitial and hole.[17] Following a suggestion of Brooks,[18] an approximate relation is,

$$K=6aD/n, \quad (2)$$

where a is the lattice spacing and n is the ratio of the number of holes to the number of lattice sites without irradiation. At thermodynamic equilibrium,

$$n=\beta e^{-E/kT} \quad (3)$$

where E is the energy required to form a hole (about 1 ev), k is Boltzmann's constant, T is the temperature and β is the order of 100.[19]

The order of magnitude of the steady-state number of displacements can now be calculated from Eqs. (1), (2) and (3) using $a=2.3\times10^{-8}$ cm, $E=1$ ev, $n\cong10^{-16}$, $D=4.7\times10^{-24}$ cm^2/sec[20]. For a flux of 10^{12} deuterons/cm^2 sec the value for B is about 10^{16} displacements/cm^3 sec. At the creep temperature of 260°C, a value for N of about 10^{16} displacements per cubic centimeter is obtained. This steady-state value is approximately 1 atom in 10 million, much lower than 1 atom in a 1000 as calculated for no annealing.

The time constant for Eq. (1) is,

$$t^*=1/(BK)^{\frac{1}{2}}, \quad (4)$$

and calculated to be the order of one-half second. Typical bombardments of 10 to 15 hours are long compared with this time and insured the attainment of the steady-state number of displacements.

b. Effect of displacements on dislocation.—A dislocation is a lattice disruption involving some 10^3 atoms. On the average, however, only 1 atom in 10^7 is displaced in equilibrium under irradiation. It is difficult to picture this density of displaced atoms having any appreciable effect on the movement of the dislocations.

2. *Thermal Spikes*

The temperature rise in the path of a fast deuteron penetrating copper can be estimated in the following way. The average space rate of energy loss of a 16-Mev deuteron along its range is about 500 Mev/cm. Only about one thousandth of this energy is dissipated directly to the nuclei in the solid; the remainder is given to the electrons. This electronic energy spreads out rapidly through the lattice and is transferred only very slowly to the nuclei because of the large mass difference; it cannot produce small regions of high temperature.

Only the temperature, i.e., thermal motion of the nuclei, can have an effect on creep. The rate of energy loss to the nuclei is about $1/1000\times500$ Mev/cm$=0.5$ Mev/cm. The average lattice spacing in Cu is 2.3×10^{-8} cm so that the deuteron loses 10^{-2} ev per atom plane to the nuclei.

When the energy is shared by 10 atoms, i.e., thirty degrees of freedom, the temperature rise is only 4C°. As a result we have very small volumes being raised but a few degrees in temperature. Very small regions along the path of the relatively few high energy copper recoils will rise in temperature to as high as 10^4°C. However, it has little meaning to speak of the temperature of just a few atoms and this temperature will last only some 10^{-11} second.

IV. CONCLUSION

The creep rate of OFHC copper wire at 260°C and 10,000 psi is not affected by deuteron bombardment of an intensity of 10^{12} deuterons/cm^2 sec. This statement is valid within the precision of the experiment, about 20 percent. These results are in agreement with the theoretical calculations presented. Consequently it does not seem justified to use the results of Andrade's experiments as a general indication of the effect of radiation on creep.

The author wishes to acknowledge the assistance of Drs. W. E. Johnson and A. J. Allen in conducting the experiments. Discussions of the manuscript with Drs. S. Krasik and D. Halliday were most helpful. In addition, my colleagues of the Solid State Physics Group have offered many helpful suggestions.

[17] H. B. Huntington and F. Seitz, Phys. Rev. **61**, 315 (1941).

[18] F. C. Brooks (private communication). The author is indebted to Dr. Brooks for his discussions of this problem.

[19] M. A. Mott and R. W. Gurney, *Electronic Processes in Ionic Crystals* (Oxford University Press, London, 1948), p. 31.

[20] C. J. Smithells, *Metals Reference Book* (Interscience Publishers, Inc., New York, 1949), p. 404.

JOURNAL OF APPLIED PHYSICS VOLUME 23, NUMBER 11 NOVEMBER, 1952

Diffraction of a Shock or an Electromagnetic Pulse by a Right-Angled Wedge*

JOSEPH B. KELLER
Institute for Mathematics and Mechanics, New York University, New York, New York
(Received May 14, 1952)

Graphs of the theoretical pressure distribution resulting from diffraction of a weak shock by a rigid right-angled corner are presented and compared with graphs of measured pressure distributions. The agreement is found to be satisfactory. A graph of the electric field resulting from diffraction of an electromagnetic pulse by a perfectly conducting right-angled corner is also presented.

IN a previous article[1] the problem of diffraction of an electromagnetic or acoustic pulse (or weak shock) by a wedge or corner was solved. In the present note the results of two calculations based on that solution are given, as well as a comparison of the calculated results with experimental measurements. The agreement between theory and experiment is found to be satisfactory.

A pulse is assumed to approach a right-angled wedge with its front parallel to one face of the wedge, and to hit it at time $t=0$. Part of the pulse continues past the wedge, part is reflected back by the wedge, and in addition a diffracted wave originates from the vertex of the wedge. If c is the propagation speed in the medium surrounding the wedge, the diffracted wave is confined to a circle of radius ct at time t, with its center at the vertex. It is the field in this circle which is of interest.

The two cases considered refer to two different boundary conditions on the wedge. In the first case the field quantity is assumed to vanish on the wedge. This applies to an electromagnetic pulse and a perfectly conducting wedge, with the electric field parallel to the edge. The results are shown in Fig. 1, the lines $v=$ constant being the level lines, or lines of constant electric field strength. The radial coordinate is r/ct, where r is the distance of a point from the edge of the wedge, and t is the time. Thus, only the scale of the figure changes with time. The incident field strength is assumed to be 1, and the field before the pulse arrives is assumed to be zero. The pulse is not of finite duration; but rather a Heaviside pulse—the field is 1 everywhere behind the incident pulse front.

The field after diffraction is zero in front of the incident pulse, one behind it except in the diffraction circle, and zero between the reflected pulse front and the wedge. Within the circle it is less than one everywhere, but is undefined at the two singular points where the incident and reflected pulse fronts are tangent to the diffraction circle. These points are of interest in considering the relationship between the pulse solution and geometrical optics, since they correspond to shadow boundaries.[2]

The other case is that in which the normal derivative of the field quantity vanishes on the wedge. This applies to an acoustic pulse or weak shock, if the field quantity is the excess pressure and the wedge is rigid. It also applies to an electromagnetic pulse and a perfectly conducting wedge, if the field quantity is the magnetic field, which is parallel to the edge. The results are shown in Fig. 2. All the above discussion of Fig. 1 also applies to Fig. 2. The only differences are that the field is 2 between the wedge and the reflected pulse front being doubled by reflection, that there is only one singular point, and that the field is between 1 and 2 in the circle. The solution was computed from Eq. (18) of reference 1 with $\phi=\psi=\pi/4$ and $\lambda=\frac{2}{3}$.

In Fig. 3 experimental data on weak shock diffraction supplied by Dr. Donald R. White of Palmer Physical

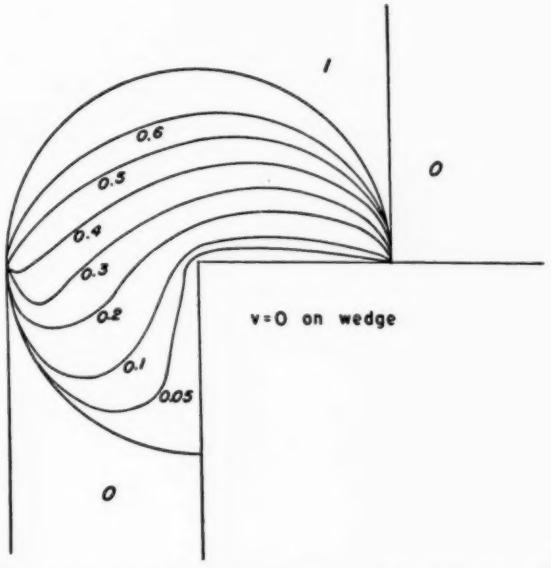

FIG. 1. Contour lines of constant electric field strength in diffraction of a pulse by a perfectly conducting right-angled wedge. The radial coordinate is r/ct and the circle is given by $r/ct=1$.

* This work was performed at Washington Square College of Arts and Science, New York University, and was supported in part by Contract No. AF-19(122)-42, with the U. S. Air Force through sponsorship of the Geophysics Research Division, Air Force Cambridge Research Center, Air Materiel Command.

[1] "Diffraction and reflection of pulses by wedges and corners," Joseph B. Keller and Albert Blank, Communications on Pure and Applied Mathematics, IV, No. 1, 75–94, June, 1951.

[2] The solution was computed from Eq. (17) of reference 1, with $\phi=\psi=\pi/4$ and $\lambda=\frac{2}{3}$.

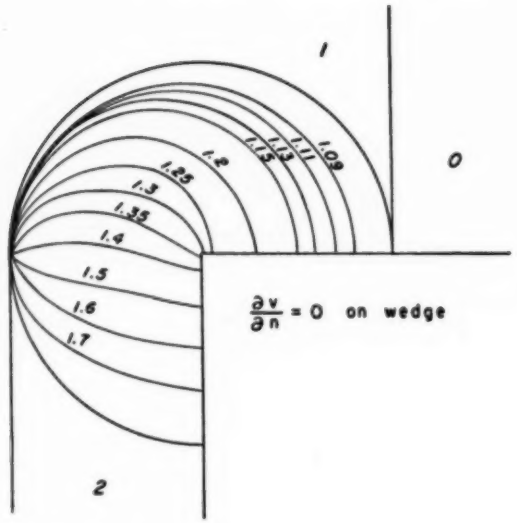

FIG. 2. Contour lines of constant excess pressure in diffraction of a shock by a rigid right angled wedge. The radial coordinate is r/ct and the circle is given by $r/ct=1$.

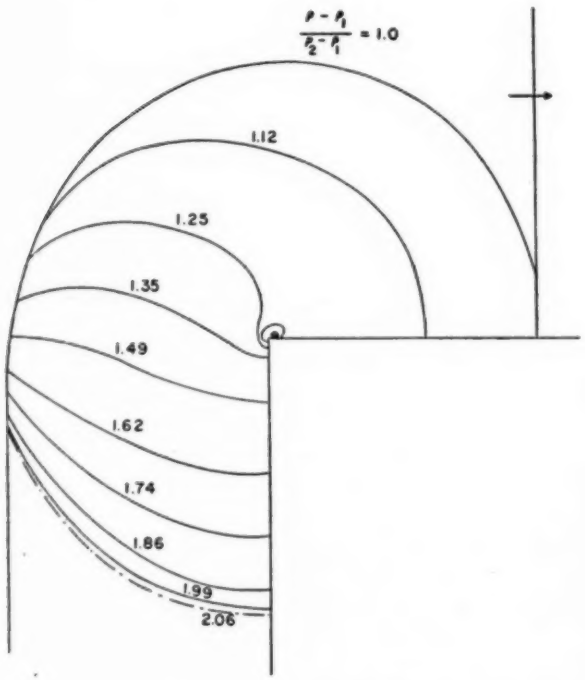

FIG. 3. Measured contour lines of constant excess density in diffraction of a shock by a rigid right angled wedge. The values of $(\rho-\rho_1)/(\rho_2-\rho_1)$ are given for each line. The incident shock density ratio $\rho_2/\rho_1=1.081$. Compare calculated contours in Fig. 2. (Courtesy of Dr. Donald R. White, Princeton University.)

Laboratory, Princeton University, is presented.[3] The lines of constant density are plotted, the numbers designating excess density divided by incident excess density. This figure is to be compared with Fig. 2. The agreement is fair although the incident pressure ratio $\rho_2/\rho_1=1.081$, indicating that the linear theory may be inadequate. A more detailed comparison of theory and experiment is shown in Fig. 4, in which the excess pressure divided by the incident excess pressure is plotted along the top and front walls of the wedge. The dashed curve is based on the calculation used in constructing

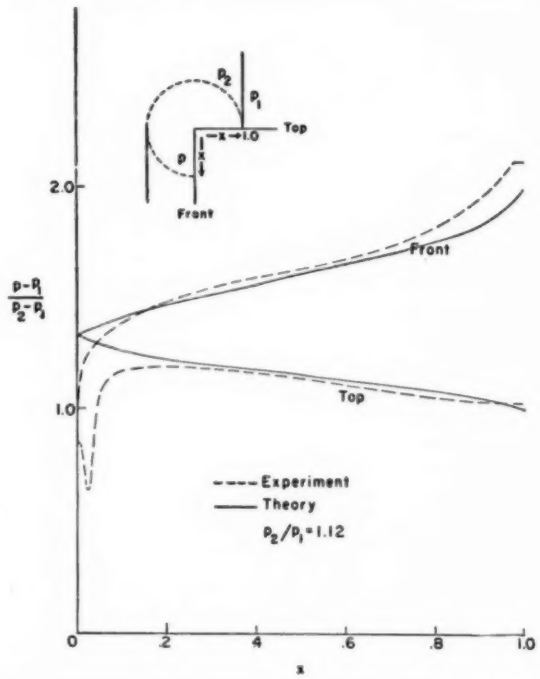

FIG. 4. Comparison of computed and measured excess pressure ratios in diffraction of a shock by a rigid right angled wedge. (Courtesy of Dr. Donald R. White, Princeton University.)

Fig. 2, the solid curve on experimental data like that of Fig. 3 with $p_2/p_1=1.12$. The agreement is satisfactory except at the vertex, where a vortex due to viscosity occurs in the experiment.

I wish to thank Mr. Leon Nemerever for performing the calculations and Professor Eugene Isaacson for his helpful interest.

[3] See "The diffraction of shock waves around obstacles and the resulting transient loading of structures," Tech. Report II-6 by White, Weimer, and Bleakeny, August 1, 1950, and Tech. Report II-3 by Walker Bleakney, March 16, 1950. Department of Physics, Princeton University. The curves are from White and Bleakney, Tech. Report II–11, "Shock loading of rectangular structures" (January 1, 1952).

JOURNAL OF APPLIED PHYSICS VOLUME 23, NUMBER 11 NOVEMBER, 1952

Initial Behavior of a Spherical Blast*

J. A. McFADDEN
Naval Ordnance Laboratory, White Oak, Silver Spring, Maryland

(Received May 28, 1952)

At time $t=0$ a unit sphere containing a perfect gas at uniformly high pressure is allowed to expand suddenly into a homogeneous atmosphere. Solutions for short times later are sought by analytic (i.e., not numerical) methods. Viscosity and heat conduction are neglected. The particle velocity, sound speed, and entropy are developed in powers of y, which is proportional to the time (more precisely, the distance moved by the head of the rarefaction wave in time t), with coefficients depending on a slope coordinate $q=(1/2N)[(2N-1)+(1-x)/y]$, where x is the radial coordinate, $N=(\frac{1}{2})(\gamma+1)/(\gamma-1)$, and γ is the ratio of specific heats. The zero-order coefficients are the plane shock-tube solution. First-order corrections are derived for the various regions. Boundary conditions are approximated for small y at the surfaces of discontinuity, and the method for matching the solutions in the different regions is outlined. This matching process is carried out for the expansion of a diatomic gas into diatomic air.

INTRODUCTION

NUMEROUS attempts[1] have been made to obtain solutions which describe the propagation of spherical blast waves in an inviscid fluid. The vast majority of the methods used require either (a) that the disturbance be weak, or (b) that the expansion obey a given similarity constraint, appropriate only for point-source explosions. The only successful solutions which avoid these restrictions were obtained by Penney and Dasgupta[2] and by Wecken,[3] who attacked some particular spherical explosion problems by the method of characteristics.

In an actual explosion the disturbances are not weak, and the volume of gas generated is finite; the dynamical behavior of this gas will invariably influence the blast waves in the surrounding fluid. Yet a straightforward numerical attack on this more complicated problem is extremely difficult. The first (and by no means least) difficulty is in starting the integration. If the initial values are given by regular functions, successive stepwise integrations soon lead to anomalous results; accordingly, shock discontinuities must be introduced at ill-defined points. Alternatively, if the initial values are discontinuous, shocks appear immediately, but the accompanying changes in the dependent variables are enormous when applied to any reasonable mesh of coordinates.

In this report an analytic method is applied to an idealized problem with discontinuous initial values—the problem of the "spherical shock tube." The behavior immediately after the "explosion" is described by analytic solutions. These solutions should provide a qualitative picture of the behavior at later times, starting values for stepping ahead numerically after the initial discontinuity has been smoothed out, and an early quantitative check on any numerical method which surmounts the starting difficulty.

1. STATEMENT OF THE PROBLEM

The following idealized blast problem is considered. A perfect gas at high pressure is held stationary by a thin spherical diaphragm of unit radius, surrounded by a second perfect gas at uniformly low pressure. (Henceforth, the inner medium will be referred to as "gas", the outer medium as "air.") At time $t=0$ the diaphragm is destroyed and the gas rushes outward, compressing the air around it.

The subsequent behavior may be described by a space-time diagram as in Fig. 1. In region A is undisturbed gas. Region B is a rarefaction wave (bounded by a "head" and a "tail") in which the gas is rapidly expanding, irrespective of the behavior outside the tail. Region C consists of rarefied gas which is moving outward. An interface or contact surface separates the gas from region D, which contains compressed air also

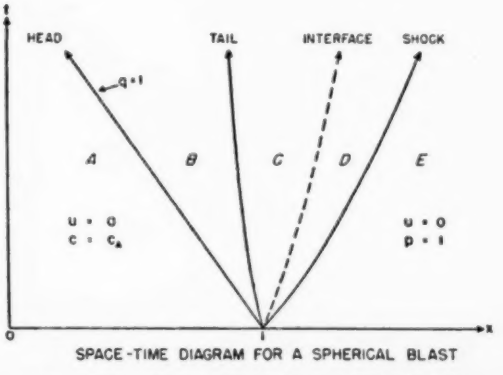

FIG. 1. Space-time diagram for a spherical blast.

* Preliminary reports on this investigation were presented to the American Physical Society at Ithaca, New York, September 12, 1951 [Phys. Rev. **84**, 611 (A) (1951)], and at New York, New York, January 31, 1952 [Phys. Rev. **86**, 600(A) (1952)].

[1] See, for example, R. Courant and K. O. Friedrichs, *Supersonic Flow and Shock Waves* (Interscience Publishers, Inc., New York, 1948), pp. 416–433; W. G. Penney and H. H. M. Pike, Rep. Phys. Soc. Progr. Phys. **13**, 46–82 (1950); R. H. Cole, *Underwater Explosions* (Princeton University Press, Princeton, 1948), Chapter 4. The problem of a spherical blast at *great* distances from the origin has been treated by G. B. Whitham, Proc. Roy. Soc. (London) **A203**, 571–581 (1950).

[2] See reference 1, W. G. Penney and H. H. M. Pike, and R. H. Cole, Chapter 4.

[3] F. Wecken, Z. ang. Math. Mech. **30**, 270–271 (1950).

moving outward. Finally, the transition from the undisturbed air in region E into region D takes the form of a shock.

This problem is the spherical analog of the plane shock tube. The spherical geometry introduces several new difficulties, among them being that (a) the spherical term in the equation of continuity prevents solution by the classical one-dimensional methods, (b) the tail of the rarefaction wave, the interface, and the shock front travel with varying speeds, and (c) the entropy varies spatially in the air behind the shock front.

If p is the pressure, ρ the density, u the particle velocity, S the entropy per mole, x the radial distance from the geometric center, and t the time, then we may assume the validity of the equations of motion for the spherical flow of an inviscid fluid in the absence of heat conduction,[4]

$$\left.\begin{aligned} \rho(u_t+uu_x)+P_x&=0,\\ \rho_t+u\rho_x+\rho(u_x+2u/x)&=0,\\ S_t+uS_x&=0, \end{aligned}\right\} \quad (1.01)$$

where the subscripts t and x denote differentiation. To these equations must be added the entropic equation of state of a perfect gas,

$$p\rho^{-\gamma}=\gamma^{-\gamma}\exp(S/c_v), \quad (1.02)$$

where $\gamma=c_p/c_v$, c_p and c_v being the (constant) specific heat capacities per mole at constant pressure and volume, respectively, and the entropy scale has been chosen so that $S=0$ when $p=1$ and $\rho=\gamma$.

A more suitable form of Eq. (1.01) is obtained by expressing p and ρ in terms of S and the sound speed $c=(\gamma p/\rho)^{\frac{1}{2}}$ and then absorbing a constant in a new "entropy" function

$$\mathcal{S}=S/c_v\gamma(\gamma-1). \quad (1.03)$$

Then

$$p=c^{2N+1}\exp(-\gamma\mathcal{S}), \quad \rho=\gamma c^{2N-1}\exp(-\gamma\mathcal{S}), \quad (1.04)$$

where $N=(1/2)(\gamma+1)/(\gamma-1)$, N not necessarily being an integer, and the equations of motion (1.01) take the following form:

$$\left.\begin{aligned} u_t+uu_x+(2N-1)cc_x-c^2\mathcal{S}_x&=0\\ (2N-1)(c_t+uc_x)+c(u_x+2u/x)&=0\\ \mathcal{S}_t+u\mathcal{S}_x&=0. \end{aligned}\right\} \quad (1.05)$$

Equations (1.05) must be satisfied in each of the five regions[5] in Fig. 1, but the solutions in regions A and E are trivial. If we take as initial conditions that $u=0$, $c=c_A$, $\mathcal{S}=\mathcal{S}_A$ (c_A and $\mathcal{S}_A$ being constants) in the gas where $0\leq x\leq 1$, and $u=0$, $c=1$, $\mathcal{S}=0$ (and therefore $p=1$) in the air where $x>1$, then for $t>0$ these conditions will prevail in regions A and E, respectively, and certain boundary conditions must be satisfied between them.

The head of the rarefaction wave travels inward at the (constant) speed of sound according to the equation

$$x_H=1-c_At. \quad (1.06)$$

Since this path is a characteristic of the differential equations (1.05), discontinuities in the derivatives of u and c are permissible there, but u, c, and $\mathcal{S}$ must be continuous; that is, when $x=x_H$,

$$u_B=0, \quad c_B=c_A, \quad \mathcal{S}_B=\mathcal{S}_A, \quad (1.07)$$

under the restriction that the rarefaction wave has not yet reached the center; that is, $0<t<1/c_A$. (Subscripts A, B, C, and D refer to the various regions.)

The tail of the rarefaction wave moves at a variable speed, either inward or outward (but always inward relative to the particles). For the plane shock tube this path is a characteristic, and we shall attempt to extend this condition to the spherical case[6] in the zero- and first-order approximations. The conditions applicable in these approximations will be specified later.

The interface between the gas and the air moves outward at varying speed. Since it is a particle path, the velocity u of the particles must approach the same limit from both sides, the limit being equal to the velocity of the surface itself. Furthermore, if the acceleration of the interface is to be finite, the pressure p must also be the same on both sides (except when $t=0$; then the acceleration is infinite). Then if x_I is the radius of the spherical interface, the boundary conditions are that, when $x=x_I$,

$$u_C=u_D, \quad t\geq 0; \quad p_C=p_D, \quad t>0. \quad (1.08)$$

The density ρ, the sound speed c, and the entropy S will be discontinuous across the interface.

The shock front moves outward into the air at a variable velocity U. Since the mass, the momentum, and the energy must be conserved across the shock, the equations of Rankine and Hugoniot are satisfied, and the particle velocity, the sound speed, and the pressure inside the shock front may be expressed in terms of the shock velocity U. For perfect "air" with $p=1$, $c=1$, and $u=0$ outside, the shock conditions are as follows,[7] where x_S is the radius of the shock: When $x=x_S$, $t>0$,

$$\left.\begin{aligned} u_D&=(2N-1)(U^2-1)/2NU,\\ c_D^2&=[(2N+1)U^2-1][U^2+(2N-1)]/4N^2U^2,\\ p_D&=[(2N+1)U^2-1]/2N. \end{aligned}\right\} \quad (1.09)$$

[4] See, for example, reference 1, R. Courant and K. O. Friedrichs, p. 29.

[5] For simplicity only one constant γ (or N) has been used; however, the method can easily be generalized to let γ change at the interface.

[6] F. Wecken, reference 3, asserts that the tail of the rarefaction wave in a spherical explosion is a weak shock, beginning with zero strength at time $t=0$ and gaining strength as time goes on. Numerical evidence for such a shock has been found by T. S. Walton at the Naval Ordnance Laboratory, by applying the dynamical shock model of v. Neumann and Richtmyer [J. Appl. Phys. **21**, 232–237 (1950)] to this spherical problem, but the method gives no information as to when the shock is formed. In the present paper the boundary conditions are satisfied to first order without a tail shock; therefore the shock must be of higher order.

[7] See, for example, reference 1, R. Courant and K. O. Friedrichs, pp. 148–149.

2. APPROXIMATION FOR SMALL TIME

It is required that we find solutions of the above problem for small times $t \ll 1/c_A$. For this purpose the following transformation of the independent variables is convenient:[8]

$$q=(1/2N)[(2N-1)+(1-x)/c_A t], \quad y=c_A t. \tag{2.01}$$

q is a linear function of the slope dx/dt of a straight line which passes through the point $x=1$, $t=0$ in the space-time diagram, and is proportional to the sound speed in region B *in the plane-wave case.* By Eq. (1.06) it follows that $q=1$ at the head of the rarefaction wave, and from Eq. (2.01) we observe that q decreases as x increases. The second variable y is the distance moved by the head in the time t.

The transformation (2.01) has the double advantage of removing the singularity at the point $x=1$, $t=0$, while also rendering the boundary conditions approximately independent of y.

Next we assume that $u(q, y)$, $c(q, y)$, and $\mathcal{S}(q, y)$ are regular functions of q and y in each of the three regions B, C, and D near the point $y=0$. Then we can attempt a power-series development in powers of y, assuming that the head of the rarefaction wave has moved a small portion of the initial gas radius; that is, $y \ll 1$. Then

$$u(q, y)=\sum_{n=0}^{\infty} u_n(q)y^n, \quad c(q, y)=\sum_{n=0}^{\infty} c_n(q)y^n,$$

$$\mathcal{S}(q, y)=\sum_{n=0}^{\infty} \mathcal{S}_n(q)y^n. \tag{2.02}$$

If the differential Eq. (1.05) are transformed by (2.01) and the series (2.02) are substituted, we obtain as a zero-order approximation three ordinary differential equations,

$$\{c_A[(2N-1)-2Nq]-u_0\}u_0' - (2N-1)c_0c_0'+c_0^2\mathcal{S}_0'=0, \tag{2.03}$$

$$(2N-1)\{c_A[(2N-1)-2Nq]-u_0\}c_0'-c_0u_0'=0, \tag{2.04}$$

$$\{c_A[(2N-1)-2Nq]-u_0\}\mathcal{S}_0'=0, \tag{2.05}$$

where the symbol ($'$) denotes differentiation with respect to q. The first-order equations are as follows:

$$\{c_A[(2N-1)-2Nq]-u_0\}u_1' + (2c_AN-u_0')u_1-(2N-1)c_0c_1' + [2c_0\mathcal{S}_0'-(2N-1)c_0']c_1+c_0^2\mathcal{S}_1'=0, \tag{2.06}$$

$$-c_0u_1'-(2N-1)c_0'u_1 + (2N-1)\{c_A[(2N-1)-2Nq]-u_0\}c_1' + [2c_AN(2N-1)-u_0']c_1=-4Nc_0u_0, \tag{2.07}$$

$$-\mathcal{S}_0'u_1+\{c_A[(2N-1)-2Nq]-u_0\}\mathcal{S}_1' + 2c_AN\mathcal{S}_1=0. \tag{2.08}$$

[8] Another form of this transformation and the subsequent power series is used by F. Wecken, reference 3.

Approximations higher than the first order in y will not be considered in this paper.

For each order of approximation to the differential equations, an appropriate approximation to the boundary conditions must be used. The condition at the head is the simplest, for there $q=1$, independently of y. For zero order, from Eq. (1.07),

$$u_0(1)=0, \quad c_0(1)=c_A, \quad \mathcal{S}_0(1)=\mathcal{S}_A, \tag{2.09}$$

and, for all higher orders,

$$u_n(1)=0, \quad c_n(1)=0, \quad \mathcal{S}_n(1)=0; \quad n=1, 2, 3, \cdots. \tag{2.10}$$

At the tail, at the interface, and at the shock, q varies with y. We may write

$$\left.\begin{aligned} q_T&=q_{T0}+q_{T1}y+0(y^2),\\ q_I&=q_{I0}+q_{I1}y+0(y^2),\\ q_S&=q_{S0}+q_{S1}y+0(y^2),\end{aligned}\right\} \tag{2.11}$$

where q_{T0}, q_{I0}, and q_{S0} are related by the first of equations (2.01) to the slopes of the respective paths at $t=0$, and q_{T1}, q_{I1}, and q_{S1} are undetermined constants. For the time being, only zero-order conditions can be specified at these points.

We shall attempt to make the zero-order values of u, c, and $\mathcal{S}$ continuous across the tail (which would then be a characteristic, to zero order). Then the zero-order condition can be written at $q=q_{T0}$,

$$\begin{aligned} u_0(q_{T0}-0)&=u_0(q_{T0}+0),\\ c_0(q_{T0}-0)&=c_0(q_{T0}+0),\\ \mathcal{S}_0(q_{T0}-0)&=\mathcal{S}_0(q_{T0}+0).\end{aligned} \tag{2.12}$$

If the tail is a characteristic, its slope is $dx/dt=u-c$, since the disturbance is moving inward at sonic speed relative to the particles. Then the difference function (u_0-c_0) at $q=q_{T0}$ is the initial velocity of propagation of the tail, and is equal to the value of $(x_T-1)/t$ along the tangent to the tail at $t=0$ in the space-time diagram; therefore, by Eq. (2.01),

$$u_0(q_{T0})-c_0(q_{T0})=c_A[(2N-1)-2Nq_{T0}]. \tag{2.13}$$

In similar fashion, we may use Eqs. (1.04) and (1.08) to approximate the conditions at the interface to zero order.

$$\left.\begin{aligned} u_0(q_{I0}-0)&=u_0(q_{I0}+0),\\ c_0^{2N+1}(q_{I0}-0)\exp[-\gamma\mathcal{S}_0(q_{I0}-0)]&\\ =c_0^{2N+1}(q_{I0}+0)\exp[-\gamma\mathcal{S}_0(q_{I0}+0)]&.\end{aligned}\right\} \tag{2.14}$$

But the velocity in (2.14) is the initial velocity of the interface and is equal to the value of $(x_I-1)/t$ along the tangent to the interface at $t=0$ in the space-time diagram; therefore, by Eq. (2.01),

$$u_0(q_{I0})=c_A[(2N-1)-2Nq_{I0}]. \tag{2.15}$$

At the shock, we may apply Eqs. (1.04) and (1.09) and write the following zero-order conditions:

$$\left.\begin{aligned} u_0(q_{S0}+0)&=(2N-1)(U_0^2-1)/2NU_0,\\ c_0^2(q_{S0}+0)&\\ &=[(2N+1)U_0^2-1][U_0^2+(2N-1)]/4N^2U_0^2,\\ c_0^{2N+1}(q_{S0}+0)&\exp[-\gamma\mathcal{S}_0(q_{S0}+0)]\\ &=[(2N+1)U_0^2-1]/2N, \end{aligned}\right\} \quad (2.16)$$

where U_0 is the initial velocity of the shock. As in the case of the interface, q_{S0} and U_0 may be related by

$$U_0=c_A[(2N-1)-2Nq_{S0}]. \quad (2.17)$$

3. SOLUTION FOR ZERO ORDER

The assumption of solutions of the type (2.02) leads to zero-order solutions identical with those of a plane shock tube. To prove this statement, let us first examine Eq. (2.05). The only physically realistic solution is that $\mathcal{S}_0'=0$ in each of the regions B, C, and D. By the boundary conditions, $\mathcal{S}_0$ must be constant in the entire gaseous sphere,

$$\mathcal{S}_0=\mathcal{S}_A, \quad 1\geq q>q_{I0}. \quad (3.01)$$

In region D the "entropy" assumes a different constant value C_0.

$$\mathcal{S}_0=C_0, \quad q_{I0}>q>q_{S0}. \quad (3.02)$$

Next we may substitute $\mathcal{S}_0'=0$ into Eqs. (2.03) and (2.04). The resulting equations may be added and subtracted, respectively; then we obtain the following pair of equations:

$$\{c_A[(2N-1)-2Nq]-(u_0\pm c_0)\}\times[u_0'\pm(2N-1)c_0']=0. \quad (3.03)$$

(These are the equations for plane isentropic flow.) This system has four possible solutions, depending on which factors are set equal to zero. In three cases, the functions are linear in q; in the fourth, the functions are constant. For the rarefaction zone B, only the following linear solution is compatible with the boundary condition (2.09) at the head:

$$u_0=c_A(2N-1)(1-q), \quad c_0=c_Aq, \quad 1\geq q\geq q_{T0}. \quad (3.04)$$

This equation describes a centered simple rarefaction wave.[9] In regions C and D the boundary conditions require that we choose constant solutions. For region C, the following solution agrees with (3.04) at $q=q_{T0}$:

$$u_0=c_A(2N-1)(1-q_{T0}), \quad c_0=c_Aq_{T0}, \quad q_{T0}\geq q>q_{I0}. \quad (3.05)$$

In region D we employ new constants A_0 and B_0.

$$u_0=A_0, \quad c_0=B_0, \quad q_{I0}>q>q_{S0}. \quad (3.06)$$

By using Eq. (2.14) for the interface, we may match the solutions (3.02) and (3.06) with (3.01) and (3.05). Then

$$A_0=c_A(2N-1)(1-q_{T0}), \quad (3.07)$$

$$B_0^{2N+1}\exp(-\gamma C_0)=(c_Aq_{T0})^{2N+1}\exp(-\gamma\mathcal{S}_A). \quad (3.08)$$

At the shock we substitute the solutions (3.02) and (3.06) into (2.16); then

$$A_0=(2N-1)(U_0^2-1)/2NU_0, \quad (3.09)$$

$$B_0^2=[(2N+1)U_0^2-1][U_0^2+(2N-1)]/4N^2U_0^2, \quad (3.10)$$

$$B_0^{2N+1}\exp(-\gamma C_0)=[(2N+1)U_0^2-1]/2N. \quad (3.11)$$

Equations (3.07)–(3.11) must be solved for the five constants A_0, B_0, C_0, q_{T0}, and U_0. This problem involves the solution of the equation

$$[c_A(2N-1)(1-q_{T0})]^2=\frac{(2N-1)^2}{2N+1}\,\frac{(p_Aq_{T0}^{2N+1}-1)^2}{2Np_Aq_{T0}^{2N+1}+1} \quad (3.12)$$

for q_{T0}, where $p_A=c_A^{2N+1}\exp(-\gamma\mathcal{S}_A)$, the pressure in region A. After q_{T0} is determined, the other constants can be calculated from Eqs. (3.07)–(3.11). Furthermore q_{S0} may be found by the substitution of U_0 into (2.17). Now all the constants of the zero-order problem can be regarded as known except q_{I0}. If we let $u_0(q_{I0})=A_0$ in Eq. (2.15), we find that

$$A_0=c_A[(2N-1)-2Nq_{I0}]. \quad (3.13)$$

If we then eliminate A_0 between Eqs. (3.07) and (3.13), we find the following relation between q_{I0} and q_{T0}:

$$q_{I0}=(2N-1)q_{T0}/2N. \quad (3.14)$$

4. FIRST-ORDER SOLUTIONS IN THE VARIOUS REGIONS

Solutions of the first-order Eqs. (2.06), (2.07), and (2.08) yield the first spherical corrections to the plane-wave solution. These equations can be solved when u_0, c_0, and $\mathcal{S}_0$ are known functions of q.

For the rarefaction zone B, these functions are taken from Eqs. (3.01) and (3.04). Then the appropriate first-order equations are the following:

$$qu_1'-(4N-1)u_1+(2N-1)qc_1'+(2N-1)c_1=c_Aq^2\mathcal{S}_1', \quad (4.01)$$

$$qu_1'+(2N-1)u_1+(2N-1)qc_1'-(4N^2-1)c_1=4c_AN(2N-1)q(1-q), \quad (4.02)$$

$$q\mathcal{S}_1'-2N\mathcal{S}_1=0. \quad (4.03)$$

These equations may be solved together with the boundary conditions (2.10) at the head. As we should expect, $\mathcal{S}_1$ is zero throughout the region, since these gas particles have not crossed any shock front. We find the

[9] See, for example, R. Courant and K. O. Friedrichs, reference 1, pp. 104–106.

following solutions for the first-order coefficients in region B, if $N\neq 1, 2$:

$$u_1=-\frac{c_A(2N-1)q}{2}\,\frac{2(N-2)-3(N-1)q+(N+1)q^{N-1}}{(N-1)(N-2)}, \tag{4.04}$$

$$c_1=-\frac{c_Aq}{2}\,\frac{2(N-2)(2N-1)-(N-1)(4N-3)q+(3N-1)q^{N-1}}{(N-1)(N-2)}, \tag{4.05}$$

$$s_1=0, \tag{4.06}$$

$$1\geq q>q_T.$$

Note that if $N=3, 4, 5, \cdots$ then u_1 and c_1 are polynomials of degree N. If $N=1, 2$, the solutions are logarithmic. $N=2$ is of interest, since then $\gamma=5/3$ (monatomic gas). For $N=2$,

$$u_1=-(3c_Aq/2)[3q\log q+2(1-q)], \tag{4.07}$$

$$c_1=-(c_Aq/2)[5q\log q+6(1-q)], \tag{4.08}$$

$$s_1=0, \quad 1\geq q>q_T. \tag{4.09}$$

For all N, both u_1 and c_1 vanish as $q\to 0$; therefore in a complete rarefaction there is no first-order change in the speed of the first particles to escape into vacuum.

Next let us determine the first-order solutions in region C. For this region the functions u_0, c_0, and s_0 are taken from Eqs. (3.01) and (3.05). The following differential equations result:

$$[(2N-1)q_{T0}-2Nq]u_1'+2Nu_1-(2N-1)q_{T0}c_1'+c_Aq_{T0}^2s_1'=0, \tag{4.10}$$

$$-q_{T0}u_1'+(2N-1)[(2N-1)q_{T0}-2Nq]c_1'+2N(2N-1)c_1=-4c_AN(2N-1)q_{T0}(1-q_{T0}), \tag{4.11}$$

$$[(2N-1)q_{T0}-2Nq]s_1'+2Ns_1=0. \tag{4.12}$$

These equations have the following general solutions ($N\neq 0, \frac{1}{2}$):

$$u_1/c_A=k_1[(N-1)q_{T0}-Nq]+k_2N[q_{T0}-q]-k_3q_{T0}^2/2N \tag{4.13}$$

$$c_1/c_A=\frac{k_1[(N-1)q_{T0}-Nq]-k_2N[q_{T0}-q]}{2N-1}-2q_{T0}(1-q_{T0}) \tag{4.14}$$

$$s_1=-(k_3/2N)[(2N-1)q_{T0}-2Nq], \tag{4.15}$$

$$q_T>q>q_I,$$

where k_1, k_2, and k_3 are constants of integration. If we use the formula (3.14) in the entropy Eq. (4.15), we find that as $q\to q_{I0}$, $s_1\to 0$ irrespective of k_3. Then by Eqs. (3.01) and (2.11) it follows that

$$s(q_I+0, y)=s_A+0(y^2)$$

at the interface. This conclusion is in agreement with the physical statement that the interface is a particle path.

In region C the series (2.02) are equivalent to double series in integral powers of t and $(x-x_{I0})$, where $x_{I0}=1+y[(2N-1)-2Nq_{I0}]$, the zero-order approximation to the radius of the interface.

In region D the solutions are completely analogous to those in region C. For convenience, A_0 is partially eliminated in favor of q_{I0} by equation (3.13). The first-order coefficients are the following:

$$u_1=(K_1/2)[2c_AN(q_{I0}-q)-B_0]+(K_2/2)[2c_AN(q_{I0}-q)+B_0]-B_0^2K_3/2c_AN, \tag{4.16}$$

$$c_1=\frac{K_1[2c_AN(q_{I0}-q)-B_0]-K_2[2c_AN(q_{I0}-q)+B_0]}{2(2N-1)}-\frac{2A_0B_0}{c_A(2N-1)}, \tag{4.17}$$

$$s_1=-K_3(q_{I0}-q), \tag{4.18}$$

$$q_I>q>q_S,$$

where K_1, K_2, and K_3 are new constants of integration. The essential difference between these formulas and the solutions (4.13), (4.14), and (4.15) is that the zero-order value of sound speed changes at the interface.

In the above solutions, the constants c_A and N are given for the entire problem and q_{T0}, q_{I0}, A_0, and B_0 are known from the zero-order solution. The methods for determining k_1, k_2, k_3, K_1, K_2, and K_3 will be discussed subsequently.

5. FIRST-ORDER BOUNDARIES AND BOUNDARY CONDITIONS

In order to write the boundary conditions to first order, we must first specify the location of the boundaries; that is, we must relate the first-order terms in Eqs. (2.11) to the solutions at known points.

In the first place, if the tail is a characteristic (to first order), then along the tail,

$$dx_T/dt = u(q_T+0, y) - c(q_T+0, y) + 0(y^2). \quad (5.01)$$

If we express x_T and t in terms of q_T and y by Eqs. (2.01), replace the right member of (5.01) by appropriate partial sums for region B, without specifying u_1 and c_1 but making use of (3.04), and then eliminate q_T by the first of Eqs. (2.11), we find that the constant q_{T1} can be represented by

$$q_{T1} = -[u_1(q_{T0}) - c_1(q_{T0})]/2c_A N, \quad (5.02)$$

where $u_1(q_{T0})$ and $c_1(q_{T0})$ may be obtained from Eqs. (4.04) and (4.05), respectively, or, if $N=2$, from (4.07) and (4.08). By those Eqs., u_1 is always greater than c_1 for a given value of q in the range $0<q<1$; therefore q_{T1} is negative and the acceleration of the tail at $t=0$ is positive.

Next we shall prove that to first order the solutions can all be made continuous across the tail. Let us postulate the following boundary conditions:

$$\left.\begin{aligned} u(q_T+0, y) - u(q_T-0, y) &= 0(y^2), \\ c(q_T+0, y) - c(q_T-0, y) &= 0(y^2), \\ \mathcal{S}(q_T+0, y) - \mathcal{S}(q_T-0, y) &= 0(y^2). \end{aligned}\right\} \quad (5.03)$$

It is now to be proved that the appropriate partial sums of (2.02) can be made to satisfy these three conditions.

(a) It follows immediately that the entropy can be made continuous to first order if $k_3=0$.

(b) Consider the linear combination $[u-(2N-1)c]$. In region C, this combination is independent of k_1, and as $q\to q_T$ the term containing k_2 becomes of second order, since $q_T - q_{T0} = 0(y)$. Then if $k_3=0$ the limit at $q=q_T-0$ depends (to first order) only on c_A, N, and q_{T0}. In region B, the same linear combination may be evaluated at $q=q_T+0$. q_T can be eliminated by means of Eqs. (2.11) and (5.02), and by the difference of Eqs. (4.01) and (4.02) the resulting combination of $u_1(q_{T0})$ and $c_1(q_{T0})$ can be expressed in terms of c_A, N, and q_{T0}. The result is the same as at $q=q_T-0$; therefore the given combination of u and c can be matched (to first order) at the tail, irrespective of both k_1 and k_2.[10]

(c) Consider a second linear combination $[u+(2N-1)c]$. In region C, this combination is independent of k_2. By means of the solutions in regions B and C and Eq. (5.02), we find that (with $k_3=0$) this combination can be matched (to first order) if k_1 assumes the following values: For $N\neq 1, 2$,

$$k_1 = \frac{2N-1}{(N-1)(N-2)} \times [(N-2) - 2(N-1)q_{T0} + Nq_{T0}^{N-1}], \quad (5.04)$$

and for $N=2$,

$$k_1 = 6q_{T0}\log q_{T0} + 3(1-q_{T0}). \quad (5.05)$$

(d) In conclusion, if k_1 is given by (5.04) or (5.05) and $k_3=0$, then the solutions in regions B and C satisfy all three conditions (5.03), irrespective of k_2.

Consider next the location of the interface. The interface follows a particle path; therefore, along it,

$$dx_I/dt = u(q_I+0, y). \quad (5.06)$$

We may proceed as we did with Eq. (5.01), thereby determining q_{I1}. If we define

$$A_1 = u_1(q_{I0}+0), \quad (5.07)$$

then we find that

$$q_{I1} = -A_1/4c_A N. \quad (5.08)$$

Note that the denominator in (5.08) is $4c_A N$; whereas in (5.02) it was only $2c_A N$.

Now we can approximate the boundary conditions (1.08). Since u_0 is constant on both sides of the interface, the function $[u(q_I\pm 0, y) - u(q_{I0}\pm 0, y)]$ is of $0[(q_I - q_{I0})y]$, and therefore of $0(y^2)$. Then in a first-order calculation we may satisfy the first of conditions (1.08) at $q=q_{I0}$ instead of at q_I, and the same reasoning applies to the pressure condition. By Eqs. (2.14) the zero-order terms cancel, and the appropriate first-order condition is

$$u_1(q_{I0}+0) = u_1(q_{I0}-0), \quad (5.09)$$

where the arguments $(q_{I0}\pm 0)$ indicate from which region the solutions are calculated. The first-order pressure condition may be found in a similar way. The relation (1.04) is substituted for pressure; then c and $\mathcal{S}$ are expanded in power series in y, and both sides of the equation are developed by the binomial theorem. The zero-order pressures cancel by the second of Eqs. (2.14), and $\mathcal{S}_1$ is removed from both sides of the equation since it is of $0(y)$ at the interface. Then the resulting boundary condition is the following:

$$c_1(q_{I0}+0)/c_A q_{T0} = c_1(q_{I0}-0)/B_0. \quad (5.10)$$

Along with the two boundary conditions at the interface we must prescribe an algebraic relation between the acceleration constant A_1 and the solutions at q_{I0}. Such a relation will be given by Eq. (5.07).

Finally we may consider the shock front. By the definition of the shock velocity,

$$dx_S/dt = U, \quad (5.11)$$

along the path of the shock. If we expand U by the

[10] A more detailed proof is given by the author in NAVORD Report 2378.

equation

$$U=U_0+U_1y+0(y^2), \tag{5.12}$$

then U_1 is analogous to A_1, and the determination of q_{S1} is similar to that of q_{I1}. Then

$$q_{S1}=-U_1/4c_AN. \tag{5.13}$$

As in the case of the interface, the first-order boundary conditions can be expressed at q_{S0} instead of at q_S. By the development of Eqs. (1.09) and the substitution of the zero-order conditions (2.16), we find the following:

$$u_1(q_{S0}+0)=(2N-1)(U_0^2+1)U_1/2NU_0^2, \tag{5.14}$$

$$c_1(q_{S0}+0)=[(2N+1)U_0^4 +(2N-1)]U_1/4N^2B_0U_0^3, \tag{5.15}$$

$$S_1(q_{S0}+0)=A_0^2U_1/B_0^2U_0. \tag{5.16}$$

In the right members all quantities are known from the zero-order solution except U_1.

The specification of the boundary conditions is now complete, and those at the head and at the tail have been satisfied explicitly. The remaining conditions are just sufficient for the determination of the remaining constants. The relation (5.07) can be used to express k_2 in terms of A_1. The three shock conditions (5.14), (5.15), and (5.16) provide formulas for K_1, K_2, and K_3 in terms of U_1. Finally the solutions are substituted into the two interface conditions (5.09) and (5.10), which may then be solved simultaneously for A_1 and U_1. In the following section the results will be given for a particular case of N.

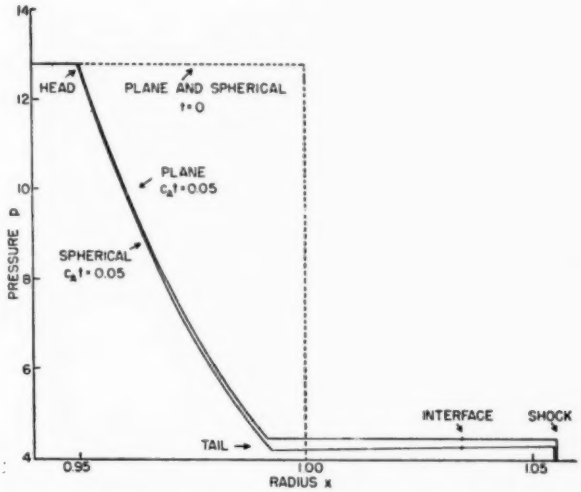

FIG. 2. Pressure distribution in plane and spherical blasts.

6. PARTICULAR SOLUTION FOR $\gamma=1.4$

Let us consider the case of a diatomic gas ($\gamma=1.4$) surrounded by diatomic air. If $\gamma=1.4$, then $N=3$ and the solutions in zone B become especially simple. The remaining constants are given by the following formulas:

$$k_2=2A_1/c_Aq_{T0}-(5/2)(1-q_{T0})(3q_{T0}-1), \tag{6.01}$$

$$K_1+K_2=-\frac{5}{9U_0}\left[\frac{3(3U_0^2+1)}{U_0^2-1}U_1+\frac{7U_0^2-1}{c_A}\right], \tag{6.02}$$

$$K_1-K_2=\frac{5}{18B_0U_0^2}\,\frac{21U_0^6-151U_0^4+11U_0^2-25}{(U_0^2+5)(U_0^2-1)}U_1-\frac{10}{3}\,\frac{B_0}{c_A}, \tag{6.03}$$

$$K_3=-6c_AA_0^2U_1/B_0^2U_0(U_0-A_0), \tag{6.04}$$

$$A_1=\frac{5}{36}\,\frac{9U_0^4+16U_0^2-1}{U_0^2(U_0^2-1)}U_1+\frac{5}{3}\,\frac{B_0^2}{c_A}, \tag{6.05}$$

$$U_1=-\frac{2U_0(U_0^2-1)}{c_A}\,\frac{6B_0^2U_0+c_Aq_{T0}(U_0^2+5)+9c_A^2q_{T0}(1-q_{T0})(5-3q_{T0})U_0}{(9U_0^4+16U_0^2-1)+6c_Aq_{T0}U_0(3U_0^2+1)}. \tag{6.06}$$

Consider next a numerical example. If the initial pressure ratio is 12.8173 and the initial density ratio ratio 3.9560, then the resulting curve for pressure *vs* radius at the time $y=c_At=0.05$ is shown in Fig. 2. Pressure was calculated from c and S by (1.04), and the constants q_{T1}, q_{I1}, and q_{S1} were used to determine the positions of the various surfaces of discontinuity. For comparison, the zero-order pressure (or the pressure in a plane shock tube with the same initial conditions) for the same instant is displayed in the same diagram. The two pressures are identical inside the head of the rarefaction wave, but everywhere else the spherical model has the lower pressure, especially at the tail. In regions C and D the pressure gradient is positive and is discontinuous at the interface. The plane shock pressure ratio is 4.5:1; the corresponding spherical ratio is about 4.33:1. The pressure at the spherical interface is about 4.29 and the tail pressure is about 4.24. We also notice that the spherical tail has accelerated and therefore lies to the right of the plane tail, but the spherical interface and shock have decelerated.

The method given in this paper is easily extended to cylindrical symmetry or to corresponding spherical or cylindrical *implosions*.

The author wishes to thank Dr. G. Kuerti, Dr. L. H. Thomas, and Mr. T. S. Walton for numerous helpful suggestions in the solution of this problem.

Letters to the Editor

Note on Love Waves in a Homogeneous Crust Laid upon Heterogeneous Medium

SUSHIL CHANDRA DAS GUPTA
Hooghly Mohsin College, Chinsurah, West Bengal, India
(Received May 14, 1952)

LOVE discussed the propagation of the transverse waves in a homogeneous superficial layer laid upon another homogeneous subjacent material, differing in rigidity and density from that of the layer.[1] Ernest Meissner (1921)[2] attempted to solve the case of a heterogeneous material in which the density varied as $\rho_0(1+\delta z)$, while the rigidity was proportional to $G_0(1+\delta z)^2$. He only pointed out the way to proceed, without going into detailed discussions as the process involved much mathematical difficulties. Jeffreys (1928)[3] considered a homogeneous layer over a heterogeneous medium where density was constant and rigidity varied as $[1+(z/\lambda)]^2$, λ being a constant length.

We shall discuss in this paper the cases of a homogeneous layer over a medium where (I) the density and rigidity change according to some exponential law and (II) density varies as $[1+(z/\lambda)]$ whereas rigidity varies as $[1+(z/\lambda)]^2$.

I. Let us take the x and y axis in the horizontal plane boundary of the lower medium and z axis vertically upwards. Suppose, the thickness of the upper layer is T and the density and rigidity are ρ and μ, respectively. The density and rigidity in the lower layer are supposed to be given by $\rho=\rho' e^{pz}$, $\mu=\mu' e^{pz}$ where ρ' and μ' are density and rigidity at the boundary of the lower layer and p is a negative constant.

The equation of motion in the upper layer for Love waves is

$$\frac{\mu}{\rho}\left(\frac{\partial^2 v}{\partial x^2}+\frac{\partial^2 v}{\partial z^2}\right)=\frac{\partial^2 v}{\partial t^2}$$

or

$$\beta^2\left(\frac{\partial^2 v}{\partial x^2}+\frac{\partial^2 v}{\partial z^2}\right)=\frac{\partial^2 v}{\partial t^2} \quad \text{where} \quad \beta^2=\frac{\mu}{\rho}. \tag{1}$$

Let $v=Y_1\cos k(x-ct)$, where Y_1 is a function of z only. Therefore,

$$\frac{d^2Y_1}{dz^2}-k^2Y_1=-\frac{k^2c^2}{\beta^2}Y_1,$$

or

$$\frac{d^2Y_1}{dz^2}+s^2Y_1=0, \tag{2}$$

where

$$s^2=k^2\left(\frac{c^2}{\beta^2}-1\right). \tag{3}$$

The equation of motion in the lower layer is,

$$\frac{\partial}{\partial x}\left(\mu\frac{\partial v}{\partial x}\right)+\frac{\partial}{\partial z}\left(\mu\frac{\partial v}{\partial z}\right)=\rho\frac{\partial^2 v}{\partial t^2}. \tag{4}$$

On putting $v=Y\cos k(x-ct)$ we get,

$$\frac{d}{dz}\left(\mu\frac{dY}{dz}\right)-\mu k^2Y=-\rho k^2c^2Y. \tag{5}$$

Let $Z=(\mu)^{\frac{1}{2}}Y$. Hence Eq. (5) transforms to

$$\frac{d^2Z}{dz^2}+Z\left[\frac{\rho k^2c^2}{\mu}-k^2-\frac{1}{2\mu}\frac{d^2\mu}{dz^2}+\frac{1}{4\mu^2}\left(\frac{d\mu}{dz}\right)^2\right]=0. \tag{6}$$

Since $\mu=\mu' e^{pz}$ and $\rho=\rho' e^{pz}$, the equation is

$$\frac{d^2Z}{dz^2}+Z\left[\frac{\rho' k^2c^2}{\mu'}-k^2-\frac{p^2}{4}\right]=0,$$

or

$$\frac{d^2Z}{dz^2}-Z\left[k^2\left(1-\frac{c^2}{\beta'^2}\right)+\frac{p^2}{4}\right]=0, \tag{7}$$

where $\beta'^2=\mu'/\rho'$.

In order that there may be vibration which diminishes gradually downwards we must have

$$n^2=k^2\left(1-\frac{c^2}{\beta'^2}\right)+\frac{p^2}{4} \tag{8}$$

positive. Solution of (7) is then given by

$$Z=A_1e^{nz}+B_1e^{-nz}$$

or

$$Y=e^{-pz/2}(A_1e^{nz}+B_1e^{-nz}), \tag{9}$$

where A_1, B_1 are constants. Solution of (2) is given by

$$Y_1=C\cos(sz)+D\sin(sz) \tag{10}$$

where C, D are constants.

But we have the boundary conditions to be satisfied by Y and Y_1. Firstly at the surface $z=T$, the normal component of stress Y_z must be zero, i.e.,

$$\mu\frac{dY_1}{dz}\bigg|_{z=T}=0. \tag{11}$$

Secondly, as the waves propagate without deeply penetrating into the interior of the material we have displacement

$$Y=0 \quad \text{as} \quad z=-\infty. \tag{12}$$

On the interface the displacement Y and traction $\mu dY/dz$ are continuous. Therefore,

$$\left.\begin{aligned} Y&=Y_1 \\ \mu\frac{dY_1}{dz}&=\mu' e^{pz}\frac{dY}{dz}\end{aligned}\right\} \quad \text{and} \quad \text{at} \quad z=0. \tag{13}$$

From (10) and (12) we get

$$Y=A_1e^{[n-(p/2)]z}, \tag{14}$$

as n is clearly greater than $p/2$ for (8). From (14), (10), and (13),

$$A_1=C \tag{15}$$

$$\mu'\left(n-\frac{p}{2}\right)A_1=\mu sD. \tag{16}$$

From (10) and (11)

$$D\cos(sT)-C\sin(sT)=0. \tag{17}$$

From (15), (16), and (17), eliminating A_1, C, D, we get the frequency equation as

$$s\tan(sT)=\frac{\mu'}{\mu s}\left(n-\frac{p}{2}\right), \tag{18}$$

or

$$\tan\left\{\left(\frac{c^2}{\beta^2}-1\right)^{\frac{1}{2}}kT\right\}=\frac{\mu'}{\mu[(c^2/\beta^2)-1]^{\frac{1}{2}}}\left[\left\{k^2\left(1-\frac{c^2}{\beta'^2}\right)+\frac{p^2}{4}\right\}^{\frac{1}{2}}-\frac{p}{2}\right]. \tag{19}$$

From (8) $n^2=k^2[1-(c^2/\beta'^2)]+(p^2/4)$ is positive, if $\beta'>c$. If $c>\beta$, s is purely imaginary so that $s\tan(sT)$ is negative. The right-hand side of (18) is evidently positive. So $c>\beta$ and s is wholely real. There is then a possible real solution of (19) if $\beta'>c>\beta$. If $p=0$ we get the case in a homogeneous medium.

II. We consider now the homogeneous crust of density ρ and rigidity μ over a heterogeneous material where density $\rho=\rho'[1+(z/\lambda)]$ and rigidity $\mu=\mu'[1+(z/\lambda)]^2$. ρ', μ' are the density and rigidity at the boundary of the lower layer. z axis is taken downwards. λ is a constant. The thickness of the upper layer is taken to be T. As in Eqs. (2) and (3), transverse vibration in the upper layer is given by

$$\frac{d^2Y_1}{dz^2}+s^2Y_1=0,$$

where

$$s^2=k^2\left(\frac{c^2}{\beta^2}-1\right). \tag{20}$$

Therefore,

$$Y_1=A\cos(sz)+B\sin(sz). \tag{21}$$

As before, motion in the lower layer is given by

$$\frac{d^2Z}{dz^2}+Z\left[\rho\frac{k^2c^2}{\mu}-k^2-\frac{1}{2\mu}\frac{d^2\mu}{dz^2}+\frac{1}{4\mu^2}\left(\frac{d\mu}{dz}\right)^2\right]=0, \tag{22}$$

where $Y=(\mu)^{\frac{1}{2}}Z$. Putting $\mu=\mu'[1+(z/\lambda)]^2$ and $\rho=\rho'[1+(z/\lambda)]$ we get

$$\frac{d^2Z}{dz^2}+Z\left[\frac{\rho'k^2c^2}{\mu'[1+(z/\lambda)]}-k^2\right]=0. \tag{23}$$

Let us now assume $\xi=2(kz+b)$, where $b=k\lambda$. Equation (22) is then

$$\frac{d^2Z}{d\xi^2}+\left[-\frac{1}{4}+\frac{\hat{p}}{\xi}\right]Z=0, \tag{24}$$

where $\hat{p}=bc^2/2\beta'^2$, where $\beta'^2=\mu'/\rho'$. Solution of Eq. (24) is given by

$$Z=CW_{\hat{p},\frac{1}{2}}(\xi)+DW_{-\hat{p},\frac{1}{2}}(-\xi), \tag{25}$$

where W is the Whittaker function and C and D are constants. Therefore,

$$Y=\frac{1}{2(kz+b)}[C'W_{\hat{p},\frac{1}{2}}\{2(kz+b)\}+D'W_{-\hat{p},\frac{1}{2}}\{-2(kz+b)\}]. \tag{26}$$

As given by Whittaker (1927),[4]

$$W_{k,m}(z)=e^{-\frac{1}{2}z}z^k\left\{1+O\left(\frac{1}{z}\right)\right\}$$

and

$$W_{-k,m}(-z)=e^{\frac{1}{2}z}(-z)^{-k}\left\{1+O\left(\frac{1}{z}\right)\right\}. \tag{27}$$

Compare (26) and (27) and assume the boundary condition (12), i.e., $Y=0$ as $z=+\infty$, and take

$$Y=C'\frac{W_{\hat{p},\frac{1}{2}}\{2(kz+b)\}}{2(kz+b)}. \tag{28}$$

The boundary conditions are the same as in (11), (12), and (13). Hence the frequency equation is

$$s\tan(sT)=-\frac{\mu'}{\mu}\frac{\dfrac{d}{dz}\left[\dfrac{W_{\hat{p},\frac{1}{2}}\{2(kz+b)\}}{2(kz+b)}\right]_{z=0}}{\left[\dfrac{W_{\hat{p},\frac{1}{2}}\{2(kz+b)\}}{2(kz+b)}\right]_{z=0}}; \tag{29}$$

but

$$\frac{\dfrac{d}{dz}\left[\dfrac{W_{\hat{p},\frac{1}{2}}\{2(kz+b)\}}{2(kz+b)}\right]_{z=0}}{\left[\dfrac{W_{\hat{p},\frac{1}{2}}\{2(kz+b)\}}{2(kz+b)}\right]_{z=0}}$$

$$=\frac{\dfrac{d}{dz}\left[-\dfrac{1}{2\pi i}\Gamma(\hat{p})e^{-(kz+b)}\{2(kz+b)\}^{\hat{p}-1}\times\int_{\infty}^{0+}(-t)^{-\hat{p}}\left\{1+\dfrac{t}{2(kz+b)}\right\}^{\hat{p}}e^{-t}dt\right]_{z=0}}{\left[-\dfrac{1}{2\pi i}\Gamma(\hat{p})e^{-(kz+b)}\{2(kz+b)^{\hat{p}-1}\times\int_{\infty}^{0+}(-t)^{-\hat{p}}\left\{1+\dfrac{t}{2(kz+b)}\right\}^{\hat{p}}e^{-t}dt\right]_{z=0}}$$

$$=-k+\frac{k(\hat{p}-1)}{b}-\frac{k\hat{p}}{2b^2}\frac{\int_{\infty}^{0}(-t)^{-\hat{p}}t\left(1+\dfrac{t}{2b}\right)^{\hat{p}-1}e^{-t}dt}{\int_{\infty}^{0}(-t)^{-\hat{p}}\left(1+\dfrac{t}{2b}\right)^{\hat{p}}e^{-t}dt}$$

$$=-k\left\{\left(1-\frac{c^2}{\beta'^2}\right)+\frac{1}{b}\right\}-\frac{k\hat{p}}{2b^2}\frac{\int_{\infty}^{0}(-t)^{-\hat{p}}t\left(1+\dfrac{t}{2b}\right)^{\hat{p}-1}e^{-t}dt}{\int_{\infty}^{0}(-t)^{-\hat{p}}\left(1+\dfrac{t}{2b}\right)^{\hat{p}}e^{-t}dt}; \tag{30}$$

but

$$\frac{\int_{\infty}^{0}(-t)^{-\hat{p}}\left(1+\dfrac{t}{2b}\right)^{\hat{p}-1}e^{-t}dt}{\int_{\infty}^{0}(-t)^{-\hat{p}}\left(1+\dfrac{t}{2b}\right)^{\hat{p}}e^{-t}dt}=\frac{\int_{0}^{\infty}t^{-\hat{p}+1}\left(1+\dfrac{t}{2b}\right)^{\hat{p}-1}e^{-t}dt}{\int_{0}^{\infty}t^{-\hat{p}}\left(1+\dfrac{t}{2b}\right)^{\hat{p}}e^{-t}dt}$$

is essentially positive, as the functions within the integrals are positive within the positive range. If, then, $c<\beta'$ the right-hand side of (30) is negative. Now, if $c>\beta$, s is wholely imaginary and $s\tan(sT)$ is negative. But the right-hand side of (29) is positive. Hence, possible real solution of (29) can be obtained if $\beta'>c>\beta$.

If in Eq. (30) $\lambda\to\infty$, the frequency Eq. (29) is

$$s\tan(sT)=\frac{\mu'}{\mu}\left\{k\left(1-\frac{1}{2}\frac{c^2}{\beta'^2}+\frac{1}{8}\frac{c^4}{\beta'^4}\cdots\right)\right\},$$

which converges to Love's frequency equation if $\beta<c<\beta'$ i.e.,

$$\tan\left\{kT\left(\frac{c^2}{\beta^2}-1\right)^{\frac{1}{2}}\right\}=\frac{\mu'}{\mu}\left[\frac{1-(c^2/\beta'^2)}{(c^2/\beta^2)-1}\right]^{\frac{1}{2}}.$$

[1] A. E. H. Love, *Some Problems of Geodynamics* (1911), p. 160.
[2] F. Meissner, Vierteljahr. Natur. forch. Gessels (Zurich, 1921), p. 181.
[3] H. Jeffreys, Monthly Notices Roy. Astron. Soc. (Geo. Sup.) **2**, 101–111 (1928).
[4] E. T. Whittaker and G. N. Watson, *Modern Analysis*, pp. 339 and 343.

Creep of Zinc Single Crystals under Direct Shear

ELLIOT H. WEINBERG
Department of Physics, State University of Iowa, Iowa City, Iowa
(Received August 5, 1952)

ROOM temperature measurements on the creep of single crystals of 99.99 and 99.999 percent zinc under direct shear have been made in this laboratory on 5 crystals whose basal planes were oriented parallel to the shear direction. The empirical creep law proposed by Tyndall,[1] $s=at^m$, has been verified on all of these with m approximately equal to 0.6.

A single run was carried on for over 100 hours, measurements starting with a strain of about 5 microradians and extending to about 3 degrees. No deviation from the above law was observed over the entire range. Further evidence has been obtained to suggest that bending, as a result of rotation of some lattice planes with respect to others, is the cause of observed discrepancies in tensile creep tests, even at small strain values. Rapid annealing of strain hardening takes place only when the lattices have not been bent.

The Bauschinger effect has also been investigated, using the direct shear apparatus. Reversal of the stress shortly after the completion of a creep run produced creep at extremely low stress values, the exact value being quite dependent on the time between the runs. The Bauschinger effect can be looked upon as an extension of the very slight creep recovery that is known to occur in strained single crystals.[2]

[1] E. P. T. Tyndall, J. Appl. Phys. **21**, 939 (1950).
[2] R. E. Holland, thesis, State University of Iowa, (1944).

Creep of Zinc Single Crystals

DONALD O. THOMPSON
Department of Physics, The State University of Iowa, Iowa City, Iowa
(Received August 5, 1952)

FURTHER evidence for the creep law $S=At^M$ for zinc single crystals as proposed by Professor Tyndall has been obtained.[1] The experimental procedure is essentially that outlined in reference 1. However, the apparatus is entirely different, making use of electrical strain gauge wires as the measuring element.

In these experiments single crystals have been prepared from 99.99 percent purity zinc. Geometrically, the crystals are 0.5 cm² in cross section and about 15 cm long. The cross-sectional shape

is that of an equilateral triangle, making for convenience in mounting the strain gauges.

It is found that for all crystals investigated thus far (7), the value of M is close to 0.5 at room temperature. This value is quite reproducible from test to test. Further, this value of M seems to be quite independent of the state of the crystal, i.e., its value at room temperature is the same whether the run follows a thorough anneal or is taken soon after a previous run. The dependence of M upon stress is certainly not very pronounced for the stresses used in this work.

Three crystals having primary orientations of 60°, 70°, and 80° and the angle between one of the translation directions and the direction of the projection of the length of the specimen into the basal plane close to zero have been strained at elevated temperatures and in the same general strain region as that indicated in reference 1. It is found for these three crystals that M increases rapidly with temperature and fits best the equation $M=M_0\exp(-H/RT)$. H is about 3400 cal/mole. Values of M from 0.2 to 3.3 have been observed. The average temperature at which M has the value 1 is about 60°C. It is also noted that the stress at which the creep begins at the various temperatures is not significantly different from the room temperature values.

[1] E. P. T. Tyndall, J. Appl. Phys. **21**, 939 (1950), and Report of Carnegie Institute of Technology and ONR Symposium on Plastic Deformation of Crystalline Solids, May, 1950.

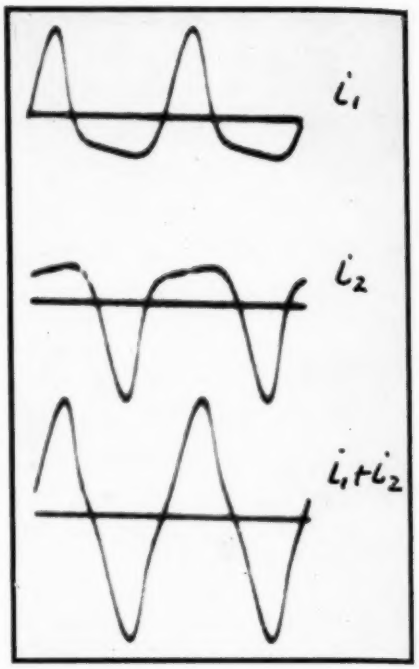

FIG. 1.

Comments on "A Mathematical Analysis of Parallel Connected Magnetic Amplifiers with Resistive Loads"

H. S. KIRSCHBAUM
Ohio State University, Columbus, Ohio
(Received August 4, 1902)

IN a recent paper published under the title above in the *Journal of Applied Physics*, June, 1952, pp. 625–629, Professor Pipes presents an analysis of magnetic amplifier systems using mathematical procedures whose working knowledge may be most useful and of great interest to anyone concerned with such nonlinear problems. It is very regretable, however, to recognize some serious initial misconceptions which impair the validity of the treatment and of the results presented in the paper.

The author writes the differential voltage equations of the two branch loops of the output circuit

$$E_m \sin\omega t = R_L\cdot(i_1+i_2)+R_w\cdot i_1+N\dot{\phi}_a, \tag{2.2}$$
$$E_m \sin\omega t = R_L\cdot(i_1+i_2)+R_w\cdot i_2-N\dot{\phi}_b, \tag{2.3}$$

and recognizes that in practical instances the output winding resistances are very small in comparison to the load resistance, i.e., $R_w \ll R_L$. Hence by making the assumption $R_w=0$, the above equations are modified into

$$E_m \sin\omega t = R_L\cdot(i_1+i_2)+N\dot{\phi}_a,$$

and

$$E_m \sin\omega t = R_L(i_1+i_2)-N\dot{\phi}_b,$$

whence by subtraction the conclusion is drawn:

$$\dot{\phi}_a+\dot{\phi}_b=0. \tag{2.9}$$

On the other hand, from the original equations (2.2) and (2.3), by subtraction

$$0=R_w(i_1-i_2)+N(\dot{\phi}_a+\dot{\phi}_b). \tag{2.10}$$

Now use is made of the approximate relation (2.9) into (2.10), thus obtaining

$$0=R_w(i_1-i_2), \tag{2.11}$$

from which the further conclusion is drawn:

$$i_1=i_2. \tag{2.12}$$

All subsequent developments are based on this unwarranted result.

Apparent departures from logical consistency may be all but infrequent in the solution of engineering problems when approximations are introduced in the process. But utmost care is needed when this is done, and responsibility rests with the writers to check on the physical meaning of the approximation and also on the use to which it shall be put subsequently.

In the case in question, since R_0 is assummed to be other than zero, the crucial point leading to the conclusion $(\dot{\phi}_a+\dot{\phi}_b)=0$ rests only with the assumption $R_w=0$, no matter how large or small R_L is. This conclusion results really from Eq. (2.10), which could have been written directly as the voltage differential equation of the loop described along the external sides of the two branch circuits and linking both cores. Of course, if the resistance of this loop is zero, $N(\dot{\phi}_a+\dot{\phi}_b)$ is constant and $N(\dot{\phi}_a+\dot{\phi}_b)=0$. This identity expresses the so-called idealized condition of nonconstrained magnetization. When the loop resistance is other than zero, the identity may or may not be used reasonably well in the way of approximation in some appropriate steps of a problem. (Clues about the legitimacy of the procedure must be obtained for this by checks performed experimentally or otherwise.)

No immediate conclusion can be drawn in any case about the value of (i_1-i_2), as we know only that

$$(i_1-i_2)=(\dot{\phi}_a+\dot{\phi}_b)/R_w.$$

Certainly it does not appear legitimate to assume $R_w=0$, as needed to derive Eq. (2.11), and to make use at the same time of the hidden assumption $R_w\neq 0$ to proceed from Eq. (2.11) to Eq. (2.12). In other words, if R_w is different from zero (no matter how "small") $(\dot{\phi}_a+\dot{\phi}_b)$ will also be not quite zero and nothing is known about the ratio of these two quantities. And if $R_w=0$ exactly, then also $\dot{\phi}_a+\dot{\phi}_b=0$ exactly and $i_1-i_2=0/0$. In no case can be drawn the conclusion that $(i_1-i_2)=0$.

The enclosed oscillogram presents some experimental evidence on this matter. The tests have been performed on a magnetic amplifier with cores of transformer steel with the circuitry given in Fig. 1 of the paper. $R_L/R_w\cong 65$, and R_0 has been chosen large enough to keep the control current i_0 practically constant, as assumed further by the author in Eq. (2.15). Output voltage and currents are near the center of design of this amplifier. Under these conditions the instantaneous values of i_1 and i_2 are by no means equal; nor is $i_L=2i_1$.

The condition $i_1=i_2$ can be met approximately in the experimentation by making $R_w>R_0$ (on an equal turns basis), but then

it is well established that i_0 contains most remarkable even harmonics in violation of Eq. (2.15).

Conclusing that one may agree with the author that conditions (2.12) and (2.15) jointly simplify greatly his subsequent manipulations, one must recognize that their simultaneous acceptance is not in the least justifiable in the problem treated.

It appears also very strange that the expression (3.23) derived for the steady-state load current contains a second harmonic term as well as a sizable direct current component, which flows through the load resistance without being sustained by any dc voltage source in the output. This is only a result to the first approximation (which hereby would appear to be a rather poor one to start with). But the next sentence conveys to the reader the impression that higher order approximations modify only slightly such peculiar findings by the presence of harmonies of higher order and smaller magnitude.

As a minor point, some reservation could be made about the name of "effective time constant" of the amplifier proposed for the expression (3.19). Other considerations aside, this quantity does not express the influence of some most significant factors (e.g., R_0 and R_w), determining what is commonly understood as transient response of this amplifier.

Comments on H. S. Kirschbaum's Letter*

LOUIS A. PIPES
University of California, Los Angeles, California
(Received August 18, 1952)

THE approximate analysis on which the discussion of the magnetic amplifier circuit is based may be put in a clearer form by introducing the following notation:

$$k=R_w/R_L, \tag{1}$$

$$F_1=\frac{E_m\sin(wt)}{R_L}-\frac{N\dot{\phi}_a}{R_L}, \tag{2}$$

$$F_2=\frac{E_m\sin(wt)}{R_L}+\frac{N\dot{\phi}_b}{R_L}. \tag{3}$$

In this notation, Eqs. (2.2) and (2.3) of the paper may be written in the convenient form,

$$(1+k)i_1+i_2=F_1, \tag{4}$$

$$i_1+(1+k)i_2=F_2. \tag{5}$$

It is desired to investigate the conclusions that may be reached when $R_w\ll R_L$ so that $k\to 0+$.

If the Eqs. (4) and (5) are solved for i_1 and i_2, the results are:

$$i_1=\frac{(1+k)F_1-F_2}{(2k+k^2)}, \tag{6}$$

and

$$i_2=\frac{(1+k)F_2-F_1}{(2k+k^2)}. \tag{7}$$

It is seen that as k approaches $0+$, i_1 and i_2 increase in magnitudes indefinitely unless,

$$F_1=F_2=F. \tag{8}$$

Since, from physical considerations, the currents i_1 andi_2 are always finite, this condition must be satisfied for very small values of k. Hence if (8) is substituted into (6) and (7) the results are,

$$i_1=\frac{F}{2},\quad i_2=\frac{F}{2}\quad\text{as}\quad k\to 0+. \tag{9}$$

The condition (8) leads to,

$$\dot{\phi}_a+\dot{\phi}_b=0. \tag{10}$$

From (9) it is concluded that,

$$i_1=i_2. \tag{11}$$

All this is based on the assumption that the currents of the magnetic amplifier satisfy the simple equations (2.2) and (2.3) and that there are no leakage fluxes and other effects to destroy the symmetry of the configuration of the circuit on which the analysis is based.

Professor Kirschbaum points out that in a practical amplifier, even with $k=\frac{R_w}{R_L}=\frac{1}{65}=0.0154$, the observed values of i_1 and i_2 are far from those predicted on the basis that $k=0+$. This indicates the importance of checking the conditions (10) and (11) on which the subsequent analysis is based before applying it to special amplifiers.

The fact that direct current components are sometimes sustained in nonlinear circuits is one that has been observed ferquently. An example of this is found in Helmholtz's *Theory of Combination Tones.*[1]

* H. S. Kirschbaum, J. Appl. Phys. **23**. 1278 (1952).
[1] See H. Bateman, *Partial Differential Equations of Mathematical Physics* (Cambridge University Press, Cambridge, 1932), pp. 497–499.

Remarque on Critical Reflections of Elastic Waves at Free Surfaces

W. S. JARDETZKY
Columbia University, New York, New York
(Received July 14, 1952)

IT is well known that the functions,

$$\varphi=(A_1e^{ikz\tan e}+A_2e^{-ikz\tan e})e^{ik(x-ct)},$$
$$\psi=(B_1e^{ikz\tan f}+B_2e^{-ikz\tan f})e^{ik(x-ct)}, \tag{1}$$

represent trains of plane waves propagating in a solid half-space and having the phase velocity c. The first terms of the right-hand members (1) are incident waves, compressional or distortional, making with the x axis angles e or f, respectively. The second terms are the reflected waves. For an incident P wave we have to put $B_1=0$, for an incident SV wave it is $A_1=0$. The boundary conditions, the vanishing stresses at the free surface of an elastic body, $z=0$, yield the ratios of amplitudes A_2/A_1, B_2/A_1, For example, it is in case of a P wave

$$\frac{A_2}{A_1}=\frac{4\tan e\tan f-(1+3\tan^2 e)^2}{4\tan e\tan f+(1+3\tan^2 e)^2},$$
$$\frac{B_2}{A_1}=\frac{-4\tan e(1+3\tan^2 e)}{4\tan e\tan f+(1+3\tan^2 e)^2}. \tag{2}$$

In a recent paper Goudier and Bishop[1] have shown that in the critical case of the grazing incidence, $e=0$, one should make use of functions

$$\varphi=A_0 4\sqrt{2}\exp[ik(x-\alpha t)]+A_0 ikz\exp[ik(x-\alpha t)]$$
$$\psi=-A_0\exp[ik(-z\sqrt{2}+x-\alpha t)] \tag{3}$$

instead of (1), since (1) fail to represent trains of waves. Similar expressions (two terms for ψ) hold for an incident SV wave.

The conclusion that for the grazing incidence the integrals of wave equations should be taken in the form (for an incident P wave, if α is the velocity of its propagation).

$$\varphi=(A'+A''z)e^{ik(x-\alpha t)}$$
$$\psi=B''e^{-ikz\tan f}e^{ik(x-\alpha t)} \tag{4}$$

is correct, but it was obtained by rather artificial assumptions. It was, for example, assumed that the amplitudes are infinite, but the product, say A_1e, tends to a finite limit (A_0).

It seems to be earlier overlooked that in this limit case, when the grazing incidence is discussed, the first factors in (1) do not represent more the general integral of the equation

$$\frac{d^2F}{dz^2}+\left(\frac{c^2}{\alpha^2}-1\right)k^2F=0, \tag{5}$$

which has to be satisfied, if a solution of the wave equation $\nabla^2\varphi=\frac{1}{\alpha^2}\frac{\partial^2\varphi}{\partial t^2}$ is taken in the form

$$\varphi=F(z)e^{ik(x-ct)}. \tag{6}$$

The grazing incidence, $e=0$, corresponds, namely, to the case of two equal roots of the characteristic equation of (5) $\Delta=e^{(\tau_1+\tau_2)z}(\tau_2-\tau_1)=0$, where

$$\tau_{1,2}=\pm ik\left(\frac{c^2}{\alpha^2}-1\right)^{\frac{1}{2}}=\pm ik\tan e. \tag{7}$$

Thus, instead of taking $F=C_1e^{\tau_1 z}+C_2e^{\tau_2 z}$ one has, for $e=0$, i.e. $c=\alpha$, the general integral in the form

$$F(z)=C_1e^{\tau_1 z}+C_2ze^{\tau_1 z}=C_1+C_2z \tag{8}$$

since in our case $\tau_1=0$. This holds for an incident P wave as well as for an incident SV wave. In the first case, the equation $2+3\tan^2 e=\tan^2 f$ gives for $e=0$, $\tan f=\pm\sqrt{2}$ as it is in the solution by Goudier and Bishop.

It is obvious that the solution of the form (4) represents a plane wave with amplitudes increasing if $z\to\infty$. Whether a physical meaning can be attached to it or not, remains an open question.

[1] J. N. Goudier and R. E. D. Bishop J. Appl. Phys. 23, 124–126 (1952).

Comments on "Remarque on Critical Reflections of Elastic Waves at Free Surfaces"

J. N. GOODIER
Stanford University, Stanford, California
(Received August 26, 1952)

MR. Jardetzky says that the result of the paper (Goodier and Bishop) was obtained by "rather artificial assumptions."

The limiting process was used only to find the result, and in the result itself nothing infinite (i.e., "artificial") remains.

Also, Mr. Jardetzky points out that for $e=0$, the ordinary wave solution fails and a special form is required. This special form is what the paper provides. Mr. Jardetzky's procedure provides another way of arriving at it once its existence is realized —by passing right over the limiting process and finding solutions to the wave equation of the type (6) when $e=0$.

In the paper we preferred the limiting process because it preserves connection with the ordinary case of nongrazing incidence. We recognized that it was necessary to verify the solution so obtained, as appears in the statement "It is readily verified by substitution . . ." following Eq. (8) of the paper.

I am not clear as to whether the statement "It seems to be earlier overlooked . . ." refers to an earlier section of the paper or to the earlier literature. I have assumed the former.

The Resistance of a Truncated Hemisphere

W. R. SMYTHE
Department of Physics, California Institute of Technology, Pasadena, California
(Received April 21, 1952)

THE question of the resistance of a truncated hemisphere recently arose in connection with a physical problem. The top of a solid hemisphere of radius a and resistivity τ is sliced off by a plane at a distance b from the base. The resistance between the two plane faces is required. The lower limit obtained by breaking up the truncated hemisphere into a stack of thin disks with perfectly conducting faces and calculating their resistance in series is

$$R_l=\frac{\tau}{\pi a}\tanh^{-1}\frac{b}{a}=\frac{\tau}{\pi a}\tanh^{-1}h.$$

An upper limit may be obtained by breaking up the truncated hemisphere into a nest of coaxial shells with insulating surfaces whose boundaries in the cylindrical coordinates ρ, z are given by

$$\rho a=\rho_0(a^2-z^2)^{\frac{1}{2}},$$

where ρ_0 is the radius of the base of the shell and calculating their resistance in parallel. The result is

$$R_u=\frac{\tau[h-(1-h^2)\tanh^{-1}h]}{2\pi a(1-h^2)}\left[\ln\frac{h=(1-h^2)\tanh^{-1}h}{2(1-h^2)\tanh^{-1}h}\right]^{-1}.$$

The limits approach each other as h approaches zero. The differences in the limits in percent of the lower limit for various values of h are:

h	0.2	0.4
R_u-R_l	0.9 percent R_l	2.8 percent R_l
0.5	0.6	0.8
5.0 percent R_l	8.6 percent R_l	24 percent R_l

If a correction of half this amount is added to the lower limit the error cannot exceed the correction and is probably much smaller.

Light Scattering by Pure Polystyrene*

F. BUECHE
Department of Physics, University of Wyoming, Laramie, Wyoming
(Received August 18, 1952)

IT has been shown that solid noncrystalline polymers scatter much more light than one would expect from theoretical considerations.[1,2] The scattering has rightly been attributed to inhomogeneities in the solid but until now it has been impossible to decide the nature of the inhomogeneities. We shall show that solid polystyrene, when pure, scatters about the same amount of light as a normal liquid scatters due to its density fluctuations.

Preliminary experiments were carried out by polymerizing freshly distilled styrene in sealed test tubes without catalyst. The light scattered at an angle of 90° ($\lambda=4358$) by the resultant polymer was measured while the samples were still in the glass tubes. Using a specially constructed temperature jacket, the samples could be held at a known temperature. The scattering was standardized by measuring the scattering of benzene in the same test tubes before beginning the experiments.

Even though great care was taken to purify the styrene and avoid contamination, the resultant solid polymer always gave a high scattering which was not reproducible from sample to sample. Upon heating these samples it was found that the scattering decreased by more than a factor three when the temperature was raised from 100 to 200°C. The readings on any one sample were repeatable and equilibrium seemed to be reached as fast as the temperature became constant.

After careful investigation it has become clear that the reason for this behavior is the presence of impurities formed by degradation of the polymer during polymerization. We had until that time followed the common procedure of polymerizing one day at 100°C and then slowly raising the temperature to 180°C to remove bubbles. Even though the samples had been swept with nitrogen and sealed off from air, and though no visible coloring had occurred, some decomposition had undoubtably taken place. In those cases where the sample had been heated hot and long enough to cause a yellow tint to appear, the scattering was much more intense. Indeed, such samples actually gave off a blue-green fluoresence when exposed to violet light. No attempt has been made to determine the nature of the decomposition products.

To clarify the situation further, samples were polymerized at 90°C. These showed a much lower scattering. It was found that, using unpolarized light having $\lambda=4358$, the ratio of the light scattered at an angle of 90° for polystyrene to that of freshly distilled benzene held in the same tubes was 1.45 ± 0.05 at 30°C. The polymer's scattering was found to be essentially insensitive to temperature in the range 20 to 150°C. although a small (about 5 percent) increase with rising temperature is indicated. Un-

fortunately this is within the limit of possible error of the experiments. Certainly no large change occurs at T_g (found to be about 83° from volume expansion measurements). Also, data on polymerized styrene-benzene mixtures indicates that the pure polymer does not scatter in excess of the value one would estimate from extrapolations based on the scattering of its solutions.

The above results indicate that the structure of the polymer, at least in regard to density fluctuations, is essentially the same above and below T_g.

The great importance of the above findings for those using optical elements made of plastics should be obvious.

The author is indebted to Dr. A. M. Bueche for suggestions in connection with this work.

* This work was done at Cornell University under a contract with the Synthetic Rubber Division of the R.F.C. in connection with the U. S. Government's synthetic rubber program.

[1] P. Debye and A. M. Bueche, J. Appl. Phys. **20**, 518 (1949).
[2] P. Debye and A. M. Bueche, J. Chem. Phys. **18**, 1423 (1950).

Organization and Entropy

JEROME ROTHSTEIN
Signal Corps Engineering Laboratories, Fort Monmouth, New Jersey
(Received July 11, 1952)

STATISTICAL entropy has long been recognized as a measure of missing information or lack of organization (disorder). Precise formulation of the information concept[1] leads, via the measurement-communication analogy,[2] to recognizing that physical information is essentially negative entropy. We will attempt to show that (a) precise formulation of the concept of organization leads to its characterization as a kind of negative entropy (b) organization partakes of the nature of information encoded in structure (c) the organization concept leads to nontrivial generalization of the entropy-information concept (d) measurement, and interaction in general appear in a new light against the background of these concepts (e) theory can be considered as organization of observation.

Information is conveyed by making choices from a set of alternatives. The greater the initial uncertainty as to what the choices will be, the greater the amount of information conveyed when choices are made. Both the uncertainty and information are measured by a function defined on the set of alternatives called "entropy." Measurement, by choosing from the set of alternatives constituting the possible results of a measuring procedure, yields "physical information." This leads to a physical "informational entropy" identical except for a constant depending on choice of units, with ordinary physical entropy. A simple example may make this clearer. If a message is one of a group of N equivalent (equiprobable) messages, any of which might be selected, then selection of one conveys an amount of information $\log N$. If each message consists of n selections from M symbols then $N=M^n$. In Planck's entropy definition, $S=k\log P$ where P is the number of independent wave functions compatible with given energy and volume of the system. If measurement puts the system in an eigenstate, the entropy is reduced to zero and "physical information" equal to $\log P$ has been obtained. We may write $S=-kI$, where I is information. This is demonstrable for general stochastic nature of the message ensemble (arbitrary assignment of weights), including discrete, continuous, or mixed distributions.

The essential idea of organization is that a number of elements are coupled somehow so that they are not completely independent of one another, as opposed to the unorganized state in which they are mutually independent. We propose the following characterization of organization. Consider a set of elements, each associated with its own set of alternatives. For each set of alternatives an entropy is defined. Define a complexion as a set of selections, one from each set of alternatives. An entropy is defined for the set of complexions. If the entropy of the set of complexions is the sum of the entropies of the sets of alternatives associated with the elements, then the elements are said to have zero organization. The set of complexions has maximum entropy for zero organization. If the interaction between elements is so strong that only one complexion is possible, then the set of complexions has zero entropy and organization is maximum. In the general case the interactions (correlations, couplings, linkages, constraints, orders, instructions) in which the organization consists serve to narrow the ensemble (or set) of possible complexions. The entropy of the set of complexions is thus less than the sum of the entropies of the sets of alternatives. We define the amount of organization as the excess of the latter over the former. It is clear that organization measures how much information has been introduced into (or how much entropy has been taken away from) the ensemble of complexions because of the interactions. We have thus demonstrated (a) and (b). We remark that a complexion need not be defined only for a denumerable set of elements as above. For a continuum the complexion entropy would be an integral over the set of sets of alternatives (Lebesgue-Stieltjes or perhaps more general integrals for more complicated cases) with similar conclusions.

Many examples of (c) can be cited, (d) and (e) being among them. We mention besides them only an application to systems and system engineering design [needed in (e)] and the definition of entropy and temperature for metastable states.

Let us define a system as an organization (i.e., coupled elements individually associated with sets of alternatives) with a function (task, program, behavior pattern, objective). A function is a mapping of one set of alternatives, the input, into another set, the output. For example, a measuring system maps a set of states of an object of interest into the set of indications, a communication system maps a set of messages from a source into a set of messages at a destination, a transportation system maps a set of starting points into a set of destinations, a diagnostic system maps a set of malfunctionings into a set of disorders, and a curative system maps a set of disorders into a set of treatments. A system obviously organizes input and output considered as a pair of elements. An entropy can be calculated for the function (i.e., the organized input-output). The system is optimal if it has minimal entropy consistent with its function. This minimal entropy must be at least as great as that of the function. The excess of actual over minimal entropy is called the redundancy of the system. The actual function performed by a given system may have a higher entropy than that of the function desired. The excess of the former over the latter we call the noise entropy. It is a measure of information loss due to noise in a communication system, due to errors in a measuring system, and of unreliability in a general system. Proper use of redundancy can combat noise in communication—in general it can enhance system reliability ("factor of safety"). It is clear that system engineering design in general comes under the same philosophy as communication system design.

We now verify (e) and show that a theoretical system is a system in the above sense. Its function is to map a set of data (input, initial conditions, state-defining variables) into a set of predictions (output, conditions or state at another time). A theory with adjustable parameters is redundant, thereby being able to combat the "noise" of unexpected results of measurement. The simplest theory for a given function is the least redundant (optimal) and is preferred. Any theoretical law is a coupling between elements individually associated with sets of alternatives. Ohm's law, for example, couples the elements current and voltage, the sets of alternatives being the sets of possible results of measurement of these quantities.

The discussion so far has implicitly covered (d), but some additional remarks may be worth making. Interaction in general is equivalent to organization of the interacting elements. Physical information, obtainable only from measurement, requires organization of object of interest and indicating means. Similarly for communication with message source the object of interest. Organization (interaction) can be symmetrical between a pair of elements, whereas the communication or measurement coupling is unsymmetrical. This seems like another aspect of dynamical

reversibility (organization via theory) and phenomenological irreversibility (entropy increase accompanying measurement).

Lastly we discuss entropy and temperature for a system in a metastable state. For stable equilibrium, we can define temperature by $(\partial S/\partial E)_V=1/T$. In a metastable state, however, adding energy dE to the system may precipitate a large entropy change, and the equation is of little use as it stands. Now the entropy of the metastable state is less than that of the equilibrium state by the organization or information specifying the metastable state, i.e., $S=S_{equ}-kI$. From a statistical viewpoint, this organization or information is a kind of constraint, selection rule, or exclusion principle which prevents the molecules from populating the energy states or cells in phase space in the usual way. If we now require dE to be added to the metastable system subject to the condition that the same constraints hold, we find that $(\partial S/\partial E)_{V,I}=1/T$ gives a definition of temperature which seems quite satisfactory. The above holds for a somewhat wider concept of metastable than the conventional one, e.g., NaOH in a closed container which also holds a stoppered bottle of HCl. Constant organization means here that adding dE does not unstopper the bottle.

To conclude, organization appears to extend the entropy concept in a significant way. We hope to treat the above and further aspects of the entropy-measurement-information-organization complex of ideas in more detail in the near future.

[1] N. Wiener, *Cybernetics* (John Wiley & Sons, Inc., New York, 1950). C. E. Shannon, Bell System Tech. J. **27**, 279, 623 (1948).
[2] J. Rothstein, Science **114**, 171 (1951); Phys. Rev. **85**, 135 (1952).

Preferred Crystal Orientation in Ferromagnetic Ceramics

A. L. Stuyts, G. W. Rathenau, and E. W. Gorter
Philips Research Laboratories, N. V. Philips Gloeilampenfabrieken, Eindhoven, The Netherlands
(Received August 18, 1952)

A CLASS of ferromagnetic hexagonal iron oxide compounds has been dealt with in a previous communication.[1] The compound $BaFe_{12}O_{19}$, which is the prototype of these compounds, is the main ingredient of a new sintered permanent magnet material. For a material consisting of fine crystals oriented at random $(BH)_{max}$ values of $0.8-1.1\times10^6$ gauss-oersted were obtained.

By orienting the crystals of this oxide in a magnetic field, prior to sintering, $(BH)_{max}$ values up to 3.0×10^6 have now been achieved.

The anisotropy of the remanence value $B_r\|/B_r\perp$ increases with increasing sintering temperature, which proves that the texture is improved by grain growth. So far this phenomenon had been observed only for metallic textures.[2] A discussion on the magnetization process and on the improvement of the texture by grain growth will be given elsewhere.[3]

We wish to acknowledge the valuable cooperation of Mr. A. H. Hoekstra and Mr. G. Weber in obtaining materials with high $(BH)_{max}$ values.

[1] Went, Rathenau, Gorter, and van Oosterhout, Philips Tech. Rev. **13**, 194 (1952).
[2] G. W. Rathenau and G. Baas, Physica **17**, 117 (1951).
[3] Rathenau, Smit, and Stuyts, Z. Physik.

Electrical Resistivity of Artificial Graphite

Jun Okada and Tatsuo Ikegawa
Technical Research Laboratory, Tokai Electrode Manufacturing Company, Fujisawa, Japan
(Received August 11, 1952)

ARTIFICIAL graphites are, in general, made by the process of molding (or extruding) the mixture of pulverized coke calcined at the proper temperatures and pitch and heating up to higher temperatures. Many characteristics of artificial graphites are, therefore, varied by these manufacturing conditions.

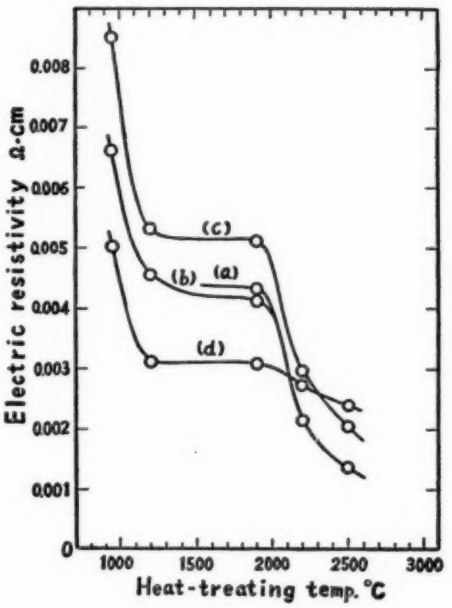

FIG. 1. The curves of electric resistivities of the specimens measured at room temperature, which are indicated as function of the heat-treating temperatures. (a), (b), (c), and (d) are the curves of the specimens including the cokes preheat-treated at 500°C, 1300°C, 1700°C, and 2400°C, respectively.

The purpose of this study is to find some effects on the electric resistivity of the artificial graphite influenced by the preheating temperatures (or calcined temperatures) of the raw coke employed in making artificial graphites.

The raw materials employed to be made into specimens were petroleum coke preheated at 500°C, 1300°C, 1700°C, and 2400°C, respectively, and coal-tar pitch. These contents were ten parts of petroleum coke and four parts of coal-tar pitch by weight. With the exception of the preheating temperatures of the raw cokes, all the same conditions were employed in order in making these specimens. The specimens were heat-treated step by step up to higher temperatures, and the electric resistivities of the specimens were measured at room temperature. Apparent densities of the specimens heat-treated above 1300°C were approximately the same value, 1.4 g/cm³.

The electric resistivities of the specimens measured at room temperature were indicated in Fig. 1 as a function of the heat-treating temperatures. The tendency of these electric resistivity *vs* heat-treating temperature curves is in good agreement with the well-known results measured by the other investigators.[1] Quantitatively, however, these resistivity values differ from each other.

Comparing the electric resistivities of the specimens heat-treated up to 2500°C with each other, the lower the preheat-treating temperature of the raw coke employed in making the specimen, the smaller the resistivity of the specimen. It seems that the fact is attributed to the effect of the boundaries between the coke grain and the carbonized pitches. It is probable that the peripheries of the raw coke preheated at lower temperatures are linked to the neighboring layers of the carbonized pitch in the early stages of the carbonization process, since they have had more bonded hydrogen atoms and/or free valencies. Therefore, the domains lying near these boundaries have good graphitizability and their resistivities decrease considerably. On the other hand, the peripheries of the raw coke preheated at higher temperatures are presumably combined with the neighboring layers of carbonized pitch by formation of criss-cross bonds and fine pore structures,[1,2] which are hardly graphitizing, since they

are more stabilized energitically. Consequently, the electric resistivity of the specimen, including the preheated at lower temperatures, is smaller than the preheated at higher temperatures.

The specimen including the coke preheated at 1700°C has larger electric resistivity than that preheated at 1300°C in the carbonization process under 950°C, although in the coke grain itself the resistivity of the coke preheated at 1700°C is a little smaller than that of the coke preheated at 1300°C. From this fact, it is probable that the larger resistive structures are formed at the boundaries between coke grains and carbonized pitches in the early stages of carbonization process.

It is improbable in this case that the growth of the crystallites depends on the quantity of the stress induced by the thermal expansion of the coke grains so that the resistivities of the specimens differ from each other.

It is important in industry that the boundaries between the coke grains and the neighboring carbonized pitches have considerable effects on the electric resistivity.

[1] S. Mrozowski, Phys. Rev. **85**, 609 (1952).
[2] R. E. Franklin, Proc. Roy. Soc. (London) **A209**, 196 (1951).

Emissivity for CO_2 at Elevated Pressures*

R. J. Holm,† D. Weber, and S. S. Penner
Guggenheim Jet Propulsion Center and Jet Propulsion Laboratory, California Institute of Technology, Pasadena, California
(Received August 26, 1952)

TOTAL absorptivity measurements have been carried out at room temperature as a function of partial pressure of CO_2 and of total pressure using nitrogen as pressurizing gas. The results of these investigations are summarized in Fig. 1. Appropriate values at a total pressure of one atmos are compared with emissivity data published by Hottel and Mangelsdorf (1935) in Figs. 2 and 3.

The principal conclusions reached as the result of the present investigations are:

(a) At atmospheric pressure and room temperature, the results of total absorptivity measurements are in reasonably good agreement with the emissivity data of Hottel and Mangelsdorf, the difference increasing somewhat as the optical density is raised.

(b) At pressures in excess of one atmos, the absorptivity (and hence the emissivity) is quite insensitive to changes in total pressure. Thus, between 1.0 and 21 atmos total pressure, the measured values of total absorptivity at fixed optical density are equal within the rather wide limits of error (±15 percent) of the present preliminary investigations. This result can be understood in terms of the ratio of rotational line width to rotational line spacing, which is relatively large for triatomic molecules such as CO_2. There are no apparent reasons why the observed insensitivity of emissivity to total pressure cannot be extrapolated to elevated temperatures. Thus, although the collision half-width of the rotational lines decreases roughly inversely as the square root of the absolute temperature, it also increases linearly with total pressure. Hence the ratio of half-width to line spacing at 3000°K and 20 atmos should be comparable to conditions at 300°K and 11 atmos. Therefore, it appears unlikely that a large error is made if radiant heat transfer calculations involving CO_2 at elevated pressures are based on emissivity data for CO_2 determined at atmospheric pressure. The preceding statement should not be extrapolated indiscriminately to other molecules.[1]

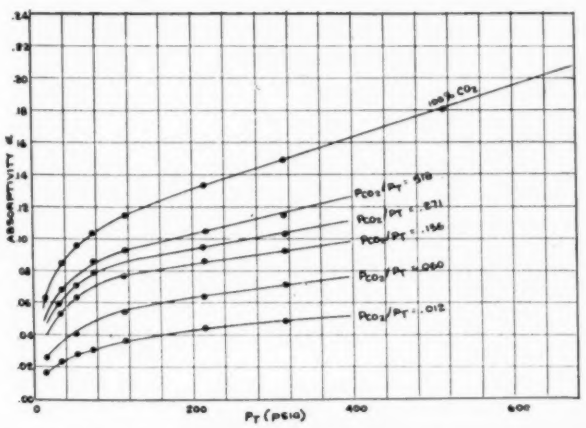

FIG. 1. Absorptivity α as a function of P_T for various fractional pressures of CO_2 at room temperature. The CO_2 was pressurized with nitrogen.

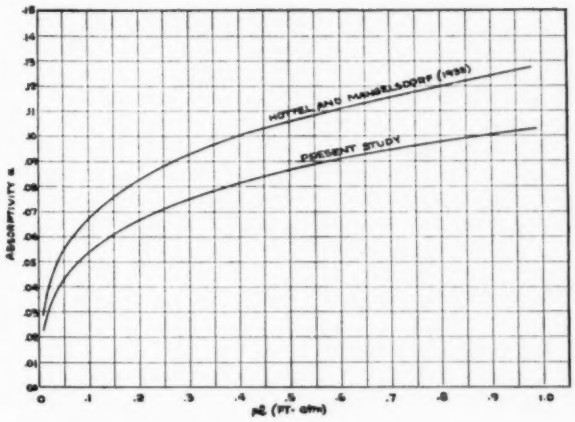

FIG. 2. Comparison of absorptivities for CO_2 at room temperature and atmospheric pressure with emissivities of Hottel and Mangelsdorf ($0 \leqslant p\ell$, ft-atmos $\leqslant 1.0$).

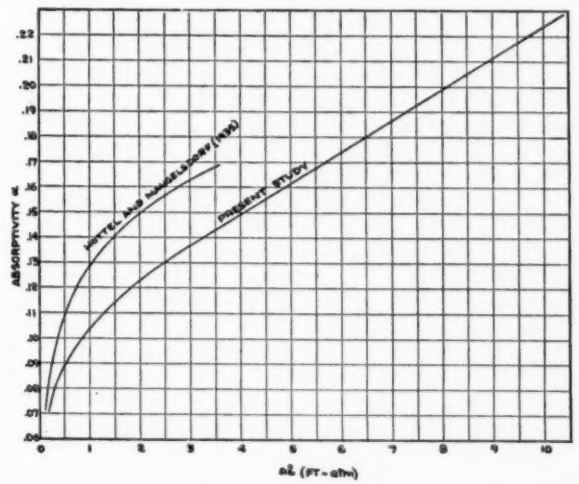

FIG. 3. Comparison of absorptivities for CO_2 at room temperature and atmospheric pressure with emissivities of Hottel and Mangelsdorf ($0 \leqslant p\ell$, ft-atmos $\leqslant 10$).

* This paper presents, in part, the results of one phase of research carried out at the Jet Propulsion Laboratory, California Institute of Technology, under Contract No. DA-04-495-ORD 18, sponsored by the U. S. Army Ordnance Department. Supported, in part, by the ONR under Contract Nonr-220(03), NR 015 210.

† This article is based, in part, on a thesis submitted by R. J. Holm to the graduate school of the California Institute of Technology, in partial fulfillment of requirements for the degree of Aeronautical Engineer, June, 1952.

[1] For details concerning emissivity calculations on diatomic gases at elevated pressures, see S. S. Penner, J. Appl. Phys. **21**, 685 (1950) or J. Appl. Mech. **18**, 53 (1951).

Books Reviewed

Antennas: Theory and Practice

By Sergei A. Schelkunoff and Harald T. Friis. Pp. 639 +xxii. John Wiley & Sons, Inc., New York, 1952. Price $10.00.

This book contains a comprehensive and detailed discussion of the theory and practice of the design of antennas. The readability of the book is enhanced by the very large number of clear diagrams which illustrate the behavior of the antennas. Although the book is full of equations, as is natural for the subject, great emphasis has been placed on physical insight. The authors are successful in their attempt "to avoid the use of advanced mathematical theorems, and to keep in more intimate contact with the physical aspects of our problem . . . ."

The book contains 19 chapters of which 5 are devoted to fundamental ideas and 3 are concerned with directivity, reciprocity, and related subjects. Conventional antennas and arrays of antennas are described in 7 chapters which constitute one-third of the book. Horns, slot antennas, reflectors, and lenses are described in the last 4 chapters. The properties of many antenna systems are developed both quantitatively and qualitatively from the limiting cases of two coaxial conducting cones. This approach is full of physical suggestiveness, an example of which is the calculation of the effect of the diameter on the lines of average power flow.

The authors state in the preface, "We have written it (the book) primarily for students and practitioners of radio engineering." Each of the first 13 problems is followed by a set of problems suitable for students. It is stated in the preface that "calculus is the only essential mathematical prerequisite." Although this statement is optimistic, it is true that a person experienced in electrical circuits can read most of the book with only a "working knowledge of general physics and calculus."

The problem of giving a simple mathematical treatment of a subject as difficult as antenna theory is not easy. The extensive use of physical insight and, in particular, the reliance on physical arguments to avoid mathematical difficulties makes the book very instructive for engineers and physicists. Unfortunately, this practice will make the book more difficult for mathematicians who are trying to learn the subject. Mathematicians will undoubtedly prefer the more formal approach of Aharoni's book on antennas. This attempt at simplification sometimes defeats itself. For example, in order to avoid the appearance of using vector analysis, vector quantities are printed in the same italic type as scalar quantities with an occasional loss of clarity.

Dr. Schelkunoff and Dr. Friis have made many original contributions to the theory and practice of antenna design. The book under review leaves one in no doubt of their mastery of the subject. The publishers are to be congratulated on a well-printed and substantially bound book which appears to be free of misprints.

C. W. Horton
The University of Texas

Phase Microscopy

By Alva H. Bennett, Helen Jupnik, Harold Osterberg, and Oscar W. Richards. Pp. 320. John Wiley & Sons, Inc., New York, 1951. Price $7.50.

This pioneer book treats the history, theory, and applications of Zernike's phase-contrast method in microscopy. In principle, (1) the object chosen is transparent and contains regions of very slightly less or greater refractive index than the surrounding material; (2) the object is illuminated with a hollow cone of light from an annular stop at the principal focus of the condenser; (3) the parallel light which passes through the object plane undeviated forms an image of the condenser annulus at the back focal plane of the objective, and then passes on to supply the background illumination at the usual image plane just within the principal focus of the eyepiece lens; (4) the light which is deviated by the inhomogeneities in the object forms images of those regions at the usual image plane; (5) a phase plate with an annular region differing in optical path (phase)—usually by $\lambda/4$—from the rest of the plate is put at the back focus of the objective so that only the undeviated light passes through the annular region; (6) the small differences in phase between deviated and undeviated beams are increased by retarding or accelerating one or the other beam by an appropriate phase plate; (7) interference between deviated and undeviated light at the image plane makes visible as amplitude (brightness) differences the slight and otherwise invisible phase differences between the regions of the object which differ in refractive index.

The authors, who have been leaders throughout the ten-year period of development of phase microscopy in this country, have produced a scholarly research monograph. The theoretical aspects are set forth in three progressively more detailed and rigorous chapters presupposing a thorough knowledge of the construction and optical principles of the ordinary compound microscope. Even the most elementary exposition (Bennett) fails to define terms such as diffraction and dispersion and falls short of the clarity of explanation attained, for example, by Burch and Stock, while the intermediate and full dress derivations (Osterberg) require a degree of familiarity with the terminology and format of geometrical optics, a level of mathematical background, and an ability and inclination to pursue the often cumbersome and pedestrian argument from theorem to theorem, which are probably not possessed by many practical microscopists to whom the phase microscope can be an extremely useful research tool. The physicist, however, will find formal treatments of the influence of object size, spacing, and periodic structure, conditions for brightest and darkest contrast, effects of varying plate absorption as well as retardation, influence on resolving power, relation of N. A. to contrast, limiting values for retardation in the object, and so on.

Jupnik's chapter relates theory to practice as seen in the basic design of phase microscope optics, notation system for plates, manufacturing problems, specifications of various commercial instruments and accessories, procedures for aligning and adjusting the phase microscope, and in various special fields such as variable, polarized, ultraviolet, color, and vertical illumination phase microscopy. An interesting section on the empirical effects of varying object size and the dimensions, absorption, and retardation of phase plates correlates qualitatively with theoretical findings and defines practical limits and sources of artifact.

In three chapters Richards gives instructions for preparing a variety of materials for examination, and a very comprehensive survey of the applications of the phase microscope in biology, medicine, and industry. The results are sometimes considered analytically, but much of the matter presented forms merely a choppy and rather repetitious catalog of the materials examined and the types of phase plate used. This useful guide to the literature could have been given more concisely in tabular form.

The book is well illustrated and indexed, has a bibliography giving almost all the literature on both theory and practice through 1950, and is remarkably free from typographical errors. A tendency toward prolixity in understandable in view of the considerable amount of hitherto unpublished personal research material presented. Bias in favor of the instruments manufactured by the authors' employer is satisfactorily restrained.

John B. Buck
National Institute of Arthritis and Metabolic Diseases

Crystal Growth

By H. E. Buckley. Pp. 571+xv. John Wiley & Sons, Inc., New York, 1951. Price $9.00.

Dr. Buckley, head of the Crystallography Department at Manchester University, gives us in this book a painstaking digest of a century of literature on crystal growth, as well as of his own experiments in this field. The first part of the book gives

short descriptions of methods which have been used to grow single crystals, mostly for experimental purposes. Then follow several chapters on theories of crystal growth, in which the author attempts to present fairly the frequently incompatible views found in the literature. Later chapters deal with etch figures, dendritic growth, and the influence of additives on growth habit; in this last field the author's contributions have been particularly important.

The reader is left with a feeling of lack of unity, which to some is inherent in the complexity of the subject, and in the divergent backgrounds of those who have treated it. To any one who intends to work actively in the field of crystal growth, this book is invaluable as a compendium of the art; the physicist in related fields, will, in the reviewer's opinion, get a more vivid impression of the current situation from the Discussion on Crystal Growth of the Faraday Society in 1949. Editing, illustrations, and typography are excellent.

HANS JAFFE
The Brush Development Company

The High Pressure Mercury Vapour Discharge

BY W. ELENBAAS. Pp. 173+xii, Figs. 80. North-Holland Publishing Company, Amsterdam, 1951. Price $4.00.

Here is the first book to be devoted entirely to the physics of the high pressure mercury discharge. The author is chief physicist in charge of the development of discharge lamps at the Philips Lamp Works, Eindhoven, The Netherlands. He has contributed a long series of very original papers on high pressure mercury discharges and is a foremost authority on the subject. He has based his book largely on his own work, although the work of others is generously treated. The book, like the author's papers, is outstanding for conciseness and clarity of presentation.

The book is devoted primarily to discharges burning axially in elongated tubes of hard glass or quartz. The tubes usually have activated electrodes and operate with all the mercury vaporized. A rare gas is usually present for starting purposes. Pressures from 0.1 to 300 atmospheres are treated but, the discussion centers around discharges at about 1 atmosphere.

The author starts from the low pressure mercury discharge and by elementary considerations shows what is happening as the mercury pressure is raised; why the discharge constricts, changes color and becomes more efficient as a light source. The processes are then dealt with quantitatively and the results compared with the experimental findings. This is the general method followed throughout, an admirable balance being kept between theory and experiment. The result is that a large amount of fundamental material has been systematized and presented in a relatively small volume.

Fundamental to the book is the concept of the existence of thermal equilibrium between the electrons at their temperature Te($\sim$6000°K at the axis) and the mercury atoms, at least in so far as the population of their lower excited states is concerned and their degree of ionization. The observed intensities of the spectral lines and the gradient are satisfactorily accounted for on this basis. The translational motions of the atoms are characterized by a gas temperature Tg, slightly lower than Te. Considerable attention is paid to the elementary processes by which the thermal equilibrium is brought about and the factors governing the excess of Te over Tg.

The author shows that the temperature of the discharge depends mainly on the quantity of mercury m and the watts loading L, each per cm of tube length. This leads to the concept of similar discharges, i.e., discharges in tubes of different diameter but having the same temperature at corresponding points. Of course, the voltage gradient and pressure depend also on the diameter, d. Formulas are developed for connecting the "effective" temperature, brightness, gradient, pressure, etc., with m, L, and d. The author discusses his own and other determinations of Te and Tg and selects the most reasonable temperature scale for his calculations.

Some of the special topics treated are the continuous spectrum; convection currents and their effects; the effects of magnetic fields, of added rare gas, of added metals like Cd or Zn, of heating the wall, etc.

The illustrations are of good size. The mathematical treatment is relatively simple. Only a few minor typographical errors have been noted.

The book is a must for designers of high pressure descharge lamps. It is highly recommended to all who are interested in arc discharges at higher pressures.

CARL KENTY
Lamp Division
General Electric Company

The Scientific Papers of James Clerk Maxwell

EDITED BY Q. S. NIVEN. Pp. 806. Dover Publications, New York, 1952. Price $10.00.

This is a reprint, bound in one volume, of the 1890 two-volume edition of the collected papers by the greatest theoretical physicist of the 19th century. The collection begins with a paper by the 15 year old Maxwell "On the Description of Oval Curves" which was communicated to the Royal Society of Edinburgh in 1846 by the celebrated Professor James Forbes; and ends with an article on "Harmonic Analysis" contributed to the 9th Edition of the Encyclopedia Britannica in the year of his death 1879. Between these papers we find many of the greatest contributions in the entire history of physics. After his early studies in Scotland had led to first class mathematical papers on "The Theory of Rolling Curves" and the "Equilibrium of Elastic Solids," Maxwell entered Cambridge where he studied with Stokes and during these undergraduate years his publications practically ceased. However, after his undergraduate examinations were over (he was second Wrangler, and shared with Routh, the senior Wrangler, the first Smith's Prize) he stayed on at Cambridge, became a Fellow of Trinity College, and began the series of distinguished publications which only ended with his untimely death in his 49th year. There are a number of papers on the theory of colors in which he extends the ideas of Thomas Young, and introduces the "Color Box" which was the first practical device for the mixing and studying of colors. Maxwell's work in color also led to important results concerning color blindness.

Then comes the paper "On Faraday's Lines of Force" read in 1855 before the Cambridge Philosophical Society. As an undergraduate he had thoroughly studied Faraday's *Experimental Researches* and in this first of his electrical papers he demonstrates the relation of the laws of Ampere with the results of Faraday.

In 1856 Maxwell became Professor of Natural Philosophy at Marischal College, Aberdeen and during his 4 year tenure of this position he produced outstanding research papers on electrical, mathematical, and color theory subjects, and in addition made two major contributions to entirely new fields. The first is a treatise of nearly 100 pages on the "Stability of the Motion of Saturn's Rings" which received the Adams Prize for 1857. In this work Maxwell proved that the rings are not solid but must be composed of disconnected particles and that for certain radii stability is completely impossible, thus explaining the dark bands in the ring structure. This study led Maxwell to the "Dynamical Theory of Gases" and the first paper on this subject appeared in 1860, and although largely superseded by his later work, nevertheless introduces the first statement of the distribution of molecular velocities according to the law of errors, proves the equality of the kinetic energy of different types of molecules in equilibrium, and defines the concept of gas viscosity.

In 1860 Maxwell began 5 years as Professor at King's College in London. This was a most important change, for he not only moved to the center of scientific work in England, but became personally acquainted with Faraday. In this most productive period of his life he made additional contributions to the theory of color and color vision, and revised and elaborated his kinetic theory of gases culminating in 1865 in the masterful Bakerian

Lecture on the "Viscosity and Internal Friction of Air and Other Gases" which describes the classic experiment using oscillating disks to prove that the coefficient of viscosity is independent of gas pressure within wide limits. But the London period was important above all for the development of his contributions to electromagnetism, and in 1864 he presented to the Royal Society his work on "A Dynamical Theory of the Electromagnetic Field," without question the greatest scientific paper of the 19th century. In this he develops his general equations for the electromagnetic field, and proves that light should be electromagnetic in nature. Here is the comparison of the velocity of electromagnetic disturbances deduced from measurements by Weber and Kohlrausch with the direct velocity of light determinations of Fizeau and of Foucault ending with Maxwell's conclusion that "the number of electrostatic units in one electromagnetic unit of electricity is according to our result, equal to the velocity of light in air or vacuum."

The heavy work of the London professorship, however, undermined Maxwell's health and he was forced to resign. During the years 1865–1871 he resided at Glenlair in Scotland where he prepared his treatise on "Heat" and wrote most of his magnificant work on "Electricity and Magnetism," in which his earlier contributions were correlated and generalized and in which he developed his work on conduction in dielectrics into the great concept of the "displacement current." The quiet and secluded life of Glenlair was broken by annual visits to London and Cambridge and a tour of Italy in 1867, but the succession of scientific papers continued unbroken, including his notable contributions of the reciprocity theorem of stresses in elastic structures and the analysis of uniformly loaded beams.

In 1871 Maxwell left his Scottish lair to become the first Cavendish Professor at Cambridge and Director of the new laboratory given by the Duke of Devonshire in honor of his famous scientific ancestor. Maxwell's new duties were many, including supervision of the new laboratory and obtaining the aparatus for it, lecturing, guiding students in research, and participating in the general affairs of the University, especially in modernizing the famous Tripos examinations, principally by questions which he himself prepared. In these first Cambridge years he also finished the treatise on "Electricity and Magnetism" (1st edition in 1873) and then put in final form his contributions to the "Dynamical Theory of Gases," generalizing his earlier work to include concepts introduced by Boltzmann.

A labor of love in the Cambridge period was his editing the unpublished "Electrical Researches" of the Honorable Henry Cavendish in whose honor the Cavendish Laboratory was named. His own scientific publications, however, continued—on geometrical optics, capillary action, thermodynamics, and a delightful series of articles in *Nature* on Faraday, Helmholtz (the great champion of his electrical work on the Continent), Loschmidt's experiments, molecules, soap bubbles, Van der Waals equation, evidence for the molecular constitution of bodies, the protection of buildings from lightning, and the telephone. Finally, there is the masterful group of semipopular discourses written for the famous 9th edition of the Encyclopedia Brȷtannica. These include an article "Atom," tracing the development of this concept from the Greeks to Maxwell's own time, exhaustive treatments of capillary action and diffusion, and one on the "Ether." In this later paper, after discussing the failure of all experiments (including one by Maxwell himself) measuring effects dependent on the first power of the ratio of the earth's speed to that of light in detecting "motion through the ether," he concludes that this motion can only be observed in an experiment sufficiently sensitive to measure the square of this ratio, and that this is beyond the bounds of experimental possibility. This conclusion by Maxwell proved to be the challenge which the young Albert Michelson accepted to devise his interferometer and the famous experiment performed in Cleveland by himself and E. W. Morley, giving the null result which led to the next great advance from Maxwell's electrodynamics at the hands of Albert Einstein. Maxwell, however, was not destined to see these developments, nor the experimental confirmation by Henrich Hertz of his prediction of the propagation of electromagnetic waves in free space, as he died in 1879.

R. S. Shankland
Case Institute of Technology

Synthesis of Electronic Computing and Control Circuits

By the Staff of the Computation Laboratory of Harvard University. Pp. 278. Harvard University Press, Cambridge, Massachusetts, 1951. Price $8.00.

The problem of the design of switching circuits for the channeling of information in large scale digital computers has acheived an importance ranking with the problem of adequate storage of the information.

Synthesis of Electronic Computing and Control Circuits is accordingly presented by Aiken and his co-workers of the Harvard Computation Laboratory as their approach to the systematic development of switching circuits. As such, the book starts with a discussion of vacuum tubes used as logical operators, proceeds to a general discussion of switching functions of two, three, and then n variables, and continues with a discussion of the minimizing chart as a means of manipulating switching functions. This encompasses the first five chapters. The remainder of the book concerns itself with a discussion of such switching circuits as triggers, rings, coding systems, adders, accumulators, and multipliers; the language of this discussion being the mathematics which was developed in the first five chapters. Chapter X deals with rectifiers as logical elements, and discusses such typical circuits as multiposition switches.

While the subject matter covered in this book is reasonably complete, at this stage of the game at least, the general impression obtained by this reviewer, which was further corroborated by the experience gained in teaching a course on the logic of switching circuits, was that a much clearer understanding could have been obtained if the mathematical formalism had been simplified. The Boolean algebra, while admittedly in need of improvement, seemed more readily comprehended than the algebra presented here.

Another point of criticism is the emphasis given to the minimizing charts. These charts are extensively used throughout the book, and one gathers that this is the only method of reducing a logical statement to minimum form. However, it is known that a "minimum" form may be obtained by means of the chart, but not necessarily the minimum form. This should have been stated more clearly in the text.

As one of the early books in the field, *Synthesis . . .* should prove to be a handy reference for the practicing engineer and mathematician. However, an engineer approaching this field with but little background will find this book disconcertingly difficult to understand, primarily because of the mathematical formalism adopted for manipulating the logic.

It is this reviewer's hope that considerable attention will be given to this problem by the authors before the second edition appears.

H. Fleisher
IBM Engineering Laboratory

Thermodynamics of Alloys

By Carl Wagner. Pp. 161+viii. Addison-Wesley Press, Cambridge, Massachusetts, 1952. Price $6.50.

This small book is an English translation with some revision and additions of Wagner's article, "Thermodynamik metallischer Mehrstoffsysteme," published in Masing's *Handbuch der Metallphysik*. The book is not a general text on the subject. It "stresses the compilation and evaluation of thermodynamic data." The nine-page Chapter 4 illustrates the specialized scope which the book sets up for itself. Entitled "Relations between Thermodynamic Functions and the Phase Diagram," the chapter makes no mention of such general topics as thermodynamically possible forms of phase diagrams that the title would certainly involve

in a general text, but only treats the relations from the one point of view that information regarding relative integral molar free energies may be obtained from experimentally determined phase diagrams and a knowledge of the heats of transition.

Chapters 2 and 3 describe the derivation of thermodynamic quantities from statistical considerations of disordered and ordered alloys, respectively, while the last three chapters (5, 6, and 7) describe experimental methods for determining free energies, activities, etc.

The specialized story is competently and briefly told. It is up-to-date (some of the material is appearing currently in the scientific journals). Certainly one of the most useful features of the book is the alloy index, where the reader is directed to experimental data for 317 alloy systems.

WILLIAM M. BALDWIN
Case Institute of Technology

Electronic and Ion Impact Phenomena

BY H. S. W. MASSEY AND E. H. S. BURHOP. Pp. 669+xviii, Figs. 286. Oxford University Press, Inc., New York, 1952. Price $14.00.

The advances in the field of atomic physics resulting from new instrumentation and stimulated by studies in gaseous electronics and the upper atmosphere since World War II make it desirable and important that the basic experimental data be correlated with the recent developments in the modern mathematical physical methods of analysis, in particular, the quantum mechanics. One of the leading experts in this field is H. S. W. Massey, whose book, *Theory of Atomic Collisions*, now in its second edition and published in collaboration with N. F. Mott, is the basic authority on this aspect of investigation. Since World War II, Massey, together with his two very able colleagues, E. H. S. Burhop and D. R. Bates, intensively have been pushing the interpretation of the newer data in terms of proper collision theory. In consequence of their studies they, as well as many others, have recognized the necessity of a book bridging the gap between the classical analysis analysis of Mott and Massey and the more direct findings of the experimental physicist. The authors have undertaken a monumental task in the book under review, in trying to present the experimental data closely correlated with the wave mechanical analysis of the complicated and extensive field of electronic and ionic phenomena. The procedure throughout the book consists, under each chapter heading, of a general statement indicating the scope of the experimental and theoretical subjects to be considered. They then proceed to give a brief survey of the experimental methods and findings, followed by the quantum-mechanical interpretation of the data. In general, the emphasis is on the experimental technique and data rather than on the more intricate quantum theoretical interpretation. However, enough of the latter is given to orient the reader and to guide his reading and further thinking in the proper channels. The text coverage is as follows: Chapter I: Passage of Electrons Through Gases; Chapter II: Experimental Analysis of the Cross Sections for Impact of Electrons with Atoms; Chapter III: Electron Collisions with Atoms—Theoretical Description; Chapter IV: Collisions of Electrons with Molecules; Chapter V: Reflection and Secondary Emission from Surfaces Due to Electron Bombardment; Chapter VI: Electron Collisions Involving Emission of Radiation; Chapter VII: Collisions Between Atoms Under Gas-Kinetic Conditions; Chapter VIII: The Passage of Homogeneous Beams of Positive Ions or Neutral Atoms Through Gases; Chapter IX: The Collision of Positive Ions and Neutral Atoms with Surfaces; Chapter X: a very brief summary on Recombination of Ions.

By and large, the most satisfactory sections of the book are those dealing with electronic collisions, about which there is most information and for which the theory has been more completely developed. Needless to say, an extensive treatise of this sort—written by a group who are primarily mathematical physicists—will have its limitations. This stems from the lack of direct experience and familiarity with the experimental field and from the rather specialized professional bias in viewing phenomena which the quantum-mechanical analysis enjoins on its exploiter. It is, therefore, not surprising that the analysis and discussion of experimental procedures and data is not always of the best and that sometimes the decisions as to the relative merits of different studies is not always correct. Some ignorance of post-war developments is displayed, especially applying to the considerable work in the United States, although some attempt has been made to correct this sketchily in Appendix I. There is also the natural tendency to stress and discuss particularly those experimental developments which bear more closely on the phases of collision behavior amenable to quantum theoretical analysis and shirking the aspects which are most important to those engaged in research in gaseous electronics, i.e., the lower energy impact phenomena.

Disregarding the weaknesses indicated above, the authors have done a remarkably good piece of work and give to the physicist and engineer an indispensable contribution for the further development —experimental and theoretical—of modern atomic physics. The book should be in the personal libraries of all physicists interested in this work and should readily be available to engineers and others engaged in applications of modern atomic physics.

LEONARD B. LOEB
University of California

The Nature of Some of Our Physical Concepts

BY P. W. BRIDGMAN. Pp. 64, Figs. 4. Philosophical Library, Inc., New York, 1952. Price $2.75.

For the past twenty-five years the writings of Professor Bridgman, based on his idea of operational analysis, have attracted wide attention. Not only has he applied his technique to matters of physical theory, but he has ventured far beyond the conventional bounds of the physicist to inquire into matters in psychology, human relations, and politics. Bridgman himself says that there is nothing mysterious in his technique, that it is only a sincere and honest attempt to recognize and describe what one really does in analyzing a physical experiment, in developing a physical theory, or in talking about ideas.

This book brings together three lectures, delivered at the University of London in 1950, and later published individually in Britain.

The first lecture includes a sketch of the author's method of operational analysis. He is anxious to point out that by operational analysis he means merely an analysis of what the physicist really does in carrying out and interpreting his experiments and observations. He does not in any sense mean to restrict it to purely physical operations. He classifies operations as "instrumental" on the one hand and "paper and pencil" on the other. A subcategory of the "paper and pencil" operations he describes as verbal operations, answers to the question "what would you say under such and such conditions?"

In the other two later lectures Bridgman analyzes various thermodynamic problems and points out the necessity of extending thermodynamics beyond reversible processes to the irreversible processes of which the world is largely made up. He calls attention to the necessity of recognizing the creation of entropy and defines an appropriate creation function for certain simple situations. With the help of this creation function he is able to carry through an analysis of thermoelectric processes which avoids the difficulty previously experienced by Kelvin in separating the reversible from the irreversible parts.

The first lecture is somewhat philosophical in tone; but whether or not one is interested in the philosophy, the thermodynamic analysis of the second two lectures suggests a way in which its powerful methods may be applied more widely than heretofore. This little book itself is merely suggestive, but it is very effective in creating a desire to delve more deeply into Bridgman's extensive writings along these lines.

W. V. HOUSTON
The Rice Institute

Other Books Received

Impact of Science on Society. This is a UNESCO periodical, a quarterly, which was founded two years ago to focus the attention of leaders of thought in all nations upon science as a powerful social force. It has been completely revised in content, style, and format. Annual subscriptions are available for $2.50 through the International Documents Service, Columbia University Press, New York City.

Technion Yearbook. Edited by WILLIAM COHEN. Vol. 10. Pp. 360. Published by American Technion Society, 80 Fifth Avenue, New York City, an organization devoted to the support of the Haifa Technion, Israel's Institute of Technology, and the advancement of science and technology in Israel. The publication contains twenty-five original papers on science and technology, including a section on "Israel—Democracy in Action," which delineates the progress achieved by the new State's scientific institutions and its industry.

Journal of the Mechanics and Physics of Solids. The first number of this international research journal has been issued in October, 1952. It will be published quarterly by the Pergamon Press, Ltd., 2, 3, and 5, Studio Place, Kinnerton Street, London, S.W.1. The publishers' American agents are Messrs. Lange, Maxwell, and Springer, Inc., 122 East 55 Street, New York 22, New York.

This journal will contain original research papers, both theoretical and experimental, of a high standard. The following subjects to be included will give an indication of the scope of the journal: creep; fatigue; elastic and plastic properties of engineering metals; stress analyses of structure and continua; significance of material tests; and rationale of technological forming processes.

The journal will be edited by Professor W. M. Baldwin, Jr., Case Institute of Technology, Department of Metallurgical Engineering, Cleveland 6, Ohio, and Dr. Rodney Hill, Department of Theoretical Mechanics, The University, Bristol 8, England. The Editors will be assisted by an Advisory Board.

Die Fabre (Colour). The first edition of this scientific journal was published some time ago, edited by Dr.-Ing. habil. Manfred Richter, Berlin. The number of readers of this very specific, scientific journal can only be very small. Some of our readers—as far as they work on this particular subject—therefore may be interested in the announcement of this new journal. The publisher is Verlag fur Angewandte Wissenschaften G.m.b.H., Wiesbaden, Rheinstrasse 79.

JOURNAL OF APPLIED PHYSICS VOLUME 23, NUMBER 11 NOVEMBER, 1952

Announcements

All Members Will Receive *Physics Today*

As a result of successful efforts to increase outside income, the American Institute of Physics will be able in 1953 to send *Physics Today* to all members. This service will be rendered without adding in any way to the financial burdens of the Societies or their members. It is being undertaken in response to a growing demand and it accords with the recommendation of a Committee appointed to advise the Institute on its future course with respect to *Physics Today*.

There are now nearly 15,000 physicists in the Institute. A group so large, driven ever to greater specialization by the development of their field, can only with the greatest difficulty maintain unity and combine strength in advancing commonly held objectives. The Institute was originally established by physicists to solve this very problem and *Physics Today* has come to be perhaps its most effective instrument. One medium of communication going to all is vitally needed if physicists are to gain the advantages of community action and meet the demands of professional responsibility. It is on these grounds that extraordinary measures seem justified to give *Physics Today* general circulation. It will begin with the January, 1953, issue.

HENRY A. BARTON